Environmental magnetism and magnetostratigraphy of the Pliocene and Pleistocene sediments of the Heidelberg Basin

DISSERTATION

zur Erlangung des akademischen Grades eines Doktors

der Naturwissenschaften (Dr. rer. nat.)

in der Bayreuther Graduiertenschule für Mathematik und Naturwissenschaften (BayNAT)

der Universität Bayreuth

vorgelegt von

Stephanie Scheidt

aus Offenbach am Main, Germany

Bayreuth, 2018

Die vorliegende Arbeit wurde in der Zeit von Februar 2012 bis Dezember 2017 im und in Kooperation mit dem Gesteins- und Paläomagnetiklabor Grubenhagen des Leibniz Institut für Angewandte Geophysik (LIAG) in Einbeck, Deutschland, angefertigt. Die Betreuung vor Ort oblag Herrn Dr. Christian Rolf (LIAG). An der Universität Bayreuth wurde die Arbeit durch Herrn Professor Dr. Ludwig Zöller und Herrn Dr. Ulrich Hambach (beide angehörige des Lehrstuhl Geomorphologie sowie BayCEER) betreut.

Dissertation eingereicht am: 08.01.2018

Zulassung durch das Leitungsgremium: 29.01.2018

Wissenschaftliches Kolloquium: 05.06.2018

Amtierender Direktor: Prof. Dr. Dirk Schüler

Prüfungsausschuss:

Prof. Dr. Ludwig Zöller   (Gutachter)

Prof. Dr. Helga de Wall   (Gutachterin)

Prof. Dr. Daniel Frost   (Vorsitz)

Prof. Dr. Martin Obst

Content

List of Figures

3. Study 2 – Magnetomineralogical characterisation

4. Study 3 – Enviromagnetic characterisation

List of Tables

1. Synopsis

2. Study 1 – Magnetic polarity stratigraphy

3. Study 2 – Magnetomineralogical characterisation

List of Abbreviations

AF	Alternating field
AFT	Apatite-fission track analysis
AGM	Alternating Gradient Magnetometer
ARM	Anhysteretic remanent magnetisation
BGR	Bundesanstalt für Geowissenschaften und Rohstoffe (Federal Institute for Geosciences and Natural Resources)
ChRM	Characteristic remanent magnetisation
CLG curve	Cumulative log Gaussian curve
DFG	German Research Foundation
DP	Dispersion parameter
EDX	Energy-dispersive X-ray microanalysis
FORC	first-order reversal curves
GAD	Geocentric axial dipole
GMB	Gauss-Matuyama boundary
GPTS	Geomagnetic polarity timescale
HLNUG	Hessisches Landesamt für Naturschutz, Umwelt und Geologie (Hessian Agency for Nature Conservation, Environment and Geology)
IFm	Iffezheim Formation
iNHG	intensification of the northern hemisphere glaciation
IRD	Ice rafted debris
IRM	Isothermal remanent magnetisation
IR-RF	Infrared radiofluorescence
LFm	Ludwigshafen Formation
LGB	Landesamt für Geologie und Bergbau Rheinland-Pfalz (Geological Survey of Rhineland-Palatinate)
LGRB	Landesamt für Geologie, Rohstoffe und Bergbau Baden-Württemberg (Geological Survey of Baden-Württemberg)
LIAG	Leibniz Institute for Applied Geophysics
MAD	Maximum angular derivation
MBB	Matuyama-Brunhes boundary

MD	Multi-domain
MFm	Mannheim Formation
MS	Magnetic Susceptibility
NRM	Natural remanent magnetisation
OSL	Optically stimulated luminescence
P36	Core Ludwigshafen Parkinsel P36
PCA	Principle component analysis
PSD	Pseudo single-domain
SEM	Scanning electron microscope
SGG curve	Skewed generalized Gaussian curve
SD	Single-domain
SP	Super-paramagnetic
TD	Total depth
URG	Upper Rhine Graben
VFm	Viernheim Formation
WD-XRF	Wavelength-dispersive X-ray fluorescence spectrometer

Abstract

The Heidelberg Basin is a broad basin structure in the northern part of the Upper Rhine Graben (URG) in southwestern Germany. The quasi-continuous Miocene to Pleistocene sedimentary infill is mainly fluvial in origin; however, it also includes minor lacustrine intercalations and sporadic pedogenic overprints. The basin has received increased attention from the geoscientific community as a result of the Heidelberg Basin Drilling Project, in which long drill cores (between 300m and 500m) have been obtained from three areas within the basin (Ludwigshafen, Viernheim, and Heidelberg). The combined efforts of scientists from various disciplines have been directed towards obtaining a better understanding of the geological evolution of the basin, including the effects of climate change and tectonics.

This PhD work was intended to establish a comprehensive temporal framework for the entire sequence using magnetic polarity stratigraphy and to assess the palaeoenvironmental evolution of the basin through detailed investigations of the mineral magnetism and environmental magnetism of the sediments. The highly energetic environment in which the sediments were deposited represents a particular challenge in this work; the signal of environmental change is affected by variations in grain size and sedimentary composition and interrupted by hiatuses. However, the results of the three studies presented here reveal that the Heidelberg Basin is an outstanding archive of climate and environmental changes. Furthermore, this work demonstrates that rock magnetic analyses of fluvial sediments can produce valuable information on palaeoenvironments and the evolution of palaeoclimatic conditions.

Age constraints extending to the Pliocene-Pleistocene boundary are obtained by identifying the majority of the boundaries that separate magnetic chrons and subchrons. An age model that averages out short-term variations is applied to the portions of the cores below the Gauss-Matuyama boundary (GMB). Thereby, ages of >4 Ma and >5 Ma are deduced for the deepest portions of the Heidelberg and Viernheim cores, respectively. Core P36 from the Ludwigshafen area is affected by strong drilling-induced overprinting, by which its older parts provide no age information.

A wide range of techniques and methods are applied in mineral magnetic characterisation. Among other properties, magnetic susceptibility and natural remanent magnetisation (NRM) intensities were determined for bulk samples and magnetically extracted fractions. Further, measurements of isothermal remanent magnetisation (IRM) were performed, and backfield IRM curves and hysteresis curves were obtained. Thermomagnetic measurements of magnetic extracts, first-order reversal curves (FORCs) and coercivity analyses of bulk samples are shown to be particularly useful in disentangling the complex magnetic mineralogy. The results of the rock magnetic techniques are

complemented by scanning electron microscopy with energy dispersive X-ray (SEM/EDX) spectroscopic analyses of selected magnetic minerals and wavelength dispersive X-ray fluorescence (WD-XRF) analyses of bulk samples.

Considering all of the results, the cores are divided into two sub-sections based on their magnetic mineralogical characteristics. The boundary between the sub-sections is located just below the Pliocene-Pleistocene boundary and is defined at the GMB. The lower parts of the P36 and Viernheim cores generally display relatively weak magnetic characteristics; authigenic haematite, haemo-ilmenite, Fe-chromite and goethite dominate the magnetic mineral assemblage. The upper parts of these cores are dominated by sulphides, especially greigite. Ilmenite, Fe-chromite, and strongly corroded magnetite remainders are present. The magnetic mineral assemblage of the Heidelberg core differs from those of the other two cores in that its lower and upper parts contain greigite and detrital haematite, respectively. This disparity is assumed to be related to greater rates of subsidence and accumulation at the Heidelberg site and inputs of Lower Triassic clastics from the Neckar River catchment.

Combined with information available from the literature, the rock magnetic data are interpreted to indicate that the climate within the study area was Mediterranean to subtropical during the Pliocene. Repeated fluctuations of the groundwater table drove redox fluctuations in the floodplain areas. Climatic and environmental conditions changed rapidly at the very end of the Pliocene. The mineral magnetic record preserves evidence of groundwater level stabilisation and climatic cooling. Variations in the magnetic mineralogy of the Pleistocene-age portions of the cores are not readily attributed to changes in climatic conditions. The future incorporation of information from palynological and clay mineralogical studies is expected to add to the outcomes of this study substantially.

This work supplements existing knowledge of the palaeoenvironmental and palaeoclimatic evolution of northwestern Europe with information obtained in a region from which few data were previously available. In particular, continental sedimentary records rarely preserve information on the progressive intensification of glaciation in the Northern Hemisphere. The sequence of events recorded in the sediments of the Heidelberg Basin is tentatively placed in the context of scenarios that are based on similar sequences of events that have been reconstructed elsewhere in the Northern Hemisphere. Thus, this study reveals that the Heidelberg Basin preserves an exceptional record of the evolution of the climate of the Northern Hemisphere from a greenhouse state to an icehouse state.

Zusammenfassung

Das Heidelberger Becken ist eine weite, Beckenstruktur im nördlichen Oberrheingraben in Südwest-Deutschland. Die miozäne bis pleistozäne, quasi-kontinuierlich abgelagerte Beckenfüllung ist vorwiegend fluvialen Ursprungs, enthält jedoch untergeordnet auch lakustrine Einschaltungen und sporadisch pedogene Überprägungen. Das Becken rückte verstärkt in den Blickpunkt der geowissenschaftlichen Gemeinschaft, als das Bohrprojekt `Heidelberger Becken´ Tiefbohrkerne (zwischen 300 m und 500 m) aus drei Bereichen des Beckens (Ludwigshafen, Viernheim, Heidelberg) der wissenschaftlichen Bearbeitung zur Verfügung stellte. Die kollektiven Anstrengungen der Wissenschaftler aus verschiedenen Disziplinen galten dem besseren Verständnis der geologischen Evolution des Beckens, inklusive der Einflüsse von Klimaveränderung und Tektonik.

Diese Dissertation hatte zum Ziel mittels Magnetostratigraphie einen Zeitrahmen für die gesamte Abfolge zu etablieren und die Entwicklung der Paläoumweltentwicklung durch eine detaillierte magnetomineralogische und umweltmagnetische Charakterisierung der Sedimente darzustellen. Die Bedingungen des hochenergetischen Ablagerungsmilieus stellen hierbei eine besondere Herausforderung dar. Die Signale der Umwelt- und Klimaveränderungen werden durch Korngrößen-effekte und Kompositionsvariationen überlagert und durch Hiaten unterbrochen. Ungeachtet dieser Bedingungen, zeigen die Ergebnisse der drei hier präsentierten Studien, dass das Heidelberger Becken ein hervorragendes Archiv für Klima und Umweltbedingungen darstellt. Darüber hinaus konnte gezeigt werden, dass gesteinsmagnetische Analysen an fluvialen Sedimenten wertvolle Informationen zur Paläoklima- und Paläoumweltentwicklung beisteuern können.

Die chronostratigraphische Einstufung bis runter zur Pliozän-Pleistozän Grenze beruht im Wesentlichen auf der Erfassung von magnetostratigraphischen Chronen und Sub-Chronen. Die Altersdaten der Kernbereiche unterhalb der Gauß-Matuyama Grenze (GMB) wurden mittels eines Altersmodels hergeleitet, in dem kurzzeitige Variationen herausgemittelt werden. So konnten Alter von >4 Millionen Jahre und >5 Millionen Jahre für die tiefsten Bereiche der Kerne Heidelberg und Viernheim bestimmt werden. Der Kern P36 aus dem Ludwigshafener Gebiet ist durch eine starke, bohrinduzierte Remanenz überprägt und liefert daher im pliozänen Bereich keine Altersdaten.

Die magnetomineralogische Charakterisierung der Sedimente beruht auf einer Anzahl verschiedener Techniken und Methoden. Unter anderem, wurde die magnetische Suszeptibilität und die natürliche remanente Magnetisierung (NRM) von Gesamtprobenmaterial und von magnetisch extrahierten Mineralen bestimmt. Weiterhin wurden Messungen der Erwerbs- und -Rückkurven der isothermalen remanenten Magnetisierung (IRM) sowie Hysteresekurven durchgeführt. Es stellte sich heraus, dass thermomagnetische Messungen von magnetischen Extrakten, sowie ‚first order reversal

curve' (FORC) Messungen und Koerzivitätsanalysen von Gesamtprobenmaterial besonders gut geeignet sind, der komplexen Magnetomineralogie auf den Grund zu gehen. Die Ergebnisse der gesteinsmagnetischen Techniken werden durch eine Kombination von Rasterelektronenmikroskop Analysen und energiedispersiver Röntgenspektroskopie (SEM/EDX) ausgewählter magnetischer Minerale und wellenlängendispersiven Röntgenfluoreszenzanalysen (WD-XRF) des Gesamtproben-materials vervollständigt.

Unter Berücksichtigung aller Resultate werden die Kerne auf Basis ihres magnetomineralogischen Charakters in zwei Teile untergliedert. Die Grenze befindet sich knapp unterhalb des Pliozän-Pleistozän Übergangs, die durch die GMB definiert ist. Der untere Teil der Kerne P36 und Viernheim ist generell schwacher magnetisch als der obere. Authigener Hämatit, Hämo-Ilmenit, Eisen-Chromit und Goethit dominieren die Magnetomineralogie. Der obere Teil dieser Kerne ist dagegen durch Sulfide (insbesondere Greigit) dominiert. Ilmenit, Eisen-Chromit und stark korrodierte Reste von Magnetit-Mineralen sind ebenfalls vorhanden. Die Vergesellschaftung der magnetischen Minerale vom Kern Heidelberg unterscheidet sich deutlich von der der anderen zwei Kerne: Greigit ist auch im unteren Teil vorhanden und der obere Teil enthält detritischen Hämatit. Die Unterschiede werden vermutlich durch höhere Subsidenz- und Akkumulationsraten und durch den Eintrag triassischer Sedimente aus dem Einzugsgebiet des Neckars bedingt.

Durch die Kombination der gesteinsmagnetischen Interpretation mit den in der Literatur verfügbaren Informationen zeichnet sich ein mediterranes bis subtropisches Klima-Szenario ab. In den Flussauen führten wiederkehrende Schwankungen des Grundwasserspiegels zu Redox-Fluktuationen. Am Ende des Pliozäns änderten sich die Klima- und Umweltbedingungen rapide. Die magnetomineralogischen Hinweise deuten auf eine Stabilisierung des Grundwasserspiegels und auf eine Abkühlung der klimatischen Verhältnisse. Variationen der magnetischen Minerale der quartären Kernbereiche können nicht ohne weiteres als Klimaindikatoren verwendet werden. Es wird jedoch erwartet, dass das Einbinden von Resultaten palynologischer Studien oder tonmineralogischer Analysen diesbezüglich weitere Erkenntnisse liefern wird.

Diese Arbeit ergänzt das bestehende Wissen über den Verlauf der Paläoumwelt- und Paläoklimaentwicklung über eine Region von Nordwest-Europa, in der bislang nur wenig Information verfügbar ist. Besonders Daten zum Verlauf der Intensivierung der Vereisung der nördlichen Hemis-phäre sind selten in kontinentalen Sedimenten dokumentiert. Die in den sedimentären Archiven des Heidelberger Beckens gespeicherten Abläufe der klimatischen Ereignisse werden mit Szenarien verglichen, die ähnliche Abläufe andernorts in der nördlichen Hemisphäre belegen (Atlantik, China, Russland). Hierdurch wird deutlich, dass im Heidelberger Becken eine exzeptionelle Aufzeichnung der

Entwicklung des nordhemisphärischen Treibhausklimas zum Eishausklima erhalten ist.

1. Synopsis

1.1. Objectives and working hypotheses

This PhD thesis focuses on the application of palaeomagnetic and environmental magnetic analyses of unconsolidated, water-saturated fluvial sediments of the Heidelberg Basin. This work was intended to demonstrate the potential and challenges of applying the methods of rock magnetism to these kinds of deposits in an extensive case study, and two main objectives were to be achieved. In the first step, a consistent magnetic polarity stratigraphy for the complete succession of the Heidelberg Basin was to be established. This magnetic polarity stratigraphy would then provide a chronological framework for all of the subsequent analyses. The second aim involved improving our understanding of the evolution of the basin through the identification of applicable rock magnetic proxies. A detailed mineral magnetic characterisation of the sediments was performed to permit successful evaluation of the climatic and environmental evolution of the Heidelberg Basin.

Due to the lack of comparable studies in fluvial sediments, it was not clear how detailed the extractable information would be; moreover, it was not clear which special characteristics of the facies needed to be considered. The initial working hypothesis refers to these circumstances in terms of two fundamental assumptions:

> ***The fluvial succession of the Heidelberg basin hosts information on the polarity of the Earth's magnetic field (i.e., a magnetic polarity stratigraphy can be established) and on environmental and climatic change (i.e., proxies can be identified).***

However, the Heidelberg Basin was recognised to represent a unique opportunity. It was hoped that the first terrestrial reference profile for the Pliocene and Pleistocene in Europe would result from this work. Furthermore, correlations of the climate data from the Heidelberg Basin with those obtained from marine sediment cores and ice cores were envisaged.

1.2. An overview of the Heidelberg Basin

The Heidelberg Basin has different names in the literature. In addition to the recently introduced name `Heidelberg Basin´, it is also called `Heidelberger Loch´ (Salomon, 1927). These names are related to the geological situation and geographical location of the basin.

The Heidelberg Basin is a large subsidence depression that is situated in the northern part of the Upper Rhine Graben (URG) in Germany (fig. 1.1). It extends over roughly 150 km along the eastern boundary fault of the URG and has a maximum width of approximately 35 km. The centre of subsidence is situated in the southeastern part of the basin and within the city of Heidelberg.
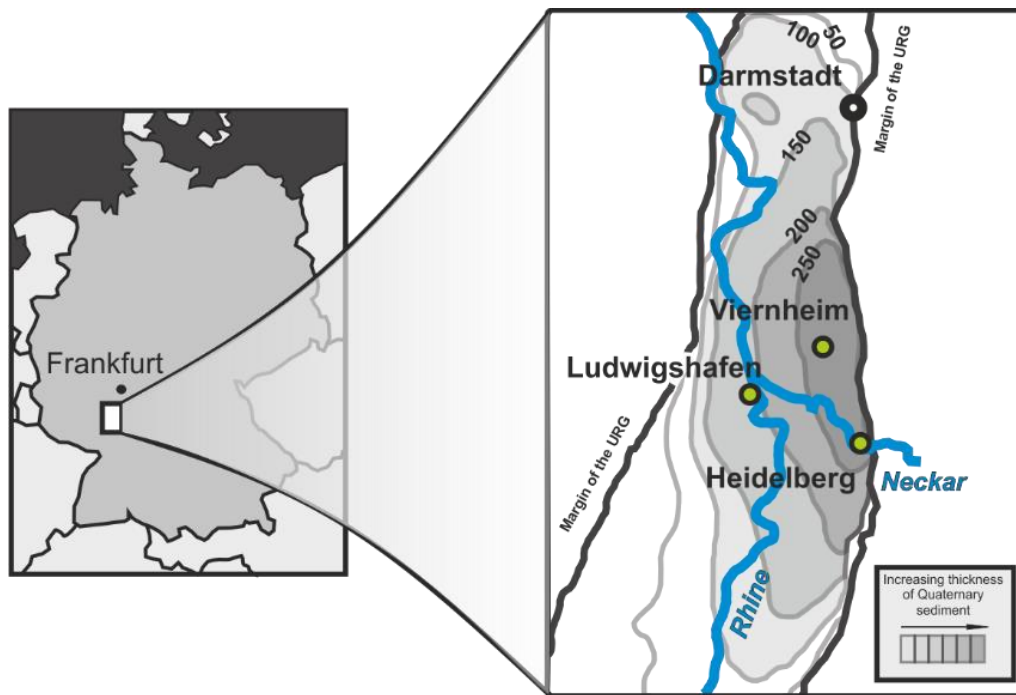
Figure 1.1:
A map of Germany (left) indicating the location of the Heidelberg Basin, which makes up part of the Upper Rhine Graben. In the site map on the right, the thickness of the Pleistocene infill of the Heidelberg Basin is shown (illustration after Bartz (1974)). The green dots indicate the drill sites from which sample material was obtained for this PhD study (cf. section 1.3 and 1.5).

The ongoing subsidence began in the Oligocene (Schumacher, 2002) and has led to sequences of Quaternary and Tertiary sediments that exceed 2000 m in thickness (Buness et al., 2008). The succession is interrupted only by fluvial erosion events. Glacial erosion had no effect within the basin, due to its geographical location. The main part of the basin infill is derived from the Rhine River and its precursors along their courses from the Alps to the North Sea Basin (Preusser, 2008). In addition, the alluvial fan of the Neckar River has had a large impact on the deposits within the Heidelberg region. Except for the deposits of the Neckar River, the grain size of the sediments generally ranges from coarse sand to silty clay. Due to regional lithological variations, different lithostratigraphic nomenclatures are used within the three federal states of Germany (Hesse, Baden-Württemberg, Rhineland-Palatinate) that meet within the Heidelberg Basin to describe the sedimentary succession. A consistent lithostratigraphy that includes 4 units was adopted only in 2011. From top to bottom, the new lithostratigraphic units are the Mannheim Formation (MFm), the Ludwigshafen Formation (LFm), the Viernheim Formation (VFm), and the Iffezheim Formation (IFm). Short descriptions of these formations are given in table 1.1. Additional information on the characteristics of the lithostratigraphic formations is given in chapters 2.3, 3.2, and 4.3. The German LithoLex provides exact definitions of these lithostratigraphic units (Ellwanger et al., 2010a, Ellwanger et al., 2010b, Hoselmann et al., 2010,

Weidenfeller et al., 2010). The translation between the former designations and the new units is explained in Gabriel et al. (2013).

Table 1.1:
Short description of the characteristics of the lithostratigraphic units (rewritten after Scheidt et al. 2015).

Lithostratigraphic unit	Short description
Mannheim Formation (MFm)	A basal layer of gravel followed by several fluvial cycles (mainly grey, calcareous sand). The monotone sequence is sporadically interrupted by fine partially organic overbank and oxbow sediments.
Ludwigshafen Formation (LFm)	Fluvial sediments with intercalations of lacustrine sediments. The fluvial sands fine upward to carbonate-rich grey silts and clays. Sequences end occasionally with humic layers composed of black to brown-black silty clays, occasionally accompanied by peat beds.
Viernheim Formation (VFm)	Dominant fine to medium sands alternate with gravelly sand with silty to clayey intervals Carbonate content of up to 30 %, greenish-grey colours and a high amount of mica are characteristic.
Iffezheim Formation (IFm)	A stack of several fluvial cycles (grey, partially kaolinitic sands) and palustrial, pedogenetically influenced, fine clastic sediments. Mostly carbonate-free, coloured clays are abundant. Isolated carbonate nests occur.

1.3. The Heidelberg Basin Drilling Project

The Heidelberg Basin Drilling Project began to take shape in 2002. The Heidelberg Basin was recognised as a distal sediment trap for Alpine sedimentary material that had the potential to function as a sedimentary record of environmental and climate changes. The project was intended to provide an improved understanding of the geological evolution of the basin and to permit assessment of the effects of climate change and tectonics (Gabriel et al., 2008). Furthermore, it was hoped that the controversy surrounding the stratigraphic classification of the sediments of the Heidelberg Basin would come to an end. This dispute had continued since the first deep drilling, named `Radium Sol Therme´, was performed within the city of Heidelberg between 1913 and 1918 (cf. section 1.4).

The Heidelberg Basin Drilling Project was carried out as a collaborative effort of the Leibniz Institute for Applied Geophysics (LIAG) and the geological surveys of Baden-Wuertemberg (LGRB), Hesse (HLNUG), and Rhineland-Palatinate (LGB). Drill cores obtained from three sites within the basin provided the pivotal issue. Three 300-m-long drill cores were obtained in 2002, 2006 and 2009 during groundwater exploration work at the Parkinsel in the city of Ludwigshafen. These cores are named P34, P35, and P36. In 2006, the geological survey of Hesse contributed a 350-m-long core obtained from a site near the city of Viernheim. The UniNord1 and UniNord2 cores were made available by the LIAG, the geological survey of Baden-Wuerttemberg, and some financiers. Due to unexpected problems, the drilling of core UniNord1 in 2006 was stopped at a depth of approximately 190 m. In

2009, the target depth of 500 m was achieved during the drilling of UniNord2 at a nearby site. Thus, the UniNord core represents a composite. The Viernheim, Ludwigshafen and Heidelberg cores were obtained from the geographical centre, the western margin, and the centre of subsidence of the basin, respectively, and represent three different facies zones.

The pre-project studies to the Heidelberg Basin Drilling Project were executed using core P34 and additional cores and outcrops in the same region. Based on these results, Ellwanger et al. (2005) suggested that considerable insights into the regional and supra-regional climatic and environmental evolution during the Pliocene-Pleistocene would result from the Heidelberg Drilling Project. Moreover, Ellwanger et al. (2005) pointed out the possibility that the project would enable correlation of the history of Alpine and northern glaciation. The project was envisaged as an extensive research effort that would include studies from various geoscientific disciplines. A preliminary sketch of the project included 18 proposals. The objectives of the project included characterisation of global climate changes at the Pliocene-Pleistocene boundary, (neo-)tectonic development in the northern URG, palaeoclimatology and climate proxies, and the sedimentary architecture of the basin, as well as basin modelling. A joint application to the German Research Foundation (DFG) was submitted in 2007 and included 9 studies. None of these projects were approved. However, after resubmission in 2009, three studies were funded by the DFG:

- ***Palynological analysis in Quaternary Sediments of the Upper Rhine Graben: stratigraphy, palaeoecology, and palaeoclimatology;*** Thomas Lit (University of Bonn)
- ***Sediment facies, flow rate and subsidence in the Heidelberg Basin;*** Frank Sirocco (University of Mainz)
- ***Environmental magnetism and magnetostratigraphy of Plio-Pleistocene sedimentary successions of the Heidelberg Basin;*** Christian Rolf (LIAG), Ulrich Hambach (University of Bayreuth)

Publications related to the Heidelberg Drilling Project are shown in section 1.4.1.

1.4. State of the research

Because this work can be considered from several perspectives, this chapter is divided into three main parts. A comprehensive outline discusses the published scientific work related to the Heidelberg Basin sediments. The reconstructed environmental evolution of northwestern and central continental Europe is then briefly summarised. Finally, the availability of work with objectives similar to this PhD study is shown.

1.4.1. Scientific work conducted at sediments of the Heidelberg Basin

The initial scientific evaluation of the sediments of the Heidelberg Basin was hampered by the absence of methods for determining the ages of sediment over the complete succession. Access to the sequences was provided by the first deep drilling (Radium Sole Therme), which was performed between 1913 and 1918. Salomon (1927) analysed the drill cuttings and identified the upper boundary of the Pliocene at a depth of 397 m by means of lithological criteria. Bartz (1953) re-evaluated the available data and suggested that the Pliocene-Pleistocene boundary should be positioned at a depth of 382 m. Schneider and Schneider (1975) shifted the divide further upwards, to a depth of 330 m. This value was obtained by geophysical measurements of the Radium Sole Therme borehole. Fezer (1997) suggested that the Pliocene-Pleistocene boundary at the centre of the Heidelberg Basin should be placed at a depth of 650 m. He correlated the stratigraphy of the Radium Sole Therme drill core with data from the Entensee core drilled in Heidelberg in 1973. The site where the Entensee core was drilled is located approximately 1 km north-northwest of the first drilling site (Conrads and Schneider, 1977).

The Heidelberg Basin Drilling Project (cf. 1.3) produced an increase in the scientific attention devoted to the Heidelberg Basin. Seismic measurements made during the geophysical pre-site survey indicated that the strata are continuous, with insignificant disturbance by faults (Buness et al., 2008). Furthermore, in this study, the depocenter of the basin was identified using the strongest negative gravimetry anomaly of the URG within the city of Heidelberg. Hunze and Wonik (2008) conducted the first correlation of the drill sites using borehole logging data. Other preliminary studies presented lithostratigraphic descriptions of the cores drilled in Heidelberg (Ellwanger et al., 2008), Ludwigshafen (Weidenfeller and Knipping, 2008) and Viernheim (Hoselmann, 2008).

Preliminary rock magnetic analyses revealed that the Pliocene-Pleistocene boundary is associated with a characteristic shift in the rock magnetic parameters (Rolf et al., 2008) that appears to coincide with a marked change in the heavy mineral signature of the sequence throughout the basin (Hagedorn, 2004, Hagedorn and Boenigk, 2008, Hoselmann, 2008). Tatzel et al. (2015) and Reiter et al. (2015) performed provenance analyses on the sedimentary material of the Viernheim core using detrital thermochronology, zircon thermochronology, geochemistry, U/Pb dating, and heavy mineral analyses. A number of biostratigraphic approaches were implemented during the preliminary stages of the Heidelberg Basin Drilling Project. The results included the identification of a number of age/depth tie points in the Heidelberg (Hahne et al., 2008, Hahne et al., 2012), Ludwigshafen (Knipping, 2008) and Viernheim (Wedel, 2008) cores. Further age determinations were later provided by optically stimulated luminescence (OSL) dating of the upper parts of the Viernheim (Lauer et al., 2010) and Heidelberg (Li et al., 2017) cores, as well as IR-RF dating (Lauer et al., 2011) and apatite fission track (AFT) analyses (Reiter et al., 2013) of sample material obtained from the Viernheim core.

Although these studies emphasize different aspects, they contribute to our knowledge of the evolution of the basin, which can be used to reconstruct the environmental and climatic history of continental Europe in greater detail.

1.4.2. Late Pliocene and Pleistocene climatic conditions in northwestern and Central Europe

The late Pliocene and Pleistocene climatic and environmental evolution of central and northwestern Europe has primarily been reconstructed from geomorphological observations (Eismann, 2002, Grube et al., 1986, Rzechowski, 1986) and pollen analyses (Cepek, 1986, Rousseau et al., 1992, Salcher et al., 2017, Zagwijn, 1985, Zagwijn, 1992). However, current analyses of other palaeobotanical material (spores, fruits, seeds, leaves, and wood) and mammal remains provide additional and detailed information on the nature of terrestrial ecosystems, the temperature conditions that prevailed throughout the year, and precipitation amounts (e.g., Mosbrugger et al., 2005, Utescher et al., 2012, Utescher et al., 2000, van Dam, 2006). Because terrestrial archives are highly fragmentary and usually lack robust age constraints, substantial parts of this body of knowledge are derived from more continuous records, such as ice cores (Seierstad et al., 2014) and marine sediments (various ODP drillings; e.g., Lisiecki and Raymo, 2005, Tiedemann et al., 1994). In particular, the reconstruction of sea surface temperatures (Dowsett and Poore, 1990, Dowsett and Poore, 1991, Haug et al., 2005, Rodrigues et al., 2017) and the identification of ice-rafted debris in North Atlantic drill cores (Bailey et al., 2013, Tiedemann et al., 1994) are widely used in reconstructions of climatic conditions during the Pliocene and Pleistocene and particularly at the Pliocene-Pleistocene transition.

Taken together, the available data provide a picture of a warm and humid Pliocene climate with successively decreasing mean annual temperatures (Haywood et al., 2000, Mosbrugger et al., 2005, Suc et al., 1997). During the late Pliocene (~2.7 Ma), the intensification of Northern Hemisphere glaciation (iNHG) was accompanied by a marked increase in seasonality (Hennissen et al., 2015) and changes in vegetation in continental Europe (Heumann and Litt, 2002, Teodoridis et al., 2017). Today, this course of events is widely accepted in the literature. In contrast, the forcing mechanisms that drove the iNHG remain controversial. Possible factors that may have initiated the iNHG include changes in orbital parameters (Berger, 1988, Milankovitch, 1930), tectonic uplift of the Rocky Mountains and the Himalaya (Raymo and Ruddiman, 1992, Ruddiman and Kutzbach, 1989), regional tectonic activity at high northern latitudes (Knies et al., 2014, Poore et al., 2006), changes in seafloor spreading rates (Raymo, 1994), closure of the Panama Seaway (Bartoli et al., 2005, Haug and Tiedemann, 1998, Utescher et al., 2017), changes in atmospheric CO_2 levels (Bartoli et al., 2011, Lunt et al., 2008, Raymo and Ruddiman, 1992, Sigman et al., 2004), and various changes in North Atlantic circulation patterns (Fedorov et al., 2006, Haug et al., 2005, Lunt et al., 2008, Marlow et al., 2000,

Raymo et al., 1992, Utescher et al., 2017). Additional suggestions can be found in the literature; however, this list is not intended to be exhaustive.

In northwestern Europe, climate conditions during the Pleistocene were characterised by cyclic changes between warm and cool periods. Analyses of marine $\delta^{18}O$ and $\delta^{13}C$ records reveal that these cycles followed the 41-ka obliquity cycle until the middle Pleistocene (Mudelsee and Stattegger, 1997). Thereafter, the climatic response of the Northern Hemisphere ice sheets was dominated by the 100-ka eccentricity cycles (Clark et al., 2006, Lawrence et al., 2010, Raymo et al., 1992). The correlations between the rhythmic responses of marine proxies with the terrestrial changes reflected by biostratigraphic data are still not perfectly evident (Šibrava, 1986a) and are pending in the most cases. The same is true for the correlation of the ice core records with records from continental Europe. In addition, multiple glacial histories of the European mainland exist. A number of attempts have focused on correlating the northern glaciations with the Alpine glaciations (Šibrava, 1986b, Brunnacker et al., 1982, Brunnacker, 1986, Bowen et al., 1986). The achievement of this goal has been hampered particularly by the lack of numerical dating methods for sediments >100 ka in age (Ehlers, 2011) and by the small number of continuous sedimentary records.

Only a very brief overview of the climatic evolution of northwestern Europe is given here. For additional information, the reader is referred to reviews on this topic (De Schepper et al., 2014, Lisiecki and Raymo, 2007, Mosbrugger et al., 2005, Ravelo et al., 2007, Raymo, 1994, Utescher et al., 2012) and references therein.

1.4.3. Rock magnetic and palaeomagnetic techniques applied to fluvial sediments

The geological records associated with fluvial systems are generally well studied in northwestern Europe. The response of alluvial architectures to changes in climate and other environmental conditions, such as uplift, subsidence or changes in base level, are recorded in fluvial deposits and are thus widely used to reconstruct the evolution of landscapes (e.g., Blum and Törnqvist, 2000, Foreman et al., 2012, Tucker and Slingerland, 1997, Bridgland and Westaway, 2008a, Bridgland and Westaway, 2008b, Westaway and Bridgland, 2014). Rock magnetic techniques have been used in a number of studies to identify the sources of suspended sediment or anthropogenic pollution (e.g., Desenfant et al., 2004, Jordanova et al., 2004, Kayvantash et al., 2017, Oldfield et al., 1979, Walling and Woodward, 1995, Zhang et al., 2011). In contrast, very few analyses of fluvial sediments apply magnetostratigraphic techniques and environmental magnetic characterisation methods. The studies listed below have been published in international science journals.

Johnson et al., 1986 applied magnetic polarity stratigraphy to fluvial sediments in an eastern Andean foreland basin in Argentina. The sedimentary material was mainly deposited within an arid

environment with ephemeral streams. The magnetic mineral assemblage consists entirely of magnetite, maghemite and haematite. The magnetic polarity stratigraphy is based on 261 samples, and the authors determined a Miocene to early Pleistocene age for the succession, which exceeds 5 km in thickness. The detected polarity zones were correlated with the GPTS using two isolated fission track ages.

Studies of the Neogene Siwalik Formation in Pakistan (Johnson et al., 1982), India (Johnson et al., 1983) and Nepal (Rösler et al., 1997) represent additional examples of magnetostratigraphic analyses of fluvial deposits. Hundreds of samples were collected in each of these studies. The Siwalik Formation is a synorogenic sedimentary sequence with a thickness that exceeds 6 km (Johnson et al., 1982). Magnetite, maghemite and haematite are the main carriers of the remanent magnetisation (Rösler et al., 1997). Radiometric dating of volcanic ashes has been applied in two studies to confirm the magnetostratigraphic results.

Pan et al. (2011) applied magnetic polarity stratigraphy to create a stable temporal framework in the context of reconstructing landscape evolution from a fluviolacustrine profile exposed in the eastern Ordos Plateau of China. The composite profile consists of 6 sections that cover a time interval that extends from 8.3 to 3.7 Ma. This study indicated that magnetite is the major contributor to the remanent magnetisation.

Han et al. (1997) analysed an approximately 100-m-thick fluviolacustrine sequence contained within the Guanzhong basin in central China. The magnetic polarity stratigraphy given in this study is based on samples taken at 50-cm-intervals. Environmental conditions were reconstructed using palynological methods. Although the sediments examined in the studies discussed above are mainly Miocene in age, the deposits examined by Han et al. (1997) accumulated contemporaneously with the sediments of the Heidelberg Basin (i.e., in the Pliocene and Pleistocene). Again, the carriers of the magnetisation are Fe oxide minerals.

Examples of analyses of at least partly fluvial sediments made accessible by deep drilling are provided by a study of an ~1700-m-long core from Osaka Bay in southwestern Japan (Biswas et al., 1999) and by analyses of 7 cores obtained from the Po Plain in central-northern Italy that range in length from 144 m to 220 m (Scardia et al., 2006). In the study conducted in Japan (Biswas et al., 1999) samples were collected at 10-m intervals; however, the sample spacing was reduced to 1 m near polarity changes. Scardia et al. (2006) applied an average sampling frequency of 5 m. The deepest materials examined in these studies are dated to the late Pliocene and the early Pleistocene, respectively. Biostratigraphic and/or radiometric data are reported in both studies and underpin the stratigraphic results. Sulphides are identified as part of the magnetic mineral assemblage only in the data from the Po Plain.

These briefly outlined studies represent most of the available work on Pliocene-Pleistocene successions of (at least partly) fluvial sediment published in the last few decades. These studies are few for many reasons. In addition to the rarity of thick sedimentary deposits of this age, fluctuations in the depositional environment lead to superimposed effects. The seasonal variations in the water levels of rivers result in episodic accumulation and erosion events and distort the magnetic record. Discharge variations may additionally lead to inconsistent mineralogical compositions and particle size distributions. The effects of these characteristics on rock magnetic data produce serious complications in the interpretation of environmental magnetic and magnetostratigraphic data or even prevent the derivation of conclusive results. Secular variations and palaeo-intensity curves cannot be correlated because the amplitudes of natural variations are in the same range as the noise introduced by environmental disturbances. These disturbances include changes in grain size and composition and possibly the alignment of magnetic minerals with currents. Established techniques for the magnetic determination of grain size from the ratios of certain magnetic measurements (Day et al., 1977, Dearing et al., 1997, King et al., 1982, Maher, 1988) must also be questioned for these reasons. Thus, environmental magnetic analyses must employ more time-consuming analyses, such as first-order reversal curves (FORCs), and magnetic polarity stratigraphy can make use only of reversals of the Earth's magnetic field. However, such records must be assessed carefully. Even after deposition, the situation does not become simple. During diagenesis, the formation of new magnetic minerals and the degradation rates of detrital magnetic minerals are affected by periodic water table fluctuations and local drainage conditions (Kraus and Aslan, 1993, Kraus, 2002). Thus, fluvial sediments show high temporal and spatial variability that hamper correlations even over short distances.

In the case of Pliocene-Pleistocene fluvial sediments, the lack of independent age control represents an additional challenge. Any remains are usually not sufficiently preserved to permit the application of biostratigraphic approaches, and age determinations using other methods (e.g., radionuclides, cosmogenic nuclides, and OSL) either do not apply to the entire time interval or feature unacceptably large uncertainties. As a consequence, temporal assignments frequently cannot be made for short sequences.

1.5. Sample materials

This work considers 1150 m of core from the Viernheim, Ludwigshafen Parkinsel and Heidelberg UniNord sites (cf. section 1.3.). After inspection of the three cores from the Ludwigshafen Parkinsel site, core P36 was chosen for sampling. This core is characterised by a comparatively fine grain size distribution and was in better condition overall. Cores P34 and P35 were discarded from further consideration. All of the selected cores were bisected and sampled at an interval of approximately 50

cm. Sections with sediments coarser than medium sand were not sampled. Sampling was performed at different times. Most of the samples from the Viernheim, UniNord 1, and UniNord 2 cores were obtained before this PhD project was begun. However, re-sampling was performed where the reliability of the data was questionable or a finer sampling interval was desired. Additional core material was taken for preparation of magnetic extracts (study 2; after Petersen et al. (1986), von Dobeneck et al. (1987)) and WD-XRF analysis (study 3).

Most of the samples were sawed out of the dried material, producing cubes with an edge length of 2.2 cm. Some cylindrical specimens were obtained from the Viernheim core (only) by pushing a one-inch-wide tube into the cut surface of the bisected working half. This sampling procedure was followed only in sections with low internal coherency to determine whether a palaeomagnetic signal could be extracted. These samples were soaked in stone hardener and sawed into specimens with a length of 2.2 cm. Shorter leftovers were also used for analysis. Samples for vibrating sample magnetometer (VSM) measurements were sawed out of the cubic or cylindrical specimens. If the primary fabric was not preserved, the sedimentary material was collected in plastic bags and used only for rock magnetic analysis (not for magnetic polarity stratigraphy). Table 1.2 shows the total number of samples considered in this PhD study.

Table 1.2*:*
The numbers of different types of samples that were obtained from the individual cores and are considered in this PhD study are listed.

	Viernheim	**P36**	**Heidelberg**
Cubic samples	256	159	445
Cylindrical samples	116	-	-
VSM samples	76	113	117
Extracts	40	28	43
SEM/EDX	-	30	-
WD-RFX	40	10	-

Note that a reversal identified in the two cores obtained from the UniNord sites showed an offset of only ~1 m. Therefore, the two cores are treated as being one in this study. This composite core is also called the UniNord core or the Heidelberg core. All of the cores contain the four lithostratigraphic units described in section 1.2.

1.6. An outline of the applied methods of rock magnetism

The techniques applied are well established in the Earth sciences. The following discussion provides a short introduction to the methodologies used. For more detailed information, the reader is

referred to the relevant literature, which is also indicated below. The devices used for the measurements are listed in table 1.3.

1.6.1. Magnetic polarity stratigraphy

Magnetic polarity stratigraphy came to the fore as a method for dating and correlating rock sequences in the 1960s (Cox et al., 1963, Cox et al., 1964) and took root during the 1970s (Butler and Opdyke, 1979, Chan and Alvarez, 1983). Palaeodirections are extracted from samples through measurements of the remanent magnetisation of oriented samples during stepwise demagnetisation experiments. Generally, the most stable direction is assumed to represent the direction of the Earth's magnetic field during acquisition of the characteristic remanent magnetisation (ChRM). Care must be taken if highly coercive minerals (e.g., haematite and goethite) are part of the magnetic mineral assemblage because alternating field (AF) demagnetisation is not suitable to erase the remanent magnetisation carried by these minerals. Both thermal and AF experiments are therefore applied in this study. The data from these measurements are investigated using principal component analysis (PCA) via the least-squares fitting technique (Kirschvink, 1980) and shown in Zijderveld diagrams (Zijderveld, 1967). Note that only the inclination values are considered because the cores of the Heidelberg Basin are not oriented with respect to their azimuthal directions. Chronostratigraphic ages are obtained through the identification of changes in the recorded earth magnetic field from either normal to reversed polarity or vice versa and the correlation of these switching points with the geomagnetic polarity timescale (GPTS; after Cande and Kent (1995), as shown in Ogg (2016)).

The reliability of the data used to establish the magnetic polarity stratigraphy was facilitated by careful selection of measurements during sampling and data processing. Core material that was characterised by relatively coarse grain sizes or visible damage to the sedimentary fabric was discarded. The determined ChRM was used only if the maximum angular deviation (MAD) calculated through PCA analysis in the Remasoft 3.0 program (Chadima and Hrouda, 2006) was ≤ 12°. Additionally, most of the specimens with very shallow inclination values were eliminated from the data set, to exclude the possibility that opposing palaeodirections might be induced by rotation. Finally, the possibility of overprinting by the later formation of authigenic minerals is rebutted by evidence regarding the origin of the magnetic mineral assemblage (cf. 3.5.2.).

Table 1.3*:*

This table shows the equipment used to perform the individual measurements and the locations of the laboratories in which the analyses were performed.

Procedure	Device	Laboratory
Measurement of magnetic susceptibility (MS)	Minikappa KLF-3 kappabridge (AGICO, Brno, CZ).	Leibniz Institute for Applied Geophysics (LIAG), Germany
	Minikappa KLF-3 kappabridge (AGICO, Brno, CZ).	Ludwig-Maximilian University of Munich, Germany
Measurement of frequency dependency of MS	A Magnon VFSM Susceptibility Bridge (MAGNON Int., Dassel, FRG)	Leibniz Institute for Applied Geophysics (LIAG), Germany
measurement of remanent magnetisations	cryogenic magnetometer (760 SRM-RF-SQUID, 2 G Enterprises, Mtn. View, CA, USA); if intensity > 10 Am^{-1}: Magnon Spinner Magnetometer (MAGNON Int., Dassel, FRG)	Leibniz Institute for Applied Geophysics (LIAG), Germany
	liquid-heliumfree, superconducting rock magnetometer (760 SRM-DC-4 K, WSGI, Sand City, CA, USA)	Ludwig-Maximilian University of Munich, Germany
Alternating field demagnetisation	Magnon MI AFD 300 demagnetiser (MAGNON Int. Dassel, FRG)	Leibniz Institute for Applied Geophysics (LIAG), Germany
	D-Tech D2000 AF demagnetiser (ASC Scientific, Carlsbad, CA, USA)	Ludwig-Maximilian University of Munich, Germany
Thermal demagnetisation	thermal specimen demagnetiser model TSD-2 (Schoenstedt Instruments Company, Virginia, USA)	Ludwig-Maximilian University of Munich, Germany
Acquisition of anhysteretic remanent magnetisation (ARM)	Magnon MI AFD 300 demagnetiser (MAGNON Int., Dassel, FRG)	Leibniz Institute for Applied Geophysics (LIAG), Germany
Acquisition of isothermal remanent magnetisation (IRM)	Magnon PM II Pulse Magnetizer (MAGNON Int. Dassel, FRG)	Leibniz Institute for Applied Geophysics (LIAG), Germany
Thermomagnetic measurement	Vibration sample magnetometer EZ7 (MicroSense, Lowell, MA, USA)	Leibniz Institute for Applied Geophysics (LIAG), Germany
Hysteresis measurement	Vibration sample magnetometer EZ7 (MicroSense, Lowell, MA, USA)	Leibniz Institute for Applied Geophysics (LIAG), Germany
	Vibration sample magnetometer EV9 (MicroSense, Lowell, MA, USA)	Institute of Geophysics, Academy of Sciences of the Czech Republic
Measurement of first order reversal curves	Princeton Measurements Alternating Gradient Magnetometer AGM, Model MicroMag 2900	University of Bremen, Germany
SEM/EDX	SEM (backscattered electrons; FEI Sirion 200, Type D1625) combined with EDX (Ametek, Genesis 4000)	Institute for Geosciences and Natural Resources (BGR), Germany
WD-RFX	PANalytical Axios wavelength-dispersive X-ray fluorescence spectrometer	Institute for Geosciences and Natural Resources (BGR), Germany

1.6.2. Magnetic mineralogy

The characterisation of the magnetic mineralogy is based on the fundamental principles of rock magnetism, which are well described in various textbooks and scientific articles (e.g., Dunlop and Özdemir, 2001, Stacey, 2012). Generally, the determination of the magnetic mineral content and its grain size spectra becomes more complicated as the number of magnetic components increases. Because multi-component systems in fluvial sedimentary material are the rule, rather than the exception, the identification of the characteristics of a magnetic inventory is rarely straightforward.

In this work, the characterisation of the full spectra of magnetic components results from the combination of findings obtained by several measurements. Initially, the variations of bulk sample magnetic parameters are determined: mass specific MS (χ), frequency dependency of MS (κ_F), natural remanent magnetisation (NRM), anhysteretic remanent magnetisation (ARM), isothermal remanent magnetisation (IRM), and hysteresis parameter.

Several ratios and parameters can be calculated from the bulk sample measurements mentioned above, and these quantities may provide more detailed information on magnetic granulometry (e.g., Day et al., 1977, Dearing et al., 1997, King et al., 1982, Maher, 1988) or the relative contributions of materials with particular coercivity values (Thompson and Oldfield, 1986). Of these ratios, only the Day plot and the S-ratio (Thompson and Oldfield, 1986) were successfully applied. This work follows Bloemendal et al., (1992) by defining the S-ratio as

$$(1 + (BF\_IRM_{-0.3T} / IRM_{2.7T})) / 2 \tag{1-1}$$

Here, $BF\_IRM_{-0.3T}$ represents the remanent magnetisation determined at a backfield of 300 mT, which is obtained after exposing the sample to a field of 2.7 T.

To exclude the paramagnetic fraction of the sample material, magnetic extraction was performed (Petersen et al., 1986, von Dobeneck et al., 1987). Then, IRM, hysteresis and temperature dependent behaviour were determined of these extracts and compared to the bulk sample material.

Unlike the above-mentioned bulk sample measurements, high-temperature experiments observe the behaviour of the sample material during heating and cooling between 40°C and 700°C. The change of the magnetisation in a field of 1 T ($I_{S(T)}$) as well as the increase or decrease of the MS (κ_T) indicate the presence or absence of certain minerals or mineral groups. However, $I_{S(T)}$-curves indicating only the specific blocking temperatures of the minerals, while κ_T-curves showing additionally thermal activation phenomenon, such as the Hopkinson peak, for example. The κ_T-curves did not attribute additional information to the knowledge of the magnetic mineralogy and are thus, not published in any work of this project. Another performed experiment is the progressive thermal demagnetisation of a three-

component IRM (Lowrie, 1990). In such experiments, the carriers of the magnetisation are detected by identification of the blocking temperatures of minerals in three different coercivity ranges (cf. section 2.5 and 2.7).

Further unravelling of the magnetic components was carried out through coercivity analysis of the IRM acquisition curves (cf. section 3.4.6.; Egli, 2003, Egli, 2004b, Kruiver et al., 2001, Robertson and France, 1994) and high-quality FORC analyses (cf. section 3.4.5; Pike et al., 1999, Roberts et al., 2000 Both of these approaches enable determination of the switching field distribution of the magnetic particles in a sample. The coercivity analysis used in this work models the remanence properties of the bulk sample material as a set of skewed generalised Gaussian (SGG) functions. For this purpose, the Mag-Mix software package (Egli, 2003, Egli, 2004) is applied. In this approach, magnetic components are defined in terms of their chemical compositions, their magnetic grain size spectra and their mineral shapes. For example, two chemically identical magnetite populations are recognised as different components if the specimens of one group combine single-domain (SD) characteristics with similar grain shapes (e.g., magnetofossils), and the other group consists of irregularly shaped, multi-domain (MD) individuals with differing grain sizes (e.g., detrital minerals). Each magnetic component identified within the sample material is represented by one SGG function, which is characterised by four parameters (for details see Egli (2003)). The summed contributions of the individual components reproduce the shape of the IRM acquisition curve (fig. 1.2).
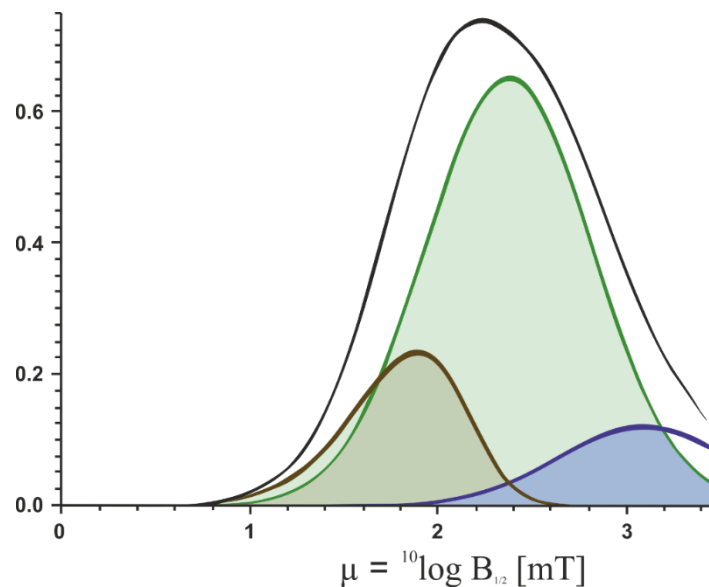
Figure 1.2:

The model result of an analysis performed using GECA (a part of the Mag-Mix software package of Egli (2003), (2004a)) shows the three individual SSG functions (brown, blue, green) and the summed curve (black) that resembles the IRM acquisition curve of sample U185.06 from the UniNord core.

FORC analysis is based on a set of partial hysteresis loops (called FORCs) measured consecutively at regularly spaced field increments. FORC diagrams are obtained from these data (for details see Roberts et al. (2000)). The resulting contour diagrams indicate the distribution of the coercivity of the components within the sample material and additionally provide information on grain size ranges and the occurrence of particle interactions. The FORC analyses are performed with the VARIFORC software package (Egli, 2013) that enables the analysis of stacks of identical FORC measurements from individual samples. This strategy increases the quality of the results obtained from very weak samples.

Rock magnetic methods are supplemented by scanning electron microscopy with energy dispersive X-ray spectroscopy (SEM/EDX; cf. section 3.4.1.) of magnetically extracted material and wavelength-dispersive X-ray fluorescence analysis (WD-XRF; cf. section 4.6.3) of bulk sample material. SEM/EDX is a surface analytical technique. A high-energy electron beam is used to liberate electrons from the surface of the uncoated sample material. Analyses of the characteristics of the resulting backscattered electrons and X-rays result in quantitative elemental compositions. Images are also obtained from the backscattered electrons.

The WD-XRF analyses serve to determine the elemental compositions of sample materials through detecting the intensities of X-rays at certain wavelengths. To carry out these analyses, the bulk sample material is converted into fused glass specimens. The specimens are irradiated by X-ray beams, whereby the elements are excited simultaneously. The transmitted X-rays are diffracted according to their wavelengths and finally detected to produce quantitative major elemental compositions.

1.6.3. Environmental magnetism

Environmental magnetism began to play a role at the end of the 1970s (Evans and Heller, 2003, Oldfield et al., 1979, Maher and Thompson, 1999, Thompson and Oldfield, 1986). This suite of methods includes a variety of techniques that can decode the magnetic signals of various rocks and other carriers of magnetic information (e.g., air filters) with the aim of assessing environmental conditions and changes.

The interpretation of the environmental magnetic record presented in this work is based on the rock magnetic measurements and analyses described briefly above. The identified magnetic properties and mineral associations indicate or exclude certain environmental conditions. The sum of all of the identified magnetic characteristics, combined with geological and geochemical observations, show the progressive evolution of the sedimentary material.

1.7. Results and discussion

The results of the three studies included in this PhD work are closely intertwined. A preliminary characterisation of the magnetic mineralogy is included in the first publication, which focuses on magnetic polarity stratigraphy. In turn, the second publication, which addresses the characterisation of magnetic minerals, also includes a discussion of further aspects of the reliability of the stratigraphic classification and also briefly presents an interpretation of the environmental and climatic implications of this classification. The environmental and climatic implications are the topics of the third manuscript. In the following outline, the final results are arranged by subject and briefly discussed, regardless of the primary publications that present the individual results.

1.7.1. Magnetic polarity stratigraphy
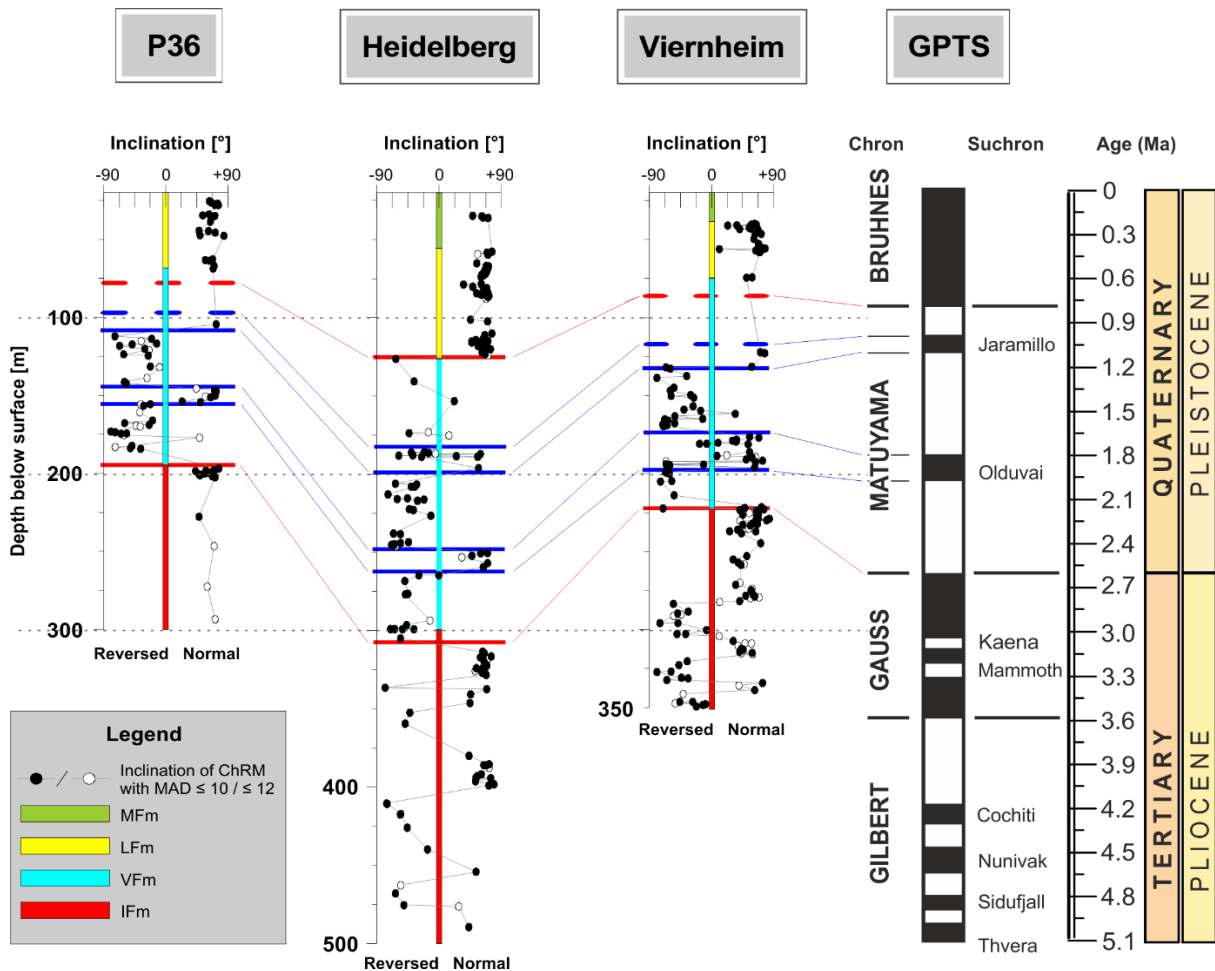
Figure 1.3*:*

Magnetic polarity stratigraphy of core P36 and the Heidelberg and Viernheim cores based on ChRM values with median angular deviation (MAD) values of 10 or 12, respectively. Correlation with the GMTS after Cande and Kent (1995), as shown in Ogg et al. (2016), is shown for the Pleistocene part.

The ChRM of the uppermost two lithostratigraphic units (MFm and LFm) shows almost exclusively normal polarity (fig. 1.3). However, the data obtained from the Heidelberg core indicate a reversal at 125.18 m ± 1.05 m; this reversal falls within the LFm but is very close to the boundary with the subjacent VFm at 126.40 m. Due to the poor preservation of palaeomagnetic signals in coarse sedimentary material, this reversal is not documented in the Viernheim core and core P36. Instead, large data gaps compromise the magnetostratigraphic records in these cores. Fortunately, the Heidelberg core contributes a small number of isolated reversed data points; these points require the upper VFm to correspond to the Matuyama chron. Consequently, the top of the Matuyama Chron in the Viernheim core and core P36 is suggested to be located within the data gaps and in the vicinity of the lithostratigraphic boundary between the VFm and the LFm. Downcore, the onset of higher data density in the VFm starts with normally magnetised specimens. This section is correlated with the Jaramillo subchron in all of the cores. The occurrence of mixed normal and reversed polarities in the Heidelberg core is assumed to originate from the formation of authigenic minerals long after the deposition of the sediments. The subjacent alternation from predominantly reversed to normal and back to reversed polarity is attributed to the lower part of the Matuyama chron, which includes the normal Olduvai subchron.

The top of the Tertiary part of the succession is defined by the Gauss-Matuyama boundary (GMB). Within the Viernheim core, this reversal coincides with the boundary between the VFm and the IFm. Here, evidence for a discordant contact between the lithostratigraphic units is provided by the heavy mineral analyses (Hoselmann, 2008). Similar circumstances are assumed to apply to core P36, but the lack of palaeomagnetic data in the lowermost part of the VFm hampers the localisation of the top of the Gauss chron. Again, the Heidelberg core provides crucial information on stratigraphic affiliations by revealing that the GMB occurs at the very top of the IFm. Below, clear association of the identified polarity changes with particular stratigraphic positions is hardly achievable. A large number of different scenarios are possible because the number, extent and position of hiatuses are all unknown. The most plausible correlation scheme is obtained through the use of assumptions that focus on deposition over longer time periods (>0.5 Ma). In this regard, the accumulation space of a continuously subsiding basin is assumed to be constant. Furthermore, it is suggested that the age-depth relationship of the laterally complex depositional pattern of a fluvial system, which is actually step-like, can be approximated by an almost linear, smooth curve. Finally, it is expected that longer chrons or subchrons have a higher preservation potential than short ones.

The application of these assumptions in the interpretation of the data lead to minimum ages for the deepest parts of the Viernheim and Heidelberg cores of 5.235 Ma and 4.187 Ma, respectively (fig. 1.4, 2.9). These ages represent the most plausible correlation scheme; though other solutions are also

possible. The drilling-induced overprinting of the IFm inhibited the correlation of core P36 with the GPTS.

Viernheim

1) 222.12 m +/- 0.16 m
2) 282.85 m +/- 0.62 m
3) 303.51 m +/- 0.74 m
4) 318.00 m +/- 2.27 m
5) 333.04 m +/- 0.76 m
6) 339.99 m +/- 1.24 m

Heidelberg

1) 309.20 m +/- 4.27 m
2) 349.32 m +/- 3.08 m
3) 370.01 m +/- 10.27 m
4) 404.68 m +/- 5.74 m
5) 475.08 m +/- 0.24 m
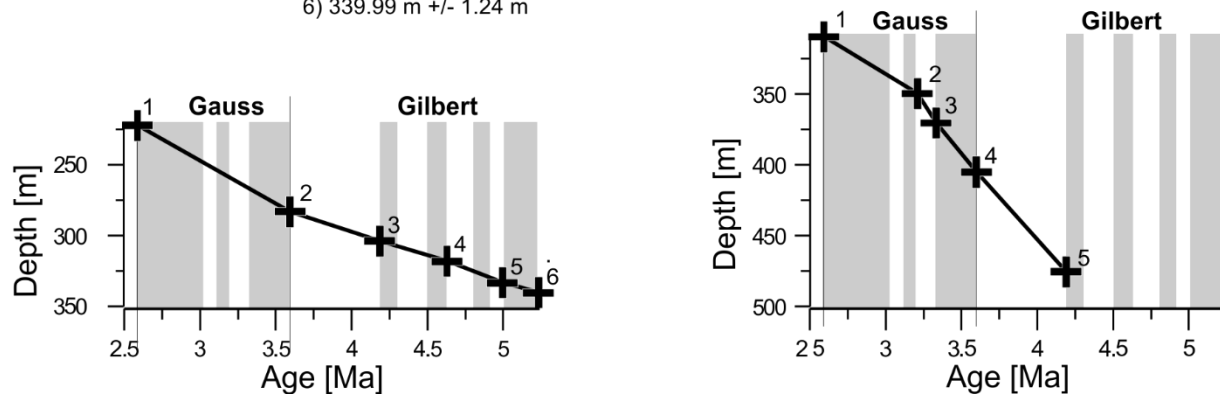
Figure 1.4:

Final age-depth correlation of the Pliocene palaeomagnetic data from the Viernheim (left) and Heidelberg cores (right) with the GPTS (after Cande and Kent (1995), as shown in Ogg et al. (2016)), shown as grey (normal) and white (reversed) bars (redrawn after Scheidt et al. (2015)).

The interpretation of the magnetic polarity stratigraphy is largely consistent with the results of any method applied to the sequence (cf. 1.4.1). However, two exceptions are noted here. First, the results of a pollen analysis of the lower part of the Heidelberg core (Hahne et al., 2012, Hahne et al., 2008) does not conform with the results presented here (see remarks to study 1 for background information). Second, these results contradict the interpretation of a single (U-Th-Sm)/He thermochronology age determined from the Viernheim core and presented by Reiter et al. (2013). A comprehensive overview on age determination methods that were applied to the sequences of the Heidelberg Basin and the results obtained using these methods is given in section 4.4.

Although the sequence contained in the Heidelberg Basin provides a quasi-continuous sedimentary record, the magnetic polarity stratigraphy is not suitable for establishing a terrestrial reference profile for the Pliocene and Pleistocene in Europe, as initially anticipated. The deficiencies arise mainly from the dynamics of the depositional environment. Due to the occurrence of sections with coarser grains, the magnetostratigraphic record is discontinuous, hampering clear localisation of polarity changes in the upper parts of the cores. Although the lack of short-lived magnetic excursions and events in the record may result from the sampling interval used, data gaps or hiatuses are also possible explanations. Finally, variations in the grain size spectra and mineralogical compositions prevent fine tuning of the age-depth model using relative palaeo intensity or secular variations of the earth magnetic field. However, besides the age determinations, the identification of age tie points

from reversals allows the estimation of accumulation rates within the Heidelberg Basin. Although these accumulation rates represent averages over relatively long time scales, they provide important evidence on the course of subsidence within the basin. These data can be included in reconstructions of the structural development of the URG.

1.7.2. Magnetic mineral characterisation

The successful identification of the magnetic mineral inventory of the sediments of the Heidelberg Basin requires combining the results from different techniques. The ARM data do not contribute information to the magnetic mineral characterisation discussed in the following.

Bulk sample measurements reflect the integrated responses of all magnetic components in a sample. Thus, the resulting data are used to show general trends within the succession. The increases in MS and the NRM values close to the top of the IFm are less pronounced in the Heidelberg core than in the Viernheim core and core P36 (fig. 1.5 and 3.7, 4.2, 4.3, 4.4).
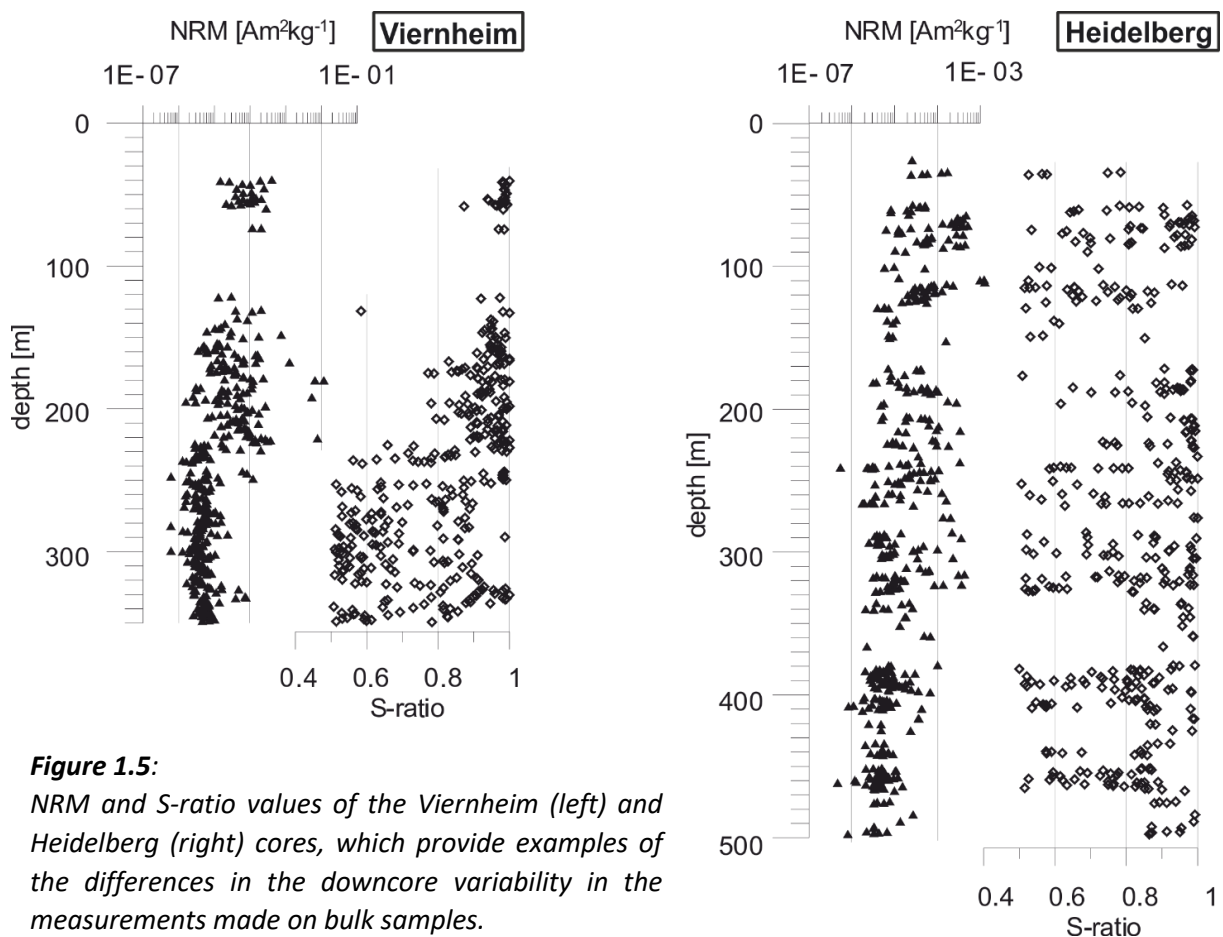
Figure 1.5:
NRM and S-ratio values of the Viernheim (left) and Heidelberg (right) cores, which provide examples of the differences in the downcore variability in the measurements made on bulk samples.

Additionally, the S-ratios of the Heidelberg core are widely scattered in all of the lithostratigraphic units, not only in the Tertiary part (fig. 1.5). Thus, these bulk sample measurements indicate clear

differences in the distributions of high coercivity minerals and ferrimagnetic minerals among the lithostratigraphic formations and the cores, respectively.

SEM/EDX analyses of magnetically extracted minerals were performed to gain an overview of the magnetic mineral inventory of core P36 and its chemical composition. Quantitative statements cannot be made on the basis of these analyses because certain minerals and grain sizes are preferentially collected by the extraction apparatus. Moreover, only a small number of grains in each sample were selected for closer inspection. However, the analyses indicate that the Pleistocene part of the succession is dominated by greigite with different growth habits (fig. 3.3). Tiny single crystals, framboids, and aggregates occur together. Some heavily corroded magnetite grains are also found. The Tertiary part of the succession is strongly depleted in magnetically extractable minerals. Haematite is present as specularite and as pseudomorphs after pyrite. The specularite is sometimes slightly pitted. Only a very few grains of Ti-magnetite were identified. Fe-chromite spinel and Ti-enriched Fe-chromite are recognised in the complete succession (fig. 4.4). It is shown that the downcore variations in the Ti/Fe-ratio of the non-sulphidic minerals increase significantly from one lithostratigraphic unit to the next. Except from a few outliers, the maximum values of this ratio are 1.4, 1.8 and 4.0 for the LFm, the VFm, and the IFm, respectively (fig. 1.6).
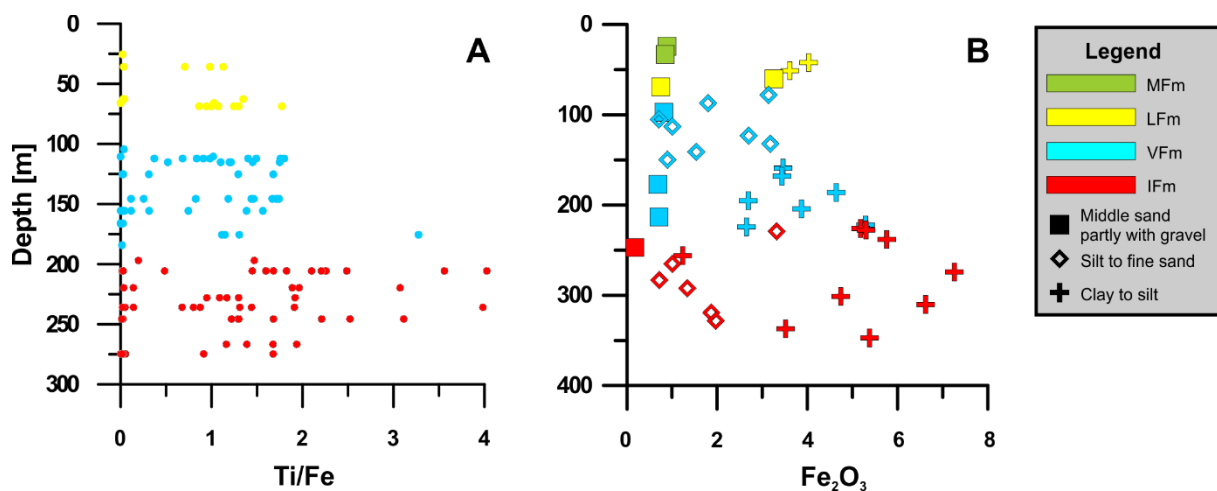
Figure 1.6:
A) Distribution of Ti/Fe-ratios determined from EDX measurements of single magnetic minerals derived from core P36. The colour coding of the closed circles refers only to the lithostratigraphic units. Redrawn after Scheidt et al. (2017). B) Fe_2O_3 values determined from WD-XRF measurements of bulk sample material from the Viernheim core.

Most prominent is the change close to the Pliocene-Pleistocene boundary. In this context, the elemental distribution of bulk sample material obtained by WD-XRF analysis of the Viernheim core and

core P36 is remarkable. This distribution shows that the fines within the IFm contain greater amounts of Fe_2O_3 than comparable sediments of the younger lithostratigraphic formations (fig. 1.6).

The findings of the EDX and XRF analyses are consistent with the results of progressive thermal demagnetisation experiments of the three-component IRM of bulk sample material obtained from core P36. Here, maghemite and/or magnetite are recognised as rather unusual carriers of the remanent magnetisation, whereas high coercivity minerals (haematite and goethite) and sulphides (most likely greigite) dominate the Tertiary- and Pleistocene-age lithostratigraphic units, respectively (fig. 2.6).

Thermomagnetic measurements under a field of 1 T performed on minerals extracted magnetically from all cores results in the identification of three groups of thermomagnetic behaviour within the lithostratigraphic units (fig. 1.7 and 3.6).

A) Samples that are characterised by monotonically decreasing curves are attributed to pure oxide minerals (magnetite, maghemite, ferro-chromite, haemo-ilmenite, and haematite) and occur in the IFm, the VFm and the LFm.

B) Samples with demagnetisation curves that show a monotonic decrease that is followed by an increase in magnetisation between 400°C and 450°C and a rapid loss of magnetisation at approximately 550°C are attributed to a mixture of oxide minerals. The peak is likely induced by the conversion of pyrite. These curves were exclusively recognised in the IFm.

C) Curves that show an increase in magnetisation beginning at ~250°C with multiple subsequent peaks are attributed to the presence of sulphides in the samples. With a very few exceptions, this type of thermal behaviour is found only in the VFm and the LFm.
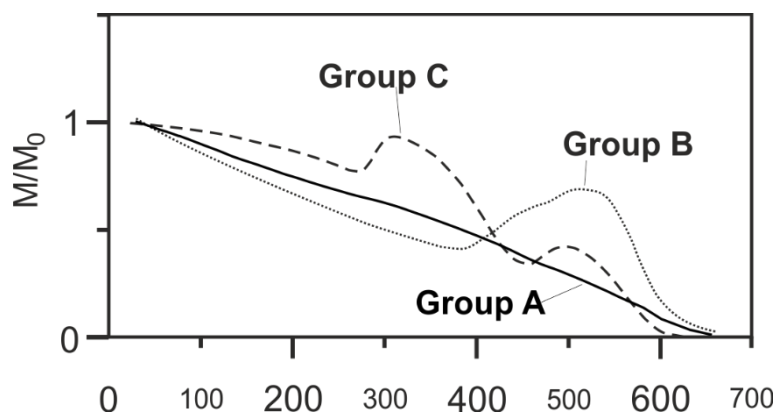
Figure 1.7:

Sample heating curves belonging to the groups A, B, and C.

The thermomagnetic measurements and the EDX analyses provide information that is key in the interpretation of the data obtained from the <u>coercivity analyses</u>. As a result, 6 coercivity groups are distinguished, of which up to 5 coexist in the sample materials (fig. 3.11). The coercivity groups represent particular minerals. In order of increasing coercivity, these groups represent magnetite and chromite; magnetite and sulphides; sulphides; sulphides and haemo-ilmenite; haematite; and goethite. The repeated assignment of magnetite and sulphide minerals to different groups results from overlaps in the coercivity ranges. Coercivity variations in these minerals are likely caused by lattice defects, variations in their chemical compositions, or grain size changes. The distribution pattern of the coercivity groups divides the Viernheim core and core P36 into two parts. The lower (Tertiary) part is mainly influenced by haematite, goethite, and haemo-ilmenite, which are high coercivity minerals with weak magnetic moments. The upper (Pleistocene) part of the cores is dominated by an association of low coercivity minerals, primarily ferrimagnetic sulphides and magnetite. In contrast, in the Heidelberg core, haematite and sulphides are universally present. The results of the coercivity analysis fully explain the trends disclosed by the bulk sample measurements.

Another interesting aspect of the coercivity analysis concerns the narrow coercivity distributions associated with the sulphide components. These shapes point towards the presence of non-interacting SD-particles (Newell, 2005), which are usually contributed by magnetofossils (Egli, 2004a, Egli et al., 2010, Heslop et al., 2014, Ludwig et al., 2013). However, the <u>FORC analyses</u> of the bulk sample materials call into question the presence of these particles in the sample material. The presence of magnetofossils would result in a characteristic FORC signature (central ridge) that carries substantial parts of the magnetisation. The central ridges in the sample materials carry <2% of the total remanent magnetisation (fig. 3.10). Thus, they are suggested to represent an elemental part of the greigite signatures, which is only visible in high-quality FORC diagrams. This theory is reinforced by the occurrence of similar features in the FORC diagrams presented by other studies (e.g., Rowan and Roberts, 2006). Besides this essential clarification, FORC diagrams reveal information on the magnetic components and their individual grain sizes. The characteristic asymmetric contours of SD greigite dominate most of the FORC diagrams in this study. In some samples, the signature is combined with that of PSD magnetite. High coercivity central ridges are recognised in two FORC diagrams and are attributed to SD haematite and/or goethite particles of unknown origins. Here, different sources are likely.

Finally, the <u>hysteresis measurements</u> performed in this study reinforce the results discussed above. The shapes of the loops in fields > 300 mT, i.e., whether they are open or closed, indicate the presence or absence of high coercivity minerals, respectively (fig. 3.8). The positions of samples on Day plots (Day et al., 1977) are shown to be difficult to interpret for multi-component samples. The

interpretation of samples influenced by high coercivity minerals are declared to be invalid because the materials do not reach saturation. However, the hysteresis loops of the magnetically extracted minerals are assigned to thermomagnetic group C, following the mixing trend of Roberts et al. (2011). Correct determination of the sizes of magnetic grains thus appears to be possible (inlet in fig. 3.8). In accordance with the FORC analyses, the samples obtained from the VFm and LFm are dominated by SD greigite.

All of the analyses employed in this study indicate a division of the Viernheim core and core P36 into two parts with distinct

magnetomineralogical behaviour. These findings can be explained as a result of changes in provenance, as shown by heavy mineral analyses (Hagedorn, 2004, Hagedorn and Boenigk, 2008), or they may be caused by variations in the degree of diagenetic overprinting of the individual units. In this context, it is important to note that changes in the rock magnetic proxies occur at the top of the IFm and thus before the extension of the drainage area of the Rhine is recognised in the sedimentary material. Therefore, the change in rock magnetic proxies is interpreted to be mainly driven by the effects of climate on diagenesis.

1.7.3. Climatic and environmental implications of the rock magnetic results

When combined with the geological information provided by other studies of the Heidelberg Basin, the results of the magnetic mineral characterisation (cf. section 1.4.1.) indicate the following evolution of the climate and the environment.

During the Pliocene, the depositional conditions of the Heidelberg Basin were dominated by meandering stream channels accompanied by anastomosing sub-environments and interconnected lakes (Przyrowski and Schäfer, 2015). During the deposition of thick pelitic overbank deposits, warm climatic conditions prevailed, as indicated by the formation of authigenic haematite. However, the occurrence of pseudomorphs of haematite after pyrite and the pitted surfaces of specularite point towards alternating reducing and oxidizing conditions. This suggestion is reinforced by the widespread occurrence of mottling in varying degrees; mottling indicates the influence of groundwater (Kraus and Aslan, 1993, Kraus, 2002). Our rock magnetic findings are also interpreted as indicating redox cycles. Under these conditions, sulphides form at the expense of magnetite during reducing conditions. Subsequently, the sulphides break down when oxic conditions dominate. Through the repetition of these processes, most of the ferrimagnetic minerals are transformed into poorly crystalline Fe(III) phases (Byrne et al., 2015, Ginn et al., 2017). The presence of these phases are recognised in the IFm as high Fe_2O_3 values in the WD-XRF analyses. The rises and falls of the groundwater table may have been induced by supra-seasonal cycles. The bulk sample parameters indicate that a rapid transition

towards the conditions that prevailed during the Pleistocene occurred during the deposition of the very top of the IFm. These portion of the succession was most likely not strongly influenced by redox cycles, which hints at a stabilisation of the groundwater level.

The Heidelberg core, however, reveals a different environmental history, given the preservation of sulphide minerals and the occurrence of relatively little mottling within the IFm. Here, fluctuations of the groundwater table had a smaller effect. The cause is presumed to be related to the Neckar alluvial fan and the subsidence pattern of the basin, but cannot be characterised in greater detail here.

The Pleistocene part of the Heidelberg Basin sedimentary succession was substantially influenced by stable reducing conditions, as indicated by the abundance of greigite and the rarity of mottling. Consequently, the groundwater table was not heavily affected by repeated rises and falls. Furthermore, the general lack of authigenic haematite indicates the prevalence of cooler conditions than in Pliocene times. The interbedded horizons with lower S-ratios may have developed due to changes in climatic conditions. This hypothesis requires confirmation by further data, such as that provided by palynological analyses. The high proportion of haematite in the Pleistocene part of the Heidelberg core is related to the denudation of the Triassic hinterland, the products of which were transported into the study region and deposited in the Neckar River alluvial fan; thus, it has no climatic explanatory power.

Beyond its significance for the reconstruction of local and regional climatic and environmental conditions, the Heidelberg Basin sedimentary record can be placed within a larger context. The recorded palaeoclimatic evolution is consistent with the results of pollen analyses, MS measurements, $\delta^{18}O$ records and other proxies used in many studies performed at a variety of locations in the Northern Hemisphere; examples include loess deposits in China (Ding et al., 2005, Nie et al., 2014, Nie et al., 2016), lake deposits in Russia (Brigham-Grette et al., 2013, Nowaczyk et al., 2013), and marine sediments from the Pacific (Haug et al., 2005), and Atlantic (Lang et al., 2014, Lawrence et al., 2010 Oceans. Thus, the evidence from the Heidelberg Basin record fits harmoniously into the reconstructed pattern of the development of the climate of the Northern Hemisphere from a greenhouse state to an icehouse state. In particular, the onset of the iNHG has rarely been documented in terrestrial sediments in Europe; thus, the Heidelberg Basin record is of considerable scientific value. The recorded change in the hydrological regime likely indicates rapid changes in the environment at the end of the Pliocene within the catchment area farther south in Germany. It is tentatively presumed that this hydrological change was driven by the supply of greater amounts of water due to the initial glaciation of the Alps and an increase in the consistency of this water supply. This hypothesis is not contradicted

by the later connection of the Alpine Rhine with the Palaeo-Rhine (Preusser 2008), because Reiter et al. (2015) suggested that sediment delivery from the Alpine region occurred from 4.2 Ma onwards.

All things considered, the sedimentary archive of the Heidelberg Basin provides information on the local (i.e., Heidelberg Basin-specific) evolution of climate during the Pliocene and Pleistocene. This information also increases our understanding of climate changes within regional (northwestern Europe) and even hemispheric contexts. In the future, these results should be implemented in simulations of palaeoclimate evolution.

1.8. Conclusion

The Heidelberg Basin represents a rare opportunity to study the environmental and climatic changes that occurred in terrestrial northwestern Europe during the Pliocene and Pleistocene. A conclusive temporal framework for the complete succession is provided by magnetic polarity stratigraphy. Accordingly, the boundaries between youngest magnetic reversals are found to lie close to the lithostratigraphic boundaries. The Brunhes-Matuyama boundary is placed close to the contact between the LFm and the VFm; the GMB is situated at the very top of the IFm. The chronostratigraphic framework for the older parts are based on three assumptions that aim to average out short-term variations. Thus, the deepest parts of the Heidelberg and Viernheim cores are found to have ages of >4 Ma and >5 Ma, respectively. Due to drilling-induced overprinting, the lowermost part of core P36 cannot be correlated with the GPTS.

The data presented in this study provide evidence for a rapid change in climatic and environmental conditions at the end of the Pliocene. Considerable thicknesses of fine pelitic sediment accumulated during the Pliocene. These deposits are largely coloured by authigenic haematite. Hence, climatic conditions warmer and dryer than today affected the succession. The sediments contained in the Viernheim core and core P36 are characterised by varying degrees of mottling. This, as well as the habits and compositions of the magnetic minerals indicate fluctuations in the groundwater table. These fluctuations produced redox cycles, which led to the breakdown of ferrimagnetic minerals in favour of poorly crystalline Fe(III) phases. Consequently, the deposits are poor in magnetite and sulphides. Haematite, goethite, Fe-chromite, and haemo-ilmenite are the dominant magnetic minerals. The groundwater fluctuations are assumed to have occurred due to supra-seasonal (orbital or sub-orbital) cycles. The effects of these cycles seem to be superimposed in the Heidelberg core; the magnetic mineral inventory of the Pliocene strata indicates considerable amounts of greigite. Additionally, the occurrence of mottling is clearly reduced. Relatively stable reducing conditions are

thus inferred to have occurred. The reasons are open to speculation, but may be connected to the Neckar alluvial fan or high subsidence rates.

At the end of the Pliocene, the climatic conditions changed. The preservation of magnetite remainders and the persistence of greigite point towards the cessation of the redox cycles. Instead, persistently high levels of the groundwater table and generally stable reducing conditions are suggested to have occurred. The change in the mineral magnetic characteristics temporally precede the change in the sediment source, which occurred due to extension of the catchment area of the Rhine River, and is thus most likely to be a climatic signal. The variations in the rock magnetic parameters in the Pleistocene parts of the cores may represent interglacial periods. A more detailed investigation requires further information obtained via pollen analysis or other scientific approaches; these data are not yet available.

The environmental and climatic evolution suggested by the rock magnetic record of the Heidelberg Basin is consistent with scientific results derived from various studies carried out in the Northern Hemisphere. In particular, documentation of the iNHG in chronologically well-constrained records from the European mainland is exceptionally rare. Elucidation of the details of the evolution of climatic conditions in northwestern Europe during the Pliocene and Pleistocene is expected when the results of rock magnetic analyses are combined with those of additional studies, such as pollen analytical work or clay mineralogy.

This PhD work demonstrates that fluvial systems can be successfully analysed by the methods of magnetic polarity stratigraphy and environmental magnetism, despite the presence of hiatuses and the influence of reducing diagenesis. The strategy employed here may serve as a methodological template for comprehensive characterisations of multi-component fluvial systems.

1.9. Contributions and contributors to this PhD work

In total, this PhD work includes three studies that are based on an extensive collection of samples and data. Most of the samples from the Heidelberg and Viernheim cores were collected and prepared by the technical staff of the LIAG (Marianne Klick, Kathrin Worm, Lena Wallbrecht) before I began this PhD project. I collected the samples from core P36 with the help of Kathrin Worm and Lena Wallbrecht. Additional samples were taken from the Viernheim and Heidelberg cores by me. The preparation (sawing and labelling) of the samples from core P36 and the additional material sampled of the Viernheim and Heidelberg cores was mainly conducted by Lena Wallbrecht; I made minor contributions to this part of the work. Most of the magnetic extraction procedures (sample preparation, processing of the extracts, rinsing, and drying) were carried out by me with the help of

Lena Wallbrecht and a student assistant (Maria Schaarschmidt). The MS determinations, the NRM, ARM, IRM measurements, and the AF demagnetisation experiments were mainly performed by the technical staff of the LIAG (Marianne Klick, Lena Wallbrecht, Kathrin Worm) at the Grubenhagen laboratory before I joined the project. After I joined the project, I contributed to this work. However, Lena Wallbrecht and Kathrin Worm continued to produce data. Some of the measurements were additionally carried out by student interns at the laboratory. The procedures used to carry out the VSM measurements were defined by me. The sample material was processed by me with the help of Lena Wallbrecht. The experiments performed in other laboratories were largely carried out by me, including the thermal and alternating field demagnetisation experiments at the Niederlippach laboratory of the Ludwig-Maximilian University of Munich (Germany); the measurements performed using the VSM at the Institute of Geophysics, Academy of Sciences (Prague, Czech Republic); and the FORC measurements at the University of Bremen (Germany). Manuela Weiss, a technical staff member at the Niederlippach laboratory, completed one thermal demagnetisation experiment after my time in the laboratory was finished, and Dr. T. Frederichs performed FORC measurements of one sample. The SEM/EDX analyses were performed by Sabine Stäger, a technical staff member of the Federal Institute for Geosciences and Natural Resources (BGR) of Germany, under my direction. Several helpful discussions with Dr. Stefan Kaufhold (BGR) helped me to interpret these data. The sample preparation for the WD-XRF analyses and the relevant measurements were performed without my help by Frank Korde, a technical staff member at the BGR.

I bear full responsibility for the analyses and utilisation of the data, though my co-authors provided a conceptual background and discouraged erroneous interpretations in discussions. In the application of coercivity analysis and FORC analysis (second publication, chapter 3) I had to learn to use software developed by Dr. Ramon Egli (ZAMG, Vienna). During email correspondence regarding the configurations and settings used in this software, he provided important information on the interpretation of the data.

All three manuscripts were completely prepared by me as first author, including all figures and tables. The co-authors reviewed the manuscripts and made suggestions for improvement, and I then revised the manuscript. Finally, the language was checked by the professional service of American Journal Experts. In total, the following contributions to the work are estimated:

Sampling and sample preparation:

- Sampling: Technical staff members: 75 %; S. Scheidt: 25 %
- Sample preparation cubic specimens: Technical staff members: 95 %; S. Scheidt: 5 %
- Sample preparation cylindrical specimens: Technical staff members: 100 %

- Sample preparation VSM: S. Scheidt: 80 %; Technical staff members: 20 %
- Sample preparation magnetic extracts: S. Scheidt: 60 %; Student assistance: 20 %; Technical staff members: 20 %;
- Sample preparation FORC analysis: S. Scheidt: 100 %

Measurements:

- Measurement of NRM, ARM, IRM, and all types of MS measurements: Technical staff members: 80%; S. Scheidt: 15 %; student assistance: 5 %
- Processing of AF demagnetisation experiments: Technical staff members: 70 %; S. Scheidt: 25 %; student assistances: 5 %
- Processing of thermal demagnetisation experiments: S. Scheidt 100 %
- VSM Measurements (cycles from IRM, Hysteresis, thermomagnetic measurement): S. Scheidt 70 %, technical staff members: 30 %
- FORC measurements: S. Scheidt: 95 %; T. Frederichs: 5 %

Publication 1 (chapter 2):

- Data interpretation: S. Scheidt: 80 %; U. Hambach: 10 %; C. Rolf: 10 %
- Manuscript preparation: S. Scheidt: 100 %
- Figure and table preparation: S. Scheidt: 100 %
- Comments to improve the manuscript and the figures: U. Hambach: 60 %, C. Rolf: 40 %

Publication 2 (chapter 3):

- Data interpretation: S. Scheidt: 76 %; R. Egli: 16 %; C. Rolf 3 %, U. Hambach: 3 %; F. Frederichs: 2 %; S. Kaufhold: 1 %
- Manuscript preparation: S. Scheidt: 100 %
- Figure and table preparation: S. Scheidt: 100 %
- Comments to improve the manuscript and the figures: R. Egli: 55 %; U. Hambach 20 %; C. Rolf: 20 %; T. Frederichs: 5 %

Publication 3 (chapter 4):

- Data interpretation: S. Scheidt: 100 %
- Manuscript preparation: S. Scheidt: 100 %
- Figure and table preparation: S. Scheidt: 100 %
- Comments to improve the manuscript and the figures: U. Hambach 70 %; C. Rolf: 30 %

1.10.   References

BAILEY, I., HOLE, G. M., FOSTER, G. L., WILSON, P. A., STOREY, C. D., TRUEMAN, C. N. & RAYMO, M. E. 2013. An alternative suggestion for the Pliocene onset of major northern hemisphere glaciation based on the geochemical provenance of North Atlantic Ocean ice-rafted debris. *Quaternary Science Reviews,* 75**,** 181-194.

BARTOLI, G., HÖNISCH, B. & ZEEBE, R. E. 2011. Atmospheric CO_2 decline during the Pliocene intensification of Northern Hemisphere glaciations. *Paleoceanography,* 26. PA4213, doi: 10.1029/2010PA002055

BARTOLI, G., SARNTHEIN, M., WEINELT, M., ERLENKEUSER, H., GARBE-SCHÖNBERG, D. & LEA, D. 2005. Final closure of Panama and the onset of northern hemisphere glaciation. *Earth and Planetary Science Letters,* 237**,** 33-44.

BARTZ, J. 1953. Revision des Bohr-Profils der Heidelberger Radium-Sol-Therme. *Jahresberichte und Mitteilungen des Oberrheinischen Geologischen Vereins***,** 101-125.

BARTZ, J. 1974. Die Mächtigkeit des Quartärs im Oberrheingraben. *In:* ILLIES, J. H. & FUCHS, K. (eds.) *Approaches to Taphrogenesis.* Stuttgart: Schweizerbart.

BERGER, A. 1988. Milankovitch theory and climate. *Reviews of Geophysics,* 26**,** 624–657.

BISWAS, D. K., HYODO, M., TANIGUCHI, Y., KANEKO, M., KATOH, S., SATO, H., KINUGASA, Y. & MIZUNO, K. 1999. Magnetostratigraphy of Plio-Pleistocene sediments in a 1700-m core from Osaka Bay, southwestern Japan and short geomagnetic events in the middle Matuyama and early Brunhes chrons. *Palaeogeography, Palaeoclimatology, Palaeoecology,* 148**,** 233-248.

BLOEMENDAL, J., KING, J., HALL, F. & DOH, S. J. 1992. Rock magnetism of Late Neogene and Pleistocene deep-sea sediments: Relationship to sediment source, diagenetic processes, and sediment lithology. *Journal of Geophysical Research: Solid Earth (1978–2012),* 97**,** 4361-4375.

BLUM, M. D. & TÖRNQVIST, T. E. 2000. Fluvial responses to climate and sea-level change: a review and look forward. *Sedimentology,* 47**,** 2-48.

BOWEN, D., RICHMOND, G., FULLERTON, D., ŠIBRAVA, V., FULTON, R. & VELICHKO, A. 1986. Correlation of Quaternary glaciations in the Northern Hemisphere. *Quaternary Science Reviews,* 5**,** 509-510.

BRIDGLAND, D. & WESTAWAY, R. 2008a. Climatically controlled river terrace staircases: a worldwide Quaternary phenomenon. *Geomorphology,* 98**,** 285-315.

BRIDGLAND, D. R. & WESTAWAY, R. 2008b. Preservation patterns of Late Cenozoic fluvial deposits and their implications: results from IGCP 449. *Quaternary International,* 189**,** 5-38.

BRIGHAM-GRETTE, J., MELLES, M., MINYUK, P., ANDREEV, A., TARASOV, P., DECONTO, R., KOENIG, S., NOWACZYK, N., WENNRICH, V. & ROSÉN, P. 2013. Pliocene warmth, polar amplification, and stepped Pleistocene cooling recorded in NE Arctic Russia. *Science,* 340**,** 1421-1427.

BRUNNACKER, K. 1986. Quaternary stratigraphy in the lower Rhine area and northern Alpine foothills. *Quaternary science reviews,* 5**,** 381-386.

BRUNNACKER, K., LÖSCHER, M., TILLMANNS, W. & URBAN, B. 1982. Correlation of the Quaternary terrace sequence in the lower Rhine valley and northern Alpine foothills of central Europe. *Quaternary Research,* 18**,** 152-173.

BUNESS, H., GABRIEL, G. & ELLWANGER, D. 2008. The Heidelberg Basin drilling project: Geophysical pre-site surveys. *E & G (Quaternary Science Journal),* 57**,** 338-366.

BUTLER, R. F. & OPDYKE, N. D. 1979. Magnetic polarity stratigraphy. *Reviews of Geophysics,* 17**,** 235-244.

BYRNE, J. M., KLUEGLEIN, N., PEARCE, C., ROSSO, K. M., APPEL, E. & KAPPLER, A. 2015. Redox cycling of Fe (II) and Fe (III) in magnetite by Fe-metabolizing bacteria. *Science,* 347**,** 1473-1476.

CANDE, S. C. & KENT, D. V. 1995. Revised calibration of the geomagnetic polarity timescale for the Late Cretaceous and Cenozoic. *Journal of Geophysical Research: Solid Earth,* 100**,** 6093-6095.

CEPEK, A. 1986. Quaternary stratigraphy of the German Democratic Republic. *Quaternary science reviews,* 5**,** 359-364.

CHADIMA, M. & HROUDA, F. 2006. Remasoft 3.0 a user-friendly paleomagnetic data browser and analyzer. *Travaux Géophysiques,* 27**,** 20-21.

CHAN, L. S. & ALVAREZ, W. 1983. Magnetic polarity stratigraphy. *Reviews of Geophysics,* 21**,** 620-626.

CLARK, P. U., ARCHER, D., POLLARD, D., BLUM, J. D., RIAL, J. A., BROVKIN, V., MIX, A. C., PISIAS, N. G. & ROY, M. 2006. The middle Pleistocene transition: characteristics, mechanisms, and implications for long-term changes in atmospheric pCO_2. *Quaternary Science Reviews,* 25**,** 3150-3184.

CONRADS, H. & SCHNEIDER, E. 1977. Hydrogeologische und brunnentechnische Probleme bei der Wassererschließung aus dem tiefen Pleistozän des Oberrheingrabens für die Stadtwerke Heidelberg AG. *Brunnenbau, Bau von Wasserwerken, Rohrleitungsbau,* 1**,** 5-10.

COX, A., DOELL, R. R. & DALRYMPLE, G. B. 1963. Geomagnetic Polarity Epochs and Pleistocene Geochronometry. *Nature*, 198, 1049-1051.

COX, A., DOELL, R. R. & DALRYMPLE, G. B. 1964. Reversals of the earth's magnetic field. *Science,* 144**,** 1537-1543.

DAY, R., FULLER, M. & SCHMIDT, V. A. 1977. Hysteresis properties of titanomagnetites; grain-size and compositional dependence. *Physics of The Earth and Planetary Interiors,* 13**,** 260-267.

DE SCHEPPER, S., GIBBARD, P. L., SALZMANN, U. & EHLERS, J. 2014. A global synthesis of the marine and terrestrial evidence for glaciation during the Pliocene Epoch. *Earth-Science Reviews,* 135**,** 83-102.

DEARING, J., BIRD, P., DANN, R. & BENJAMIN, S. 1997. Secondary ferrimagnetic minerals in Welsh soils: a comparison of mineral magnetic detection methods and implications for mineral formation. *Geophysical Journal International,* 130**,** 727-736.

DESENFANT, F., PETROVSKÝ, E. & ROCHETTE, P. 2004. Magnetic signature of industrial pollution of stream sediments and correlation with heavy metals: case study from South France. *Water, Air, & Soil Pollution,* 152**,** 297-312.

DING, Z., DERBYSHIRE, E., YANG, S., SUN, J. & LIU, T. 2005. Stepwise expansion of desert environment across northern China in the past 3.5 Ma and implications for monsoon evolution. *Earth and Planetary Science Letters,* 237**,** 45-55.

DOWSETT, H. J. & POORE, R. Z. 1990. A new planktic foraminifer transfer function for estimating Pliocene-Holocene paleoceanographic conditions in the North Atlantic. *Marine Micropaleontology,* 16**,** 1-23.

DOWSETT, H. J. & POORE, R. Z. 1991. Pliocene sea surface temperatures of the north atlantic ocean at 3.0 Ma. *Quaternary Science Reviews,* 10**,** 189-204.

DUNLOP, D. J. & ÖZDEMIR, Ö. 2001. *Rock magnetism: fundamentals and frontiers*, Cambridge university press.

EGLI, R. 2003. Analysis of the field dependence of remanent magnetization curves. *Journal of Geophysical Research: Solid Earth,* 108, 2081, doi:10.1029/2002JB002023, B2.

EGLI, R. 2004a. Characterization of individual rock magnetic components by analysis of remanence curves. 1. Unmixing natural sediments. *Studia Geophysica et Geodaetica,* 48**,** 391-446.

EGLI, R. 2004b. Characterization of individual rock magnetic components by analysis of remanence curves. 2. Fundamental properties of coercivity distributions. *Physics and Chemistry of the Earth, Parts A/B/C,* 29**,** 851-867.

EGLI, R. 2013. VARIFORC: An optimized protocol for calculating non-regular first-order reversal curve (FORC) diagrams. *Global and Planetary Change,* 110**,** 302-320.

EGLI, R., CHEN, A. P., WINKLHOFER, M., KODAMA, K. P. & HORNG, C. S. 2010. Detection of noninteracting single domain particles using first-order reversal curve diagrams. *Geochemistry, Geophysics, Geosystems,* 11, Q01Z11, doi: 10.1029/2009GC002916.

EHLERS, J. 2011. *Das Eiszeitalter,* Heidelberg, Spektrum Akademischer Verlag.

EISMANN, L. 2002. Quaternary geology of eastern Germany (Saxony, Saxon-Anhalt, South Brandenburg, Thuringia), type area of the Elsterian and Saalian stages in Europe. *Quaternary Science Reviews,* 21**,** 1275-1346.

ELLWANGER, D., GABRIEL, G., HOSELMANN, C., LÄMMERMANN-BARTHEL, J. & WEIDENFELLER, M. 2005. The Heidelberg drilling project (Upper Rhine Graben, Germany). *Quaternaire. Revue de l'Association française pour l'étude du Quaternaire,* 16**,** 191-199.

ELLWANGER, D., GABRIEL, G., HOSELMANN, C., WEIDENFELLER, M. & WIELANDT-SCHUSTER, U. 2010a. Mannheim-Formation. *Litholex (online database).* 03.11.2010 ed.

http://www.bgr.bund.de/litholex: Federal Institute for Geosciences and Natural Resources (BGR).

ELLWANGER, D., GABRIEL, G., SIMON, T., WIELANDT-SCHUSTER, U., GREILING, R. O., HAGEDORN, E.-M., HAHNE, J. & HEINZ, J. 2008. Long sequence of Quaternary Rocks in the Heidelberg Basin Depocentre. *E & G (Quaternary Science Journal),* 57**,** 316-337.

ELLWANGER, D., GRIMM, M., HOSELMANN, C., HOTTENROTT, M., WEIDENFELLER, M. & WIELANDT-SCHUSTER, U. 2010b. Iffezheim-Formation. *Litholex (online database).* 03.11.2010 ed. http://www.bgr.bund.de/litholex: Federal Institute for Geosciences and Natural Resources (BGR).

EVANS, M. E. & HELLER, F. 2003. *Environmental Magnetism - Principles and Applications of Enviromagnetics,* San Diego, Academic Press.

FEDOROV, A., DEKENS, P., MCCARTHY, M., RAVELO, A., BARREIRO, M., PACANOWSKI, R. & PHILANDER, S. 2006. The Pliocene paradox (mechanisms for a permanent El Niño). *Science,* 312**,** 1485-1489.

FEZER, F. 1997. 220 m Altpleistozän im Heidelberger Loch. *E & G (Quaternary Science Journal),* 47**,** 145-153.

FOREMAN, B. Z., HELLER, P. L. & CLEMENTZ, M. T. 2012. Fluvial response to abrupt global warming at the Palaeocene/Eocene boundary. *Nature,* 491**,** 92.

GABRIEL, G., ELLWANGER, D., HOSELMANN, C. & WEIDENFELLER, M. 2008. Preface: The Heidelberg Basin Drilling Project. *E & G (Quaternary Science Journal),* 57**,** 253-260.

GABRIEL, G., ELLWANGER, D., HOSELMANN, C., WEIDENFELLER, M. & WIELANDT-SCHUSTER, U. 2013. The Heidelberg Basin, Upper Rhine Graben (Germany): a unique archive of Quaternary sediments in Central Europe. *Quaternary International,* 292**,** 43-58.

GINN, B., MEILE, C., WILMOTH, J., TANG, Y. & THOMPSON, A. 2017. Rapid Iron Reduction Rates Are Stimulated by High-Amplitude Redox Fluctuations in a Tropical Forest Soil. *Environmental Science & Technology,* 51**,** 3250-3259.

GRUBE, F., CHRISTENSEN, S., VOLLMER, T., DUPHORN, K., KLOSTERMANN, J. & MENKE, B. 1986. Glaciations in north west Germany. *Quatery science reviews,* 5**,** 347-358.

HAGEDORN, E.-M. 2004. *Sedimentpetrographie und Lithofazies der Jungtertiären und Quartären Sedimente im Oberrheingebiet.* Dissertation, Universität zu Köln.

HAGEDORN, E.-M. & BOENIGK, W. 2008. The Pliocene and Quaternary sedimentary and fluvial history in the Upper Rhine Graben based on heavy mineral analyses. *Netherlands Journal of Geosciences,* 87**,** 19-30.

HAHNE, J., ELLWANGER, D., FRANZ, M., STRITZKE, R. & WIELAND-SCHUSTER, U. 2012. Pollenanalytische Untersuchungsergebnisse aus dem baden-württembergischen Rheinsystem Oberrheingraben, Hochrhein, Oberschwaben - eine Zusammenfassung des aktuellen Kenntnisstandes. *LGRB-Informationen,* 26**,** 121-162.

HAHNE, J., ELLWANGER, D. & STRITZKE, R. 2008. Evidence for a Waalian thermomer pollen record from the research borehole Heidelberg UniNord, Upper Rhine Graben, Baden-Württemberg. *E & G (Quaternary Science Journal),* 57**,** 403-410.

HAN, J., FYFE, W. S., LONGSTAFFE, F. J., PALMER, H. C., YAN, F. H. & MAI, X. S. 1997. Pliocene-Pleistocene climatic change recorded in fluviolacustrine sediments in central China. *Palaeogeography, Palaeoclimatology, Palaeoecology,* 135**,** 27-39.

HAUG, G. H., GANOPOLSKI, A., SIGMAN, D. M., ROSELL-MELE, A., SWANN, G. E., TIEDEMANN, R., JACCARD, S. L., BOLLMANN, J., MASLIN, M. A. & LENG, M. J. 2005. North Pacific seasonality and the glaciation of North America 2.7 million years ago. *Nature,* 433**,** 821-825.

HAUG, G. H. & TIEDEMANN, R. 1998. Effect of the formation of the Isthmus of Panama on Atlantic Ocean thermohaline circulation. *Nature,* 393**,** 673-676.

HAYWOOD, A., SELLWOOD, B. & VALDES, P. 2000. Regional warming: Pliocene (3 Ma) paleoclimate of Europe and the Mediterranean. *Geology,* 28**,** 1063-1066.

HENNISSEN, J. A. I., HEAD, M. J., DE SCHEPPER, S. & GROENEVELD, J. 2015. Increased seasonality during the intensification of Northern Hemisphere glaciation at the Pliocene–Pleistocene boundary ~2.6 Ma. *Quaternary Science Reviews,* 129**,** 321-332.

HESLOP, D., ROBERTS, A. P. & CHANG, L. 2014. Characterizing magnetofossils from first-order reversal curve (FORC) central ridge signatures. *Geochemistry, Geophysics, Geosystems,* 15**,** 2170-2179.

HEUMANN, G. & LITT, T. 2002. Stratigraphy and paleoecology of the Late Pliocene and Early Pleistocene in the open-cast mine Hambach (Lower Rhine Basin). *Netherlands Journal of Geosciences,* 81**,** 193-199.

HOSELMANN, C. 2008. The Pliocene and Pleistocene fluvial evolution in the northern Upper Rhine Graben based on results of the research borehole at Viernheim (Hessen, Germany). *E & G (Quaternary Science Journal),* 57**,** 286-315.

HOSELMANN, C., ELLWANGER, D., GABRIEL, G., WEIDENFELLER, M. & WIELANDT-SCHUSTER, U. 2010. Viernheim-Formation. *Litholex (online database).* 03-11-2010 ed. http://www.bgr.bund.de/litholex: Federal Institute for Geosciences and Natural Resources (BGR).

HUNZE, S. & WONIK, T. 2008. Sediment Input into the Heidelberg Basin as determined from Downhole Logs. *E & G (Quaternary Science Journal),* 57**,** 367-381.

JOHNSON, G. D., OPDYKE, N. D., TANDON, S. & NANDA, A. 1983. The magnetic polarity stratigraphy of the Siwalik Group at Haritalyangar (India) and a new last appearance datum for Ramapithecus and Sivapithecus in Asia. *Palaeogeography, Palaeoclimatology, Palaeoecology,* 44**,** 223-249.

JOHNSON, N. M., JORDAN, T. E., JOHNSSON, P. A. & NAESER, C. W. 2009. Magnetic Polarity Stratigraphy, Age and Tectonic Setting of Fluvial Sediments in an Eastern Andean Foreland Basin, San Juan Province, Argentina. *In:* ALLEN, P. A. & HOMEWOOD, P. (eds.) *Foreland Basins.* Blackwell Publishing Ltd., doi: 10.1002/9781444303810.ch3.

JOHNSON, N. M., OPDYKE, N. D., JOHNSON, G. D., LINDSAY, E. H. & TAHIRKHELI, R. 1982. Magnetic polarity stratigraphy and ages of Siwalik Group rocks of the Potwar Plateau, Pakistan. *Palaeogeography, Palaeoclimatology, Palaeoecology,* 37**,** 17-42.

JORDANOVA, D., HOFFMANN, V. & FEHR, K. T. 2004. Mineral magnetic characterization of anthropogenic magnetic phases in the Danube river sediments (Bulgarian part). *Earth and Planetary Science Letters,* 221**,** 71-89.

KAYVANTASH, D., COJAN, I., KISSEL, C. & FRANKE, C. 2017. Magnetic fingerprint of the sediment load in a meander bend section of the Seine River (France). *Geomorphology,* 286**,** 14-26.

KING, J., BANERJEE, S. K., MARVIN, J. & OZDEMIR, O. 1982. A comparison of different magnetic methods for determining the relative grain size of magnetite in natural materials; some results from lake sediments. *Earth and Planetary Science Letters,* 59**,** 404-419.

KIRSCHVINK, J. 1980. The least-squares line and plane and the analysis of palaeomagnetic data. *Geophysical Journal International,* 62**,** 699-718.

KNIES, J., MATTINGSDAL, R., FABIAN, K., GRØSFJELD, K., BARANWAL, S., HUSUM, K., DE SCHEPPER, S., VOGT, C., ANDERSEN, N. & MATTHIESSEN, J. 2014. Effect of early Pliocene uplift on late Pliocene cooling in the Arctic–Atlantic gateway. *Earth and Planetary Science Letters,* 387**,** 132-144.

KNIPPING, M. 2008. Early and Middle Pleistocene pollen asssemblages of deep core drillings in the northern Upper Rhine Graben, Germany. *Netherlands Journal of Geosciences,* 87**,** 51-65.

KRAUS, M. J. 2002. Basin-scale changes in floodplain paleosols: implications for interpreting alluvial architecture. *Journal of Sedimentary Research,* 72**,** 500-509.

KRAUS, M. J. & ASLAN, A. 1993. Eocene hydromorphic paleosols: significance for interpreting ancient floodplain processes. *Journal of Sedimentary Research*, 63, 453-463.

KRUIVER, P. P., DEKKERS, M. J. & HESLOP, D. 2001. Quantification of magnetic coercivity components by the analysis of acquisition curves of isothermal remanent magnetisation. *Earth and Planetary Science Letters,* 189**,** 269-276.

LANG, D. C., BAILEY, I., WILSON, P. A., BEER, C. J., BOLTON, C. T., FRIEDRICH, O., NEWSAM, C., SPENCER, M. R., GUTJAHR, M., FOSTER, G. L., COOPER, M. J. & MILTON, J. A. 2014. The transition on North America from the warm humid Pliocene to the glaciated Quaternary traced by eolian dust deposition at a benchmark North Atlantic Ocean drill site. *Quaternary Science Reviews,* 93**,** 125-141.

LAUER, T., FRECHEN, M., HOSELMANN, C. & TSUKAMOTO, S. 2010. Fluvial aggradation phases in the Upper Rhine Graben—new insights by quartz OSL dating. *Proceedings of the Geologists' Association,* 121**,** 154-161.

LAUER, T., KRBETSCHEK, M., FRECHEN, M., TSUKAMOTO, S., HOSELMANN, C. & WEIDENFELLER, M. 2011. Infrared radiofluorescence (IR-RF) dating of middle pleistocene fluvial archives of the Heidelberg Basin (Southwest Germany). *Geochronologia,* 38**,** 23-33.

LAWRENCE, K., SOSDIAN, S., WHITE, H. & ROSENTHAL, Y. 2010. North Atlantic climate evolution through the Plio-Pleistocene climate transitions. *Earth and Planetary Science Letters,* 300**,** 329-342.

LI, Y., TSUKAMOTO, S., FRECHEN, M. & GABRIEL, G. 2017. Timing of fluvial sedimentation in the Upper Rhine Graben since the Middle Pleistocene: constraints from quartz and feldspar luminescence dating. *Boreas,* 47, 256-270.

LISIECKI, L. E. & RAYMO, M. E. 2005. A Pliocene-Pleistocene stack of 57 globally distributed benthic $\delta^{18}O$ records. *Paleoceanography,* 20. PA1003. doi:10.1029/2004PA001071

LISIECKI, L. E. & RAYMO, M. E. 2007. Plio–Pleistocene climate evolution: trends and transitions in glacial cycle dynamics. *Quaternary Science Reviews,* 26**,** 56-69.

LOWRIE, W. 1990. Identification of ferromagnetic minerals in a rock by coercivity and unblocking temperature properties. *Geophysical Research Letters,* 17**,** 159-162.

LUDWIG, P., EGLI, R., BISHOP, S., CHERNENKO, V., FREDERICHS, T., RUGEL, G., MERCHEL, S. & ORGEIRA, M. 2013. Characterization of primary and secondary magnetite in marine sediment by combining chemical and magnetic unmixing techniques. *Global and Planetary Change,* 110**,** 321-339.

LUNT, D. J., FOSTER, G. L., HAYWOOD, A. M. & STONE, E. J. 2008. Late Pliocene Greenland glaciation controlled by a decline in atmospheric CO_2 levels. *Nature,* 454**,** 1102-1105.

MAHER, B. A. 1988. Magnetic properties of some synthetic sub-micron magnetites. *Geophysical Journal,* 94**,** 83-96.

MAHER, B. A. & THOMPSON, R. 1999. *Quaternary climates, environments and magnetism,* Cambridge, University Press.

MARLOW, J. R., LANGE, C. B., WEFER, G. & ROSELL-MELÉ, A. 2000. Upwelling intensification as part of the Pliocene-Pleistocene climate transition. *Science,* 290**,** 2288-2291.

MILANKOVITCH, M. 1930. Mathematische Klimalehre und astronomische Theorie der Klimaschwankungen. *Handbuch der Klimatologie,* 1.

MOSBRUGGER, V., UTESCHER, T. & DILCHER, D. L. 2005. Cenozoic continental climatic evolution of Central Europe. *Proceedings of the National Academy of Sciences of the United States of America,* 102**,** 14964-14969.

MUDELSEE, M. & STATTEGGER, K. 1997. Exploring the structure of the mid-Pleistocene revolution with advanced methods of time-series analysis. *International Journal of Earth Sciences: Geologische Rundschau,* 86**,** 499.

NEWELL, A. J. 2005. A high-precision model of first-order reversal curve (FORC) functions for single-domain ferromagnets with uniaxial anisotropy. *Geochemistry, Geophysics, Geosystems,* 6, Q05010, doi: 10.1029/2004GC000877.

NIE, J., SONG, Y. & KING, J. W. 2016. A review of recent advances in red-clay environmental magnetism and paleoclimate history on the Chinese Loess Plateau. *Frontiers in Earth Science,* 4**,** 27. doi: 10.3389/feart.2016.00027

NIE, J., ZHANG, R., NECULA, C., HESLOP, D., LIU, Q., GONG, L. & BANERJEE, S. 2014. Late Miocene–early Pleistocene paleoclimate history of the Chinese Loess Plateau revealed by remanence unmixing. *Geophysical Research Letters,* 41**,** 2163-2168.

NOWACZYK, N. R., HALTIA, E. M., ULBRICHT, D., WENNRICH, V., SAUERBREY, M. A., ROSÉN, P., VOGEL, H., FRANCKE, A., MEYER-JACOB, C., ANDREEV, A. A. & LOZHKIN, A. V. 2013. Chronology of Lake El'gygytgyn sediments – a combined magnetostratigraphic, palaeoclimatic and orbital tuning study based on multi-parameter analyses. *Clim. Past,* 9**,** 2413-2432.

OGG, J. G., OGG, G. & GRADSTEIN, F. M. 2016. *A Concise Geologic Time Scale: 2016,* Elsevier.

OLDFIELD, F., RUMMERY, T., THOMPSON, R. & WALLING, D. E. 1979. Identification of suspended sediment sources by means of magnetic measurements: some preliminary results. *Water Resources Research,* 15**,** 211-218.

PAN, B., HU, Z., WANG, J., VANDENBERGHE, J. & HU, X. 2011. A magnetostratigraphic record of landscape development in the eastern Ordos Plateau, China: Transition from Late Miocene and Early Pliocene stacked sedimentation to Late Pliocene and Quaternary uplift and incision by the Yellow River. *Geomorphology,* 125**,** 225-238.

PETERSEN, N., VON DOBENECK, T. & VALI, H. 1986. Fossil bacterial magnetite in deep -sea sediments from the South Atlantic Ocean. *Nature,* 320**,** 611-615.

PIKE, C. R., ROBERTS, A. P. & VEROSUB, K. L. 1999. Characterizing interactions in fine magnetic particle systems using first order reversal curves. *Journal of Applied Physics,* 85**,** 6660-6667.

POORE, H., SAMWORTH, R., WHITE, N., JONES, S. & MCCAVE, I. 2006. Neogene overflow of Northern Component Water at the Greenland-Scotland Ridge. *Geochemistry, Geophysics, Geosystems,* 7, Q06010, doi: 10.1029/2005GC001085.

PREUSSER, F. 2008. Characterisation and evolution of the River Rhine system. *Netherlands Journal of Geosciences,* 87**,** 7-19.

PRZYROWSKI, R. & SCHÄFER, A. 2015. Quaternary fluvial basin of northern Upper Rhine Graben. *Zeitschrift der Deutschen Gesellschaft für Geowissenschaften,* 166**,** 71-98.

RAVELO, A., BILLUPS, K., DEKENS, P., HERBERT, T. & LAWRENCE, K. 2007. Onto the ice ages: proxy evidence for the onset of Northern Hemisphere glaciation. *Deep Time Perspectives on Climate Change. The Micropalaeontological Society***,** 563-574.

RAYMO, M. E. 1994. The Initiation of Northern Hemisphere Glaciation. *Annual Review of Earth and Planetary Sciences,* 22**,** 353-383.

RAYMO, M. E., HODELL, D. & JANSEN, E. 1992. Response of deep ocean circulation to initiation of Northern Hemisphere glaciation (3–2 Ma). *Paleoceanography,* 7(5), 645–672, doi: 10.1029/92PA01609.

RAYMO, M. E. & RUDDIMAN, W. F. 1992. Tectonic forcing of late Cenozoic climate. *Nature,* 359**,** 117-122.

REITER, W., ELFERT, S., GLOTZBACH, C., BERNET, M. & SPIEGEL, C. 2013. Relations between denudation, glaciation, and sediment deposition: implications from the Plio-Pleistocene Central Alps. *Basin Research,* 25**,** 659-674.

REITER, W., ELFERT, S., GLOTZBACH, C. & SPIEGEL, C. 2015. Plio-Pleistocene evolution of the north Alpine drainage system: new constraints from detrital thermochronology of foreland deposits. *International Journal of Earth Sciences,* 104**,** 891-907.

ROBERTS, A. P., FLORINDO, F., VILLA, G., CHANG, L., JOVANE, L., BOHATY, S. M., LARRASOAÑA, J. C., HESLOP, D. & GERALD, J. D. F. 2011. Magnetotactic bacterial abundance in pelagic marine environments is limited by organic carbon flux and availability of dissolved iron. *Earth and Planetary Science Letters,* 310**,** 441-452.

ROBERTS, A. P., PIKE, C. R. & VEROSUB, K. L. 2000. First-order reversal curve diagrams: A new tool for characterizing the magnetic properties of natural samples. *Journal of Geophysical Research: Solid Earth,* 105**,** 28461-28475.

ROBERTSON, D. & FRANCE, D. 1994. Discrimination of remanence-carrying minerals in mixtures, using isothermal remanent magnetisation acquisition curves. *Physics of The Earth and Planetary Interiors,* 82**,** 223-234.

RODRIGUES, T., ALONSO-GARCIA, M., HODELL, D., RUFINO, M., NAUGHTON, F., GRIMALT, J., VOELKER, A. & ABRANTES, F. 2017. A 1-Ma record of sea surface temperature and extreme cooling events in the North Atlantic: A perspective from the Iberian Margin. *Quaternary Science Reviews,* 172**,** 118-130.

ROLF, C., HAMBACH, U. & WEIDENFELLER, M. 2008. Rock and palaeomagnetic evidence for the Plio-Pleistocene palaeoclimatic change recorded in Upper Rhine Graben sediments (Core Ludwigshafen Parkinsel). *Netherlands Journal of Geosciences,* 87**,** 41-50.

RÖSLER, W., METZLER, W. & APPEL, E. 1997. Neogene magnetic polarity stratigraphy of some fluviatile Siwalik sections, Nepal. *Geophysical Journal International,* 130**,** 89-111.

ROUSSEAU, D.-D., TAOUFIQ, N. B., PETIT, C., FARJANEL, G., MÉON, H. & PUISSÉGUR, J.-J. 1992. Continental late Pliocene paleoclimatic history recorded in the Bresse Basin (France). *Palaeogeography, palaeoclimatology, palaeoecology,* 95**,** 253-261.

ROWAN, C. J. & ROBERTS, A. P. 2006. Magnetite dissolution, diachronous greigite formation, and secondary magnetizations from pyrite oxidation: Unravelling complex magnetizations in Neogene marine sediments from New Zealand. *Earth and Planetary Science Letters,* 241**,** 119-137.

RUDDIMAN, W. F. & KUTZBACH, J. E. 1989. Forcing of late Cenozoic northern hemisphere climate by plateau uplift in southern Asia and the American west. *Journal of Geophysical Research: Atmospheres,* 94**,** 18409-18427.

RZECHOWSKI, J. 1986. Pleistocene till stratigraphy in Poland. *Quaternary science reviews,* 5**,** 365-372.

SALCHER, B. C., FRANK-FELLNER, C., LOMAX, J., PREUSSER, F., OTTNER, F., SCHOLGER, R. & WAGREICH, M. 2017. Middle to Late Pleistocene multi-proxy record of environmental response to climate change from the Vienna Basin, Central Europe (Austria). *Quaternary Science Reviews,* 173**,** 193-210.

SALOMON, W. 1927. Die Erbohrung der Heidelberger Radium-Sol-Therme und ihre geologischen Verhältnisse. *Abhandlungen der Heidelberger Akademie der Wissenschaften,* 14**,** 1-105.

SCARDIA, G., MUTTONI, G. & SCIUNNACH, D. 2006. Subsurface magnetostratigraphy of Pleistocene sediments from the Po Plain (Italy): Constraints on rates of sedimentation and rock uplift. *Geological Society of America Bulletin,* 118**,** 1299-1312.

SCHEIDT, S., HAMBACH, U. & ROLF, C. 2015. A consistent magnetic polarity stratigraphy of late Neogene to Quaternary fluvial sediments from the Heidelberg Basin (Germany): A new time frame for the Plio–Pleistocene palaeoclimatic evolution of the Rhine Basin. *Global and Planetary Change,* 127**,** 103-116.

SCHEIDT, S., EGLI, R., FREDERICHS, T., HAMBACH, U., & ROLF, C. 2017. A mineral magnetic characterization of the Plio-Pleistocene fluvial infill of the Heidelberg Basin (Germany). Geophysical Journal International 210(2). 743-764.

SCHNEIDER, E. F. & SCHNEIDER, H. 1975. Synsedimentäre Bruchtektonik im Pleistozän des Oberrheintal-Grabens zwischen Speyer, Worms, Hardt und Odenwald. *Münstersche Forschungen zur Geologie und Paläontologie,* 36**,** 81-126.

SCHUMACHER, M. E. 2002. Upper Rhine Graben: role of preexisting structures during rift evolution. *Tectonics,* 21: 6-1–6-17.

SEIERSTAD, I. K., ABBOTT, P. M., BIGLER, M., BLUNIER, T., BOURNE, A. J., BROOK, E., BUCHARDT, S. L., BUIZERT, C., CLAUSEN, H. B. & COOK, E. 2014. Consistently dated records from the Greenland GRIP, GISP2 and NGRIP ice cores for the past 104 ka reveal regional millennial-scale $\delta^{18}O$ gradients with possible Heinrich event imprint. *Quaternary Science Reviews,* 106**,** 29-46.

ŠIBRAVA, V. 1986a. Correlation of European glaciations and their relation to the deep-sea record. *Quaternary Science Reviews,* 5**,** 433-441.

ŠIBRAVA, V. 1986b. Scandinavian glaciations in the Bohemian Massif and Carpathian Foredeep and their relationship to the extraglacial areas. *Quaternary science reviews,* 5**,** 373-379.

SIGMAN, D. M., JACCARD, S. L. & HAUG, G. H. 2004. Polar ocean stratification in a cold climate. *Nature,* 428**,** 59-63.

STACEY, F. 2012. *The physical principles of rock magnetism*, Elsevier.

SUC, J. P., BERTINI, A., LEROY, S. A. G. & SUBALLYOVA, D. 1997. Towards a lowering of the Pliocene/Pleistocene boundary to the Gauss/Matuyama Reversal. *In:* PARTRIDGE, T. C. (ed.) *The Plio-Pleistocene boundary.* Quaternary International.

TATZEL, M., DUNKL, I. & EYNATTEN, H. 2017., U/Pb dating and heavy mineral assemblages. *Basin Research ,* 29(S1), 396-417.

TEODORIDIS, V., BRUCH, A. A., VASSIO, E., MARTINETTO, E., KVAČEK, Z. & STUCHLIK, L. 2017. Plio-Pleistocene floras of the Vildštejn Formation in the Cheb Basin, Czech Republic—A floristic and palaeoenvironmental review. *Palaeogeography, Palaeoclimatology, Palaeoecology,* 467**,** 166-190.

THOMPSON, R. & OLDFIELD, F. 1986. *Environmental magnetism,* London, Allen and Unwin.

TIEDEMANN, R., SARNTHEIN, M. & SHACKLETON, N. J. 1994. Astronomic timescale for the Pliocene Atlantic δ^{18}O and dust flux records of Ocean Drilling Program Site 659. *Paleoceanography,* 9(4), 619–638, doi: 10.1029/94PA00208.

TUCKER, G. E. & SLINGERLAND, R. 1997. Drainage basin responses to climate change. *Water Resources Research,* 33**,** 2031-2047.

UTESCHER, T., ASHRAF, A. R., DREIST, A., DYBKJAER, K., MOSBRUGGER, V., PROSS, J. & WILDE, V. 2012. Variability of neogene continental climates in Northwest Europe-a detailed study based on microfloras. *Turkish Journal of Earth Sciences,* 21**,** 289-314.

UTESCHER, T., DREIST, A., HENROT, A.-J., HICKLER, T., LIU, Y.-S. C., MOSBRUGGER, V., PORTMANN, F. T. & SALZMANN, U. 2017. Continental climate gradients in North America and Western Eurasia before and after the closure of the Central American Seaway. *Earth and Planetary Science Letters,* 472**,** 120-130.

UTESCHER, T., MOSBRUGGER, V. & ASHRAF, A. R. 2000. Terrestrial climate evolution in northwest Germany over the last 25 million years. *Palaios,* 15**,** 430-449.

VAN DAM, J. A. 2006. Geographic and temporal patterns in the late Neogene (12–3 Ma) aridification of Europe: the use of small mammals as paleoprecipitation proxies. *Palaeogeography, Palaeoclimatology, Palaeoecology,* 238**,** 190-218.

VON DOBENECK, T., PETERSEN, N. & VALI, H. 1987. Bakterielle Magnetofossilien. *Geowissenschaften in Unserer Zeit,* 5**,** 27–35.

WALLING, D. & WOODWARD, J. 1995. Tracing sources of suspended sediment in river basins: a case study of the River Culm, Devon, UK. *Marine and Freshwater Research,* 46**,** 327-336.

WEDEL, J. 2008. Pleistocene molluscs from research boreholes in the Heidelberg Basin. *E & G (Quaternary Science Journal),* 57**,** 382-402.

WEIDENFELLER, M., ELLWANGER, D., GABRIEL, G., HOSELMANN, C. & WIELANDT-SCHUSTER, U. 2010. Ludwigshafen-Formation. *Litholex (online database).* 02.11.2010 ed. http://www.bgr.bund.de/litholex: Federal Institute for Geosciences and Natural Resources (BGR).

WEIDENFELLER, M. & KNIPPING, M. 2008. Correlation of Pleistocene sediments from boreholes in the Ludwigshafen area, western Heidelberg Basin. *E & G (Quaternary Science Journal),* 57**,** 270-285.

WESTAWAY, R. & BRIDGLAND, D. R. 2014. Relation between alternations of uplift and subsidence revealed by Late Cenozoic fluvial sequences and physical properties of the continental crust. *Boreas,* 43**,** 505-527.

ZAGWIJN, W. H. 1985. An outline of the Quaternary stratigraphy of the Netherlands. *Geologie en Mijnbouw,* 64**,** 17-24.

ZAGWIJN, W. H. 1992. The beginning of the Ice Age in Europe and its major subdivisions. *Quaternary Science Reviews,* 11**,** 583-591.

ZHANG, C., QIAO, Q., PIPER, J. D. & HUANG, B. 2011. Assessment of heavy metal pollution from a Fe-smelting plant in urban river sediments using environmental magnetic and geochemical methods. *Environmental Pollution,* 159**,** 3057-3070.

ZIJDERVELD, J. D. A. 1967. AC demagnetization of rocks: analysis of results. *Methods in paleomagnetism,* 3**,** 254.

2. Study 1: A consistent magnetic polarity stratigraphy of late Neogene to Quaternary fluvial sediments from the Heidelberg Basin (Germany): A new time frame for the Plio-Pleistocene palaeoclimatic evolution of the Rhine Basin

Stephanie Scheidt[1,2], Ulrich Hambach[2, 3], Christian Rolf[1]

[1]Leibniz Institute of Applied Geophysics, Stilleweg 2, D-30655 Hannover

[2]Chair of Geomorphology, University of Bayreuth, D-95440 Bayreuth

[3]BayCEER, University of Bayreuth, D-95440 Bayreuth

Corresponding author: Stephanie Scheidt

Abstract

This work presents the results of a magnetostratigraphic survey performed on 1,150 m of core material from three sites within the Heidelberg Basin. The cores intersect one of the thickest continuous accumulations of Plio-Pleistocene fluvial sediments in western Central Europe. The resultant magnetic polarity stratigraphy includes every Quaternary polarity chron, thereby providing constant age constraint down to the Gauss-Matuyama Boundary (2.58 Ma). Older deposits cannot be unequivocally dated; instead, various age-depth models are discussed. We base our chronostratigraphic interpretation of the successions tentatively on three assumptions. A) The accommodation was almost constant over time. B) Hiatuses in the duration of subchrons (on the order of 0.2 Myr) may occur, and the actual step-like age-depth relationship is best depicted as a smooth curve with almost constant slope. C) Long chrons and subchrons have a higher preservation potential than shorter polarity intervals.

The stratigraphic scenarios with the highest probability - based upon our three assumptions - lead to minimum ages of >5.235 Ma and >4.187 Ma for the oldest parts of the Viernheim and Heidelberg cores, respectively. Consequently, this study provides the first consistent magnetic polarity stratigraphy for quasi-continuous sequences of late Neogene to Quaternary fluvial sediments in the Rhine Basin and generally in western central Europe. This methodologically independent chronostratigraphy supplies an urgently required temporal model for on-going tectonic and sedimentological studies and the reconstruction of the palaeoclimate since the Pliocene in this part of Europe.

2.1. Introduction

The precise ages of a significant number of Plio-Pleistocene continental deposits are still unknown. Changes in magnetic polarity recorded in thick sedimentary sequences provide a solid temporal framework for chronostratigraphic analysis (Cox et al., 1963; Cox et al., 1964; Cande and Kent, 1995; Opdyke and Channell, 1996). In contrast to other dating techniques (e.g., luminescence and cosmogenic nuclides), magnetic polarity stratigraphy encompasses diverse time scales, including the complete Quaternary. Thus, this technique enables the correlation of coeval different rocks and environments.

The first palaeomagnetically derived age constraints for Plio-Pleistocene sedimentary successions from continental Europe became available through the work of Van Montfrans (1971). He studied sedimentary successions in the North Sea Basin and correlated a number of stratigraphic levels with the geomagnetic polarity time scale (GPTS). In the following years, magnetic polarity stratigraphy became an important age determination tool for geologically young, onshore strata worldwide (e.g., Keller et al., 1977; Heller and Liu, 1982; Johnson et al., 1986; Appel et al., 1991; Biswas et al., 1999; Maher and Hallam, 2005b; Scardia et al., 2006). However, the current chronostratigraphic system for the Quaternary and the late Neogene in central and north-western Europe is based primarily on pollen-analysis investigations from the Netherlands and the Lower Rhine Embayment (i.e., Zagwijn, 1957, 1963, 1985; Kemna, 2008; Westerhoff et al., 2008). Although these studies are underpinned by magnetic polarity stratigraphy, the palaeomagnetic record by itself was not suitable for the establishment of the chronostratigraphic system. In addition to other reasons not specified here, this is due to the low number of appropriately long and complete sedimentary exposures for magnetostratigraphic examinations.

The Heidelberg Basin is situated in the northern Upper Rhine Graben (Figure 2.1). It has been considered an exceptional repository of a long fluvial succession. Due to the lack of satisfactory dating methods, the chronostratigraphy of these sequences has been controversial for decades (Salomon, 1927; Bartz, 1953; Fezer, 1997; Ellwanger et al., 2008).

Recently, the "Heidelberg Drilling Project" (for details, see Gabriel et al., 2008) made deep borehole material from three sites within the basin available to scientists from different disciplines. Currently, three projects aim to comprehensively describe the sediments by means of sedimentological, palynological and palaeomagnetic analysis. To provide reliable chronological constraints, comprehensive magnetic polarity stratigraphies are elaborated in this study. It should however be noted that the complexity and incompleteness of fluvial sedimentary records are a fundamental challenge for the application of magnetic polarity stratigraphy. Nevertheless, an

accessible magnetostratigraphic timeframe enables further interpretation towards a better understanding of the development of climatic and environmental conditions in the area of investigation. Furthermore, this type of work can lay the foundation for the next step toward a correlation of different continental basins in Europe.
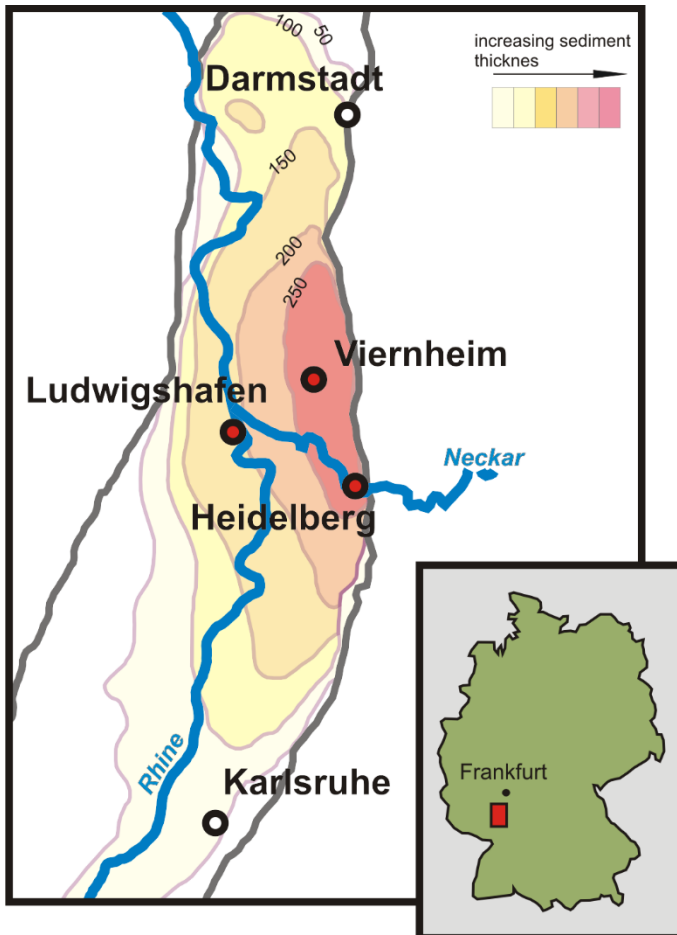
Figure 2.1:
The location of the Heidelberg Basin in Germany and the locations of the boreholes (red dots) within the basin. Illustration after Bartz (1974) shows the thickness of the sedimentary fill in the Heidelberg Basin.

Note that the lack of chronostratigraphic information in the Upper Rhine Graben has led to classification by lithological and hydrological criteria. It is a common practice to utilise the onset of the alpine mineral assemblage, i.e., the first occurrence of calcareous sediments and the change in the heavy mineral spectrum, as the 'base of the Quaternary' (Bartz, 1953; Hagedorn and Boenigk, 2008). However, the use of chronostratigraphic terms for lithostratigraphy has caused some ambiguities in the literature. For this reason, we follow the style of Buness et al. (2008). Terms that we assume to be in lithostratigraphic context are set in quotation marks (e.g., 'Quaternary') and chronostratigraphic expressions are used without quotation marks (e.g., Quaternary).

2.2. Geological settings

The Heidelberg Basin is part of the Rhine Basin, which comprises the recent catchment of the Rhine River including subsiding basins and the uplifted areas where fluvial sediments are only preserved as river terrace staircases. The Heidelberg Basin is the dominant sediment trap in the northern Upper Rhine Graben (URG) (Doebel, 1967; Doebel and Olbrecht, 1974; Bartz, 1974). The basin began to subside in the Late Oligocene (Schumacher, 2002) and created one of the thickest continental Plio-Pleistocene sedimentary successions in central Europe (Gabriel et al., 2008). The sediments have been delivered primarily by the Rhine River. In respect to the position within the basin, this superregional supply is complemented by regional and local sources (e.g., sediment load from smaller rivers, such as the Neckar and local erosion products). Consequently, different lithostratigraphic schemes have been used. This situation changed in 2011 by the introduction of a new lithostratigraphy for the northern URG, in which four units were defined. These units are the Iffezheim Formation, the Viernheim Formation, the Ludwigshafen Formation and the Mannheim Formation (from oldest to youngest), as shown in Figure 2.2. The formations are composed of clay, silt, and fine to coarse sand. Interlayers of gravelly sands and gravels are characteristic. The primarily green to grey colours of the sediments in the younger parts change in the Iffezheim Formation to dominantly orange and red silts and clays with grey veins.

Mannheim Formation	A basal layer of gravel followed by several fluvial cycles (mainly grey, calcareous sand). The monotone sequence is sporadically interrupted by fine, partially organic overbank and oxbow sediments.
Ludwigshafen Formation	Fluvial sediments with intercalations of lacustrine sediments. The fluvial sands fine upward to carbonate-rich grey silts and clays. Sequences end occasionally with humic layers composed of black to brown-black silty clays, occasionally accompanied by peat beds.
Viernheim Formation	Dominant fine to medium sands alternate with gravelly sand with silty to clayey intervals. Carbonate content of up to 30%, greenish-grey colours and a high amount of mica are characteristic.
Iffezheim Formation	A stack of several fluvial cycles (grey, partially kaolinitic sands) and palustrial, pedogenetically influenced, fine clastic sediments. Mostly carbonate-free, coloured clays are abundant. Isolated carbonate nests occur.

Figure 2.2:
General lithological description of the Plio-Pleistocene formations of the Heidelberg Basin. Data taken from Ellwanger et al. (2010a), Ellwanger et al. (2010b), Hoselmann et al. (2010), and Weidenfeller et al. (2010) in the German Litholex stratigraphic database.

In general, the sedimentary environment was characterised by fluvial cycles, lacustrine sediments, and horizons of peat and soils. An overview of the units that were previously in use and the

composition of the individual formations is given by Gabriel et al. (2013). The exact description of the new formations is given in the German lithostratigraphic lexicon (Ellwanger et al., 2010a; Ellwanger et al., 2010b; Hoselmann et al., 2010; Weidenfeller et al., 2010).

2.3. Sites and drilling procedures

This study is based on four borehole cores from three locations. The cores represent different facies zones in the Heidelberg Basin. Information on the boreholes in the different sites is provided in the following paragraphs. Additional information on the cores is provided in Table 2.1.

Table 2.1*:*
Core data and number of samples. The total number of demagnetisation experiments is shown in relation to the successfully analysed samples with MAD ≤ 10° and MAD ≤ 12°, respectively. The range of the lithological units is listed in the grey field, as provided by Weidenfeller (pers. comm.), Ellwanger et al. (2008), and Hoselmann (2008).

	Viernheim	Heidelberg UniNord 1	Heidelberg UniNord 2	Ludwigshafen P36
cored depth	0-350 m	0-190.4 m	114-115 m, 183-500 m	0-301 m
Finished in year	2002	2006	2008	2009
core recovery	ca. 97%	n/A[1]	n/A[1]	ca. 95%
core diameter	10 cm	10 cm	10 cm	12 cm
number of sampled depths	394	128	341	166
total number of cubic samples **total number of cylindrical samples**	778 117	379	968	469
AF / thermal demagnetisation	509 / 31	132 / 4	388 / 29	171 / 4
ChRM: MAD ≤ 10° / MAD ≤ 12°	138 / 162	59 / 64	86 / 97	66 / 75
Mannheim Formation	0 - 39.76 m	0 - 56.20 m	#	0 - 17.3 m
Ludwigshafen Formation	39.76 - 77 m	56.20 - 126.40 m	114 - 115 m	17.3 - 69.6 m
Viernheim Formation	77 - 225 m	126.40 - 190.40 m	183 - 298.60 m	69.9 - 199,8 m
Iffezheim Formation	225 - 350 m	#	298.60 - 500 m	199.8 - 301 m

[1] Unusable data, for details see Ellwanger and Wieland-Schuster (2012)

2.3.1. Viernheim

The Viernheim borehole site is located in the geographical centre of the Heidelberg Basin, approximately 3 km north of the city of Viernheim, in the Hessian Ried (Buchnerschneise). The borehole was drilled to a total depth (TD) of 350 m in the year 2002. To obtain an intact high-quality borehole core, the ram-coring method was applied in alternation with the wireline rotary coring method. The site represents the Pleistocene "normal facies" of the URG, which is characterised by low input of sediments from regional or local sources. The uppermost part of the core is composed solely

of gravel deposits associated with the Neckar River (Hoselmann, 2008). The core intersects the four lithostratigraphic formations and is presented in Figure 2.2.

2.3.2. Heidelberg

The cores UniNord 1 and UniNord 2 were drilled at two sites, both located at the centre of the area with the greatest subsidence in the Heidelberg Basin. Problems with the drilling procedure at the Heidelberg UniNord 1 site culminated in an early stop of the drilling at 190.4 m in 2006. The core UniNord 1 was collected using the ram-coring technique. The core includes the lithostratigraphic units down to the Ludwigshafen Formation. A second borehole (UniNord 2) was sunk at a distance of approximately 260 m north-northwest of the first drill site in 2008. Hydraulic circulation drilling was used to a depth of 183 m; beneath this depth, ram coring and wireline rotary coring was used (for details see Ellwanger and Wieland-Schuster (2012). The core of UniNord 2 starts in the Ludwigshafen Formation and ends in the Iffezheim Formation. The comparability of the two Heidelberg cores was proved by matching cored segments from UniNord 2 (114-115 m and 183-190.4 m) with the UniNord 1 core. The successful identification of a magnetic polarity reversal in both cores showed a vertical stratigraphic difference of less than 1 m. Therefore, the combined total length of 500 m of the cores is processed as one Heidelberg core in this paper.

The whole sequence of the Heidelberg core is clearly influenced by the sediment load of the Neckar River. Thus, the sedimentological characteristics of the Heidelberg borehole differ from the other cores. Taken as a whole, the sediments are coarser and the proportion of orange to red sediments decreases in favour of grey sands. An illustrated and detailed lithostratigraphic description is presented in Ellwanger and Wieland-Schuster (2012).

2.3.3. Ludwigshafen Parkinsel P36

The sedimentary successions of borehole P36 represent the evolution of the western margin of the Heidelberg Basin. The core is available from groundwater exploration and was collected via the ram core drilling technique to a TD of 301 m in 2009. The core composition is similar to the older sister cores P34 and P35. Their drill sites are located at a distance of ca. 500 m and 1,000 m from borehole P36, respectively. All cores involve the four described lithostratigraphic formations. Rhine sediments represent the major parts of the cores. Interlayers of deposits from the Pfälzerwald (Bundsandstein) emerge occasionally. The descriptions and analyses of core P36 are as yet undisclosed. Until now, only studies of the older sister cores P34 and P35 have been published, e.g., Rolf et al. (2008), Weidenfeller and Knipping (2008), and Knipping (2008).

2.4. Sampling

The liners and the borehole cores contained within were vertically bisected into two halves. The orientation of the cut face was not considered because the azimuth angel of the cores is unknown. One half was kept in flexible polyethylene tubes and stored in wooden boxes to prevent desiccation, whereas the other half used for sampling gradually dried. The cores were sampled at 0.5-m intervals. Sampling was performed preferentially in fine clastic layers (clay, silt, fine sandy layers with a clayey or silty matrix). Due to the drilling process itself, certain core segments were pervasively disturbed (e.g., flexures, drill marks, artificially re-sedimented sections, etc.). These core segments and coarser-grained sections were not sampled for the purpose of magnetic polarity stratigraphy; thus, relatively large sampling gaps occur. Most samples were taken by sawing the hardened rock into cubic specimens with a volume of approximately 10 cm^3. Additionally, 117 cylindrical samples with a diameter of 2.54 cm were cut perpendicular to the Z-axis (downhole) from unconsolidated sediments of the Viernheim core. The distribution of all 1,200 samples along the cores is presented in Table 2.1.

2.5. Methodology

The natural remanent magnetisation (NRM; before any treatment) of all samples was measured with a cryogenic magnetometer (760 SRM-RF-SQUID, 2 G Enterprises, Mtn. View, CA, USA) in the Leibniz Institute for Applied Geophysics (LIAG) palaeomagnetic laboratory at Grubenhagen, near Einbeck, Germany (Rolf, 2000). Subsequently, the low-field magnetic susceptibility (κ) of each sample was determined using the Minikappa KLF-3 kappabridge (AGICO, Brno, CZ). Alternating field (AF) demagnetisation experiments were performed with a Magnon MI AFD 300 demagnetiser (MAGNON Int. Dassel, Germany) in Grubenhagen or with a D-Tech D2000 AF demagnetiser (ASC Scientific, Carlsbad, CA, USA) in the palaeomagnetic laboratory of the Department for Earth and Environmental Sciences, Geophysics Section, University of Munich, in Niederlippach, Germany. Measurements at the Niederlippach laboratory were carried out with a liquid-helium-free, superconducting rock magnetometer system (760 SRM-DC-4K, WSGI, Sand City, CA, USA). Each AF demagnetisation started with the determination of the NRM of the specimen, followed by up to eighteen progressively increasing demagnetisation steps and was continued until the measured directions became scattered. Due to equipment characteristics and laboratory setups, the AF demagnetisation was performed up to a peak field of 300 mT in Grubenhagen and up to 150 mT in Niederlippach. In total, 1,200 specimens were subjected to AF demagnetisation experiments.

Thermal (TH) demagnetisation experiments were conducted using a thermal specimen demagnetiser model TSD-2 (Schoenstedt Instruments Company, Virginia, USA) in a magnetically shielded room at Niederlippach. In total, 68 samples were heated in steps to a maximum temperature

of 700°C to identify the entire blocking temperature spectrum of the samples and to validate the directions of the AF demagnetisation experiments. The thermal demagnetisation started with measurement of the NRM. Then, the magnetisation, presumably carried by goethite, was determined via 20°C increments between 90°C and 150°C. Increments of 50°C to 150°C were chosen for the temperature range above 150°C. Measurements of the low-field magnetic susceptibility were performed after each thermal demagnetisation step. This step allows the detection of possible alteration in the magnetic mineralogy due to heating. All specimens that exhibited unstable magnetic remanences were discarded.

In total, 11 specimens were selected for a coupled treatment of AF and thermal demagnetisation. In this case the samples were demagnetised in an alternating field and were subsequently thermally demagnetised as described above. Another three samples were heated to 150°C before they were AF demagnetised. Both experiments were performed to evaluate the influence of high-coercivity components.

The AF and thermal demagnetisation data were plotted in orthogonal vector diagrams (Zijderveld, 1967) and analysed by the program Remasoft 3.0 (Chadima and Hrouda, 2006). The characteristic remanent magnetisation (ChRM) was isolated by principle component analysis (Kirschvink, 1980). With only a few exceptions, these calculated magnetisation directions are based on at least 4 demagnetisation steps (AF ≥ 15 mT), including the origin, but not anchored to the origin (settings of the program Remasoft 3.0).

Rock magnetic parameters were used to identify the magnetic minerals that carry the remanent magnetisation. The stepwise acquisition of the isothermal remanent magnetisation (IRM) was measured in a DC peak field up to 2.75 T. The saturation isothermal remanent magnetisation (SIRM) is defined as the IRM in this peak field; even so, saturation was not reached. Three-component IRM analysis (after Lowrie, 1990) was performed on 15 samples from the Viernheim drill core. The selected specimens were exposed successively to a 2.75 T DC field along the Z-axis, a 0.4 T DC field along the Y-axis and a 0.12 T DC field along the X-axis. Subsequently, the samples were progressively thermally demagnetised in temperature increments between 20°C and 50°C up to a temperature of 660°C. The three-component IRM analysis provides information about the soft, medium and hard coercivity fraction of a rock by accounting for the unblocking temperatures of the different magnetisation carriers.

The IRM acquisition experiments were performed with a Magnon PM II pulse magnetiser, and the thermal demagnetisation of the three-component IRM was executed with a Magnon MI TD 700 demagnetisation oven (MAGNON Int. Dassel, Germany).

2.6. Results of the demagnetisation experiments

During the demagnetisation experiments, most samples exhibited a weak secondary magnetisation. These viscous remanent magnetisations (VRM) were removed by AF demagnetisation steps of < 15 mT or thermal demagnetisation at 90°C. Because a large number of samples had widely scattered demagnetisation curves, ChRM determination via principle component analysis (Kirschvink, 1980) was often not possible. Samples with stable magnetisation and maximum angular derivation (MAD) of ≤ 10° were primarily considered in this study. Inclination values with a MAD ≤ 12° were utilised if the quantity of the MAD ≤ 10° data was very low.

In Figure 2.3, examples of the demagnetisation behaviour of samples from the different formations are given. Stable magnetisation behaviour is depicted in Figures 2.3 a to d. Figures 2.3 e to f show examples of Zijderveld plots that led to doubtful ChRM directions. The reasons for the exclusion of these datasets from further interpretation are given in the respective captions.

However, due to the presence of highly coercive components, certain samples retained up to 45% of the initial NRM intensity after AF demagnetisation. In these cases, the orthogonal projections show a clearly defined demagnetisation pathway, which is followed by a cluster around a certain direction. The role of the highly coercive components in the ChRM has been revealed by the thermal demagnetisation experiments. The AF-treated samples from the Viernheim Formation through the Mannheim Formation did not exhibit significantly different directional behaviour compared to their thermally demagnetised sister samples (Figure 2.4a). Additionally, the combined AF and thermally demagnetised specimens did not reveal an intrinsic influence of a highly coercive phase on the determined ChRM. For the samples from the Iffezheim Formation, a reliable identification of the directions was often only possible by using thermal demagnetisation. However, in most cases, it was possible to determine normal and reversed polarity (Figure 2.4b). Nevertheless, the determined ChRM values of these samples are only used for the polarity determination if reliable adjacent data support their results. Unfortunately, the Iffezheim Formation in the Ludwigshafen P36 core experienced significant overprinting during the drilling process. Even if damage to the core was not visually detectable, the demagnetisation pathway clearly indicated overprinting in terms of a magnetisation parallel to the core axis (Figure 2.3h). The primary magnetisation has been completely eliminated, and therefore no data could be gained.

The total numbers of appropriate polarity results from the different boreholes are listed in Table 2.1.
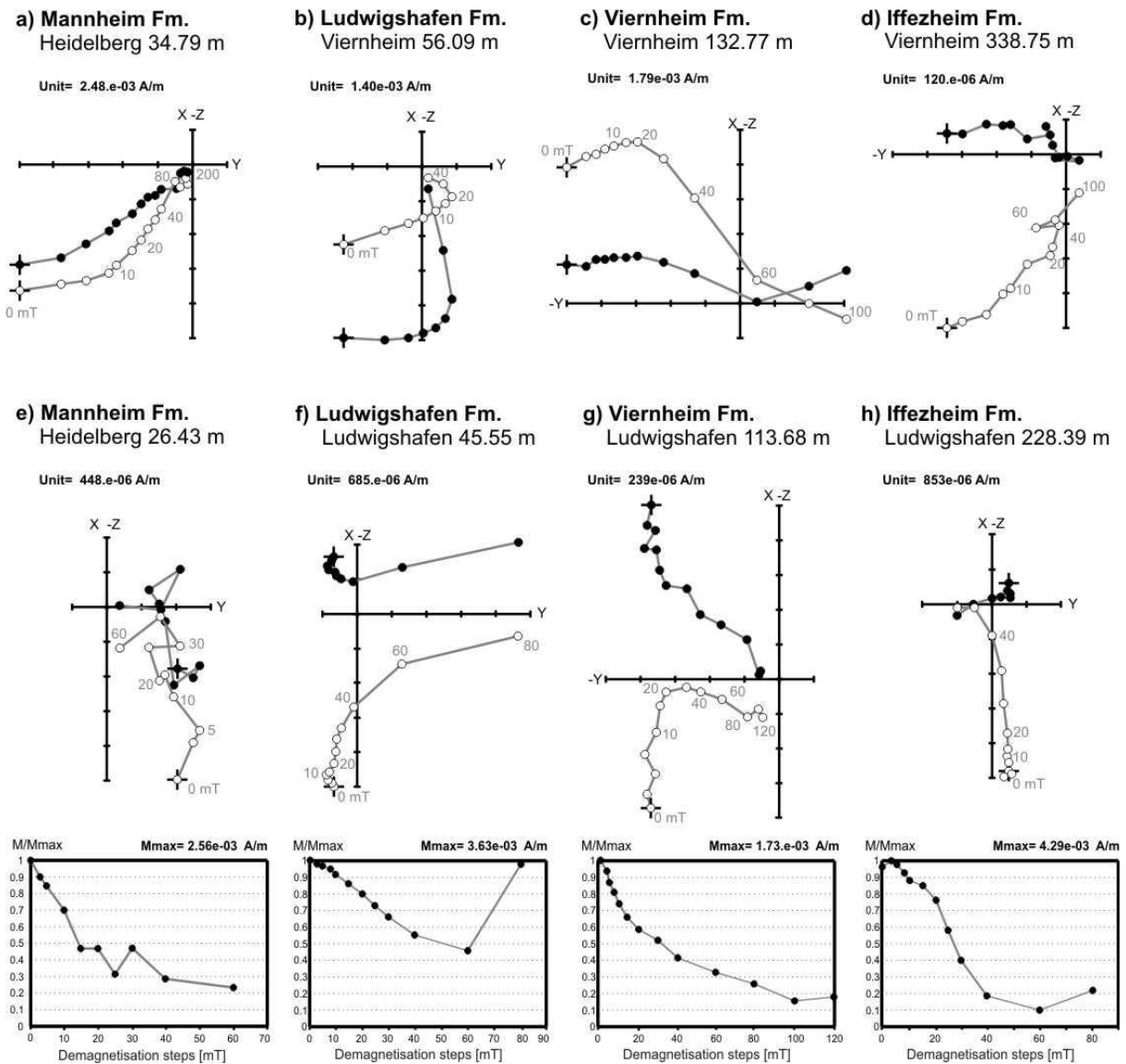
Figure 2.3:

Examples of Zijderveld demagnetisation diagrams for the different lithological units with indisputable ChRM (a-d) and Zijderveld diagrams and related normalised (M/M$_{Max}$) intensity plots of datasets with doubtful ChRM directions (e-h). Open and closed circles represent projections onto the vertical and horizontal planes, respectively. The samples are identified by the core and the depth. Because of the solely up-down orientation of the cores, the horizontal projections show arbitrary azimuths.

Mannheim Formation (a & e): The scattered data in e do not allow reliable ChRM determination.
Ludwigshafen Formation (b & f): The demagnetisation pathway in f is masked by a secondary strong gyro-remanence. Viernheim Formation (c & g): Due to the acquisition of a gyro-remanence, the demagnetisation experiment in c was stopped at 100 mT. The ChRM in g would turn from normal into reverse via slight rotation around the Y-axis. Therefore, the result was not assessed to be reliable.
Iffezheim Formation (d & e): Due to highly coercive components, a complete demagnetisation of the sample was not possible via the AF method. To avoid overloading the illustration with a point cloud, the pathway of d is depicted only up to 100 mT. The Zijderveld diagram in h shows a clear overprint due to the drilling process. The sample is magnetised parallel to the Z-axis.
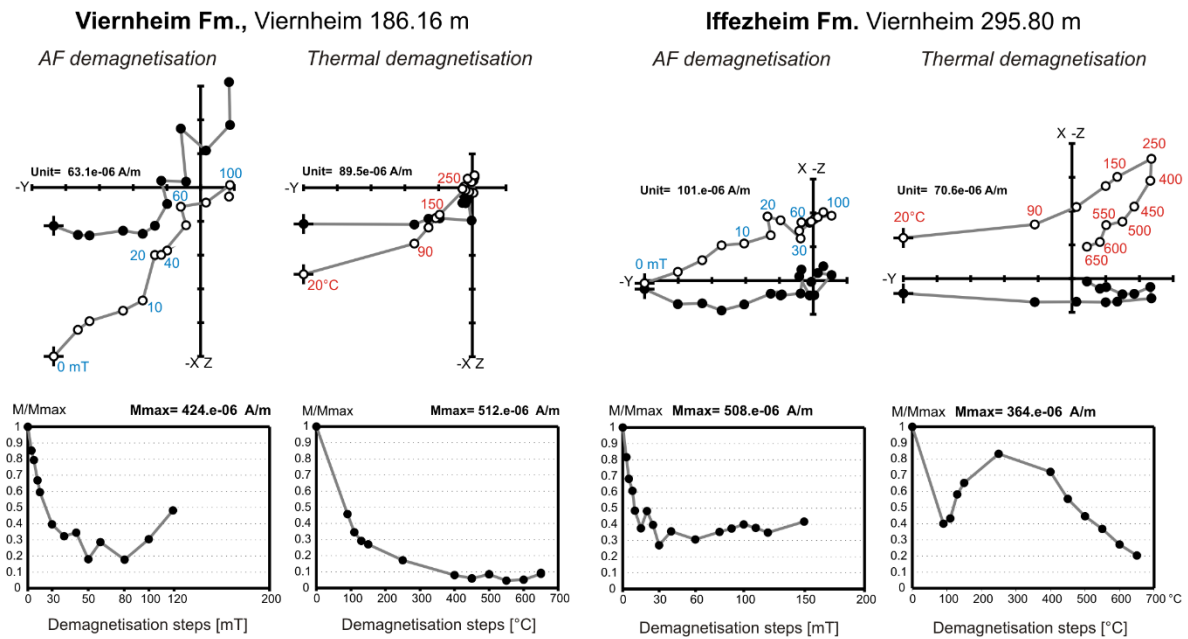
Figure 2.4:

Comparison of AF demagnetised samples (blue) and thermally demagnetised sister samples (red) from the Viernheim Formation and the Iffezheim Formation, with associated normalised (M/M$_{Max}$) intensity plots. Open and closed circles represent projections onto the vertical and horizontal planes, respectively. The samples are identified by the core name and the depth. Because of the incomplete orientation of the cores, the horizontal projections show arbitrary azimuths.

2.7. Carriers of the magnetic remanence

A general knowledge of the carriers of the magnetic remanence in a sedimentary sequence is essential for a reliable magnetostratigraphic interpretation. In this paper, we report the general temporal and spatial trends in the lithofacies of the Pliocene to Pleistocene clastics of the Heidelberg Basin. A detailed rock magnetic analysis of this long, complex sequence of mainly fluvial fine to coarse clastics is beyond the scope of this work and will be reported and discussed in a separate paper (in preparation).

The fluvial sediments from the Heidelberg Basin are characterised by variable values of initial NRM and susceptibility. The NRM ranges from 10^{-2} to 10^{2} mAm^{-1}, with a mean of 10^{1} mAm^{-1} (Figure 2.5). The mass-specific magnetic susceptibility (χ) varies between -0.5 and 432.5 $\cdot$ 10^{-8} m^{3} kg^{-1}, where the maximum value is associated with a few outliers. The mean χ values of the different formations range between 6 and 15.5 $\cdot$ 10^{-8} m^{3} kg^{-1} (Figure 2.5). The variation in the magnetic susceptibility with depth and the initial NRM correlate well and depend strongly on the lithology. The petrographic composition of the different lithostratigraphic formations differs within the cores, depending on their local

catchment areas, as described in detail in section 2.3. In general, the Iffezheim Formation exhibits significantly lower initial NRM intensities and lower magnetic susceptibilities than the younger formations. The gradual transition to higher values occurs close to the boundary of the overlying Viernheim Formation, but the transition is still within the Iffezheim Formation.
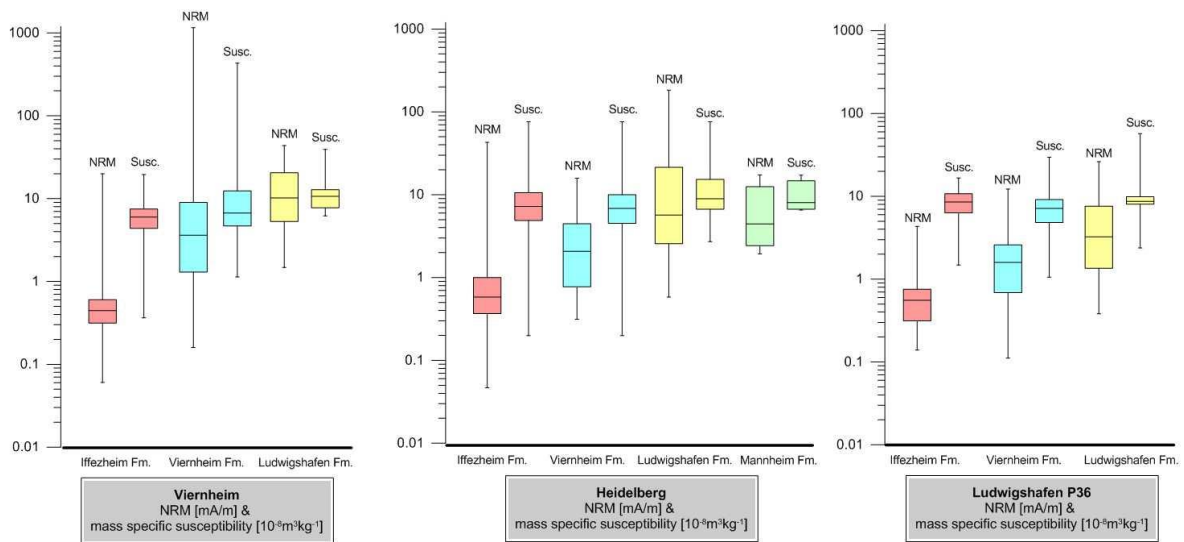
Figure 2.5:
Box-whisker plots of the NRM and the magnetic susceptibility of the different lithological formations from the three cores. A negligible number of negative values from the Iffezheim Formation are not depicted.

IRM-acquisition experiments and thermal demagnetisations of three-component IRMs suggest that this change is caused by a shift in the relative contribution of high- and low-coercivity minerals to the cumulative intensity. Towards the younger formations, the influence of the soft coercive mineralogical inventory becomes dominant. Figure 2.6 shows this general trend with a number of examples from the Viernheim core. The IRM acquisition curves of the uppermost parts of the cores rise steeply to (almost) saturation under static fields of 0.5 T (Figure 2.6a-c). Close to the boundary of the Viernheim Formation, the samples from the Iffezheim Formation acquire ca. 95% of the maximum magnetisation at 1 T; under high fields, the IRM increases continuously (Figure 2.6d). The initial gradient of the IRM acquisition curve in the lowermost parts of the cores is less steep. At 1 T, approximately 90% of the maximum magnetisation is reached. At higher fields, a steady increase is observable without reaching saturation at 2.75 T (Figure 2.6e).

This impression of a gradual change within the magnetic minerals is supported by the results from the thermal demagnetisation of a three-component IRM (Figures 2.6f-j). The influence of the soft fraction declines significantly downcore, whereas the unblocking temperatures shift successively to higher temperatures. After Lowrie (1990), the decay of the intensity of the medium and soft fraction

at 300°C indicates the presence of either pyrrhotite, Ti-magnetite, or Ti-maghemite, depending on the depositional environment. Kodama (1982), Løvlie et al. (1989) and Jordanova et al. (2010) interpret the decrease in remanence intensity between 350°C and 400°C as indicative of metastable maghemite, titanomaghemite and the presence of detrital magnetite with a maghemitised rim, respectively. A recent work on clastic continental deposits of the Po plain interpret the decay of the soft coercive component at 300°C to 350°C as indicative of iron sulphides (Scardia et al. 2006). Torii et al. (1996) discriminate between pyrrhotite and greigite based on the contribution of the coercive fractions to a composite IRM and by coercivity fractions of thermal demagnetisation behaviour. In that study, pyrrhotite-bearing samples are characterised by a coercivity spectrum ranging from soft to hard and a blocking temperature below 350°C. In the greigite-bearing samples, in contrast, more than a third of the total magnetisation is carried by the medium coercive fraction and the IRMs are completely demagnetised by approximately 320°C (Torii et al. 1996).

Based on these observations, we conclude that maghemite or maghemitised magnetite is very likely present in these samples. Furthermore, greigite is an important carrier of the magnetisation in the upper parts of the cores. This interpretation corroborates the findings by Rolf et al. (2008), who proved greigite was the dominant soft magnetic mineral to a depth of 177 m in a sister core of Ludwigshafen P36.

Approximately 30 to 40% of all samples from the Ludwigshafen Formation and the Viernheim Formation show an artificial increase in the magnetisation during AF demagnetisation, as shown in Figures 2.3c, 2.3f and 2.4a. This gyro-remanence (GRM) is another strong argument for the presence of greigite (Snowball, 1997).

The GRM is detectable down to the lithological transition zone at the top of the Iffezheim Formation. However, the course of the thermal decay of the individual IRM components in Figure 2.6i indicates a different composition of IRM carriers for the Iffezheim Formation than for the upper parts of the cores.

The vector plot of the soft fraction versus the hard fraction (Figures 2.6k-o) provides additional information on the temperature dependence of the different coercive minerals (Lowrie, 1990). Figure 2.6n clearly shows an additional change in slope at 540°C. This unblocking temperature is also evident at the lowermost parts of the core (Figure 2.6o) and is indicative of the presence of impure magnetite (Vincent et al., 1957; Smykatz-Kloss, 1974). This again is in good agreement with the findings of Rolf et al. (2008). The final decay towards zero between 540°C and 660°C might result either from maghemite or impure haematite (Özdemir and Banerjee, 1984; Tarling, 1983).

The decay of the initial intensity of the hard and medium fraction between 90°C and 150°C is a reliable indicator of the presence of goethite. The subsequent decrease of the curves in the younger lithologies indicates that magnetic sulphides might be present over a wide range of coercivity (Lowrie,

1990). However, the monotonic decrease in the intensity of the high-coercivity component in the older sequences of the core is a strong argument for a large amount of haematite, as also expected from the colour of the sediments.
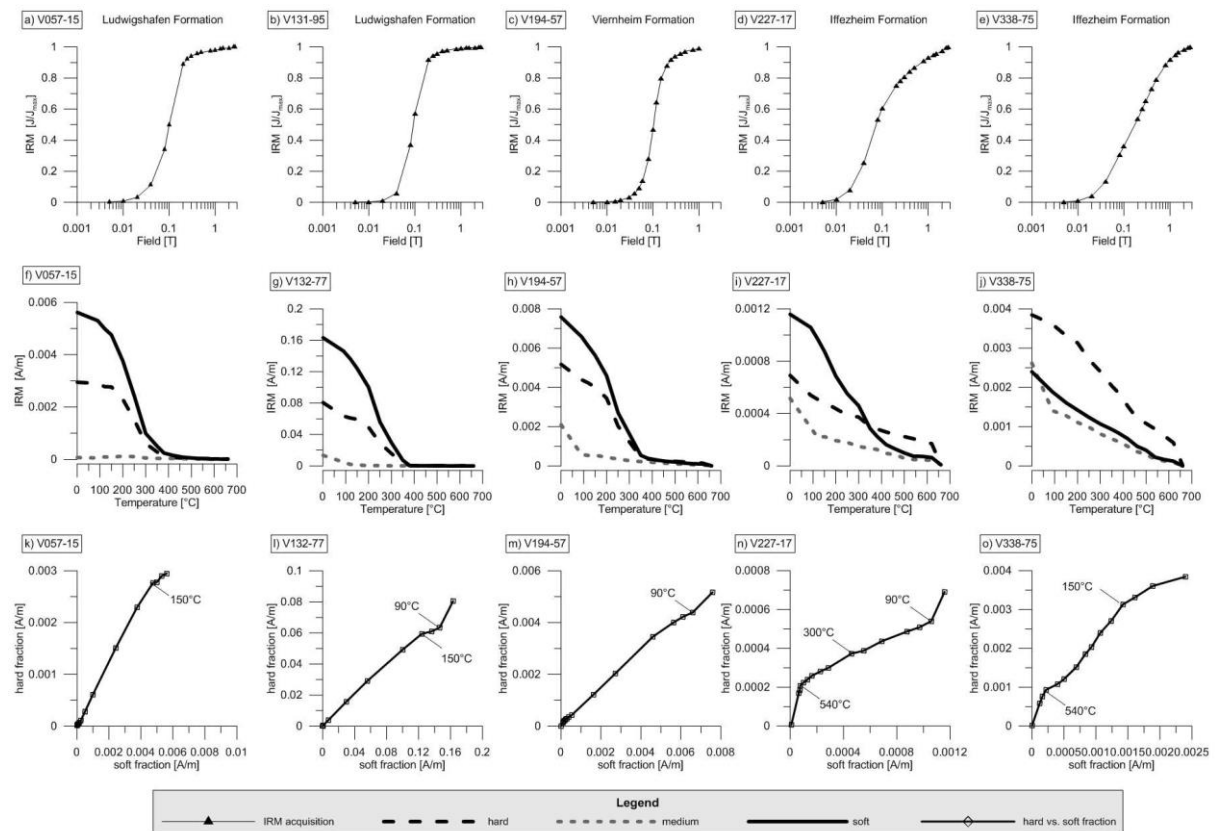
Figure 2.6:

Top row: Progressive IRM acquisition curves for selected samples from the Viernheim core. Middle row: Progressive thermal demagnetisation curves for a three-component IRM (Lowrie, 1990). The IRM was produced by magnetising the sample successively at 2.7 T along the Z-axis, 0.4 T along the Y-axis and 0.12 T along the X-axis. Bottom row: The vector plots of the composite IRM exhibit variations in the temperature dependence of the different coercivity fractions by the trajectory of the curve (Lowrie, 1990). The temperatures of prominent changes are indicated.

2.8. Magnetic polarity stratigraphy

The cores are not oriented with respect to azimuth. Consequently, identification of normal and reversed polarised sections is based only on the inclination data.

The inclination of the finer-grained sediments is on average shallower than the expected geocentric axial dipole (GAD) inclination of 67° (± secular variations) at the site (Figure 2.7). This phenomenon is even more obvious in the deeper sections of core Viernheim and core Ludwigshafen P36, which are less sandy and generally finer than the Heidelberg core. Inclination shallowing of the ChRM caused by compaction is a probable explanation for this observation, which in turn can be taken as evidence for

early acquisition of the remanence (Deamer and Kodama, 1990). Despite cautious sampling, minor effects on the angle of inclination due to the drilling process cannot be ruled out. Nevertheless, these phenomena do not affect the discrimination of stratigraphic intervals that exhibit normal and reversed polarity.
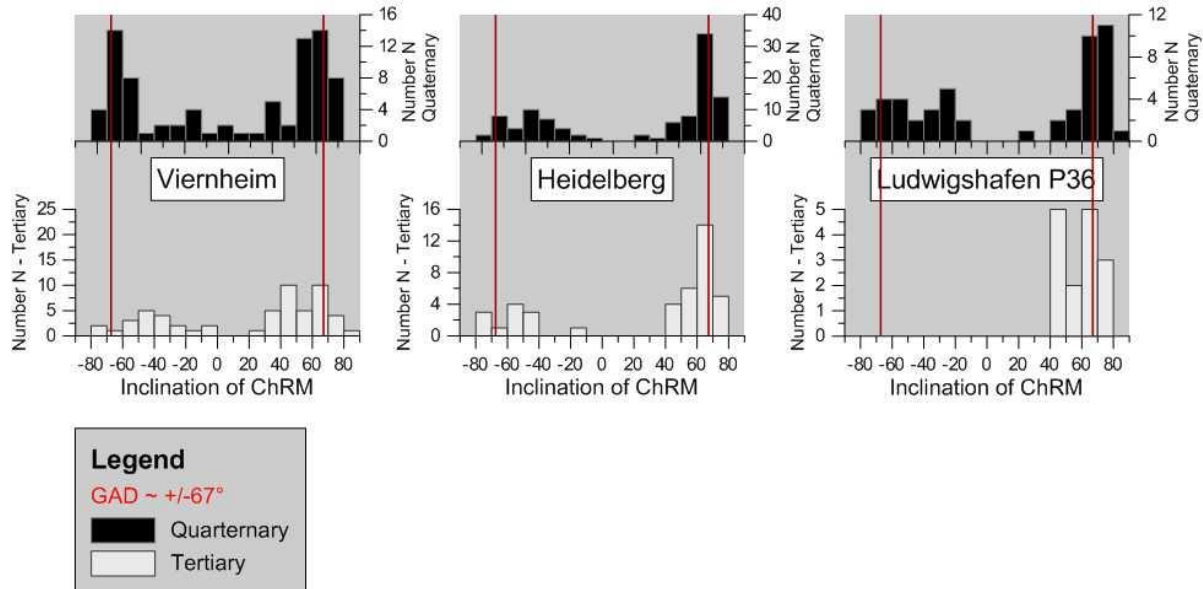
Figure 2.7*:*
Distribution of inclination of the ChRM with MAD ≤ 10° for the sediments from the Quaternary (black) and the sediments from the Tertiary (white). Note the different scales of the total amount of samples on the y-axis. The geocentric axial dipole (GAD) of the area of investigation is depicted in red.

The overall quality and reliability of the data used for the magnetic polarity stratigraphy are supported by following measures.

(1) Careful sampling of mainly fine sediments, which were (almost) not affected by the drilling procedure.

(2) Determination of the ChRM primarily based on at least 4 demagnetisation steps (AF ≥ 15 mT).

(3) Exclusive use of ChRM with MAD ≤ 10° and ≤ 12°.

(4) A sever strategy, in which (almost) all samples with low inclination values were discarded. This procedure prevents the falsification of the magnetisation direction by the slight tilting of the sample.

From the Mannheim Formation through the Ludwigshafen Formation down to the younger part of the Viernheim Formation, an exclusively normal polarity is observed and is interpreted as representative of the Brunhes normal polarity chron (Figure 2.8).
The dominance of reversed polarity throughout the underlying parts of the sequence, which mainly encompass the Viernheim Formation, suggests that these sections were deposited during the Matuyama reversed polarity chron.

The beginning of the Gauss normal polarity chron is observed below the reversed section and is clearly defined by a change to an interval of normal polarity, followed further down by alternating reversed and normal polarity sections. At Ludwigshafen P36 core, this normal polarity zone expands down to the base of the core. However, the drilling-induced overprint in the magnetisation in the lowermost parts of core P36 and the relatively small number of reliable polarity data limit the significance of the remanence data within this section. In the Ludwigshafen P36 core and the Viernheim core, the Gauss-Matuyama boundary appears just above the base of the Viernheim Formation. In the Heidelberg core, this polarity change is located at the top of the Iffezheim Formation.
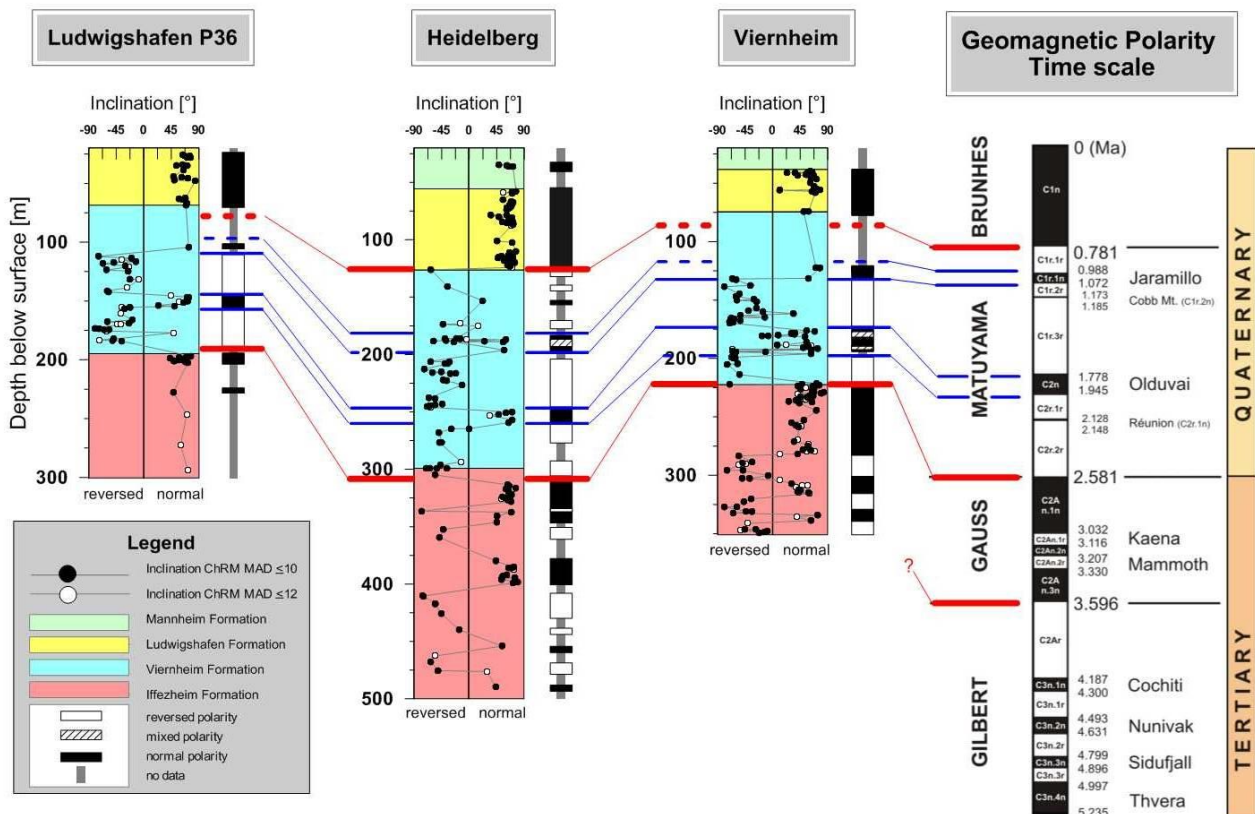
Figure 2.8:
Magnetostratigraphic correlations of the studied cores with the geomagnetic polarity time scale (GPTS). Inclinations of the ChRM are indicated. The y-axis refers to the depth below the surface. The GPTS is after Cande and Kent (1995), as shown in Ogg (2012). The range of the lithostratigraphic units are taken from previous unpublished data from the Ludwigshafen P36 core (Weidenfeller, pers. comm.), from Ellwanger et al. (2008) for the Heidelberg core and from Hoselmann (2008) for the Viernheim core.

A confident correlation of the deepest parts of the cores is not possible without additional stratigraphic and/or chronologic information. The observed pattern of normal and reversed polarity allows for quite different stratigraphic scenarios. Several age-depth correlations are discussed in the next paragraph to illustrate the most probable options.

In addition to chrons, certain shorter polarity intervals have temporal extents that make them likely to be preserved in fluvial sediments. Subchrons with durations of ≤ 0.1 Ma that occur within chrons are reported frequently, even in continental settings (e.g., Scardia et al., 2006; Pan et al., 2011). Geomagnetic excursions, in contrast, are rarely documented (e.g., Laj and Channell, 2007). In the Heidelberg core, two intervals with normal or mixed polarity stand out within the reversed Matuyama chron (Figure 2.8). These intervals most likely match the Jaramillo (C1r.1n) and Olduvai (C2n) subchrons. The top of the upper reversed section (Jaramillo) is observed in UniNord1 at 188.47 m and in UniNord 2 at 187.09 m. The existence of multi-component (reversed-normal) results at the border of chrons and subchrons can be interpreted as evidence of a stable magnetisation that was acquired at different lock-in depths (Spassov et al., 2003). The quiet uniform magnetic susceptibility values in these sections indicate a homogenous mineral assemblage.

The Viernheim and Ludwigshafen P36 cores show just one of these zones with normal or mixed polarity. A remarkable feature in this context is a data gap in both cores located in the upper part of the Viernheim Formation. These gaps occur between 74.40 and 122.17 m in Viernheim core and 68.61 and 104.37 m in the Ludwigshafen P36 core and are due to a coarse clastic facies that could not suitably record magnetic polarity. The samples with normal polarity below the gaps could still be part of the Brunhes chron, or they could represent the end of the Jaramillo (C1r.1n) subchron. To decide whether the former or the latter interpretation is favourable, we compared the data from the Viernheim and Ludwigshafen P36 cores with the results from the Heidelberg core.

Although the stratigraphic data resolution is quite low in this section, the Matuyama-Brunhes boundary is clearly detectable at the UniNord1 core at 125.18 m ± 1.05 m, which is near the Viernheim Formation - Ludwigshafen Formation boundary. We assume the relative position of the Matuyama-Brunhes boundary to be quite similar in all cores relative to the lithostratigraphic formation boundaries. Thus, we prefer to locate the position of the Matuyama-Brunhes boundary in the Viernheim and Ludwigshafen P36 cores within the data gaps and near the formation boundary (Figure 2.8).

2.9. Discussion

This study provides the first comprehensive magnetic polarity stratigraphy for the sediments of the Heidelberg Basin and for Plio-Pleistocene fluvial sequences from western Central Europe in general. The rock magnetic studies revealed different carriers of the remanent magnetisation. Related to the facies interpretations of the formations (Ellwanger et al., 2010a; Ellwanger et al., 2010b; Hoselmann et al., 2010; Weidenfeller et al., 2010), the minerals are thought to be predominantly

authigenic or formed during or shortly after the deposition of the sediments. A detailed analysis will be published later.

The fidelity of the identified magnetic minerals is controversial in the literature. Although haematite has been accepted as an important carrier of palaeomagnetic information, the reliability of greigite is frequently questioned (e.g., Horng et al., 1998; Roberts and Weaver, 2005; Nilsson et al., 2013). However, convincing studies have shown that greigite is a reliable recorder of the ChRM if greigite formation occurs roughly contemporaneous with sedimentary deposition (e.g., Fassbinder and Stanjek, 1994; Maher and Hallam, 2005a; Vasiliev et al., 2008; Van Baak et al., 2013).

In addition to the mineral composition of the sediments, the fluvial depositional environment of the Heidelberg Basin is a challenge for any palaeomagnetic approach. The analyses of discontinuous sequences, composed of unconsolidated and water-saturated clastic sediments of various grain sizes, leads to ambiguities in the correlation of polarity reversals. Short excursions might not be recorded due to the lock-in depth, and certain polarity events could be completely eroded (e.g., Bleil and von Dobeneck, 1999; Roberts and Winklhofer, 2004). However, similar successions studied in the past decades have demonstrated that it is possible to construct magnetostratigraphic records even without confidently identifying short polarity changes (e.g., Opdyke et al., 1979; Johnson et al., 1986; Scardia et al., 2006; Pan et al., 2011).

At first glance, the polarity boundaries and formation boundaries of the sequences of the Heidelberg Basin appear to occur at similar depths and suggest the occurrence of major hiatuses in the succession. Indeed, in the Viernheim core, an unconformity between the 'Pliocene' and 'Pleistocene' sediments is described by Hoselmann 2008. The distinct facies change at 177 m in borehole Ludwigshafen Parkinsel P34 (Weidenfeller & Knipping 2008) is also an indication of a disconformable contact between the Iffezheim Formation and the Viernheim Formation. However, a closer inspection of the depths of the polarity changes reveals an offset of a few meters between the Iffezheim-Viernheim Formation boundary and the Gauss-Matuyama boundary. The described unconformities between the Pliocene and Pleistocene are based on a sedimentological classification at the base of Quaternary, as discussed in the introduction of this paper.

Furthermore, distinct climatically driven lithological changes near the Gauss-Matuyama boundary are well known from terrestrial and marine archives. In the Chinese loess plateau, for instance, the Gauss-Matuyama boundary is located near but well below the lithological change from the older red clay formation (strongly weathered aeolian silt) to the first loess sediments that indicate the global change towards a cooler and drier Pleistocene climate (Sun et al., 1998). The Gauss-Matuyama boundary can be found in the North Atlantic in a similar position near but below the first evidence for ice rafted debris and a decrease in carbonate recorded in the marine sediments, both of which indicate the onset of glaciation on Greenland (Shackleton et al., 1984).

The exact depth of the polarity change at the Matuyama-Brunhes boundary is obscured by data gaps. A coincidence with the Viernheim-Ludwigshafen Formation boundary cannot be confirmed or denied. Nevertheless, unconformities are present in the succession of the Heidelberg Basin. An estimate of the temporal dimension of these hiatuses can be taken from the work of Lauer et al. (2010; 2011) on the Viernheim core. An age of 56.2 ka ± 6.3 ka was identified at a depth of 32.7 m via optically stimulated luminescence (OSL) dating. Due to partial bleaching, a minimum age model (MAM3) was applied for the fluvial samples (Lauer et al., 2010). An age of 288 ± 19 ka resulted from infrared radiofluorscence (IR-RF) dating of a sample from a depth of 39.5 m (Lauer et al., 2011). From our point of view, certain uncertainties are related to the use of two different methods and the limits of the applications. However, a significant discordance is definitely identified in the Viernheim core; thus, we expect hiatuses that last as long as subchrons to be possible.

In addition to these numerical ages, certain biostratigraphic age constraints are available for the successions of the Heidelberg Basin. Wedel (2008) analysed the fossil remains of molluscs in the Viernheim core. He identified the Tertiary-Quaternary boundary to be between 195 m and 223 m. Unpublished pollen analyses are consistent with this classification and set the Tertiary-Quaternary boundary of the Viernheim core at a depth below 221.21 m (Heumann, pers. comm). The Ludwigshafen P36 core was examined in another study that used the same method. The Tertiary-Quaternary boundary was found to be between 198.92 and 185.50 m depth (Knipping, pers. comm). Based on pollen analysis, Hahne et al. (2008) classified the sector between 180 and 181.7 m of the Heidelberg core as Waalian. He noted that different authors have reported ages between 1.1 Ma to 1.3 Ma (Zagwijn, 1985) or between 1.4 Ma to 1.6 Ma (Ogg et al., 2008) for this stage. The former age supports our interpretation in which the mixed (normal and reversed) interval between 171.46 ± 1.80 and 180.53 ± 0.29 m is classified as Jaramillo (0.988 to 1.072 Ma). With just one exception, these independent biostratigraphic findings are consistent with the magnetostratigraphy presented here. The stratigraphic interpretation of the deeper section of the Heidelberg core as solely Quaternary by Ellwanger et al. (2008) and Ellwanger and Wieland-Schuster (2012) using pollen analysis and mollusc remains contradicts our results.

Another depth for the 'Base Quaternary' in the region of Heidelberg was revealed by preliminary interpretations of seismic reflection profiles by Buness et al. (2008). The Pliocene to Pleistocene transition of the Heidelberg borehole was predicted to be at approximately 430 m depth. However, the classification of this layer was carried out with respect to the only available data at that time, the Schriesheim borehole, approximately 1 km to the north. The age determination for this stratigraphic level is not explained in the hydrocarbon industry report and, hence, remains uncertain (Elwerath Erdgas und Erdöl GmbH, 1953).

Because there are only sparse reliable age constraints for the sediments of the Heidelberg Basin, a definitive correlation of the deeper parts of the cores with the GPTS is not readily possible. The correlation of the sediments older than the Gauss-Matuyama boundary is indeed a special challenge. While insufficient data render the magnetostratigraphic interpretation of this section from core P36 impossible, the Viernheim and Heidelberg cores exhibit several polarity changes (Figure 2.8).

We checked the plausibility of different correlation variants in a series of age-depth diagrams. The plausibility of the results is based on the following assumptions:

A.) The continuous subsidence of the Heidelberg Basin began in the late Oligocene (Schumacher, 2002). We assume the complex interplay between subsidence and fluvial erosion averaged over timescales of ≥ 0.5 Ma provided an almost constant accommodation. Changes in this system might occur only on long timescales (≥ 1 Ma).

B.) Fluvial sediments in subsidence-dominated basins have a higher potential for preservation than in other tectonic settings. The constant accommodation is continuously filled. River channels run through the basin and exhibit complex lateral-erosion patterns. The resulting episodic accumulation yields discontinuously vertical basin fill (Gibbard and Lewin, 2009; Lewin and Macklin, 2003). Due to the irregular distribution of our data, we average over relatively long time intervals. In this context, we suppose the actual step-like age-depth relationship to be best depicted by an almost linear smooth curve.

C.) In such a discontinuous succession, chrons and subchrons have a higher recording probability than shorter polarity intervals. Therefore, we suppose that core sections with prominent uniform polarity correspond to longer subchrons or chrons, whereas shorter subchrons and geomagnetic events were most likely not preserved.

The resultant age-depth models are depicted in Figure2. 9. Major polarity boundaries are denoted by capital letters. The accumulation rate between the polarity boundaries in the different scenarios is calculated for each possible variant in Table 2.2. Although uncorrected for compaction, the values illustrate the changes in sediment accumulation and are therefore indicative of the evolution of the subsidence in the Heidelberg Basin.
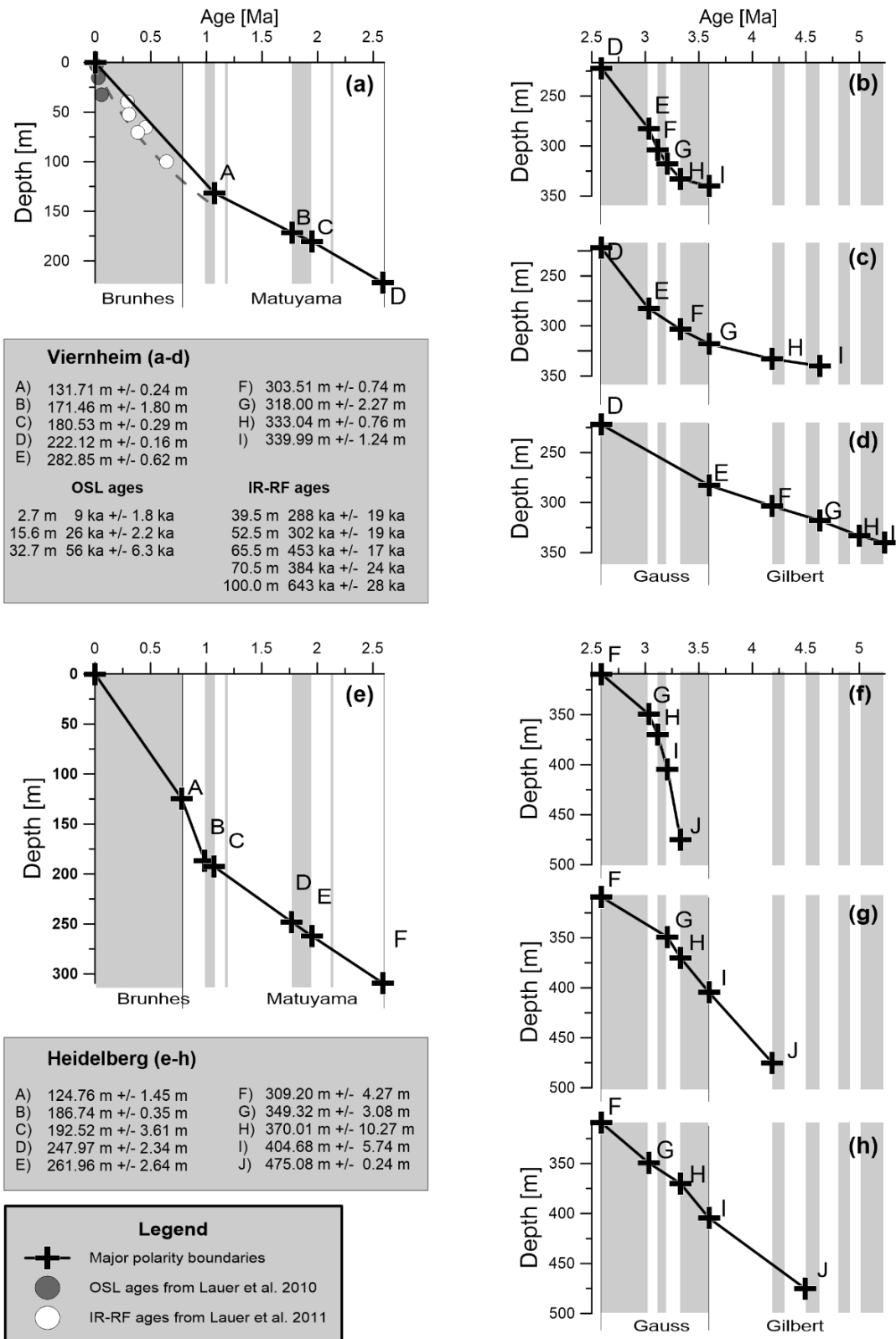
Figure 2.9:

Age-depth plots, constructed for the Viernheim and Heidelberg cores. The grey-white background in each plot refers to the GPTS. Major polarity boundaries are indicated by capital letters. The plots on the right-hand side show different scenarios for the Tertiary. The age-depth relationship of Quaternary time is depicted on the left-hand side. See text for discussion.

Table 2.2

The following tables present calculated accumulation rates (values in cm/ka). They are rotated 90° on the page and consist of several sub‑tables ("HEIDELBERG" and "VIERNHEIM", panels 8a–8h). Each is a matrix of accumulation rate between a starting boundary ("from …") and a "to" boundary.

HEIDELBERG (8a) [sections 8e / 8f]

cm/ka · to	from 0	A	B	C
A 15.97 ± 0.19	12.29 ± 0.02	from A	9.69 ± 0.10	9.26 ± 0.10
B 18.90 ± 0.87	29.94 ± 0.87	5.69 ± 0.29	from B	5.56 ± 0.06
C 17.96 ± 4.71	23.28 ± 4.71	6.87 ± 4.71	5.04 ± 1.16	from C
D 14.01 ± 0.85	12.46 ± 0.85	7.83 ± 0.34	7.94 ± 0.85	
E 13.43 ± 2.77	11.74 ± 2.77	7.82 ± 0.31	7.91 ± 0.71	
F 11.94 ± 1.08	10.20 ± 1.08	7.64 ± 0.29	7.69 ± 0.52	
G 11.52 ± 1.66	9.98 ± 1.66	7.95 ± 0.17	8.00 ± 0.34	
H 11.87 ± 15.88	10.50 ± 15.88	8.61 ± 0.50	8.68 ± 0.68	
I 12.62 ± 17.58	11.54 ± 17.58	9.82 ± 0.27	9.94 ± 0.44	
J 14.27 ± 4.85	13.74 ± 4.85	12.31 ± 0.02	12.51 ± 0.17	

VIERNHEIM (8b)

to	from D	from E	from F	from G	from H	from I
0	8.58 ± 0.01	9.33 ± 0.02	9.74 ± 0.02	9.92 ± 0.07	10.00 ± 0.02	9.45 ± 0.03
A	5.96 ± 0.03	7.71 ± 0.04	8.41 ± 0.05	8.73 ± 0.12	8.92 ± 0.04	8.25 ± 0.06
B	6.18 ± 0.24	8.83 ± 0.19	9.81 ± 0.19	10.20 ± 0.28	10.36 ± 0.16	9.23 ± 0.17
C	6.50 ± 0.07	9.46 ± 0.08	10.55 ± 0.09	10.94 ± 0.20	11.05 ± 0.08	9.69 ± 0.09
D	from D	13.74 ± 0.18	15.47 ± 0.17	15.54 ± 0.39	14.99 ± 0.12	11.72 ± 0.14
E	7.77 ± 2.77	from E	24.60 ± 1.62	20.09 ± 1.65	16.84 ± 0.46	10.13 ± 0.33
F	7.47 ± 0.81	7.38 ± 1.08	from F	15.92 ± 3.31	13.80 ± 0.70	7.60 ± 0.41
G	8.03 ± 0.43	8.07 ± 0.53	9.08 ± 1.66	from G	12.23 ± 3.31	5.65 ± 0.90
H	9.07 ± 0.94	9.27 ± 1.11	11.56 ± 2.76	12.23 ± 2.46	from H	2.61 ± 0.75
I	10.91 ± 0.44	11.35 ± 0.67	15.47 ± 1.62	24.63 ± 15.88	38.10 ± 17.58	from I
J	14.56 ± 0.17	15.44 ± 0.21	22.42 ± 0.61	42.20 ± 1.11	49.10 ± 4.91	57.24 ± 4.85

VIERNHEIM (8c)

cm/ka	E	F	G	H	I
0	9.33 ± 0.02	9.11 ± 0.06	8.84 ± 0.06	7.95 ± 0.02	7.34 ± 0.03
A	7.71 ± 0.04	7.61 ± 0.10	7.38 ± 0.10	6.46 ± 0.03	5.85 ± 0.04
B	8.83 ± 0.19	8.46 ± 0.22	8.03 ± 0.22	6.69 ± 0.11	5.89 ± 0.11
C	9.46 ± 0.08	8.91 ± 0.16	8.35 ± 0.16	6.82 ± 0.05	5.95 ± 0.06
D	13.74 ± 0.18	11.00 ± 0.24	9.53 ± 0.24	6.95 ± 0.06	5.78 ± 0.07
E	from E	6.93 ± 0.51	6.23 ± 0.51	4.35 ± 0.12	3.57 ± 0.12
F		from F	5.45 ± 1.13	3.45 ± 0.18	2.80 ± 0.15
G			from G	2.54 ± 0.51	2.12 ± 0.34
H				from H	1.57 ± 0.45
I					from I

VIERNHEIM (8d)

cm/ka	E	F	G	H	I
0	7.87 ± 0.02	7.25 ± 0.02	6.87 ± 0.02	6.66 ± 0.02	6.49 ± 0.02
A	5.99 ± 0.03	5.52 ± 0.03	5.23 ± 0.03	5.13 ± 0.03	5.00 ± 0.04
B	6.10 ± 0.13	5.46 ± 0.11	5.12 ± 0.11	5.01 ± 0.08	4.86 ± 0.09
C	6.22 ± 0.06	5.50 ± 0.05	5.13 ± 0.10	5.01 ± 0.03	4.85 ± 0.05
D	6.04 ± 0.08	5.10 ± 0.06	4.70 ± 0.12	4.61 ± 0.04	4.46 ± 0.05
E	from E	3.50 ± 0.23	3.40 ± 0.28	3.58 ± 0.10	3.49 ± 0.11
F		from F	3.26 ± 0.68	3.65 ± 0.19	3.48 ± 0.19
G			from G	4.11 ± 0.83	3.64 ± 0.58
H				from H	2.92 ± 0.84
I					from I

HEIDELBERG (8g)

to	from 0	A	B	C	D	E	F	G	H	I
G	10.89 ± 0.10	9.26 ± 0.19	7.33 ± 0.15	7.34 ± 0.31	7.05 ± 0.38	6.95 ± 0.45	6.50 ± 1.19	from G		
H	11.11 ± 0.31	9.62 ± 0.46	7.83 ± 0.45	7.86 ± 0.61	7.82 ± 0.81	7.83 ± 0.94	8.22 ± 1.96	16.82 ± 10.85	from H	
I	11.25 ± 0.16	9.94 ± 0.26	8.36 ± 0.23	8.41 ± 0.37	8.58 ± 0.44	8.67 ± 0.51	9.49 ± 0.99	14.23 ± 2.26	13.03 ± 6.02	from I
J	11.35 ± 0.01	10.29 ± 0.05	9.01 ± 0.02	9.07 ± 0.12	9.40 ± 0.11	9.53 ± 0.13	10.39 ± 0.28	12.83 ± 0.34	12.26 ± 1.23	11.91 ± 1.01

HEIDELBERG (8h)

to	from 0	A	B	C	D	E	F	G	H	I
G	11.52 ± 0.10	9.98 ± 0.20	7.95 ± 0.20	8.00 ± 0.34	8.03 ± 0.43	8.07 ± 0.53	9.08 ± 1.66	from G		
H	11.11 ± 0.31	9.62 ± 0.46	7.83 ± 0.45	7.86 ± 0.61	7.82 ± 0.81	7.83 ± 0.94	8.22 ± 1.96	6.94 ± 4.48	from H	
I	11.25 ± 0.16	9.94 ± 0.26	8.36 ± 0.23	8.41 ± 0.37	8.58 ± 0.44	8.67 ± 0.51	9.49 ± 0.99	9.82 ± 1.56	13.03 ± 6.02	from I
J	10.57 ± 0.01	9.44 ± 0.05	8.23 ± 0.02	8.26 ± 0.11	8.34 ± 0.09	8.38 ± 0.11	8.72 ± 0.24	8.61 ± 0.23	9.03 ± 0.90	7.85 ± 0.67

Table 2.2:

Calculated accumulation rates for the scenarios in Figure 2.9. The tables enable the accumulation rate between any detected major polarity boundaries to be calculated. The values are in units of cm/ka.

An application example: To read the accumulation rate between B in Figure 2.9e and H in Figure 2.9f, one starts at the white field 'from B' in the section of 'Heidelberg (2.9e)' and follows the column downwards to the line 'H' to find 8.61 ± 0.5 cm/ka. To read the accumulation rate between B in Figure 9a and H in Figure 2.9c from the table, one starts at the white field 'B' at the left-hand side of the 'Viernheim (2.9c)' table and follows the line to the right to the column 'H' to find 6.69 ± 0.11 cm/ka.

Figure 2.9a and 2.9e depict the age-depth relationship for the Quaternary sediments of the Viernheim and Heidelberg cores. The proposed solutions are in accordance with the established magnetostratigraphy, as set out above, and support the above assumptions. The OSL and IR-RF ages of Lauer et al. (2010; 2011) are also depicted in Figure 2.9a. The dashed line shows the average age-depth relationship that arises by considering these data. Compared with the lower sectors, the steeper sectors at the top can be interpreted as a periods of increased subsidence. Depending on the lithology, a decrease in the uncorrected accumulation rate could be caused by compaction.

For the Tertiary sediments, different age-depth relationships are displayed individually for Viernheim (Figure 2.9b-d) and Heidelberg (Figure 2.9f-h). Due to its temporal extent, the reversed period at the beginning of the Gilbert chron (C2Ar) is not expected to have been totally eroded. In considering all assumptions, the scenarios in Figure 2.9d and 2.9h appear to be the most plausible. These curves skip several subchrons of the GPTS and feature almost constant accumulation rates from the Pleistocene to the late Pliocene. Consequently, a few quite large hiatuses are needed to explain these figures. In these scenarios, maximum ages of 5.235 Ma and 4.493 Ma are obtained for the deepest parts of the Viernheim and Heidelberg cores, respectively.

The models 9c and 9g are still plausible but less likely with respect to our assumptions. The Viernheim scenario in 9c has an almost constant slope, but the Tertiary-Quaternary boundary is marked by an increase in the accumulation rate whereas the rate in the oldest section is very low. The Heidelberg scenario 9g is also characterised by a distinctive change in the accumulation rate and a subsequent gradual decline (Table 2.2). Higher accumulation rates could be interpreted as a result of increased subsidence and/or due to not yet recognised hiatuses. Nevertheless, both developments seem to be atypical for basins with more or less continuous subsidence like that in the Heidelberg Basin, as determined by the analysis of seismic reflection lines by Buness et al. (2008).

The solutions with the shortest possible time spans are the most unrealistic (Figures 2.9b and 2.9f). Here, the observed polarity changes are correlated with contiguous intervals of the GPTS. Tremendously higher accumulation rates would result from these solutions (Table 2.2). To explain these rates, the subsidence would need to have been fourfold and sevenfold higher than the rates calculated for the Middle and Upper Pleistocene, respectively. In addition, the subsidence would need to have levelled off suddenly at the end of the Gauss chron. Consequently, these latter solutions are not consistent with the determined assumptions. However, further evidence for the plausibility of hiatuses in the temporal order of subchrons is provided by this approach.

To limit the numbers of figures in this work, a few possible variants are not depicted in separate figures. The correlation of the points J among the plots 2.9g and 2.9h could, for example, be transposed. Therefore, the minimum age could be set at 4.187 Ma or 4.493 Ma for both scenarios.

Taken as a whole, the central message of the age-depth models would not be changed significantly by these or any other solution. We used the age-depth correlations for the selection of the most likely age-depth model and have shown that there is a high plausibility for minimum ages of >5.235 Ma and >4.187 Ma for the deepest sections of the Viernheim and Heidelberg cores, respectively. In our opinion, a detailed prediction of the age using the method of magnetic polarity stratigraphy is not possible for the lower parts of the cores.

Even though the relatively new method of burial dating using cosmogenic nuclides produces large uncertainties in complex fluvial environments (Dehnert and Schlüchter, 2008; Matmon et al., 2012), future work could use $^{26}Al/^{10}Be$ dating. For example, Dehnert et al. (2011) provided consistent age estimates for fluvial sediments from the Lower Rhine Embayment in Germany. A combination of the results of burial dating and magnetic polarity stratigraphy would certainly yield valuable results.

2.10.   Conclusions

We show the fluvial sediments of the Heidelberg Basin were able to preserve the ancient geomagnetic field through geologic time. The carriers of the remanent magnetisation changed over time and depend on lithofacies. Generally, maghemite and/or magnetite are uncommonly the remanence carriers. The Iffezheim Formation is dominated by high-coercivity minerals (haematite, goethite), whereas the younger formations are characterised by sulphides (most likely greigite).

The Gauss-Matuyama boundary is clearly defined by changes in polarity in all three cores. The Matuyama-Brunhes boundary is undoubtedly detectable in the Heidelberg core. Its position in the Viernheim and Ludwigshafen cores can be roughly estimated from its relative position with respect to the lithostratigraphic boundaries. The subchrons of Jaramillo (C1r.1n) and Olduvai (C2n) are identified with a high probability. The major remaining uncertainty concerns the correlation of the sectors below the Gauss-Matuyama boundary. Age-depth plots suggest that the Heidelberg and Viernheim cores include the Gilbert Chron. Minimum ages of >5.235 Ma and >4.187 Ma are highly plausible for the base of the Viernheim and Heidelberg cores, respectively. The large-scale correlations should not be affected by small inaccuracies. The calculated accumulation rates of the most plausible models are on the order of 5.7-29.9 and 2.9-13.0 cm/ka in the Quaternary and Tertiary, respectively.   These accumulation rates allow a quantification of the basin subsidence over timescales of ca. ≥ 1 Ma.

The obtained magnetic polarity stratigraphy provides the first exclusively palaeomagnetically based chronostratigraphic framework for the sequences of the northern URG and for fluvial Plio-Pleistocene sequences in western central Europe in general. This will enable consistent future correlation across central Europe. The change in magneto-mineralogy near to the Gauss-Matuyama boundary is an important proxy for the environmental (climatic) changes at approximately 2.58 Ma.

As already noted by Rolf et al. (2008), this worldwide climate change is marked by the initiation of Northern Hemisphere glaciation and is well documented in deep-sea sediments (Shackelton et al., 1984) and loess deposits in China (Heller and Liu, 1982). Further advances in the knowledge of superregional geological and palaeoclimatic developments can be expected from, for example, the correlation with the Plio/Pleistocene sites in the North Sea Basin (Zagwijn 1985; Maher and Hallam, 2005b, Westerhoff et al., 2008), the Pannonian Basin (Nádor et al., 2003) and the Po-Basin (Muttoni et al., 2007; Scardia et al., 2006).

Acknowledgements

References

APPEL, E., RÖSLER, W. and CORVINUS, G., 1991. Magnetostratigraphy of the Miocene-Pleistocene Surai Khola Siwaliks in west Nepal. Geophysical Journal International, 105(1), 191-198.

BARTZ, J., 1953. Revision des Bohr-Profils der Heidelberger Radium-Sol-Therme. Jahresberichte und Mitteilungen des Oberrheinischen Geologischen Vereins, 101-125.

BARTZ, J., 1974. Die Mächtigkeit des Quartärs im Oberrheingraben. In: J.H. Illies and K. Fuchs (Eds.), Approaches to Taphrogenesis. Schweizerbart, Stuttgart, pp. 78-87.

BISWAS, D.K. et al., 1999. Magnetostratigraphy of Plio-Pleistocene sediments in a 1700-m core from Osaka Bay, southwestern Japan and short geomagnetic events in the middle Matuyama and early Brunhes chrons. Palaeogeography, Palaeoclimatology, Palaeoecology, 148(4), 233-248.

BLEIL, U. and VON DOBENECK, T., 1999. Geomagnetic events and relative paleointensity records - Clues to high resolution paleomagnetic chronostratigraphies of Late Quaternary marine sediments? In: G. Fischer and G. Wefer (Eds.), Use of proxies in paleoceanography: Examples from the South Atlantic. Springer Verlag, Berlin, pp. 635-665.

BUNESS, H., GABRIEL, G. and ELLWANGER, D., 2008. The Heidelberg Basin drilling project: Geophysical pre-site surveys. E & G (Quaternary Science Journal), 57(3/4), 338-366.

CANDE, S.C. and KENT, D.V., 1995. Revised calibration of the geomagnetic polarity timescale for the Late Cretaceous and Cenozoic. Journal of Geophysical Research: Solid Earth, 100(B4), 6093-6095.

CHADIMA, M. and HROUDA, F., 2006. Remasoft 3.0 a user-friendly paleomagnetic data browser and analyzer. Travaux Géophysiques, 27, 20-21.

COX, A., DOELL, R.R. and DALRYMPLE, G.B., 1963. Geomagnetic polarity epochs and Pleistocene geochronometry. Nature, 198(4885), 1049-1051.

COX, A., DOELL, R.R. and DALRYMPLE, G.B., 1964. Reversals of the earth's magnetic field. Science, 144(3626), 1537-1543.

DEAMER, G.A. and KODAMA, K.P., 1990. Compaction-induced inclination shallowing in synthetic and natural clay-rich sediments. Journal of Geophysical Research: Solid Earth, 95(B4), 4511-4529.

DEHNERT, A. and SCHLÜCHTER, C., 2008. Sediment burial dating using terrestrial cosmogenic nuclides. E & G (Quaternary Science Journal), 57, 210-225.

DEHNERT, A. et al., 2011. Cosmogenic isotope burial dating of fluvial sediments from the Lower Rhine Embayment, Germany. Quaternary Geochronology, 6(3–4), 313-325.

DOEBEL, F., 1967. The Tertiary and Pleistocene sediments of the northern and central part of the Upper Rhinegraben. Abhandlungen des Geologischen Landesamt Baden-Württemberg, 6, 7.

DOEBEL, F. and OLBRECHT, W., 1974. An isobath map of the Tertiary base in the Rhinegraben. In: J.H. Illies and K. Fuchs (Eds.), Approches to Taphrogenesis. Schweizerbart, Stuttgart, Germany, pp. 71-72.

ELLWANGER, D. and WIELAND-SCHUSTER, U., 2012. Fotodokumentation und Schichtenverzeichnis der Forschungsbohrungen Heidelberg UniNord I und II. LGRB-Informationen, 26, 25-86.

ELLWANGER, D. et al., 2008. Long sequence of Quaternary Rocks in the Heidelberg Basin Depocentre. E & G (Quaternary Science Journal), 57(3/4), 316-337.

ELLWANGER, D., GABRIEL, G., HOSELMANN, C., WEIDENFELLER, M. and WIELANDT-SCHUSTER, U., 2010a. Mannheim-Formation, Litholex (online database). Federal Institute for Geosciences and Natural Resources (BGR), http://www.bgr.bund.de/litholex.

ELLWANGER, D. et al., 2010b. Iffezheim-Formation, Litholex (online database). Federal Institute for Geosciences and Natural Resources (BGR), http://www.bgr.bund.de/litholex.

ELWERATH_ERDGAS_UND_ERDÖL_GMBH, 1953. ERDOEL-, ERDGAS-, AUFSCHLUSSBOHRUNG SCHRIESHEIM-1, 1953. The Federal Institute for Geosciences and Natural Resources (BGR = Bundesanstalt für Geowissenschaften und Rohstoffe), Archive Hannover.

FASSBINDER, J.W. and STANJEK, H., 1994. Magnetic properties of biogenic soil greigite (Fe_3S_4). Geophysical Research Letters, 21(22), 2349-2352.

FEZER, F., 1997. 220 m Altpleistozän im Heidelberger Loch. E & G (Quaternary Science Journal), 47, 145-153.

GABRIEL, G., ELLWANGER, D., HOSELMANN, C. and WEIDENFELLER, M., 2008. Preface: The Heidelberg Basin Drilling Project. E & G (Quaternary Science Journal), 57(3/4), 253-260.

GABRIEL, G., ELLWANGER, D., HOSELMANN, C., WEIDENFELLER, M. and WIELANDT-SCHUSTER, U., 2013. The Heidelberg Basin, Upper Rhine Graben (Germany): A unique archive of Quaternary sediments in Central Europe. Quaternary International, 292, 43-58.

GIBBARD, P. and LEWIN, J., 2009. River incision and terrace formation in the Late Cenozoic of Europe. Tectonophysics, 474(1), 41-55.

HAGEDORN, E.-M. and BOENIGK, W., 2008. The Pliocene and Quaternary sedimentary and fluvial history in the Upper Rhine Graben based on heavy mineral analyses. Netherlands Journal of Geosciences, 87(1), 19-30.

HAHNE, J., ELLWANGER, D. and STRITZKE, R., 2008. Evidence for a Waalian thermomer pollen record from the research borehole Heidelberg UniNord, Upper Rhine Graben, Baden-Württemberg. E & G (Quaternary Science Journal), 57(3/4), 403-410.

HELLER, F. and LIU, T.-S., 1982. Magnetostratigraphical dating of loess deposits in China. Nature, 300(5891), 431-433.

HORNG, C.-S., TORII, M., SHEA, K.-S. and KAO, S.-J., 1998. Inconsistent magnetic polarities between greigite- and pyrrhotite/magnetite-bearing marine sediments from the Tsailiao-chi section, southwestern Taiwan. Earth and Planetary Science Letters, 164(3–4), 467-481.

HOSELMANN, C., 2008. The Pliocene and Pleistocene fluvial evolution in the northern Upper Rhine Graben based on results of the research borehole at Viernheim (Hessen, Germany). E & G (Quaternary Science Journal), 57(3/4), 286-315.

HOSELMANN, C., ELLWANGER, D., GABRIEL, G., WEIDENFELLER, M. and WIELANDT-SCHUSTER, U., 2010. Viernheim-Formation, Litholex (online database). Federal Institute for Geosciences and Natural Resources (BGR), http://www.bgr.bund.de/litholex.

JOHNSON, N.M., JORDAN, T.E., JOHNSSON, P.A. and NAESER, C.W., 1986. Magnetic polarity stratigraphy, age and tectonic setting of fluvial sediments in an eastern Andean foreland basin, San Juan Province, Argentina. Foreland basins, 63-75.

JORDANOVA, D., JORDANOVA, N., PETROV, P. and TSACHEVA, T., 2010. Soil development of three Chernozem-like profiles from North Bulgaria revealed by magnetic studies. Catena, 83(2), 158-169.

KELLER, H.M. et al., 1977. Magnetic polarity stratigraphy of the Upper Siwalik deposits, Pabbi Hills, Pakistan. Earth and Planetary Science Letters, 36(1), 187-201.

KEMNA, H., 2008. A Revised Stratigraphy for the Pliocene and Lower Pleistocene Deposits of the Lower Rhine Embayment. Netherlands Journal of Geosciences, 87(1), 91-105.

KIRSCHVINK, J., 1980. The least-squares line and plane and the analysis of palaeomagnetic data. Geophysical Journal International, 62(3), 699-718.

KNIPPING, M., 2008. Early and Middle Pleistocene pollen assemblages of deep core drillings in the northern Upper Rhine Graben, Germany. Netherlands Journal of Geosciences, 87(1), 51-65.

KODAMA, K.P., 1982. Magnetic effects of maghemitization of Plio-Pleistocene marine sediments, northern California. Journal of Geophysical Research: Solid Earth (1978–2012), 87(B8), 7113-7125.

LAJ, C. and CHANNELL, J.E., 2007. Geomagnetic Excursions. In: G. Schubert (Ed.), Treatise on Geophysics. Elsevier, Amsterdam, pp. 373-416.

LAUER, T., FRECHEN, M., HOSELMANN, C. and TSUKAMOTO, S., 2010. Fluvial aggradation phases in the Upper Rhine Graben—new insights by quartz OSL dating. Proceedings of the Geologists' Association, 121(2), 154-161.

LAUER, T. et al., 2011. Infrared radiofluorescence (IR-RF) dating of middle pleistocene fluvial archives of the Heidelberg Basin (Southwest Germany). Geochronologia, 38(1), 23–33.

LEWIN, J. and MACKLIN, M.G., 2003. Preservation potential for Late Quaternary river alluvium. Journal of Quaternary Science, 18(2), 107-120.

LØVLIE, R., STØLE, G. and SPJELDNÆS, N., 1989. Magnetic polarity stratigraphy of Pliocene-Pleistocene marine sediments from Rhodos, eastern Mediterranean. Physics of The Earth and Planetary Interiors, 54(3), 340-352.

LOWRIE, W., 1990. Identification of ferromagnetic minerals in a rock by coercivity and unblocking temperature properties. Geophysical Research Letters, 17(2), 159-162.

MAHER, B.A. and HALLAM, D.F., 2005a. Magnetic carriers and remanence mechanisms in magnetite-poor sediments of Pleistocene age, southern North Sea margin. Journal of Quaternary Science, 20(1), 79-94.

MAHER, B.A. and HALLAM, D.F., 2005b. Palaeomagnetic correlation and dating of Pli/Pleistocene sediments at the southern margins of the North Sea Basin. Journal of Quaternary Science, 20(1), 67-77.

MATMON, A., STOCK, G.M., GRANGER, D.E. and HOWARD, K.A., 2012. Dating of Pliocene Colorado River sediments: Implications for cosmogenic burial dating and the evolution of the lower Colorado River. Geological Society of America Bulletin, 124(3-4), 626-640.

MUTTONI, G. et al., 2007. Magnetostratigraphic dating of an intensification of glacial activity in the southern Italian Alps during Marine Isotope Stage 22. Quaternary Research, 67(1), 161-173.

NÁDOR, A., LANTOS, M., TÓTH-MAKK, Á. and THAMÓ-BOZSÓ, E., 2003. Milankovitch-scale multi-proxy records from fluvial sediments of the last 2.6 Ma, Pannonian Basin, Hungary. Quaternary Science Reviews, 22(20), 2157-2175.

NILSSON, A., LEE, Y.S., SNOWBALL, I. and HILL, M., 2013. Magnetostratigraphic importance of secondary chemical remanent magnetizations carried by greigite (Fe_3S_4) in Miocene sediments, New Jersey shelf (IODP Expedition 313). Geosphere, 9(3), 510-520.

OGG, G., 2012. Geomagnetic Polarity Time Scale. In: F.M. Gradstein, G. Ogg and M.D. Schmitz (Eds.), The Geologic Time Scale 2012 2-Volume Set. Elsevier.

OGG, J.G., OGG, G. and GRADSTEIN, F.M., 2008. The concise geologic time scale, 1.

OPDYKE, N.D. and CHANNELL, J. (Eds.), 1996. Magnetic Stratigraphy. International Geophysics Series, 64. Academic Press, Inc., San Diego, 346 pp.

ÖZDEMIR, Ö. and BANERJEE, S.K., 1984. High temperature stability of maghemite (γ-Fe2O3). Geophysical Research Letters, 11(3), 161-164.

PAN, B., HU, Z., WANG, J., VANDENBERGHE, J. and HU, X., 2011. A magnetostratigraphic record of landscape development in the eastern Ordos Plateau, China: Transition from Late Miocene and Early Pliocene stacked sedimentation to Late Pliocene and Quaternary uplift and incision by the Yellow River. Geomorphology, 125(1), 225-238.

ROBERTS, A.P. and WEAVER, R., 2005. Multiple mechanisms of remagnetization involving sedimentary greigite (Fe3S4). Earth and Planetary Science Letters, 231(3-4), 263-277.

ROBERTS, A.P. and WINKLHOFER, M., 2004. Why are geomagnetic excursions not always recorded in sediments? Constraints from post-depositional remanent magnetization lock-in modelling. Earth and Planetary Science Letters, 227(3-4), 345-359.

ROLF, C., 2000. Das Kryogenmagnetometer im Magnetiklabor Grubenhagen. Geologisches Jahrbuch, E52, 161-188.

ROLF, C., HAMBACH, U. and WEIDENFELLER, M., 2008. Rock and palaeomagnetic evidence for the Plio-Pleistocene palaeoclimatic change recorded in Upper Rhine Graben sediments (Core Ludwigshafen Parkinsel). Netherlands Journal of Geosciences, 87(1), 41-50.

SALOMON, W., 1927. Die Erbohrung der Heidelberger Radium-Sol-Therme und ihre geologischen Verhältnisse. Abhandlungen der Heidelberger Akademie der Wissenschaften, 14, 1-105.

SCARDIA, G., MUTTONI, G. and SCIUNNACH, D., 2006. Subsurface magnetostratigraphy of Pleistocene sediments from the Po Plain (Italy): Constraints on rates of sedimentation and rock uplift. Geological Society of America Bulletin, 118(11-12), 1299-1312.

SCHUMACHER, M.E., 2002. Upper Rhine Graben: Role of preexisting structures during rift evolution. Tectonics, 21(1), 6-1-6-17.

SHACKLETON, N.J. et al., 1984. Oxygen isotope calibration of the onset of ice-rafting and history of glaciation in the North Atlantic region. Nature, 307(5952), 620-623.

SMYKATZ-KLOSS, W., 1974. Influence of the Chemical Composition on the Curie-Temperatures of Magnetites, Differential Thermal Analysis: Application and Results in Mineralogy. Minerals and Rocks. Springer Berlin Heidelberg, Berlin, Heidelberg, pp. 118-122.

SNOWBALL, I., 1997. Gyroremanent magnetization and the magnetic properties of greigite-bearing clays in southern Sweden. Geophysicsical Journal International, 129, 624-636.

SPASSOV, S., HELLER, F., EVANS, M.E., YUE, L.P. and VON DOBENECK, T., 2003. A lock-in model for the complex Matuyama-Brunhes boundary record of the loess/palaeosol sequence at Lingtai (Central Chinese Loess Plateau). Geophysical Journal International, 155(2), 350-366.

SUN, D., AN, Z., SHAW, J., BLOEMENDAL, J. and SUN, Y., 1998. Magnetostratigraphy and palaeoclimatic significance of Late Tertiary aeolian sequences in the Chinese Loess Plateau. Geophysical Journal International, 134(1), 207-212.

TARLING, D.H., 1983. Magnetic mineralogy and magnetic identification of minerals, Palaeomagnetism. Springer, pp. 35-50.

TORII, M., FUKUMA, K., HORNG, C.S. and LEE, T.Q., 1996. Magnetic discrimination of pyrrhotite-and greigite-bearing sediment samples. Geophysical Research Letters, 23(14), 1813-1816.

VAN BAAK, C. et al., 2013. A magnetostratigraphic time frame for Plio-Pleistocene transgressions in the South Caspian Basin, Azerbaijan. Global and Planetary Change, 103, 119-134.

VAN MONTFRANS, H.M., 1971. Palaeomagnetic dating in the North Sea basin. Earth and Planetary Science Letters, 11(1), 226-235.

VASILIEV, I. et al., 2008. Putative greigite magnetofossils from the Pliocene epoch. Nature Geoscience, 1(11), 782-786.

VINCENT, E., WRIGHT, J., CHEVALLIER, R. and MATHIEU, S., 1957. Heating experiments on some natural titaniferous magnetites. Mineral. Mag, 31(239), 624-655.

WEDEL, J., 2008. Pleistocene molluscs from research boreholes in the Heidelberg Basin. E & G (Quaternary Science Journal), 57(3/4), 382-402.

WEIDENFELLER, M., ELLWANGER, D., GABRIEL, G., HOSELMANN, C. and WIELANDT-SCHUSTER, U., 2010. Ludwigshafen-Formation, Litholex (online database). Federal Institute for Geosciences and Natural Resources (BGR), http://www.bgr.bund.de/litholex.

WEIDENFELLER, M. and KNIPPING, M., 2008. Correlation of Pleistocene sediments from boreholes in the Ludwigshafen area, western Heidelberg Basin. E & G (Quaternary Science Journal), 57(3/4), 270-285.

WESTERHOFF, W., KEMNA, H. and BOENIGK, W., 2008. The confluence area of Rhine, Meuse, and Belgian rivers: Late Pliocene and Early Pleistocene fluvial history of the northern lower Rhine Embyment. Netherlands Journal of Geosciences, 87(1), 107-125.

ZAGWIJN, W., 1957. Vegetation, climate and time-correlations in the early Pleistocene of Europe. Geologie en Mijnbouw, 19, 233-244.

ZAGWIJN, W., 1963. Pollen-analytic investigations in the Tiglian of the Netherlands. Meded. Geol. Sticht. , N.S. 16, 49-71.

ZAGWIJN, W., 1985. An outline of the Quaternary stratigraphy of the Netherlands. Geologie en Mijnbouw, 64(1), 17-24.

ZIJDERVELD, J., 1967. AC demagnetization of rocks: analysis of results. Methods in paleomagnetism, 3, 254.

ZIJDERVELD, J., COLLINSON, D., CREER, K. and RUNCORN, S., 1967. AC demagnetization of rocks: analysis of results. Methods in paleomagnetism, 1, 254-286.

Remarks to study 1

The magnetic polarity stratigraphy of the Heidelberg core contradicts the results of the pollen stratigraphy published by (Hahne et al., 2008, 2012) but is in line with the pollen analysis of core P36 (performed by Dr. Knipping, University of Hohenheim, pers. com.) and the Viernheim core (performed by Dr. Heumann, University of Bonn, pers. com.). The data obtained from palynological analyses, heavy mineral analyses and the magnetic polarity stratigraphy were viewed and compared in a meeting at the University of Bonn at the beginning of 2014. The palynologists (Dr. Knipping, Dr. Heumann, and Dr. Hahne), a geologist and heavy mineral specialist (Dr. Hoselmann from the geological survey of Hesse), and I discussed these topics, and the discussion was moderated by Prof. Dr. Litt. During the meeting, the difference between the ages obtained by pollen analysis of the Heidelberg core and the remaining age results was found to represent a matter of interpretation, and a consensus was reached. Two weeks after this meeting, scientists from the geological survey of Baden-Wuertemberg informed the group that the consensus was invalid because certain arguments were not applied by Dr. Hahne. To the authors' knowledge, this disagreement remains to the present day, though no further work on this question has yet been published. The question of the stratigraphic classification is thus summarised in section 4.4.

3. Study 2: A mineral magnetic characterization of the Plio-Pleistocene fluvial infill of the Heidelberg Basin (Germany)

Stephanie Scheidt[1, 2], Ramon Egli[3], Thomas Frederichs[4], Ulrich Hambach[2, 5, 6], Christian Rolf[1]

[1]Leibniz Institute for Applied Geophysics, 30655 Hannover, Germany

[2]Chair of Geomorphology, University of Bayreuth, 95440 Bayreuth, Germany

[3]Central Institute for Meteorology and Geodynamics, 1190 Vienna, Austria

[4]Faculty 5 Geosciences, University of Bremen, 28334 Bremen, Germany

[5]BayCEER, University of Bayreuth, 95440 Bayreuth, Germany

[6]Laboratory for Palaeoenvironmental Reconstruction, Faculty of Sciences, University of Novi Sad, Serbia

Corresponding author: Stephanie Scheidt

Summary

The Heidelberg Basin (Germany) hosts a quasi-continuous sedimentary sequence of primarily fluvial sediments with pedogenetic overprints and lacustrine intercalations. This unconsolidated succession has been shown to record a consistent magnetic polarity stratigraphy of the Quaternary and the late Neogene. Previous work has reported that sulphides and high-coercive minerals are the carriers of the remanent magnetisation. Here, we provide the results of an extended mineral magnetic study that aims to disentangle the complex magnetic mineralogy. In addition, we assess the reliability of these minerals as carriers of palaeomagnetic signals. A major obstacle to the analysis of the drill cores was the large number of samples that were taken from a total core length of 1150 m. Rapid measurements on bulk samples provided only limited information on the magnetic mineralogy. In contrast, time-intensive methods such as first order reversal curves (FORC) or coercivity analyses, for example, yielded valuable information. The combined results of all the analyses consider the heterogeneous compositions of the sediments and indicate a varying palaeoenvironmental history. The Pliocene Iffezheim Formation was formed under alternating reducing and oxidising conditions. Magnetite, maghemite, haematite and goethite are the predominant magnetic minerals. Sulphides were only preserved under specific conditions. The Pleistocene sediments reflect predominantly reducing conditions during sedimentation and diagenesis. Greigite, pyrite and most likely pyrrhotite have been shown to occur. Taken together, our work provides a detailed environmental magnetic record of the Plio-Pleistocene and elucidates the capabilities and limitations of rock magnetic studies performed on fluvial dominated sedimentary successions.

Key words

Environmental magnetism; magnetic mineralogy and petrology; rock and mineral magnetism; Europe

3.1. Introduction

Rock magnetic analyses of sediment deposits represent well-established techniques for reconstructing environmental processes. A large number of studies used these techniques to examine deep-sea sediments (Robinson, 1986; Bloemendal et al., 1992), loess (Heller and Liu, 1986; Liu et al., 1993; Liu et al., 2007) and lacustrine sediments (Dearing, 1999; Nowaczyk, 2011). In many cases, these sediments contain well-defined magnetic mineral components and provide a minimum degree of continuity and relatively monotonous sedimentation mechanisms in (long-term) stable environments. An increasing number of studies on more complex systems have emerged during the last few decades. Such systems include tectonically disturbed sequences, sediments with unusual magnetic mineral assemblages, and remagnetised or diagenetically overprinted rocks (e.g., Hallam and Maher, 1994; Hounslow, 1996; Biswas et al., 1999; Maher and Hallam, 2005; Horng and Roberts, 2006; Rowan and Roberts, 2006; Lucifora et al., 2012). Despite these advances, unconsolidated fluvial sediments are still seldom the focus of rock magnetic research. Fluvial deposits are characterised by laterally and vertically irregular distributions of sedimentary bodies with interposed hiatuses of unknown duration. Variations in the primary mineralogical composition of fluvial sediments are influenced by a wide variety of factors, including changes in source areas, changes in the size and base level of the river catchment and the number of tributaries it contains, and regional subsidence. Additionally, erosion, abrasion, inundation, and transportation processes have direct effects on the sedimentary architecture and composition of deposits (Miall 2013). Further, hydrological conditions and climatic aspects, particularly seasonal variations, can lead to cyclic changes in sediment input and to alternations between oxidising and reducing conditions. Finally, in situ weathering and diagenesis affect sedimentary bodies and can cause the (partial) dissolution and alteration of existing magnetic components, as well as the formation of new minerals (Roberts, 2015). Therefore, natural fluvial sediments contain heterogeneous mixtures of magnetic minerals and display small-scaled variations in the temporal and spatial distribution patterns. Despite the considerable complexity of fluvial deposits, a small number of magnetostratigraphic and palaeomagnetic studies have demonstrated that meaningful results can be obtained (e.g., Johnson et al., 1986; Hounslow et al., 1995; Kempf et al., 1999; Scardia et al., 2006; Scheidt et al., 2015).

In this article, we present the results of a detailed rock magnetic analysis of fluvial sediments from the Heidelberg Basin, which hosts one of the thickest continental Plio-Pleistocene sedimentary successions in central Europe (Gabriel et al., 2008). A magnetostratigraphic age model for this basin has been obtained by Scheidt et al. (2015) from simple piecewise linear interpolation of age tie points corresponding to magnetic polarity changes. In this paper, we present the results of detailed rock magnetic investigations of 1150 m of core material from three sites, based on hysteresis and FORC

measurements and high-temperature measurements, as well as principal component analyses of isothermal remanent magnetisation (IRM) acquisition curves. The rock magnetic measurements are complemented by scanning electron microscopy (SEM) and energy-dispersive X-ray microanalysis (EDX). To our knowledge, this is the first integrated study of such an extensive set of samples from fluvial sediments, and it provides deeper insight into the magnetic mineralogy of unconsolidated riverine deposits. Furthermore, the results of this study support the magnetostratigraphic model of Scheidt et al. (2015), providing a solid base for a model of Pliocene and Pleistocene palaeo-environmental evolution within the region (Scheidt et al. in preparation).

3.2. Geological setting, cores and samples

The Heidelberg Basin is part of the northern Upper Rhine Graben in Germany. Continuous subsidence started in the late Oligocene (Schumacher, 2002) and led to accumulation of sedimentary sequences that are more than 2000 m in thickness at the location of the modern city of Heidelberg (Buness et al., 2008). During the evolution of the Rhine River system and its predecessors, the course of the river and its channel types changed through a complex interplay of tectonic processes and climatic influences (Preusser, 2008). Information on this evolution is archived in the sedimentary successions. In this study, we examine drill core material from three locations within the Heidelberg Basin. The coring sites correspond to the centre of subsidence of the basin (Heidelberg), the western margin (Ludwigshafen) and the geographic centre of the basin (Viernheim). Each core contains four lithostratigraphic units (Fig. 3.1), which are described below.

The lowermost Iffezheim Formation (IFm) was deposited during the Pliocene. The sediments were supplied by the adjacent Variscan massifs; thus, the heavy mineral assemblage is dominated by zircon, rutile-anatase, and tourmaline (Hagedorn & Boenigk 2008, Hoselmann 2008). The mottled reddish, orange and light grey colours of these rocks indicate oxidised fluvial floodplain deposits that were primarily deposited under reducing conditions (Bown & Kraus 1987, Kraus, 1999, 2002). The presence of pisolites and root beds is consistent with pedogenesis in a subtropical climate that experienced pronounced summer droughts. A sudden increase in unstable heavy minerals (garnet, epidote, and hornblende) accompanied by calcareous material and frequently coarser sediments is attributed to the connection of the Alpine drainage system to the Rhine (Hagedorn, 2004; Hagedorn and Boenigk, 2008; Preusser, 2008). The onset of this alpine mineral suite marks the lower boundary of the overlying lithostratigraphic formation, the Viernheim Formation (VFm) (Hoselmann et al. 2010). The change in the heavy mineral assemblage was established by Bartz (1959, 1976) and Bartz et al. (1982) as representing the Plio-Pleistocene boundary.
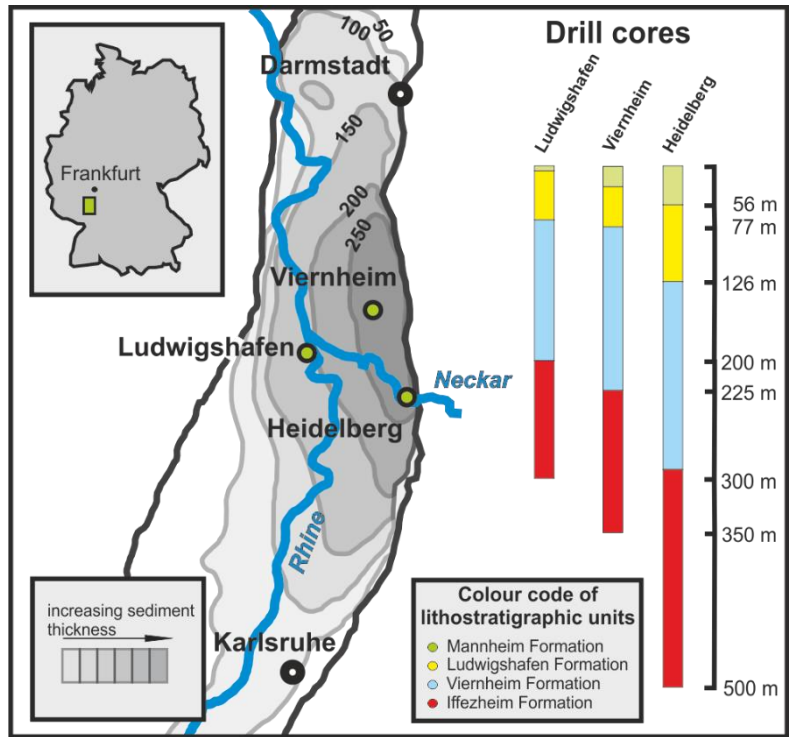
Figure 3.1:
Simplified map of the northern Upper Rhine Graben, including information on the thickness of the Quaternary sedimentary fill and the location of the coring sites (green dots; redrawn after Bartz 1974). Inset map shows the location of the basin in Germany (green square). The bars on the right-hand side of the figure illustrate the lengths of the cores and the relative proportions of the respective litho-stratigraphic units.

However, it was clarified by recent work of Scheidt et al. (2015) that the magnetic polarity change from the normal Gauss chron to the reversed Matuyama chron occurred prior to the connection of the Alpine drainage system at the top of the IFm. The pelitic strata of the IFm continue into the overlying VFm. Gradually increasing proportions of intercalated greyish fluvial sands, followed by beige and light to dark grey silts and sands, suggest a change in the hydrological regime. After the transition, a persistent high water table prevented the diagenesis and pedogenesis that would have occurred under oxidising conditions (Rolf et al. 2008). The third unit, the Ludwigshafen Formation (LFm), also consists mainly of silts and sands, as well as thin layers of peat. The Mannheim Formation (MFm), which is the uppermost unit, is composed partly of massive sequences of sand to coarse-grained gravel (Hoselmann, 2008; Weidenfeller and Knipping, 2008; Przyrowski and Schäfer, 2015). A detailed description and exact definition of the lithostratigraphic units is given in the German Litholex (Ellwanger et al., 2010a; Ellwanger et al., 2010b; Hoselmann et al., 2010; Weidenfeller et al., 2010). It should be noted that local conditions cause variations in the lithostratigraphic units between different sites. Whilst the Viernheim and P36 cores are macroscopically similar, the influence of the Neckar alluvial fan produced prominent features in the Heidelberg core. Within the Quaternary part of the

core, these include coarser grain sizes, different mineral compositions, and horizons dominated by reddish sediments that are derived from nearby outcrops of Lower Triassic sandstone (Simon 2012).

A sedimentological description of the Viernheim and Heidelberg cores can be found in Hoselmann (2008) and Ellwanger and Wieland-Schuster (2012), respectively, whereas a sedimentological microanalysis of the Mannheim Formation of the Heidelberg core has been published by Menzies and Ellwanger (2015). A detailed description of the Ludwigshafen Parkinsel P36 core is still lacking. Information on the sister cores P34 and P35 is available in Hagedorn (2004), Hagedorn and Boenigk (2008), Wedel (2008), Weidenfeller and Knipping (2008) and Westerhoff et al. (2008). General information on the sedimentary source areas of the (Palaeo-)Rhine is provided by Reiter et al. 2015 and Tatzel et al. 2015. The recently published depositional model of the northern Upper Rhine Graben by Przyrowski and Schäfer (2015) provides a fluvial facies model that shows the sedimentological composition and the fluvial cyclicity of the sediments of the Heidelberg Basin. However, their 'geohistory curve' is not consistent with the established magnetostratigraphy (Scheidt et al., 2015).

3.2.1. The Viernheim drill core

The site of the Viernheim drill core, which was obtained in 2006, is located in the Hessian Ried (Buchner-Schneise), approximately 3 km north of the city of Viernheim (N 49.565916 E 8.571516 (WGS84)). The core is enclosed in liners over its entire length of 350 m. The liners and cores were cut into 1-m pieces, which were subsequently bisected. The working halves were stored unwrapped to enable natural desiccation. Cubic specimens with a volume of ~10 cm^3 were collected at ~50 cm intervals. Interesting sections identified by visual inspection were sampled at a closer spacing. Sections consisting of medium-grained sand were sampled by cutting cylindrical samples with a diameter of 2.54 cm (1 inch) perpendicular to the core axis. Coarse sandy and gravelly sections were generally not sampled. Additional core material was taken for magnetic extractions (section 2.4) at ~10-m intervals.

3.2.2. The Heidelberg drill core

The Heidelberg site includes two cores collected from sites that are close to one another in the city of Heidelberg. The first drilling project (UniNord 1) stopped at a depth of ~190 m in 2006 (N 49.424992 E 8.663045 (WGS84)). A second drill core (UniNord 2), which is located ~260 m from the first core, was obtained in 2008 (N 49.427255 E 8.662037 (WGS84)). During the second drilling project, core was retrieved between 113 m and 114 m and from 184 m to the final depth of 500 m. The congruity of the two Heidelberg drill cores was demonstrated by the negligible (~1-m) offset between corresponding magnetostratigraphic signatures related to the Jaramillo subchron (Scheidt et al., 2015). Therefore, it was possible to merge the data obtained from the two cores into a single continuous sequence with a total length of 500 m.

Sampling of the Heidelberg cores, which were also enclosed in liners, was performed as described in section 2.1, including additional material for magnetic extractions.

3.2.3. The Ludwigshafen drill core

Several drill cores are available from groundwater exploration boreholes in the city of Ludwigshafen (N 49.469115 E 8.461574 (WGS84)). We focus on core P36, which reached a final depth of 301 m in 2009. Like the other cores, P36 was entirely enclosed in liners. The dried working half of the bisected core was sampled at 0.5-m intervals in 2012 by cutting cubic samples as described in section 2.1. Additional material was collected every ~10 m for magnetic extraction.

3.2.4. Magnetic extraction procedure

Core material for the selective extraction of magnetic minerals was gently crushed with a mortar and pestle and subsequently sieved with a 500-µm mesh. 50 g of the < 500 µm fraction were used for magnetic extraction. For this purpose, sieved material was disaggregated using ultrasonic treatment and subsequently loaded into a magnetic extraction apparatus (Petersen et al., 1986). The speed of the peristaltic pump was regulated according to the grain size of the material. To inhibit clogging, we set the speed to 50-80 rpm for sands and 30-50 rpm for silts. The extracted minerals were stored in pure ethanol to prevent oxidation processes. The extraction procedure was continued until no more mineral grains were attracted by the magnet finger. A full cycle was usually completed in ~12 hours. The extracted material was poured into a beaker with a magnet fixed at the bottom and cleaned by repeated rinsing with demineralised water and ultrasonic treatment. Finally, the solid phase was magnetically separated from the liquid phase and dried on a hot plate at ~30°C.

3.2.5. Samples for the vibrating sample magnetometer (VSM)

VSM samples were prepared only from sediments hardened in the course of drying, not from loose sediments. For this purpose, samples with an edge length of ~5 mm were cut. Only irregularly shaped samples could be obtained in this manner, due the brittle nature of the sedimentary material; thus, their volumes could not be determined.

Samples of magnetically extracted material were prepared by dispersing the extract in a drop of diamagnetic cement.

3.3. Measurement procedures

Magnetic measurements were performed in the Grubenhagen palaeomagnetic laboratory of the Leibniz Institute for Applied Geophysics (LIAG), unless otherwise specified. Different equipment was used, as specified below.

A Magnon VFSM Susceptibility Bridge was used to measure low-frequency magnetic susceptibility (χ_{lf}) and high-frequency magnetic susceptibility (χ_{hf}); the measurements were performed at 505 Hz and 5005 Hz, respectively. Natural remanent magnetisation (NRM), isothermal remanent magnetisation (IRM) and backfield IRM demagnetisation curves were measured with a 2G-760SRM-RF-SQUID three-axis cryogenic magnetometer (here abbreviated as 2G-CM (Rolf, 2000)). If the intensity of the remanent magnetisation exceeded the measurement range of the 2G-CM (10 A/m) a Magnon Spinner Magnetometer was used instead. IRMs and backfield IRMs were produced with a Magnon PM II Pulse Magnetiser.

The IRM acquisition curves were acquired in 16-20 logarithmically spaced steps up to a maximum field of 2.7 T. The magnetisation acquired at 2.7 T is here considered to represent the saturation remanence (SIRM), even in cases where the high-coercive mineral components were not completely saturated in this field. The coercivity of remanence (B_{cr}) was determined from backfield demagnetisation curves of SIRM in fields up to at least 300 mT. More detailed IRM acquisition and backfield demagnetisation curves were measured with a MicroSense EZ7 vibrating sample magnetometer (VSM) in 49-100 logarithmically distributed steps up to 1.4 or 1.8 T. This instrument was also used to measure magnetic hysteresis loops in a maximum field of 1.4 T, or 1.8 T for samples containing high-coercivity minerals. Strong-field (1 T) thermomagnetic curves $M_s(T)$ were measured with the same instrument in air between 30 and 700°C with heating/cooling rates of 30 and 50°C/min, respectively.

Hysteresis loops and IRM acquisition curves of 20 samples were measured with an EV9 VSM Vibrating Sample Magnetometer at the rock magnetic laboratory of the Institute of Geophysics, Academy of Sciences of the Czech Republic in Prague. The hysteresis parameters M_{rs}, M_s, B_{cr} and B_c were determined with the EasyVSM software by MicroSense.

The magnetic extracts from the P36 core were analysed by scanning electron microscopy (SEM, backscattered electrons; FEI Sirion 200, Type D1625) combined with energy-dispersive X-ray microanalysis (EDX; Ametek, Genesis 4000) for determination of chemical compositions. For this purpose, small amounts of the extracts were placed on carbon-tape-equipped sample holders. No coating technique was applied. The relative detection limits of EDX are within 0.1 wt. % for the main elements that are our focus. These analyses were performed in the laboratory of the Federal Institute for Geosciences and Natural Resources (BGR) (Hannover, Germany).

High-resolution first-order reversal curves (FORC) (Pike et al., 1999, Roberts et al., 2000) were measured at room temperature with a Princeton Measurements Alternating Gradient Magnetometer AGM (Model MicroMag 2900) at the Faculty 5 Geosciences, University of Bremen (Germany). Because of the long time required for a single FORC measurement (5-6 hours) and the need to perform 6-9

repeated measurements on weak specimens, only a few samples could be characterised with this technique. Suitable samples were selected according to their hysteresis properties and after preliminary low-resolution measurements, which were performed to ensure coverage of all types of FORC signatures encountered in the three cores. FORC measurement protocols were selected according to Egli et al. (2010) and extended to higher fields, if necessary, while maintaining field steps below 1 mT for the detection of high-resolution signatures (Tab. 3.1). FORC measurement processing and plotting was performed with the VARIFORC software package (Egli 2013). This software package enables the processing of multiple measurements from the same specimen for the improvement of weak signals, as well as the use of an optimised smoothing protocol for the correct representation of high-resolution features such as the central ridge and background contributions with very low signal-to-noise ratios.

Table 3.1: *List of samples analysed using FORC measurements.*

Name	Lithology	T-group	number of	Hc min/max	Hb min/max	B sat	Pauses	Average time	Anzahl FORCs (N)	Field increment [mT]
P104-37	VFm	C	8	0/120	-40/60	300	0.5s	0.1 s	450	0.515
UN036-33	MFm	A	6	0/120	-40/60	300	0.5s	0.1 s	450	0.515
			6	0/800	-80/150	1030	0.5s	0.1 s	450	2.37
UN080-22	LFm	C	6	0/160	-40/90	300	0.5s	0.1 s	450	0.667
UN458-96	IFm	A	6	0/120	-40/90	300	0.5s	0.1 s	450	0.515
			6	0/600	-40/80	800	0.5s	0.1 s	400	1.87
V043-28	LFm	C	8	0/120	-40/60	300	0.5s	0.1 s	450	0.515
V194-17	VFm	A	6	0/140	-50/70	300	0.5s	0.1 s	550	0.5
V213-87	Vfm	A	9	0/120	-40/60	300	0.5s	0.1 s	450	0.515

Note: Besides the FORC parameters, the respective lithostratigraphic units of the samples and their thermomagnetic group affiliations used in Section 4.2 are indicated.

The individual coercivity components were identified via coercivity analyses of the IRM acquisition curves using the Mag-Mix coercivity analysis software package (Egli, 2003, 2004a). The software utilises skewed generalised Gaussian curves (SGG; Egli, 2003, 2004b), which are based on cumulative log Gaussian curves (CLG) and include later improvements (Robertson and France, 1994; Stockhausen, 1998; Kruiver et al., 2001; Heslop et al., 2002; Leonhardt, 2006, Heslop and Dillon, 2007). Performing a coercivity analysis with Mag-Mix is a two-stage procedure. First, the coercivity distributions on a

logarithmic field scale are calculated from magnetisation curves (Egli, 2003). All coercivity distributions are then modelled with a linear combination of a given number *m* of identical SGG functions. That is, for the *k*-th specimen,

$$f_k(\log H) = \sum_{i=1}^{m} M_{ki} SGG(\log H, \mu_i, \sigma_i, s_i, 2) \,, \tag{1}$$

where M_{ki} is the total remanent magnetisation of the *i*-th coercivity component in the *k*-th specimen, $\mu = \log_{10}B_{1/2}$, and $B_{1/2}$ represents the median acquisition field. Furthermore, the dispersion parameter σ (referred to as DP in case of CLG functions) corresponds roughly to the logarithmic standard deviation of the coercivity distribution, the asymmetry of the coercivity distribution on a logarithmic scale is controlled by the skewness parameter *s*, and the squareness of the function is described by the squareness parameter *p*. This latter parameter is set in nearly all cases to *p* = 2 (corresponding to the squareness of a Gaussian function), as this appears to be the natural value of most magnetic components (Egli, 2004b).

To avoid incorrect estimations of the number of components present, the multi-specimen analysis function in the Mag-Mix software package was applied. Notice that all of the components are characterised by the same shape parameters μ_i, σ_i, and s_i, so this analysis is suited only to groups of samples containing the same magnetic components in different proportions. The parameters μ_i, σ_i, and s_i, are determined by minimising the root mean square of all model residuals. The main advantage of this procedure over the analysis of individual curves is that the solutions are stabilised, eliminating the well-known instability problems arising from the flexible shape of SGG functions (Egli, 2003, 2004a).

A total of 507 IRM acquisition curves measured with the 2G-CM were analysed with Mag-Mix. To handle this large number of samples, coercivity distributions taken from step one of the Mag-Mix processing were grouped into sets with similar curve shapes. Combined modelling was then applied to the members of each group. The combinations of components that were used to model groups of samples are called 'clusters' in this work. Samples that could not be modelled sufficiently within their initially assigned group were processed separately. In most cases, components of other clusters could be used.

3.4. Results and Interpretation

In the present study, a major obstacle to systematic analysis arises from the use of large amounts of bulk sample material that is extremely heterogeneous in composition, texture, and grain size spectra. For example, most bulk magnetic parameters do not support a clear sample classification, while detailed characterisations, such as coercivity analysis and FORC, were necessarily limited to a

very small number of samples. In the following, we report on the principal findings obtained with the techniques mentioned in section 3.3.

3.4.1. EDX / SEM

A combined EDX and SEM analysis was performed for 238 grains from 25 magnetic extracts of samples from P36 core. The information received on the mineralogy and chemical composition of these grains was used to gain a better understanding of the origin and the diagenetic history of the minerals. Sediments of the MFm were too coarse to be processed by our magnetic extraction apparatus. Hence, the particles examined were only obtained from the LFm (48 pc.), the VFm (101 pc.), and the IFm (89 pc.). The limited number of investigated grains does not allow for systematic interpretation of down-core trends. Nevertheless, useful information on characteristic compositions and structures was obtained.

Magnetic minerals were identified by combining visual characteristics (grain shape, surface appearance, and texture) with EDX-derived elemental abundances, whereby submicron intergrowths or subsolidus exsolution textures may lead to inconclusive results.
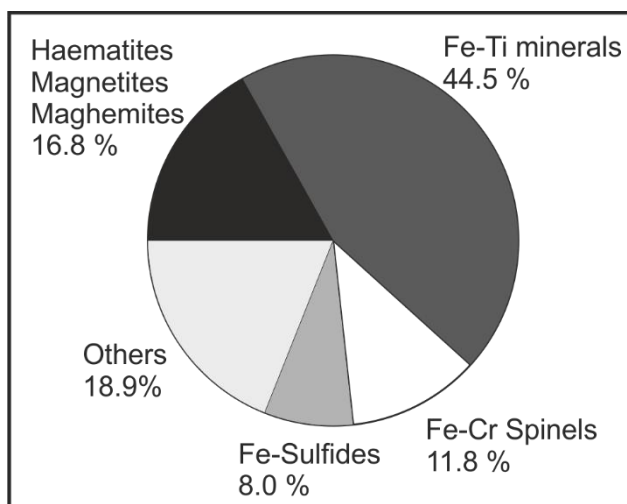
Figure 3.2:
Pie chart of minerals identified by EDX analysis. The percentages refer to the total number of 238 analysed grains.

Examination of 238 grains revealed the dominance of iron-titanium minerals (61.3%), including magnetite, maghemite, and haematite (Fig. 3.2). The majority of these minerals occur as detrital particles or microcrystalline aggregates. Idiomorphic crystals and authigenic formations appear only very occasionally. Some particles show shrinkage cracks, which typically occur during low-temperature oxidation of magnetite to maghemite (Petersen and Vali, 1987; Gapeev and Tsel'movich (1988) in Dunlop and Özdemir (1997)) or during leaching of Fe from ilmenite (Khor et al., 1996; Ahmed et al., 2010). The presence of effectively paramagnetic ilmenite in magnetic extracts can be explained by the

presence of Fe-enriched micro-structural twin-domains (Lawson and Nord, 1984; Nord and Lawson, 1989), ferrimagnetic substructures (McEnroe et al., 2002) or ferrimagnetic inclusions. Since particles that have similar chemical compositions but show dissolution features to different extents (Fig. 3.3b) can be found within the same sample, different diagenetic histories are assumed. We propose that detrital minerals with the least alteration are representative of the in situ diagenesis that has taken place within particular stratigraphic levels, with variations arising from individual burial-erosion cycles. Since physical abrasion during transport would have been destructive, the amount of in situ dissolution is likewise indicated by the fragile trellis-like habits of titanomagnetite grains showing the oxyexsolution intergrowth texture inherited from the high-temperature portion of their history (Price, 1980; Tucker and O'Reilly, 1980; Gapeev and Tsel'movich (1983) in Dunlop and Özdemir (1997).
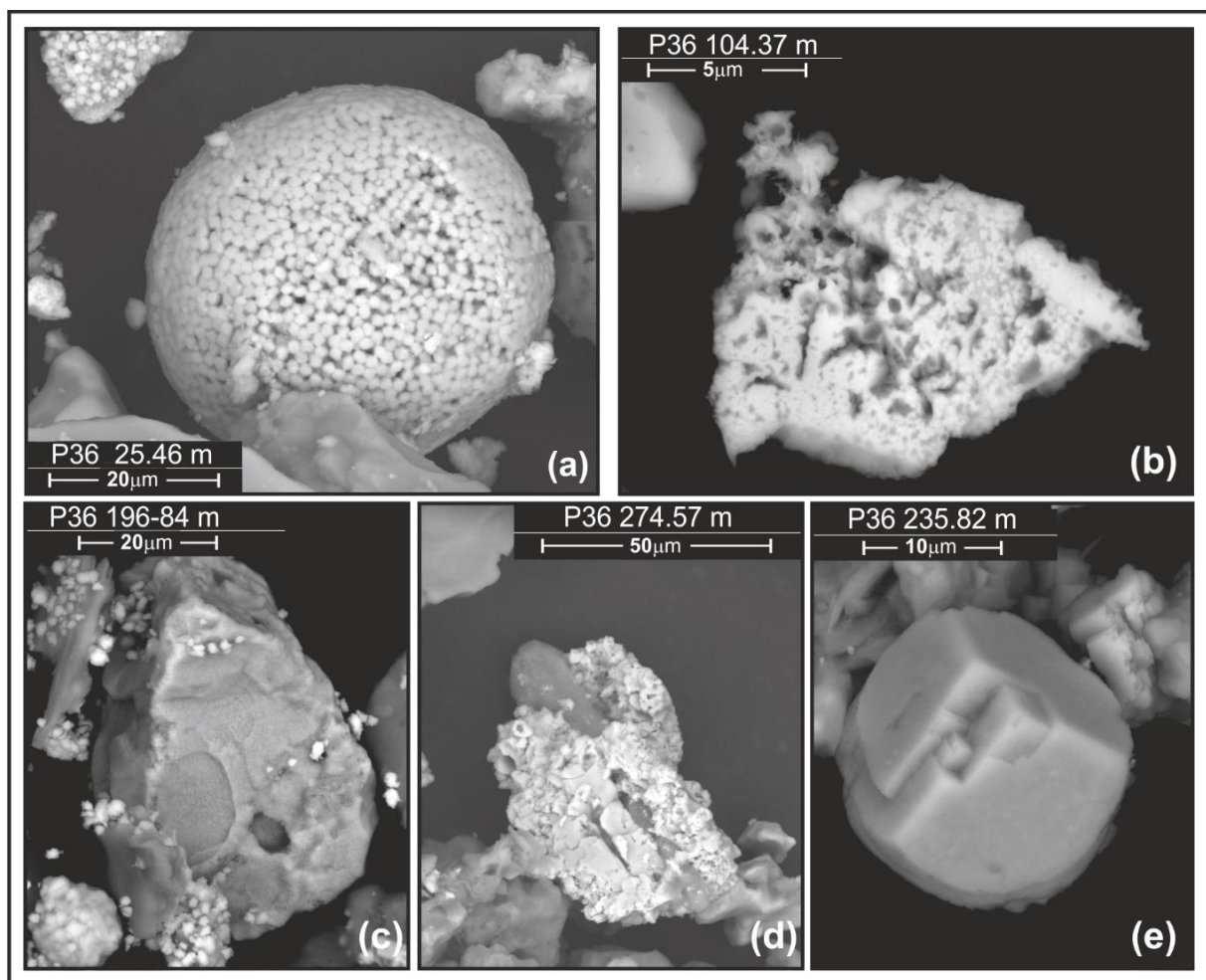
Figure 3.3:

SEM images of non-coated minerals from core P36. (a) Framboidal sulphide mineral (most likely greigite) and an irregular aggregate of sulphides consisting of larger single crystals and much smaller fine crystalline minerals (greigite, pyrite?). (b) Porous remainder of a Fe-Ti mineral; iron depletion causes the spotted appearance. (c) Ilmenite showing micro cracks on the surface and surrounded by flaky sulphide minerals. (d) Quartz grain overgrown with specularite. (e) Pseudo-morph of haematite after pyrite.

Detrital iron-chromite spinels are the second most common mineral group (11.8%) in the magnetic extracts. Chromite is only magnetically extractable if the magnetite component exceeds 40% (Hounslow, 1996). We distinguish three main mineral groups according to their Ti/Fe and Cr/Fe element ratios (Fig. 3.4):

- Titanium-free crystals from the magnetite (Fe_3O_4) - chromite ($FeCr_2O_4$) solid solution series plot along the Ti/Fe = 0 line in Fig. 3.4a.

- Ti-substituted chromites are grouped on the right-hand side of Fig. 3.4a.

- The third group, which has scattered element ratios, includes Cr-containing Fe-Ti minerals with Ti/Fe ratios between 0.024 and 1.3.

Consistent with the results of Hounslow (1996), the extent of corrosion of chromite grains increases with higher Fe content. The small amounts of manganese (mean: 0.92%, max 6%) detected in most chromites may have significant effects on their magnetic properties (Hounslow, 1996).

Iron sulphides are another important magnetic mineral group (8%). In spite of their relative small abundance (Fig. 3.2), four different morphologies were noted. The majority of all iron sulphides occurs as microcrystalline aggregates, which generally adhere to grain surfaces, when they are very small. A small number of pseudomorphic mineral fragments and tiny euhedral crystals were also found, along with a few framboidal aggregates (Fig. 3.3a, c). Perfectly round framboids (Fig. 3.3a) are generally composed of pyrite or greigite (Wilkin and Barnes, 1997). Two distinct grain size groups can be distinguished in the framboid shown in figure 3.3a. Roberts and Weaver (2005) and Roberts (2015) described similar masses of euhedral Fe-sulphides, in which the finest-grained crystals are made up of greigite, whereas the coarser ones are made up of pyrite. Due to their small size (~1 µm) and compact arrangement, the compositions of the individual crystals cannot be identified unambiguously with EDX spectra. However, because of their occurrence in the magnetic extracts, we suggest that these aggregates are composed mainly of ferrimagnetic greigite.

Finally, almost 19% of the analysed particles fall into other categories (Fig. 3.2), which collectively include non-magnetic minerals (e.g., iron carbonates, detrital zircons, and amphiboles) and unidentifiable minerals with inconclusive elemental compositions, as well as polymineralic microcrystalline aggregates.

Magnetic extracts from all stratigraphic levels contain a significant amount of silicates and aluminosilicates. Backscatter micrographs show tiny (≤1 µm), bright minerals covering some of these grains that may have caused their extraction. Paramagnetic minerals without ferrimagnetic properties that adhere to the surface are suspected to have been extracted due to ferrimagnetic inclusions.

In conclusion, the magnetic mineral assemblages of the three lithostratigraphic units, the IFm, the VFm, and the LFm, are characterised by the following main elements:

(1) The occurrence of strongly corroded magnetite remnants (similar to Fig. 3.3b) is restricted to the VFm and the LFm, whereas haematite (specularite) was exclusively identified in extracts from the IFm (Fig. 3.3e). It should be noted that the slightly pitted surfaces of some haematite particles indicate the action of iron dissolution processes after the formation and deposition of these grains.

(2) Apart from two outliers, these lithostratigraphic units yield maximum Ti/Fe ratios (Fig. 3.5) of 1.4, 1.8, and 4 for the LFm, the VFm, and the IFm, respectively. This trend can be interpreted in terms of the different origins of the minerals, as well as by changes in diagenetic conditions. A change in the sediment provenance of the Rhine River was caused by the connection of the Alpine Rhine and the Aare/Rhine system in the late Pliocene and is characterised by the appearance of an admixture of unstable heavy minerals (Hagedorn, 2004, Hagedorn and Boenigk, 2008, Hoselmann 2008). Although parts of the Quaternary deposits originated continuously from the margins of the Upper Rhine Graben and occasionally even dominate the sequence within distinctive intervals (Hagedorn and Boenigk, 2008), Ti/Fe-ratios comparable to those of the IFm were not found in the VFm and the LFm (Fig. 3.5). The magnetic minerals of the IFm are thus more influenced by iron leaching and relative enrichment in Ti and Cr, which is a typical feature of reworked and diagenetically overprinted sediments (Dimanche and Bartholome, 1976; Roberts and Turner, 1993; Hounslow et al., 1995; Hounslow, 1996; Khor et al., 1996; Wilson and Roberts, 1999; Nowaczyk, 2011; Roberts, 2015).
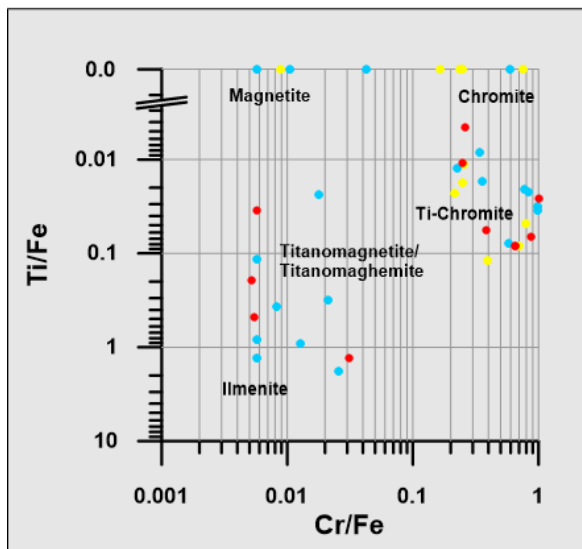
Figure 3.4:
Element ratios of Cr and Ti containing magnetic minerals extracted from core P36 measured by EDX analysis (based on atomic percentages). Unit colour code follows that used in Fig. 3.1: yellow, LFm; blue, VFm; red, IFm.
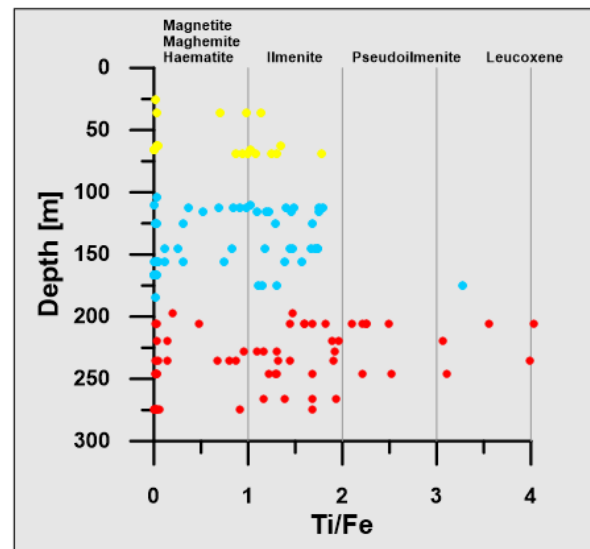
Figure 3.5:
Ti/Fe ratios of iron–titanium minerals of extracts from core P36 as a function of depth. Unit colour code follows that used in Fig. 3.1: yellow, LFm; blue, VFm; red, IFm.

According to a number of authors (e.g., van Houten, 1968) (Dimanche and Bartholome, 1976; Maher and Hallam, 2005), the chemical alteration of magnetite and ilmenite occurs after deposition, rather than during the first stages of erosion and fluvial transport. Consequently, the higher Ti/Fe-ratios of the IFm are caused by a formation history that differs from that of the LFm and the VFm. For the same reasons, differences in diagenetic conditions can be assumed, including the various biological, physical, and chemical processes that may affect magnetic mineral associations.

(3) Fe-sulphides are relatively abundant down to a depth of 196.80 m (the top of the IFm), whereas only two sulphide grains and a few traces of sulphur were found in the strata below. The identification of an iron oxide pseudomorph after pyrite at a depth of 274.57 m shows that pyrite formed authigenically and was diagenetically replaced at a later stage (Fig. 3.3e). Thus, Fe-sulphides were originally more abundantly represented in the IFm.

3.4.2. Thermomagnetic analyses

The temperature dependence of "saturation" magnetisation in a strong magnetic field provides diagnostic information about the composition of ferrimagnetic minerals through their Curie or Néel temperatures, as well as the characteristic alteration temperatures at which magnetic minerals are replaced or new magnetic minerals form. Because of the complex set of chemical reactions that occur in sediment upon heating, thermomagnetic analyses are limited to magnetic extracts, which significantly reduces the possible complications related to the alteration of non-magnetic minerals. For comparison, all curves are normalised by their initial magnetisation (Fig. 3.6).

All thermomagnetic curves can be divided into the following three main groups.

- A: Type A contains heating curves that are characterised by monotonic decreases until full disappearance of magnetisation between 600 and 700°C, which is the typical Curie temperature range of pure iron oxides (i.e., magnetite, maghemite, and haematite). Some curves show an enhanced loss of magnetisation between 450°C and 630°C.

- B: These curves are similar to type A up to 400°C, but a marked magnetisation increase that peaks between 400°C to 450°C occurs subsequently. In some cases, a main peak is followed by a secondary peak (Fig. 3.6c). A rapid magnetisation loss occurs above 550°C. Type B samples are exclusively found in the IFm.

- C: Multiple irregular peaks with relatively prominent increases between 250°C and 290°C characterise C-type heating curves. Two main groups of peaks are identifiable; the first occurs

around ~300°C and the second is found at approximately 500°C. Flat or slightly inclined sections may replace either or both peaks. Only two samples from the IFm fall into group C.

Thermal alteration processes are indicated by irreversible behaviour in all heating experiments.
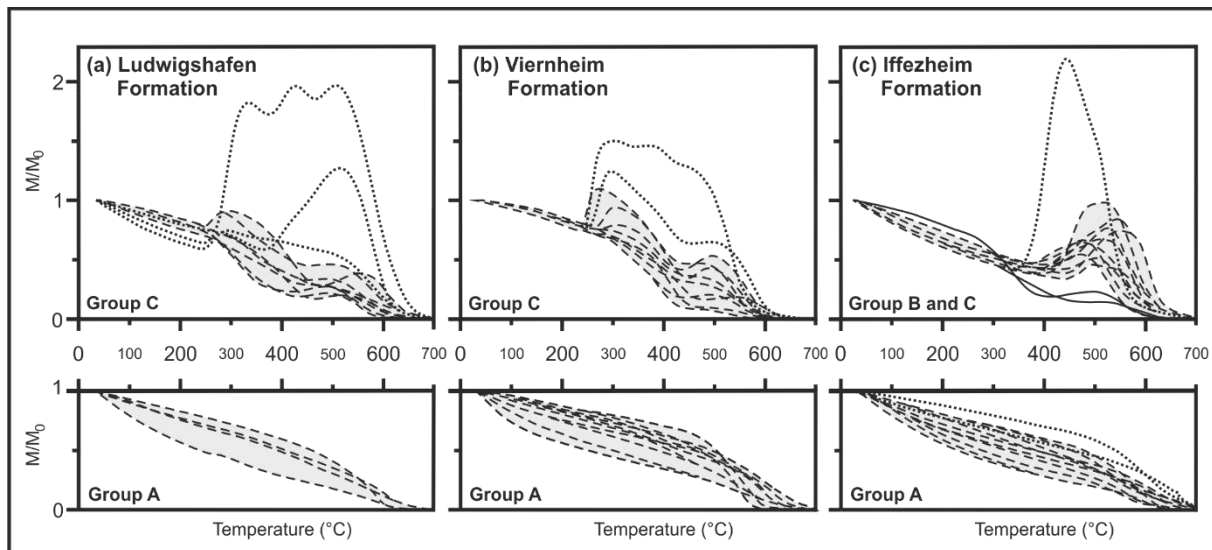
Figure 3.6*:*

Thermomagnetic measurements of samples from different lithostratigraphic units divided into groups A, B and C. Shaded areas confine regions in which the heating curves run across. Exemplary pathways are depicted using dashed lines. Outliers are shown with dotted lines. The continuous lines in (c) represent Type-C specimens. For detailed explanations, see the text.

The cooling curves start to increase between 620°C and 580 °C and have generally similar curved shapes. When little evidence for re-crystallisation processes and new mineral formations is shown by the heating curves, cooling curves fall below the heating curves (type A and some type C), and suggests the conversion of magnetic minerals into less magnetic ones (e.g., by the oxidation of magnetite into haematite). In the case of heating curves that reflect strong alteration (groups B and C), the magnetisation at the end of the heating-cooling cycle exceeds the initial one by up to a factor of 20, implying that weakly magnetic or non-magnetic minerals have been converted into strongly magnetic minerals (e.g., by the oxidation of pyrite into magnetite).

Type-A thermomagnetic curves are typical of relatively stable mineral assemblages containing magnetite, maghemite and/or haematite (e.g., Özdemir, 1990; de Boer and Dekkers, 1996; Liu et al., 2010). Curie temperatures below that of the pure magnetite end-member most likely occur due to the substitution of Fe by Cr and Ti (Schmidbauer, 1969; Gendler et al., 1979; Murthy and Krishnamacharyulu, 1994; Maksimochkin et al., 2013) or aluminium (Da Costa et al., 1995; de Boer and Dekkers, 1996). Curie temperatures exceeding that of the magnetite end-member can originate from impurities in the crystal lattice, exsolution fabrics or partial or complete oxidation to maghemite (T_C

~640°C) or haematite (T_N ~680°C) (e.g., Schmidbauer, 1969; Price, 1980; de Boer et al., 2001; Liu et al., 2010). Natural maghemite is also known to contain imperfections and internal stresses, which decrease its Curie temperature.

In addition to the abovementioned phases, minerals within the ferrimagnetic range of the haematite-ilmenite solid solution series were identified in SEM/EDX analyses of group-A samples from the IFm. These minerals are characterised by a linear dependence of the Curie temperature on the degree of Fe substitution, and these Curie temperatures range from −218°C for the ilmenite end-member to 680°C for the haematite end-member, respectively (Reynolds, 1977). We assume that ferrian ilmenites carry only a small part of the sediment magnetisation, which is not detected by thermomagnetic measurements.

The magnetisation peak that occurs at approximately 500°C for group B samples can be attributed to the conversion of thermally unstable minerals to a new magnetic phase. A strong candidate for this signature is pyrite, which starts to decompose at 400-500°C, giving rise to a magnetisation increase at approximately 500°C (Passier et al., 2001; Weaver et al., 2002, Hu et al., 2006). Paramagnetic pyrite may occur in the extracts due to intergrowth or aggregation with any ferrimagnetic minerals that are present. Alternatively, incomplete decomposition may lead to a pyrite core with an oxidised rim. Other possible but less likely candidates for the magnetisation peak seen in group B are natural chromites (Kumar and Bhalla, 1984) and siderite (Housen et al., 1996; Pan et al., 2000). The temperature range of the final magnetisation loss is indicative of the formation of impure magnetite.

Group C is characterised by the most complex thermomagnetic behaviour. The blocking temperatures are consistent with a wide range of magnetic minerals. Although some type-C specimens can be explained by multiple conversions of only one primary phase, they are more likely to reflect multicomponent mixtures with varying proportions of the minerals involved. Possible candidates are solid solutions of the paramagnetic chromite ($FeCr_2O_4$) and magnetite (Fe_3O_4) end-members. In this case, the corresponding Curie temperatures range from 0°C to 580°C (Schmidbauer, 1969; Schmidbauer, 1971; Hounslow et al., 1995). Some natural chromites are reported to be characterised by two phases, one of which has a blocking temperature between 300°C and 350°C (which is attributed to chromite), and an associated magnetite phase with a blocking temperature between 550°C and 600°C (Murthy and Krishnamacharyulu, 1994; Hounslow, 1996; Kądziałko-Hofmokl et al., 2010). The oxidation of thermally instable maghemite to haematite can also lead to a progressive magnetisation loss starting from 250°C (Verwey, 1935; Bernal et al., 1957).

The first peak at 250-270°C can be attributed to the structural transition of fine-grained pyrrhotite (Schwarz and Vaughan, 1972; Dekkers, 1989), whereas the second peak at 500°C is attributable to the

decomposition of sulphidic components. As discussed for group B specimens, pyrite is a possible contributor, along with greigite, which was previously detected in the VFm and the LFm in former studies (Rolf et al., 2008; Scheidt et al., 2015). Greigite is characterised by a moderate magnetisation decay up to 300°C, followed by a more pronounced loss. The latter signature is not observed in most of the samples, probably caused by the superposition of contributions from other minerals. After decomposition at ~340°C, a peak in intensity approximately 500°C is due to the neo-formation of magnetite (Roberts, 1995; Roberts et al., 2011).

Group C outliers are characterised by a marked magnetisation plateau between 300 and 500°C that is due to the occurrence of several peaks caused by different magnetic phases that may have formed during heating or were already present in the pristine sample material. Similar signatures are frequently found in natural sediments, and their cause is uncertain. Some similarities exist with curves arising from the reaction chain in which lepidocrocite is converted to maghemite intermediates and finally to haematite. Such conversions are usually characterised by double-peaked demagnetisation curves that contain sharp increases at ~250°C and drops between 430°C and 480°C (Gehring and Hofmeister, 1994; Gendler et al., 2005). However, multiple peaks are possible if additional magnetic phases are involved. The final demagnetisation between 500°C and 640°C can again be ascribed to the presence of impure magnetite or thermally stable maghemite, as discussed above.

3.4.3. Magnetic susceptibility

The down-core variations in mass-normalised magnetic low-frequency susceptibility (χ_{lf}) is characterised by similar trends in all three cores (Fig. 3.7). Values reach up to 345×10^{-8} m^3 kg^{-1}, and mean values of the individual formations range between 7.2 and 13.1×10^{-8} m^3 kg^{-1}. Differences between these values and those reported in Scheidt et al. (2015) arise from the measurement of a slightly different set of samples and the use of a different measuring device.

As expected, the IFm exhibits relatively low susceptibility values because of the presence of authigenic haematite formed by oxidation of the primary magnetic mineral assemblage. The highest susceptibility values are attributed to the occurrence of ferrimagnetic sulphides or heavy mineral placer in the VFm. Heavy mineral placers have occasionally been recognised by rich yields of coarse magnetic minerals in the magnetic extraction procedure.

The relative frequency dependence of magnetic susceptibility, expressed as $\chi_{fd} = 100(\chi_{lf} - \chi_{hf})/\chi_{lf}$, never exceeds 4.3%, and the low average value of 0.63% points to very small contributions from SP particles to the magnetic signal in the majority of the sediments (Tab. 3.2).

The absolute frequency dependence of susceptibility, $\Delta\chi = \chi_{lf} - \chi_{hf}$, is only roughly correlated with χ_{lf} (Fig. 3.7b). The scatter is the result of domain state and mineralogical variations, which dominate the variations in SP concentration.
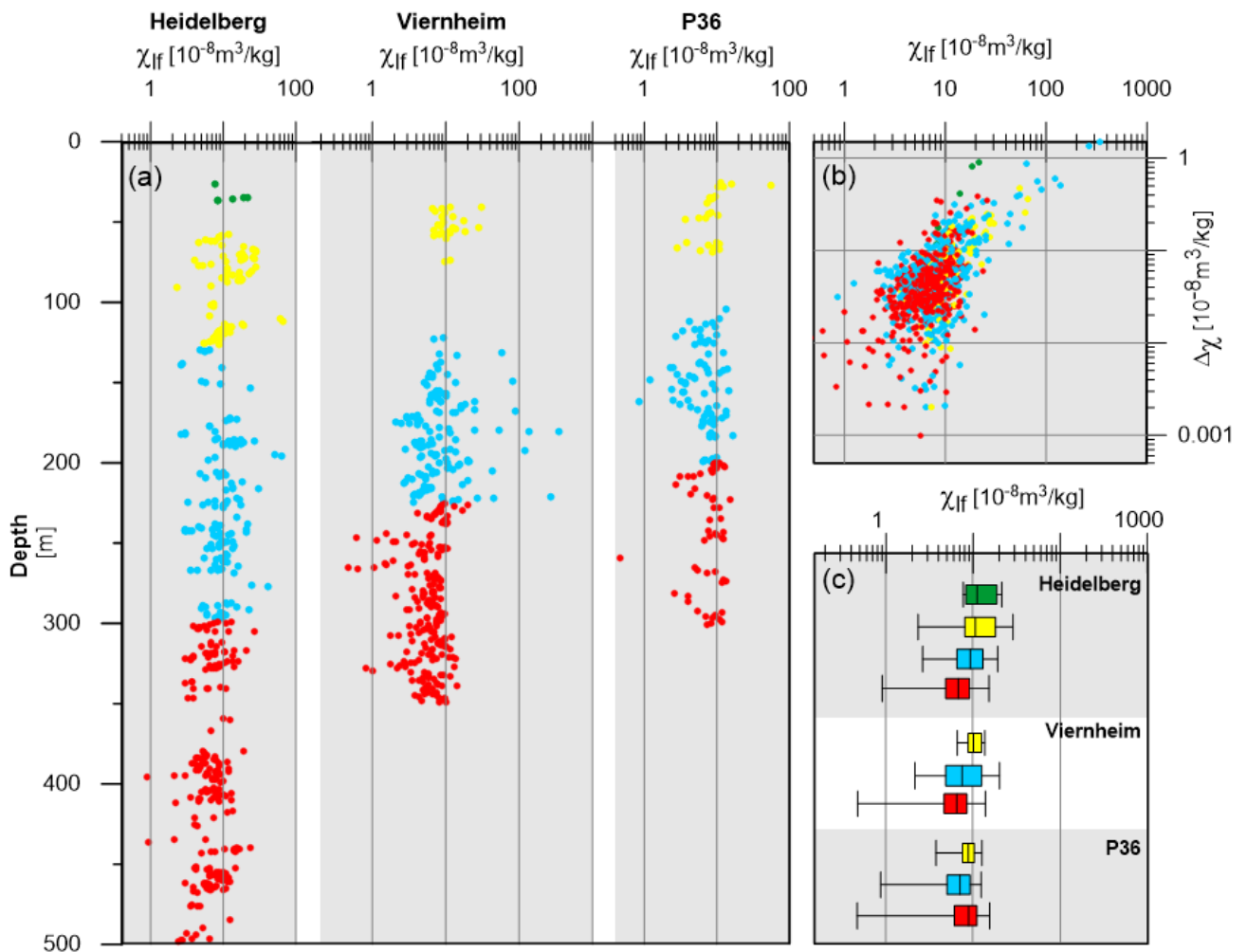
Figure 3.7:

(a) Mass-normalized susceptibility (χlf) versus core depth. (b) χlf versus absolute frequency dependence of susceptibility (χ) of bulk sample material. Four data points of the VFm within the Viernheim core with $\chi lf > 100$ and $\chi fd < 1$ are omitted to permit better visualization of the remaining data. (c) Box-and-hisker plot of susceptibility ranges. (a, b, c) Unit colour code follows that used in Fig. 3.1: green: MFm; yellow: LFm; blue: VFm; red: IFm.

Important additional information for the interpretation of frequency dependent susceptibility is gained from the dark grey/black, clayey sample material of the archived Heidelberg half-core by its susceptibility decrease to almost zero upon drying. This loss can be attributed to the oxidation of diagenetic SP sulphide particles that were originally preserved under sealed conditions.

In summary, the observed minor frequency dependence of magnetic susceptibility results either from disappearance of SP magnetite/maghemite during oxidising or reducing diagenesis (Roberts, 2015) or from oxidation of SP sulphides during desiccation of the cores and samples.

Table 3.2: Median, minimum and maximum frequency dependent susceptibility χ of the cores and the respective lithostratigraphic units.

Site	Lithostratigraphic unit	N	Median χfd	Min χfd	Max χfd
Heidelberg	MFm	6	2.59%	0.00%	4.29%
	LFm	75	0.62%	0.08%	1.15%
	VFm	128	0.66%	0.00%	1.95%
	IFm	215	0.71%	0.00%	3.52%
Viernheim	LFm	25	0.51%	0.21%	1.59%
	VFm	134	0.64%	0.00%	2.97%
	IFm	204	0.54%	0.00%	4.22%
P36	LFm	24	0.83%	0.00%	1.55%
	VFm	79	0.62%	0.00%	3.70%
	IFm	53	0.65%	0.00%	3.64%

Note: Number of measured samples (N).

3.4.4. Magnetic hysteresis

The representation of hysteresis parameters using Day plots (Day et al., 1977) are widely used for estimation of the mean domain state of magnetic mineral assemblages. Differences between the binary mixing curves of (titano)magnetites (Dunlop, 2002a, b) and of greigite-bearing samples (Roberts et al., 2011) demonstrate the dependency of the magnetisation and coercivity ratios on the composition of the sample material. Heslop and Roberts (2012) implemented a ternary mixing model with three end-members, demonstrating the difficulty of interpreting mixed mineralogy only on the basis of Day plots. Nevertheless, some clear trends can be recognised in the Day plots representing the results from 130 samples of magnetically extracted minerals and bulk sediment from the Viernheim and P36 cores (Fig. 3.8). The samples from the Heidelberg core were excluded from this analysis because they display excessive scattering. The shapes of the hysteresis loops can be divided into three categories:

(1) Those compatible with a single magnetic mineral (e.g., magnetite) with domain states varying from a single-domain (SD) end-member (e.g., Fig. 3.8c) to a multi-domain (MD) end-member (e.g., Fig. 3.8g). These loops are characterised by hysteresis parameters that form a linear trend on the Day plots. This trend is located slightly above the SD-MD mixing curve predicted for magnetite by Dunlop (2002a) (Fig. 3.8a).

(2) Due to the presence of high-coercive minerals, some loops are not saturated even in maximum fields of up to 1.8 T (e.g., Fig. 3.8h-i). The slope increase in fields higher than 1 T is attributable to a spin-flop transition that occurs in antiferromagnetic minerals such as goethite and fine-grained haema-

tite (Rochette et al., 2005). The hysteresis parameters of strongly unsaturated loops are meaningless, yielding Day plot parameters that depart significantly from the general trend of most samples. For instance, the loop in Fig. 3.8i points to a 50:50 SP-SD mixture that is not supported by the frequency dependence of magnetic susceptibility.

(3) Finally, a third category of loops saturates in fields of ~1 T but is characterised by a so-called wasp-waisted shape (Roberts et al., 1995; Tauxe et al., 1996), which is typical for binary mixtures of magnetic minerals with strongly contrasting coercivities (e.g., SD and MD or SD and SP) or a single phase affected by surface oxidation (Heisz and Hilscher, 1987). Typical examples of such loops are shown in Fig. 3.8d-
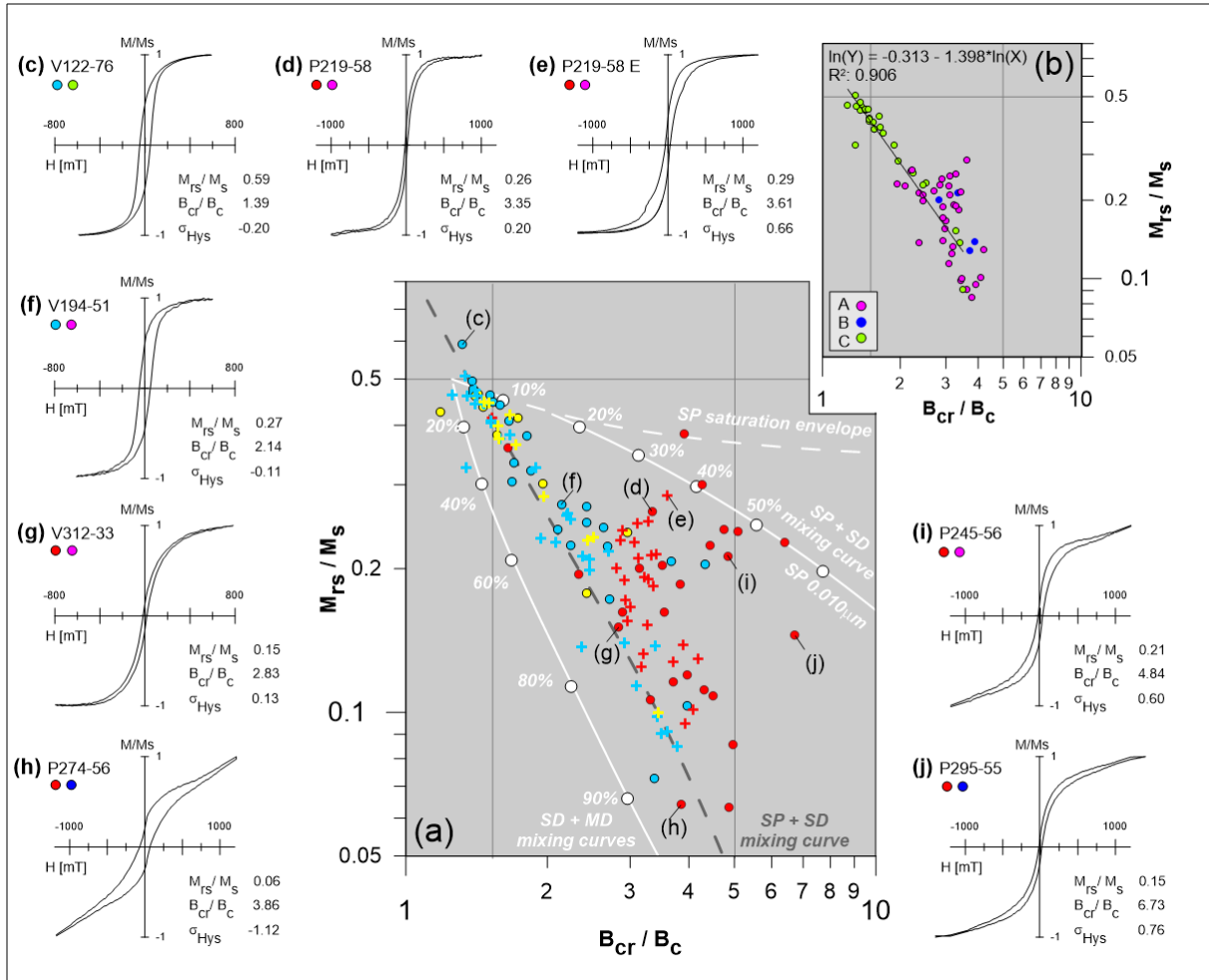
Figure 3.8:

(a) Ratios of hysteresis parameters for bulk sample material (dots) and extracted material (crosses) of the Viernheim core and core P36 in Day plots (Day et al. 1977). Mixing lines for (titano)magnetite are drawn after Dunlop (2002a; white lines). Percentages indicate portions of SD particles. SD+SP trend line for binary mixing of greigite-bearing samples after Roberts et al. (2011; dark grey dashed line) is in good agreement with the samples from the VFm and LFm. Unit colour code follows that used in Fig. 3.1: green, MFm; yellow, LFm; blue, VFm; red, IFm. (b) Day plot as in (a) showing only results from extracted materials, colour coded according to the different thermomagnetic groups. The trend line is calculated for C-type specimens of the VFm and LFm. (c–j) Exemplary hysteresis loops after paramagnetic correction. Filled circles below the label are related to the colour codes used in (a) and (b). All loops except (e) reflect bulk sample materials.

e. For the case of unsaturated loops, the hysteresis parameters of wasp-waisted loops tend to plot near the SD-SP mixing line of the Day plot, even though the corresponding samples do not contain significant amounts of SP materials, as indicated by the low frequency dependence of susceptibility discussed in section 3.4.3.

The shapes of hysteresis loops are generally described by the parameter (Fabian, 2003)

$$\sigma_{hys} = \ln\left(\frac{E_{hys}}{4M_S B_C}\right), \qquad (2)$$

where E_{hys} is the area enclosed by the hysteresis branches, M_S is the saturation magnetisation, and B_c is the coercivity. σ_{hys} quantifies the shapes of hysteresis loops by comparing E_{hys} with the area enclosed by an ideal rectangular loop with the same values of M_S and B_c. Wasp-waisted loops are characterised by $\sigma_{hys} > 0$ and potbellied loops are characterised by $\sigma_{hys} < 0$.

All of the samples that plot near the SD-SP mixing line of the Day plot (Fig. 3.8a) are characterised by large values of σ_{hys} and are thus wasp-waisted. In particular, the IFm formation contains extreme examples (Fig. 3.8i-j). Because strongly magnetic minerals, such as (titano)magnetite and greigite, are preferentially extracted, the disappearance of wasp-waisted signatures in magnetic extracts, as seen in the Day plot (Fig. 3.8b) and the σ_{hys} values (Fig. 3.9), implies the presence of high-coercive minerals with weak spontaneous magnetisation (haematite and goethite). The IFm samples, in particular, are characterised by large amounts (by mass) of antiferromagnetic minerals. However, in a few cases, magnetic extraction does not lead to a distinct decrease in

Figure 3.9:

Variations in the σhys for cores and lithological units characterizing the shape of magnetic hysteresis loops. The widely scattered results of the Heidelberg core samples do not follow the trend shown by the other two cores. Note the different vertical axes for data from bulk material (lower part) and extracted material (upper part).

σ_{hys} (e.g., Fig. 3.8d-e). This observation can be explained by the intergrowth of low- and high-coercive phases, which are not separable by the extraction procedure. In contrast, samples from the VFm and the LFm show symmetrical to potbellied shapes (Fig. 3.9). Slightly constricted hysteresis loops occur only within the A-type bulk samples but not in the corresponding extracts, and thus probably also occur due to the presence of antiferromagnetic minerals.
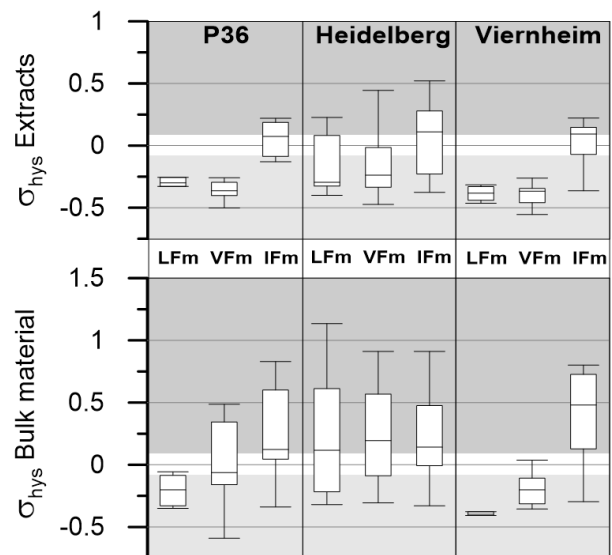
The extracts from the VFm and the LFm define a mixing trend (R^2 = 0.906), with the SD end-member being characterised by M_{rs}/M_s = 0.73 at B_{cr}/B_c = 1 (Fig. 3.8b). This trend is similar to that of greigite with M_{rs}/M_s = 0.81 at B_{cr}/B_c = 1 as the SD-end-member (Roberts et al., 2011). The properties of this end-member point to SD particles that are dominated by cubic anisotropy and have coercivity values compatible with those of greigite. Greigite is therefore the dominant ferrimagnetic component in samples from the VFm and the LFm; admixtures of other mineral phases probably generate the characteristic mixing trend seen in the Day plots (Fig. 3.8a-b).

3.4.5. First order reversal curves (FORCs)

FORC diagrams (Pike et al., 1999; Roberts et al., 2000) provide additional details about the magnetisation processes responsible for the hysteresis properties discussed in section 3.4.4. Our measurements reveal a complex mixture of magnetic minerals with different domain states that correspond to the three types of thermomagnetic curves (A, B, and C) discussed in section 3.4.2. FORC diagrams of type-C samples are characterised by roughly elliptical FORC contours that define a broad peak centred at H_c = 50-60 mT and H_b = -5 mT. This signature is indicative of greigite particles with relatively strong magnetostatic interactions that are produced by the typical growth habit of this mineral, which occurs in close-packed clusters (Roberts et al., 2011; Roberts, 1995).

The SD nature of this FORC signature is also confirmed by negative contributions in the lower-left corner of the diagrams (Fig. 3.10d, f, i), which are partially truncated in some figures (Fig. 3.10e, h). All greigite-dominated FORC diagrams also display variable contributions from a so-called central ridge, which is particularly evident in Fig. 3.10b. This feature is a horizontal, sharp ridge extending along H_b = 0 and is a characteristic signature of non-interacting SD particles (Newell, 2005) that are commonly associated with magnetofossils in various types of marine and freshwater sediments (Egli et al., 2010; Ludwig et al., 2013; Heslop et al., 2014; Roberts et al., 2014). Central ridges do not necessarily originate from magnetofossils; a chemical origin is also possible. Differentiation of biological particles from authigenically precipitated minerals may be possible through analysis of the coercivity distribution associated with the central ridge. This requires isolating the central ridge from the remaining continuous contributions of the FORC diagram using the numerical methods implemented in VARIFORC (Egli et al., 2010; Ludwig et al., 2013). Although most of the diagrams have been obtained
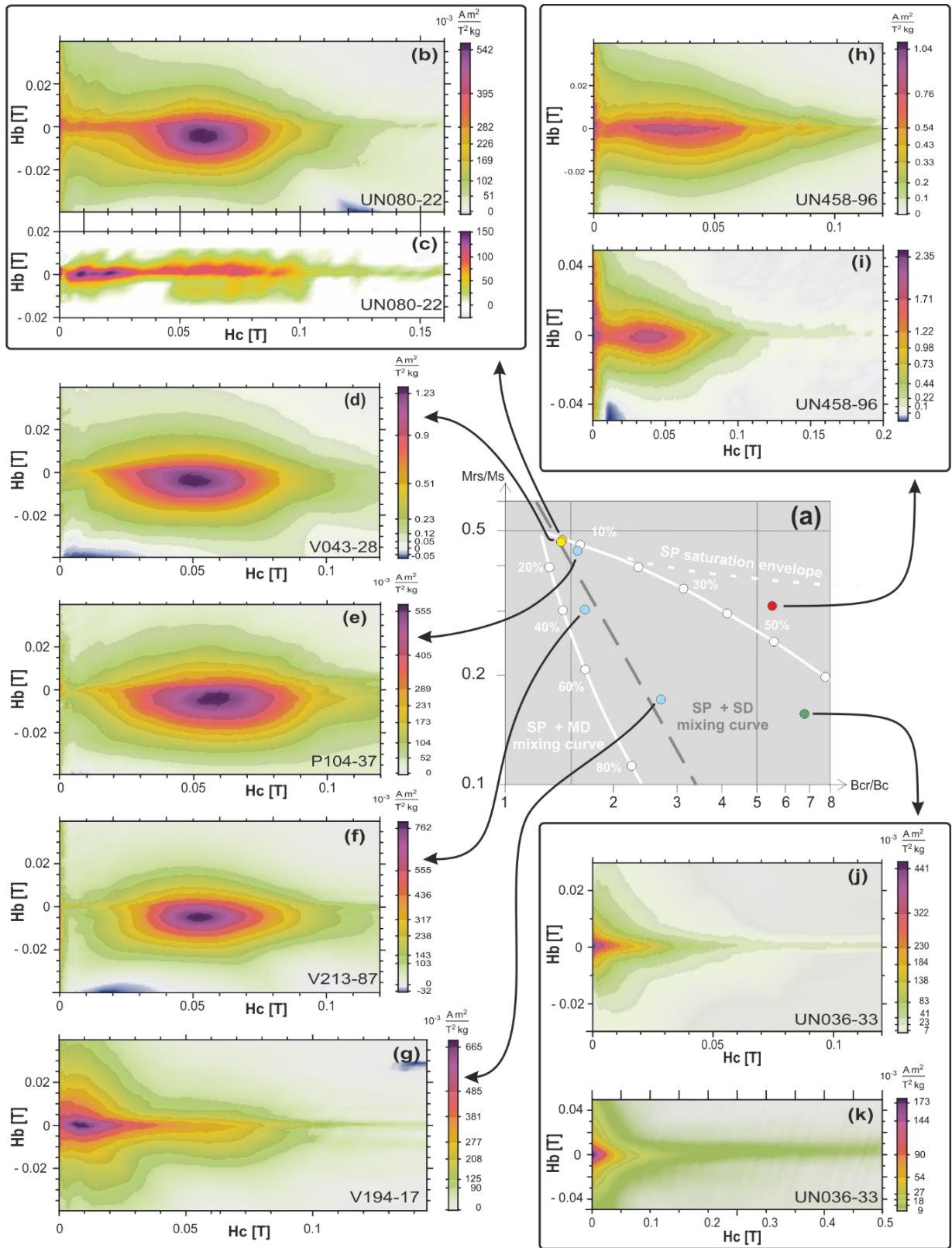
Figure 3.10:

(a) Ratios of hysteresis parameters in the Day plot (Day et al. 1977). Mixing lines for magnetite (white) and greigite (grey) are drawn after Dunlop (2002a) and Roberts et al. (2011), respectively. Unit colour code follows that used in Fig. 3.1: green, MFm; yellow, LFm; blue, VFm; red, IFm. (b,d–k) FORC diagrams calculated with VARIFORC (Egli 2013) for data from multiple runs of each sample. (c) Extracted central ridge of sample UN080-22, which is shown in panel (b). (b–f) FORC dia grams for samples affiliated with

by averaging up to nine individual sets of measurements, the residual measurement noise is still too large to support such calculations, except for sample UN080-22, where the central ridge contributes ~2% of the total remanent magnetisation (Fig. 3.10b-c). This central ridge contains two peaks at H_c = 10-20 mT and H_c = 70 mT, respectively, of which the latter is compatible with the coercivity component "BH" that is attributed to magnetofossils (Egli, 2004a). The low-coercivity peak, on the other hand, is compatible with the expected coercivity distribution of isolated, nearly equidimensional SD magnetite particles (Maher, 1988; Egli, 2004c).

Caution should be applied in the interpretation of this central ridge, given its low magnetisation (~2% of the bulk M_{rs}) in comparison to that of magnetofossil-bearing sediments (>50% of M_{rs}; e.g., Kind et al., 2011; Heslop et al., 2013; Reinholdsson et al., 2013). In fact, the entire central ridge could be part of the greigite signature. This hypothesis is supported by the fact that weak central ridges are clearly present in all greigite-bearing samples examined in this study and are also visible in high-quality FORC diagrams presented by other studies (e.g., Rowan and Roberts, 2006).

FORC diagrams of C-type samples are further characterised by high-coercivity phases, which, along with results from thermomagnetic measurements, can be interpreted as originating from SD pyrrhotite particles (Wehland et al., 2005). Interestingly, the only greigite-bearing sample showing the additional low-coercivity FORC signatures that are usually associated with pseudo-single-domain (PSD) and MD magnetite particles is also sample UN080-22. We tentatively explain this fact by assuming that primary magnetite remainders are present to a greater extent than in the other samples. The magnetisation of large magnetic minerals, which are highly diluted in the matrix of natural sample material, may be too small in relation to the main carriers to be depicted with the applied scale settings. Thus, the absence of PSD and MD signatures, for example in sample P104-37 (Fig. 3b and 10e), is not necessarily inconsistent with the detection of large iron oxide grains by SEM/EDX. It should be borne in mind that those grains were preferentially extracted and identified with electron microscopy.

FORC diagrams of thermomagnetic type-A samples V194-17, UN458-96, and UN036-33 (Fig. 3.10g-k) bear the typical signature of PSD magnetite, which consists of contour lines with increasing vertical spread at the zero-coercivity limit (e.g., Roberts et al., 2000; Muxworthy and Dunlop, 2002). This is especially clear in the case of UN036-33, where the only additional FORC signature is that of a high coercivity central ridge that will be discussed later. Surprisingly, other A-type samples seem to contain

thermomagnetic group C. Panel (g) shows an exceptional case; see the text for discussion. (h–k) FORC diagrams for samples affiliated with thermomagnetic group A. Panels (h) and (i), as well as (j) and (k), each shows measurements of the same sample. (h) and (j) are measured with the standard saturation field of 300 mT, whereas saturation fields of 800 and 1030 mT were applied for (i) and (k), respectively. Settings used to obtain the FORC measurements are listed in Table 3.1.

variable amounts of greigite, as in sample V213-87 (Fig. 3.10f).

In general, the presence of greigite in A-type samples gives an important clue to the highly variable resistance of this mineral to oxidation during the extraction procedure. Some FORC diagrams, such as V194-17 (Fig. 3.10j) and UN458-96 (Fig. 3.10h), clearly result from the superposition of two phases with PSD and greigite-like end-member properties.

Finally, the last FORC signature identifiable in our samples is a high-coercivity central ridge (Fig. 3.10i, j). This ridge extends well beyond the coercivity range of magnetite and greigite, and appears to be associated with extremely hard SD particles, as shown in high-resolution FORC measurements to H_C = 0.5 T (Fig. 3.10k). The high-coercivity central ridge is attributable to SD haematite and/or goethite particles with switching fields that are significantly lowered by thermal activation. The origin of these particles is not known. Geological observations clearly suggest different haematite sources, e.g., denudation of Triassic red beds in sample UN036-33 and authigenic growth in UN458-96 (Ellwanger et al., 2008).

3.4.6. Coercivity analysis

Coercivity analyses unravel the full complexity of the investigated sediment by identification of 30 components, of which as many as five occur simultaneously (Tab. 3.3). The components are attributable to the presence of different minerals discussed below, and can be grouped into six strongly overlapping coercivity ranges (Tab. 3.3 / Fig. 3.11) The association of individual coercivity distributions with certain mineral components is only possible with additional mineralogical information, such as thermomagnetic behaviour (groups A, B, and C), EDX analysis, and FORC measurements.

All coercivity components with median fields $B_{1/2}$ < 47 mT (μ = 1.670, shown in light blue in Fig. 3.11) are left-skewed distributions with σ-values in the range of 0.316-0.373. Several studies (e.g., Kruiver et al., 2001; Hüsing et al., 2009; Dennie et al., 2012; Just et al., 2012) interpreted these components as related to (impure) detrital magnetites with a wide range of grain sizes and oxidation states. Furthermore, maghemite, ferrochromite and, relatively low-coercive minerals from the haematite-ilmenite series may be involved (Kumar and Bhalla, 1984; Robertson and France, 1994; Grygar et al., 2003; Egli, 2004a; Schnabl et al., 2010; Brownlee et al., 2011). The contribution of these components to the SIRM reaches 74%, making them the dominant remanence carrier. As seen from the weak NRM of most samples, the concentration is low, especially in the Viernheim and P36 cores, where these minerals mainly occur in the IFm. The coercivity spectra of these magnetite-like minerals overlap in the coercivity range between $B_{1/2}$ 51 mT and 61 mT (μ = 1.707-1.785, shown in dark blue in Fig. 3.11) with those of sulphides (discussed below); thus, the peaks cannot be attributed to one of these mineral groups with certainty.
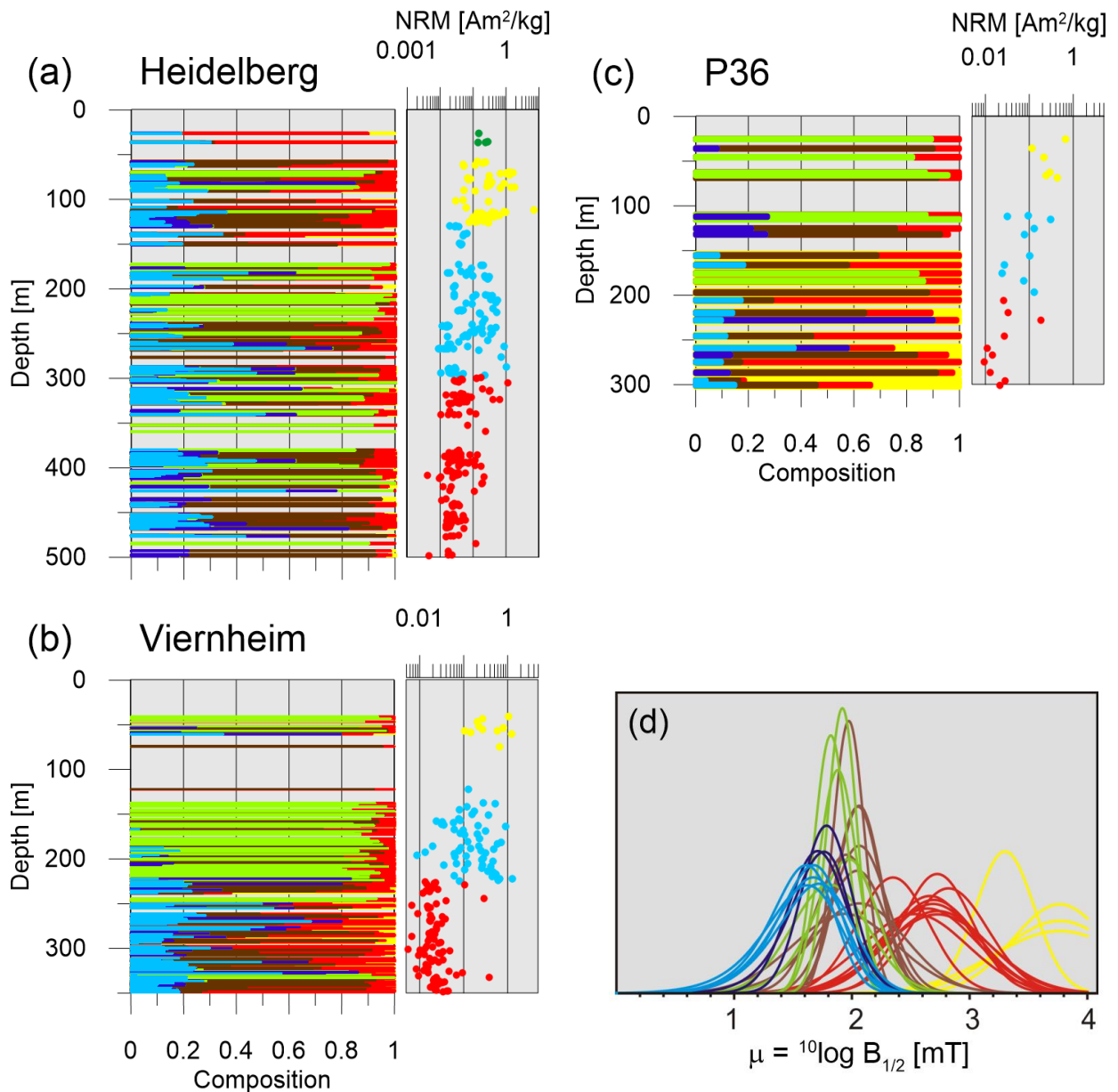
Figure 3.11:

(a–c) Composition (left) and NRM values (right) of individual samples from the cores. Compositions are indicated by colour-coded bars that show the relative portions of the respective magnetic mineralogy. Azure blue: magnetites and chromite; navy blue: magnetites and sulphides; green: sulphides; brown: sulphides and haemo-ilmenites; red: haematite; yellow: goethite. For details, see text. Unit colour code of NRM values follows that used in Fig. 3.1: green, MFm; yellow, LFm; blue, VFm; red, IFm. (d) Components used for modelling of the natural sample materials.

A major group of components is characterised by $B_{1/2}$-values ranging from 65 mT to 86 mT (μ = 1.813-1.933, green in Fig. 3.11). Frequently, two of these components can be identified within the same sample (clusters RC1 and RC3 in Tab. 3.3 and Tab. 3.4). These pairs consist of one component with small σ (not exceeding 0.16) and one with larger σ (between 0.29 and 0.33) and carry on average ~90% of the bulk SIRM; the associated samples show the largest NRM values of all of the sections.

Furthermore, all of the samples with strong contributions from these components are characterised by type-C thermomagnetic curves, which, as seen in section 3.4.4 and 3.4.5, are typical of iron sulphides. Similar combinations of coercivity components are interpreted as representing the co-occurrence of greigite magnetofossils and authigenic greigite (Vasiliev et al., 2008; Hüsing et al., 2009). The results of this study can appropriately be compared to those of Vasiliev et al. (2008); the contribution to M_{rs} of the component with small and large σ is 31-48% and ~50%, respectively (median values). In addition, the FORC diagram of sample UN080-22 closely resembles the one shown in Vasiliev et al. (2008). However, there are reasons not to attribute the narrow coercivity peak to greigite magnetofossils here. Contrary to Vasiliev et al (2008), high resolution FORCs were applied and revealed that the central ridge contribution of UN080-22 does not exceed 2% of M_{rs}. In addition, UN080-22 is composed of a higher coercive pair of components (cluster RC04) that fall within the subsequent range with $B_{1/2}$ = 87 mT to 116 mT (μ = 1.942-2.064, brown in Fig. 3.11). The properties of the components in this range vary strongly in every respect and are probably also related to oxides and sulphides.

Taken as a whole, the interpretation of the components in the $B_{1/2}$ range between 51 and 116 mT leaves many open questions. The components with larger σ-values probably include unquantifiable proportions of harder magnetites (Kruiver and Passier, 2001; Liu et al., 2007), pyrrhotite (Clark, 1984) and minerals from the ilmenite-haematite series (McEnroe et al., 2002; Brownlee et al., 2011). It should be borne in mind that previous sections have shown that these minerals co-occur with greigite. The unusually narrow coercivity distributions and relatively high coercivities of some components point towards SD magnetic particles with very uniform properties; possible candidates are magnetofossils (e.g., component BH in Egli (2004a)), both magnetite (elongated) and greigite, or quasi-ordered structures such as framboidal greigite aggregates (Rowan and Roberts, 2006), whose intrinsic FORC signature appears to be similar to that of UN080-22. None of these interpretations appears to fit all of the observed magnetic properties with our current knowledge; magnetofossils lack an appropriately large central ridge signature in FORC diagrams, and greigite magnetosomes are characterised by $B_{1/2}$ = 20-35 mT (Winklhofer et al., 2014). The coercivity argument holds also for authigenic greigite; the larger cubic magnetocrystalline anisotropy (17-26 kJ/m^3, compared to magnetite's 2.8 kJ/m^3 (Winklhofer et al., 2014) yields coercivities on the order of 40-50 mT. However, cation impurities in natural greigite, as well as unrecognised pyrrhotite lamellae, could increase the coercivity to the observed values (Winklhofer et al., 2014). The pyrrhotite lamellae hypothesis is supported by the presence of a positive internal bias field, which produces a downward shift of the central FORC maximum of greigite-bearing samples (Fig. 3.10). A magnetostatic origin of such a positive field appears unlikely, since it requires a type of loose, chain-like arrangement of SD particles that could only originate from magnetosome chains. However, magnetofossil-bearing sediments are never characterised by measurable internal bias fields (Egli et al., 2010, Ludwig et al., 2013). In conclusion,

Table 3.3: *Components determined using coercive analysis in the Mag-Mix software package (Egli 2003, 2004a), arranged in clusters.*

component	no	μ	B1/2 [mT]	σ	s	p
RC01-1	53	1.933	85.70	0.291	0.66	2.00
RC01-2	53	1.914	81.98	0.127	1.00	2.00
RC01-3	52	2.643	439.89	0.418	1.00	2.00
RC02-1	37	2.662	459.71	0.364	1.00	2.00
RC02-2	37	2.051	112.50	0.190	0.96	2.00
RC02-3	36	1.707	50.94	0.296	0.60	2.10
RC03-1	45	1.813	65.02	0.326	1.00	2.00
RC03-2	45	1.880	75.93	0.159	1.00	2.00
RC03-3	38	2.534	342.37	0.447	1.00	2.00
RC04-1	44	2.819	659.72	0.338	0.95	2.00
RC04-2	44	1.974	94.18	0.130	1.00	2.00
RC04-3	44	1.984	96.43	0.338	0.59	2.00
RC05-1	74	1.709	51.23	0.249	1.00	2.00
RC05-2	74	1.942	87.41	0.441	1.00	1.94
RC05-3	72	3.300	1995.26	0.250	0.95	2.00
RC05-4	71	2.724	529.71	0.297	0.95	2.00
RC06-1	23	1.563	36.54	0.373	0.62	2.00
RC06-2	26	1.950	89.18	0.256	0.95	2.00
RC06-3	26	2.694	494.41	0.380	0.95	2.00
RC07-1	19	2.687	486.49	0.397	0.95	2.00
RC07-2	19	2.064	115.98	0.240	1.00	2.00
RC07-3	19	1.561	36.40	0.316	0.62	2.00
RC08-1	59	2.062	115.33	0.189	1.00	2.00
RC08-2	64	1.624	42.08	0.316	0.62	2.00
RC08-3	64	2.726	532.48	0.450	0.95	2.00
RC08-4	9	3.763	5793.75	0.398	0.95	2.00
RC09-1	108	1.624	42.08	0.339	0.65	2.00
RC09-2	112	2.062	115.33	0.394	1.00	2.00
RC09-3	27	1.820	66.11	0.138	0.95	2.00
RC09-4	57	3.763	5793.75	0.490	0.95	2.00
RC09-5	111	2.726	532.48	0.431	0.95	2.00
RC10-1	30	3.763	5793.75	0.569	0.95	2.00
RC10-2	32	1.670	46.76	0.358	0.65	2.00
RC10-3	32	1.785	60.94	0.211	1.00	2.00
RC10-4	33	2.349	223.38	0.306	1.00	2.00

Note: Number of occurrences (no) and parameters (σ, μ, s, p).

Table 3.4: *Components arranged in order of ascending μ values, neglecting*

B1/2 [mT]	μ		no
36.40	1.561		19
36.54	1.563		23
42.08	1.624		172
46.76	1.670		32
50.94	1.707		36
51.23	1.709		74
60.94	1.785		32
65.02	1.813		45
66.11	1.820		27
75.93	1.880		45
81.89	1.914		53
85.70	1.933		53
87.41	1.942		74
89.18	1.950		26
94.18	1.974		44
96.43	1.984		44
112.50	2.051		37
115.33	2.062		171
115.98	2.064		19
223.38	2.349		33
342.37	2.534		38
439.89	2.643		52
459.71	2.662		37
486.49	2.687		19
494.41	2.694		26
529.71	2.724		71
532.48	2.726		175
659.72	2.819		44
1995.26	3.300		72
5793.75	3.763		96

Number of occurrences (no). Colour code as in Fig. 3.11: Azureblue: magnetites and chromite; navy blue: magnetites and sulphides; green: sulphides; brown: sulphides and haemo-ilmenites; red: haematite; yellow: goethite.

the most likely origin of the narrow coercivity components with $B_{1/2}$ = 60-100 mT is related to authigenic greigite with various degrees of cation substitution and/or pyrrhotite lamellae.

The remaining groups of coercivity components are characterised by $B_{1/2}$ values ranging from ~220 mT to ~530 mT (shown in red in Fig. 11d) and $B_{1/2}$ > 659 mT (shown in yellow in Fig. 3.11d), respectively. Because of their large coercivity, these components are generally not saturated, contributing significant uncertainty to the corresponding parameters. We expect minerals from the solid solution series from ilmenite to haematite to be associated with the components in the lower part of this coercivity range. For comparison, haematite coercivity distributions peak between 350 mT and 1000 mT as a function of grain size, stress, and chemical variations (Robertson and France, 1994; Kruiver and Passier, 2001; Kletetschka and Wasilewski, 2002; Liu et al., 2011; Dennie et al., 2012). Haematite can thus explain the intermediate components of this group. Finally, ultra-high coercivity components are associated with goethite (France and Oldfield, 2000). If components from this group are dominant, the NRM is generally low.

The overall distribution patterns of the components confirm that the succession reflected by the Heidelberg core had a different genesis than those of the other two cores. Whereas the Viernheim and P36 cores are characterised by the almost mutually exclusive occurrence of either greigite or a mixture of low-coercivity magnetite and high coercivity phases, all of the coercivity components occur in various proportions over almost the entire Heidelberg succession. This can be explained by its proximity to the graben shoulders and the influence of the Neckar River. A continuous delivery of red bed sediments from the hinterland into the Heidelberg area was provided by the Neckar and other streams. In addition, the interaction of continuous and high subsidence and a steady water supply likely led to a situation in which reducing conditions prevailed and sulphides survived.

3.5. Discussion

3.5.1. Magnetic mineralogy and environmental implications

Rock magnetic investigations reveal the presence of complex mixtures of iron oxides and sulphides, which point towards a complex formation history of the Heidelberg Basin sequences. The mineralogical composition, as well as the distribution pattern of the mottled colour variations in the Pliocene-age IFm, point to alternation of oxidising and reducing conditions during deposition and early diagenesis (Bown & Kraus 1987, Kraus, 1999, 2002). The sediments were mainly delivered from the graben shoulders and were thus primarily composed of a high proportion of stable minerals (Hagedorn and Boenigk, 2008). Upon deposition, the sediments underwent reducing diagenesis, followed by an

oxidising phase that was probably caused by repeated lowering of the groundwater table during seasonal or supra-seasonal (sub-orbital to orbital) climatic cycles. Largely humid climates gave rise to prevalent reducing conditions in which pyrite and greigite formed. Finally, the occurrence of haematite pseudomorphs after pyrite and the slightly pitted surfaces of haematite suggest an alternating sequence of oxidising and reducing conditions, during which Cr-spinels (Cr-magnetites) and ilmenites became concentrated due to their resistance to dissolution and replacement (Milliken and Mack, 1990; Hounslow, 1996; Maher and Hallam, 2005). The present appearance of the sediments exhibits pervasive oxidation of discrete horizons, as reflected by the dominance of haematite and goethite and by the occurrence of pedogenic pisolites. The haematite likely developed in arid conditions by the transformation of reactive iron into magnetite, maghemite and finally into haematite and from the oxidation of detrital precursors, respectively (e.g., Stacey and Banerjee, 1974; Turner, 1980; de Boer and Dekkers, 1996; Dunlop and Özdemir, 1997). Generally, the dissolution and/or conversion of detrital magnetic minerals become apparent by their only occasional appearance in SEM/EDX analyses and relatively low susceptibility (Fig. 3.7) and NRM values (Fig. 3.11). The magnetite-like signal observed in the thermomagnetic measurements and coercivity analyses is thus related to ferrimagnetic inclusions, which probably carry an appreciable part of the total magnetisation.

The greigite and pyrite in the IFm sediments of the Viernheim and P36 drill cores were probably destroyed during oxidising events. The frequently observed viscous magnetisations (Scheidt et al., 2015) may arise from such oxidation processes (Rowan and Roberts, 2006). If any, greigite seems to remain only in trace amounts. Since no sulphides were found in the SEM/EDX analyses, pyrite might have survived in the cores of oxidised grains, thus explaining the thermomagnetic measurements of the IFm extracts. In contrast, pyrite and its precursor greigite are preserved to a far greater extent in the sediments of the Heidelberg core, which presumably endured less frequent oxidising events. A substantial part of the differences between the rock magnetic parameters of the IFm in the Heidelberg core on the one hand and the Viernheim and P36 cores on the other hand are due to the presence or absence of greigite.

The Plio-Pleistocene-boundary is located in the uppermost part of the IFm (Scheidt et al., 2015) and coincides with a time interval characterised by major climate changes and that also featured an extension of the catchment of the Rhine River (Preusser, 2008). Accordingly, the mineral composition of the sediments from the VFm and the LFm indicate a different evolution of these Pleistocene units. In contrast to the IFm, the occurrences of haematite in the Pleistocene strata are attributed to the input of detrital material from the Neckar and the graben shoulders. Signs of authigenic formation have not been found. The Heidelberg core is particularly heavily affected by these denudation products of the Triassic hinterland, which led to a Pleistocene mineral association with significant amounts of high-coercivity constituents.

In all of the cores, the abundance of greigite indicates continued saturation of the sediment column with water, leading to overall steady reducing conditions. However, the time of formation of this mineral and the mechanism of its preservation is complex and not easily determined. A comprehensive overview of the relevant processes and key factors is provided in the literature (e.g., Heywood et al., 1991; Hoffmann, 1992; Fassbinder and Stanjek, 1994; Roberts, 1995; Wilkin and Barnes, 1997; Chang et al., 2009; Roberts et al., 2011; Roberts, 2015). For the purpose of this study, the following observations are important.

Although narrow coercivity distribution peaks are usually reported for magnetofossil components (Kruiver and Passier, 2001; Egli, 2004a, c), the bulk rock magnetic parameters (e.g., χARM/IRM (Moskowitz et al., 1993), not shown) and the lack of pronounced central ridges in the FORC diagrams are compatible with the signature of authigenic greigite. We postulate a detrital origin for most of the pyrrhotite in the Heidelberg Basin, since an authigenic origin implies unusually high pH values (>11) and elevated temperatures (~180°C) (Garrels and Christ, 1965). Outcrops of suitable igneous and metamorphic source rocks are located in the nearby Odenwald (Ramdohr, 1975). Transportation from the distal Alps also appears to have been possible, if the pyrrhotite were enclosed in minerals or mineral aggregates. Finally, minor amounts of authigenic pyrrhotite might occur as intergrowths with greigite, explaining the downward shift of the central maximum of the FORC diagrams of greigite-bearing samples.

The preservation of both sulphides points towards high accumulation rates, since detrital pyrrhotite is preserved from oxidation only if fast erosion is combined with rapid transportation and burial (e.g., Horng et al., 1998; Weaver et al., 2002; Horng and Roberts, 2006; Hu et al., 2006; Roberts, 2015). In the case of greigite, the availability of reactive iron, organic carbon, and reduced sulphur determines whether pyritisation occurs, or whether the reaction ends with the precursor minerals. High accumulation rates and rapid burial limit the availability of the reactants, thus enabling the preservation of greigite (Berner, 1970, Kao et al., 2004). In that respect, the identification of fragile magnetite remainders indicate that no shortage of iron occurred in those layers.

Furthermore, the presence of magnetic sulphide-free horizons with A-type thermomagnetic curves within sulphidic sections can also be explained by sudden depositional events that prevented pervasive reducing diagenesis.

The top layers may have been buried by sediment packages, restricting the availability of reactive sulphur and organic carbon. However, the existence of some of these A-type horizons caused by the oxidative loss of sulphide minerals, whether in situ or during storage after drilling, cannot be ruled out. Those processes are eventually associated with loss of susceptibility in the dark clayey layers, as described in section 3.4.3. In contrast, the intact habitus of minerals in some of the sandy sections and the occurrence of magnetite placers suggest prevailing non-reducing conditions.

The general lack of superparamagnetic behaviour indicates an extensive loss of fine-grained ferrimagnetic minerals, sulphides as well as oxides, which probably occurred during reducing diagenesis. In addition, both, greigite and magnetite are prone to be transferred into goethite or other oxyhydroxides under oxidising and humid conditions (e.g., Taylor et al., 2014)

Finally, the gravelly and coarse sandy sediments that are predominant within the MFm prevent meaningful interpretation of the magnetic mineralogy of this lithostratigraphic unit.

3.5.2. Reliability of palaeodirections carried by the detected minerals

The ability of magnetite-poor sediments to carry palaeomagnetic signals is still debated, especially with respect to the possibility that significant portions of the magnetic signal are carried by magnetic iron sulphides or haematite (e.g., Tauxe and Kent, 1984; Rösler et al., 1997; Liu et al., 2003; Horng and Roberts, 2006; Sagnotti et al., 2010; Nilsson et al., 2013). The possibility that these minerals formed long after deposition can greatly affect their magnetic recording reliability. Such problematic minerals are abundant in the sediments of the Heidelberg Basin.

The magnetic mineral assemblage of the IFm is mainly composed of Fe(-Ti) chromites, magnetite, (haemo)ilmenite, and high-coercive minerals, of which haematite makes up an important part of the majority of the samples (Tab. 3.3 & 3.4).

The ability of (haemo)ilmenite and Fe(-Ti) chromites to retain stable detrital remanent magnetisation (DRM) over geologically relevant times has been shown by several studies (e.g., Kumar and Bhalla, 1984; Lawson and Nord, 1984; Nord and Lawson, 1989; Hounslow et al., 1995; Hounslow and Maher, 1996; Maher and Hallam, 2005).

Based on the suggested authigenic haematite formation pathway, the recorded palaeodirections are also considered to be reliable: the surface-bound transformation of minerals into haematite occurred on the steadily subsiding floodplains of the proto-Rhine. Even though the deposited sediments might have been eroded or reworked, the formation of haematite was stopped by burial; thus, the preserved signals represent palaeomagnetic directions of the respective top layers (pDRM).

Finally, magnetites carry a part of the remanence in certain layers of the IFm. If prolonged reducing diagenesis dissolved the SD and PSD grain size fraction completely, no synsedimentary palaeomagnetic signal can be preserved. If, however, minor dissolution features indicate insignificant chemical alteration, magnetites in certain grain sizes may retain a stable palaeodirection, even after partial oxidation (Karlin and Levi, 1983; Ge et al., 2014). Magnetite and Ti-magnetite inclusions in ilmenite and other host minerals may also carry a reliable palaeomagnetic signal (Hounslow et al., 1995).

The palaeomagnetic reliability of iron sulphides is more difficult to assess. While some authors caution against the possibility of late greigite genesis (e.g., Florindo and Sagnotti, 1995; Jiang et al., 2001; Weaver et al., 2002; Roberts and Weaver, 2005; Sagnotti et al., 2005; Rowan et al., 2009), others report a stable pDRM that is related to an early diagenetic origin of this mineral (Canfield and Berner, 1987; Reynolds et al., 1999; Babinszki et al., 2007; Vasiliev et al., 2007; Frank et al., 2007). In addition, the rate of in situ greigite nucleation and growth ranges from a few years to thousands of years (Pye, 1981; Canfield and Berner, 1987; Reynolds et al., 1999).
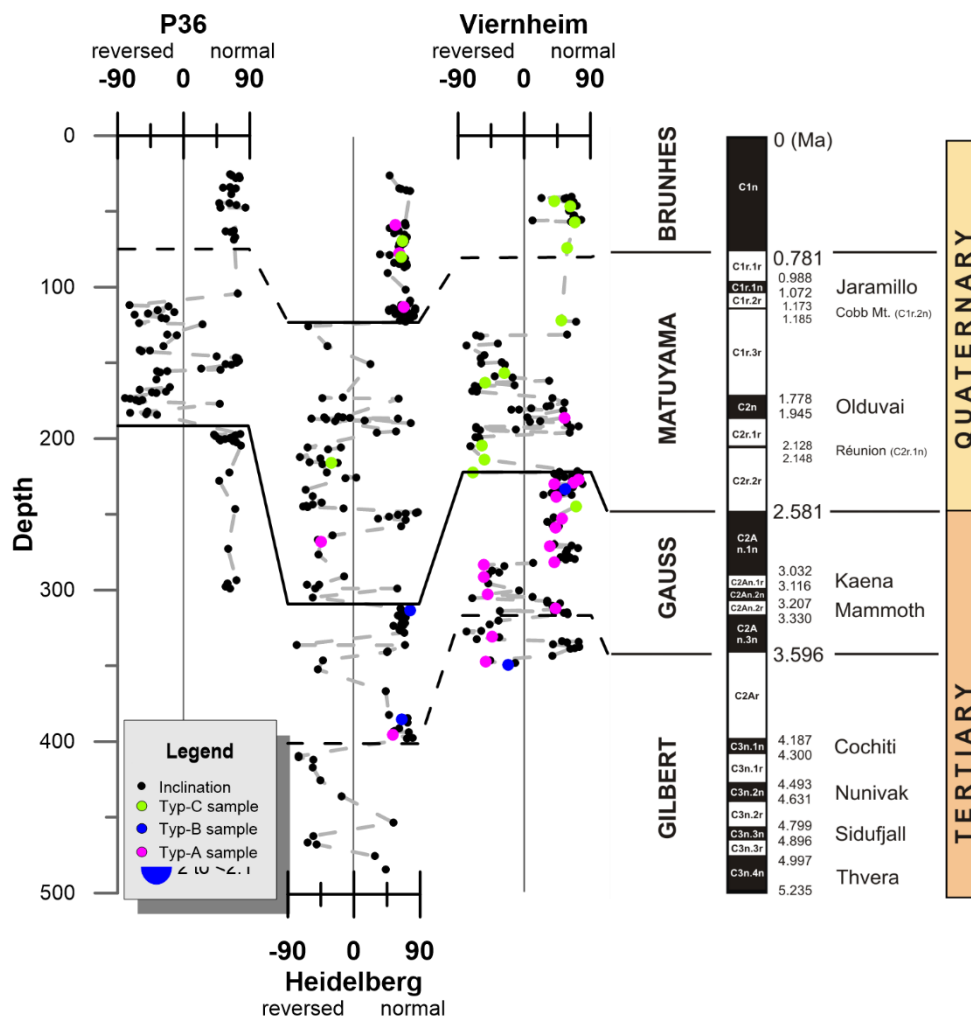
Figure 3.12:

Inclination values and deduced correlations with the geomagnetic polarity time scale (GPTS), as shown in Scheidt et al (2015). GPTS after Cande & Kent (1995),as shown in Ogg et al. (2016). Inclination values are indicated by thermomagnetic group affiliation, as in Fig. 8: pink, group A; blue, group B; green, group C; or by black filled dots if no thermomagnetic measurements were performed. Correlation lines are shown as solid lines and dashed lines for clear and inconclusive positions, respectively. The latter cases result from data gaps (for details, see Scheidt et al. 2015).

Palaeomagnetic information from the Heidelberg basin should be evaluated carefully, considering that the geological settings are characterised by episodic accumulation and erosion events. The magnetostratigraphy was obtained from samples selected after the application of stringent quality criteria that were created with the aim of isolating the characteristic remanent magnetisation (ChRM; for details see Scheidt et al. (2015)). The resultant polarity stratigraphy does not show any correlation with the magnetic mineralogy, as indicated by the thermomagnetic group affiliations (Fig. 3.12). In particular, the coincidence of DRM-carrying samples (A-type thermomagnetic properties) and samples which contain authigenic minerals (B- and C-type thermomagnetic curves) indicates the formation of pDRM-carrying authigenic minerals shortly after deposition. The insignificant occurrence of some layers showing mixed (normal and reverse) polarity within the normal Olduvai and Jaramillo events, as recorded in the Viernheim core and the Heidelberg core, respectively (Fig. 3.12; cf. (Scheidt et al., 2015)), likely results from late mineral formation but does not impair the overall good results.

3.6. Conclusions

The combined results of rock magnetic analyses and SEM/EDX observations demonstrate that meaningful results can be obtained from unconsolidated, fluvial dominated sedimentary successions from the Plio-Pleistocene of the URG. It has been shown that the interpretation of the magnetic mineralogy is very complex, due to the simultaneous occurrence of several magnetic components. In this study, the combination of EDX/SEM, thermomagnetic measurements, CLG curves and FORC diagrams enable the identification of up to five coexisting magnetic components. In contrast, bulk magnetic parameters were only able to depict general trends in terms of bulk coercivity, for example. The effects of magnetic grain size variations were superimposed by the stronger effects of the natural variances of the components; thus, they cannot be assessed.

The reconstructed magnetic mineralogy provides insights into the complex history of evolution of this basin, which can be summarised as follows. The Tertiary-age IFm underwent recurrent reducing diagenesis and subsequent oxidation events. Accordingly, most of the magnetite grains dissolved or transformed into haematite and goethite. Greigite and pyrite survived only under the moist conditions and higher accumulation rates found in the centre of subsidence (Heidelberg) and have been almost entirely oxidised in other locations within the basin. The IFm retains a primary DRM that is carried by ferrian ilmenites, titanomagnetite, Cr-Fe spinels, and impure magnetites. The haematite holds a pDRM/CRM (chemical remanent magnetisation) and imparts the distinctive colour to the sediments. During the accumulation of the Pleistocene-age VFm and LFm, reducing conditions continued, and these conditions persisted during diagenesis. Thus, sulphides became the main remanent magnetisation carriers. The magnetites were preserved mainly because of sudden sedimentation

events that restricted the availability of sulphate or organic matter. An insufficient supply of these reactants must also have stopped the pyritisation process, leading to the preservation of initially formed greigite and pyrrhotite over geological time. Magnetite and greigite magnetofossils are practically absent.

In summary, meaningful rock magnetic and palaeomagnetic results could be obtained, despite the heterogeneous and complex composition of the sediments and the enormous volume of the analysed sample set. These results enable us to disentangle the magnetic mineral compositions of fluvial dominated environments and to confirm the reliability of the magnetic polarity stratigraphy of the Heidelberg Basin (Scheidt et al., 2015). The combination of techniques used in this study may provide a template for future fluvial basin analyses.

References

AHMED, S.S., MIAH, M.Y., QUMRUZZAMAN, C., ZAMAN, M.N., ALAM, A.B. & BISWAS, P.K., 2010. Alteration and Exsolution Characteristics of Ilmenites of Moheskhali Island, Chittagong, Bangladesh, Bangladesh Journal of Scientific and Industrial Research, 45, 17-26.

BABINSZKI, E., MÁRTON, E., MÁRTON, P. & KISS, L.F., 2007. Widespread occurrence of greigite in the sediments of Lake Pannon: Implications for environment and magnetostratigraphy, Palaeogeography, Palaeoclimatology, Palaeoecology, 252, 626-636.

BARTZ, J., 1959. Gliederung des Pleistozäns im Oberrheingebiet, Zeitschrift der Deutschen Geologischen Gesellschaft, 739-781.

BARTZ, J., 1974. Die Mächtigkeit des Quartärs im Oberrheingraben. in Approaches to Taphrogenesis, pp. 78-87, eds. Illies, J. H. & Fuchs, K. Schweizerbart, Stuttgart.

BARTZ, J., 1976. Quartär und Jungtertiär im Raum Rastatt, Jh geol Landesamt Baden-Würtemberg, 18, 121-178.

BARTZ, J., VON BREILIE, G. & MAUS, H., 1982. Quartär und Jungtertiär II im Oberrheingraben im Großraum Karlsruhe, Geologisches Jahrbuch, A, 237.

BERNAL, J., DASGUPTA, D. & MACKAY, A., 1957. Oriented transformations in iron oxides and hydroxides, Nature, 180, 645-647.

BERNER, R.A., 1970. Sedimentary pyrite formation, American Journal of Science, 268, 1-23.

BISWAS, D.K., HYODO, M., TANIGUCHI, Y., KANEKO, M., KATOH, S., SATO, H., KINUGASA, Y. & MIZUNO, K., 1999. Magnetostratigraphy of Plio-Pleistocene sediments in a 1700-m core from Osaka Bay, southwestern Japan and short geomagnetic events in the middle Matuyama and early Brunhes chrons, Palaeogeography, Palaeoclimatology, Palaeoecology, 148, 233-248.

BLOEMENDAL, J., KING, J., HALL, F. & DOH, S.J., 1992. Rock magnetism of Late Neogene and Pleistocene deep-sea sediments: Relationship to sediment source, diagenetic processes, and sediment lithology, Journal of Geophysical Research: Solid Earth (1978–2012), 97, 4361-4375.

BOWN, T.M. & KRAUS, M.J., 1987. Integration of channel and floodplain suites, I. Developmental sequence and lateral relations of alluvial paleosols, Journal of Sedimentary Research, 57 (4): 587–601.

BROWNLEE, S.J., FEINBERG, J.M., KASAMA, T., HARRISON, R.J., SCOTT, G.R. & RENNE, P.R., 2011. Magnetic properties of ilmenite-hematite single crystals from the Ecstall pluton near Prince Rupert, British Columbia, Geochemistry, Geophysics, Geosystems, 12, Q07Z29, doi: 10.1029/2011GC003622.

BUNESS, H., GABRIEL, G. & ELLWANGER, D., 2008. The Heidelberg Basin drilling project: Geophysical pre-site surveys, E & G (Quaternary Science Journal), 57, 338-366.

CANDE, S.C. & KENT, D.V., 1995. Revised calibration of the geomagnetic polarity timescale for the Late Cretaceous and Cenozoic, Journal of Geophysical Research: Solid Earth, 100, 6093-6095.

CANFIELD, D.E. & BERNER, R.A., 1987. Dissolution and pyritization of magnetite in anoxie marine sediments, Geochimica et Cosmochimica Acta, 51, 645-659.

CHANG, L., ROBERTS, A.P., ROWAN, C.J., TANG, Y., PRUNER, P., CHEN, Q. & HORNG, C.S., 2009. Low-temperature magnetic properties of greigite (Fe3S4), Geochemistry, Geophysics, Geosystems, 10, Q01Y04, doi: 10.1029/2008GC002276.

CLARK, D., 1984. Hysteresis properties of sized dispersed monoclinic pyrrhotite grains, Geophysical Research Letters, 11, 173-176.

DA COSTA, G., DE GRAVE, E., BOWEN, L., DE BAKKER, P. & VANDENBERGHE, R., 1995. Temperature dependence of the hyperfine parameters of maghemite and Al-substituted maghemites, Physics and Chemistry of Minerals, 22, 178-185.

DAY, R., FULLER, M. & SCHMIDT, V.A., 1977. Hysteresis properties of titanomagnetites; grain-size and compositional dependence, Physics of The Earth and Planetary Interiors, 13, 260-267.

DE BOER, C.B. & DEKKERS, M.J., 1996. Grain-size dependence of the rock magnetic properties for a natural maghemite, Geophysical Research Letters, 23, 2815-2818.

DE BOER, C.B., DEKKERS, M.J. & VAN HOOF, T., 2001. Rock-magnetic properties of TRM carrying baked and molten rocks straddling burnt coal seams. In: Physics of the Earth and Planetary Interiors, 126, 93-108, Elsevier: Amsterdam, Netherlands, Netherlands.

DEARING, J.A., 1999. Holocene environmental change from magnetic proxies in lake sediments. In: MAHER, B. A. & THOMPSON, R. (eds.) Quaternary Climates, Environments and Magnetism. Cambridge University Press, p. 231-278.

DEKKERS, M.J., 1989. Magnetic properties of natural pyrrhotite; II, High- and low-temperature behaviour of J_{rs} and TRM as function of grain size, Physics of the Earth and Planetary Interiors, 57, 3-4, 266-283.

DENNIE, D., ELMORE, R., DENG, J., MANNING, E. & PANNALAL, J., 2012. Palaeomagnetism of the Mississippian Barnett Shale, Fort Worth Basin, Texas, Geological Society, London, Special Publications, 371, 89-106.

DIMANCHE, F. & BARTHOLOME, P., 1976. The alteration of ilmenite in sediments, Minerals Science and Engineering, 8(3), 187-201.

DUNLOP, D.J., 2002a. Theory and application of the Day plot (Mrs/Ms versus Hcr/Hc) 1. Theoretical curves and tests using titanomagnetite data, Journal of Geophysical Research: Solid Earth (1978–2012), 107, EPM 4-1-EPM 4-22.

DUNLOP, D.J., 2002b. Theory and application of the Day plot (Mrs/Ms versus Hcr/Hc) 2. Application to data for rocks, sediments, and soils, Journal of Geophysical Research: Solid Earth (1978–2012), 107, EPM 5-1-EPM 5-15.

DUNLOP, D.J. & ÖZDEMIR, Ö., 1997. Rock Magnetism: Fundamentals and frontiers, edn, Vol. 3, pp. Pages, Cambridge University Press, Cambridge.

EGLI, R., 2003. Analysis of the field dependence of remanent magnetization curves, Journal of Geophysical Research: Solid Earth, 108, 2081, doi:10.1029/2002JB002023, B2.

EGLI, R., 2004a. Characterization of individual rock magnetic components by analysis of remanence curves. 1. Unmixing natural sediments, Studia Geophysica et Geodaetica, 48, 391-446.

EGLI, R., 2004b. Characterization of individual rock magnetic components by analysis of remanence curves. 2. Fundamental properties of coercivity distributions, Physics and Chemistry of the Earth, Parts A/B/C, 29, 851-867.

EGLI, R., 2004c. Characterization of individual rock magnetic components by analysis of remanence curves. 3. Bacterial magnetite and natural processes in lakes, Physics and Chemistry of the Earth, Parts A/B/C, 29, 869-884.

EGLI, R., 2013. VARIFORC: An optimized protocol for calculating non-regular first-order reversal curve (FORC) diagrams, Global and Planetary Change, 110, 302-320.

EGLI, R., CHEN, A.P., WINKLHOFER, M., KODAMA, K.P. & HORNG, C.S., 2010. Detection of noninteracting single domain particles using first-order reversal curve diagrams, Geochemistry, Geophysics, Geosystems, 11, Q01Z11, doi:10.1029/2009GC002916.

ELLWANGER, D., GABRIEL, G., HOSELMANN, C., WEIDENFELLER, M. & WIELANDT-SCHUSTER, U., 2010a. Mannheim-Formation. in Litholex (online database) Federal Institute for Geosciences and Natural Resources (BGR), http://www.bgr.bund.de/litholex.

ELLWANGER, D., GABRIEL, G., SIMON, T., WIELANDT-SCHUSTER, U., GREILING, R., HAGEDORN, E.-M., HAHNE, J. & HEINZ, J., 2008. Long sequence of Quaternary Rocks in the Heidelberg Basin Depocentre, E & G (Quaternary Science Journal), 57, 316-337.

ELLWANGER, D., GRIMM, M., HOSELMANN, C., HOTTENROTT, M., WEIDENFELLER, M. & WIELANDT-SCHUSTER, U., 2010b. Iffezheim-Formation. in Litholex (online database) Federal Institute for Geosciences and Natural Resources (BGR), http://www.bgr.bund.de/litholex.

ELLWANGER, D. & WIELAND-SCHUSTER, U., 2012. Fotodokumentation und Schichtenverzeichnis der Forschungsbohrungen Heidelberg UniNord I und II, LGRB-Informationen, 26, 25-86.

FABIAN, K., 2003. Some additional parameters to estimate domain state from isothermal magnetization measurements, Earth and Planetary Science Letters, 213, 337-345.

FASSBINDER, J. W. & STANJEK, H. 1994. Magnetic properties of biogenic soil greigite (Fe_3S_4). Geophysical Research Letters, 21, 2349-2352. FLORINDO, F. & SAGNOTTI, L., 1995. Palaeomagnetism and rock magnetism in the upper Pliocene Valle Ricca (Rome, Italy) section, Geophysical Journal International, 123, 340-354.

FRANCE, D. & OLDFIELD, F., 2000. Identifying goethite and hematite from rock magnetic measurements of soils and sediments, Journal of Geophysical Research: Solid Earth, 105, 2781-2795.

FRANK, U., NOWACZYK, N.R. & NEGENDANK, J., 2007. Palaeomagnetism of greigite bearing sediments from the Dead Sea, Israel, Geophysical Journal International 168, 904-920.

GABRIEL, G., ELLWANGER, D., HOSELMANN, C. & WEIDENFELLER, M., 2008. Preface: The Heidelberg Basin Drilling Project, E & G (Quaternary Science Journal), 57, 253-260.

GAPEEV, A. & TSEL'MOVICH, V., 1983. Microstructure of synthetic titanomagnetite oxidized at high partial pressures of oxigen, Phys. Solid Earth, 19, 983-986.

GAPEEV, A. & TSEL'MOVICH, V., 1988. Microstructure and composition of multiphase-oxidized natural and synthetic titanomagnetites, Fiz. Zemli, 10, 42-49.

GARRELS, R.M. & CHRIST, C.L., 1965. Solutions, Minerals, and Equilibria, Harper & Raw, pp. 216-225.

GE, K., WILLIAMS, W., LIU, Q. & YU, Y., 2014. Effects of the core-shell structure on the magnetic properties of partially oxidized magnetite grains: experimental and micromagnetic investigations, Geochemistry, Geophysics, Geosystems, 15, 2021–2038, doi: 10.1002/2014GC005265.

GEHRING, A. & HOFMEISTER, A., 1994. The transformation of lepidocrocite during heating: a magnetic and spectroscopic study, Clays and Clay Minerals, 42, 409-415.

GENDLER, T., KROPÁČEK, V. & ZAPLETAL, R.K., 1979. Change of structure, phase composition and magnetic properties with the oxidation of titanomagnetites, Studia Geophysica et Geodaetica, 23, 42-54.

GENDLER, T.S., SHCHERBAKOV, V.P., DEKKERS, M.J., GAPEEV, A.K., GRIBOV, S.K. & MCCLELLAND, E., 2005. The lepidocrocite-maghemite-haematite reaction chain; I, Acquisition of chemical remanent magnetization by maghemite, its magnetic properties and thermal stability, Geophysical Journal International, 160, 815-832.

GRYGAR, T., BEZDICKA, P., DEDECEK, J., PETROVSKY, E. & SCHNEEWEISS, O., 2003. Fe_2O_3-Cr_2O_3 system revised, CERAMICS SILIKATY, 47, 32-39.

HAGEDORN, E.-M., 2004. Sedimentpetrographie und Lithofazies der Jungtertiären und Quartären Sedimente im Oberrheingebiet, Dissertation, Universität zu Köln, Köln.

HAGEDORN, E.-M. & BOENIGK, W., 2008. The Pliocene and Quaternary sedimentary and fluvial history in the Upper Rhine Graben based on heavy mineral analyses, Netherlands Journal of Geosciences, 87, 19-30.

HALLAM, D.F. & MAHER, B.A., 1994. A record of reversed polarity carried by the iron sulphide greigite in British early Pleistocene sediments, Earth and Planetary Science Letters, 121, 71-80.

HEISZ, S. & HILSCHER, G., 1987. The origin of graduated demagnetization curves of Nd · Fe · B magnets, Journal of Magnetism and Magnetic Materials, 67, 20-28.

HELLER, F. & LIU, T.-S., 1986. Palaeoclimatic and sedimentary history from magnetic susceptibility of loess in China, Geophysical Research Letters, 13, 1169–1172.

HESLOP, D. & DILLON, M., 2007. Unmixing magnetic remanence curves without a priori knowledge, Geophysical Journal International, 170, 556-566.

HESLOP, D. & ROBERTS, A., 2012. Unmixing Magnetic Hysteresis Loops. in EGU General Assembly Conference Abstracts, pp. 3758.

HESLOP, D., ROBERTS, A.P. & CHANG, L., 2014. Characterizing magnetofossils from first-order reversal curve (FORC) central ridge signatures, Geochemistry, Geophysics, Geosystems, 15, 2170-2179.

HESLOP, D., ROBERTS, A.P., CHANG, L., DAVIES, M., ABRAJEVITCH, A. & DE DECKKER, P., 2013. Quantifying magnetite magnetofossil contributions to sedimentary magnetizations, Earth and Planetary Science Letters, 382, 58-65.

HEYWOOD, B.R., MANN, S. & FRANKEL, R.B., 1991. Structure, morphology and growth of biogenic greigite (Fe_3S_4). in Proceedings of the Materials Research Society Symposium, Cambridge Univ Press, pp. 93-108.

HOFFMANN, V., 1992. Greigite (Fe_3S_4): magnetic properties and first domain observations, Physics of The Earth and Planetary Interiors, 70, 288-301.

HORNG, C.-S. & ROBERTS, A.P., 2006. Authigenic or detrital origin of pyrrhotite in sediments?: Resolving a paleomagnetic conundrum, Earth and Planetary Science Letters, 241, 750-762.

HORNG, C.-S., TORII, M., SHEA, K.-S. & KAO, S.-J., 1998. Inconsistent magnetic polarities between greigite- and pyrrhotite/magnetite-bearing marine sediments from the Tsailiao-chi section, southwestern Taiwan, Earth and Planetary Science Letters, 164, 467-481.

HOSELMANN, C., 2008. The Pliocene and Pleistocene fluvial evolution in the northern Upper Rhine Graben based on results of the research borehole at Viernheim (Hessen, Germany), E & G (Quaternary Science Journal), 57, 286-315.

HOSELMANN, C., ELLWANGER, D., GABRIEL, G., WEIDENFELLER, M. & WIELANDT-SCHUSTER, U., 2010. Viernheim-Formation. in Litholex (online database) Federal Institute for Geosciences and Natural Resources (BGR), http://www.bgr.bund.de/litholex.

HOUNSLOW, M.W., 1996. Ferrimagnetic Cr and Mn spinels in sediments: residual magnetic minerals after diagenetic dissolution, Geophysical Research Letters, 23, 2823-2826.

HOUNSLOW, M.W. & MAHER, B.A., 1996. Quantitative extraction and analysis of carriers of magnetization in sediments, Geophysical Journal International, 124, 57-74.

HOUNSLOW, M.W., MAHER, B.A. & THISTLEWOOD, L., 1995. Magnetic mineralogy of sandstones from the Lunde Formation (late Triassic), northern North Sea, UK: origin of the palaeomagnetic signal, Geological Society, London, Special Publications, 98, 119-147.

HOUSEN, B.A., BANERJEE, S.K. & MOSKOWITZ, B.M., 1996. Low-temperature magnetic properties of siderite and magnetite in marine sediments, Geophysical Research Letters, 23, 2843-2846.

HU, G., DAM-JOHANSEN, K., WEDEL, S. & HANSEN, J.P., 2006. Decomposition and oxidation of pyrite, Progress in Energy and Combustion Science, 32, 295-314.

HÜSING, S., DEKKERS, M.J., FRANKE, C. & KRIJGSMAN, W., 2009. The Tortonian reference section at Monte dei Corvi (Italy): evidence for early remanence acquisition in greigite-bearing sediments, Geophysical Journal International, 179, 125-143.

JIANG, W.-T., HORNG, C.-S., ROBERTS, A.P. & PEACOR, D.R., 2001. Contradictory magnetic polarities in sediments and variable timing of neoformation of authigenic greigite, Earth and Planetary Science Letters, 193, 1-12.

JOHNSON, N.M., JORDAN, T.E., JOHNSSON, P.A. & NAESER, C.W., 1986. Magnetic polarity stratigraphy, age and tectonic setting of fluvial sediments in an eastern Andean foreland basin, San Juan Province, Argentina, in: Foreland basins, pp. 63-75, eds Allen, P.A. & Homewookd, P., Blackwell Publishing Ltd.

JUST, J., DEKKERS, M.J., DOBENECK, T., HOESEL, A. & BICKERT, T., 2012. Signatures and significance of aeolian, fluvial, bacterial and diagenetic magnetic mineral fractions in Late Quaternary marine sediments off Gambia, NW Africa, Geochemistry, Geophysics, Geosystems, 13, Q0AO02, doi: 10.1029/2012GC004146.

KĄDZIAŁKO-HOFMOKL, M., JELEŃSKA, M., DELURA, K. & BYLINA, P., 2010. Magnetic mineralogy and paleomagnetism of serpentinized ultramafic rocks from the Braszowice-Brzeźnica fragment of sudetic paleozoic ophiolite, Acta Geophysica, 58, 269-299.

KAO, S.-J., HORNG, C.-S., ROBERTS, A.P. & LIU, K.-K., 2004. Carbon–sulfur–iron relationships in sedimentary rocks from southwestern Taiwan: influence of geochemical environment on greigite and pyrrhotite formation, Chemical Geology, 203, 153-168.

KARLIN, R. & LEVI, S., 1983. Diagenesis of magnetic minerals in recent haemipelagic sediments, Nature, 303, 327-330.

KEMPF, O., MATTER, A., BURBANK, D. & MANGE, M., 1999. Depositional and structural evolution of a foreland basin margin in a magnetostratigraphic framework: the eastern Swiss Molasse Basin, International Journal of Earth Sciences, 88, 253-275.

KHOR, L., PARKS, T., LINCOLN, F.J. & GRAHAM, J., 1996. The distribution of contaminants and the nature of the alteration products in physically separated grains of altered ilmenites, Australian journal of chemistry, 49, 847-860.

KIND, J., GEHRING, A.U., WINKLHOFER, M. & HIRT, A.M., 2011. Combined use of magnetometry and spectroscopy for identifying magnetofossils in sediments, Geochemistry, Geophysics, Geosystems, 12, Q08008, doi: 10.1029/2011GC003633.

KLETETSCHKA, G. & WASILEWSKI, P.J., 2002. Grain size limit for SD hematite, Physics of The Earth and Planetary Interiors, 129, 173-179.

KRAUS, M.J., 2002. Basin-scale changes in floodplain paleosols: implications for interpreting alluvial architecture, Journal of Sedimentary Research, 72, 500-509.

KRUIVER, P., DEKKERS, M.J. & HESLOP, D., 2001. Quantification of magnetic coercivity components by the analysis of acquisition curves of isothermal remanent magnetisation, Earth and Planetary Science Letters, 189, 269-276.

KRUIVER, P.P. & PASSIER, H.F., 2001. Coercivity analysis of magnetic phases in sapropel S1 related to variations in redox conditions, including an investigation of the S ratio, Geochemistry, Geophysics, Geosystems, 2, 1063, doi: 10.1029/2001GC000181.

LAWSON, C.A. & NORD, G.L., 1984. Remanent magnetization of a "paramagnetic" composition in the ilmenite-hematite solid solution series, Geophysical Research Letters, 11, 197-200.

LEONHARDT, R., 2006. Analyzing rock magnetic measurements: the RockMagAnalyzer 1.0 software, Computers & Geosciences, 32, 1420-1431.

LIU, C., GE, K., ZHANG, C., LIU, Q., DENG, C. & ZHU, R., 2011. Nature of remagnetization of Lower Triassic red beds in southwestern China, Geophysical Journal International, 187, 1237-1249.

LIU, Q., DENG, C., TORRENT, J. & ZHU, R., 2007. Review of recent developments in mineral magnetism of the Chinese loess, Quaternary Science Reviews, 26, 368-385.

LIU, X., SHAW, J., JIANG, J., BLOEMENDAL, J., HESSE, P., ROLPH, T. & MAO, X., 2010. Analysis on variety and characteristics of maghemite, Science China Earth Sciences, 53, 1153-1162.

LIU, X., SHAW, J., LIU, T. & HELLER, F., 1993. Magnetic susceptibility of the Chinese loess-Palaeosol sequence; environmental change and pedogenesis, Journal of the Geological Society of London, 150, Part 3, 583-588.

LIU, Z., ZHAO, X., WANG, C., LIU, S. & YI, H., 2003. Magnetostratigraphy of Tertiary sediments from the Hoh Xil Basin: implications for the Cenozoic tectonic history of the Tibetan Plateau, Geophysical Journal International, 154, 233-252.

LUCIFORA, S., CIFELLI, F., MATTEI, M., SAGNOTTI, L., COSENTINO, D. & ROBERTS, A.P., 2012. Inconsistent magnetic polarities in magnetite- and greigite-bearing sediments: Understanding complex magnetizations in the late Messinian in the Adana Basin (southern Turkey), Geochemistry, Geophysics, Geosystems, 13, Q10002, doi: 10.1029/2012GC004248.

LUDWIG, P., EGLI, R., BISHOP, S., CHERNENKO, V., FREDERICHS, T., RUGEL, G., MERCHEL, S. & ORGEIRA, M., 2013. Characterization of primary and secondary magnetite in marine sediment by combining chemical and magnetic unmixing techniques, Global and Planetary Change, 110, 321-339.

MAHER, B.A., 1988. Magnetic properties of some synthetic sub-micron magnetites, Geophysical Journal, 94, 83-96.

MAHER, B.A. & HALLAM, D.F., 2005. Magnetic carriers and remanence mechanisms in magnetite-poor sediments of Pleistocene age, southern North Sea margin, Journal of Quaternary Science, 20, 79-94.

MAKSIMOCHKIN, V., GUBAIDULLIN, R. & GAREEVA, M.Y., 2013. Magnetic properties and structure of $Fe_{2-x} Mg_x CrO_4$ chromites, Moscow University Physics Bulletin, 68, 241-248.

MCENROE, S.A., HARRISON, R.J., ROBINSON, P. & LANGENHORST, F., 2002. Nanoscale haematite–ilmenite lamellae in massive ilmenite rock: an example of 'lamellar magnetism' with implications for planetary magnetic anomalies, Geophysical Journal International, 151, 890-912.

MENZIES, J. & ELLWANGER, D., 2015. Climate and paleo-environmental change within the Mannheim Formation near Heidelberg, Upper Rhine Valley, Germany: A case study based upon microsedimentological analyses, Quaternary International, 386, 137-147.

MIALL, A., 2013. The geology of fluvial deposits: sedimentary facies, basin analysis, and petroleum geology, edn, Vol., pp. Pages, Springer.

MILLIKEN, K. & MACK, L., 1990. Subsurface dissolution of heavy minerals, Frio Formation sandstones of the ancestral Rio Grande Province, South Texas, Sedimentary Geology, 68, 187-199.

MOSKOWITZ, B.M., FRANKEL, R. & BAZYLINSKI, D., 1993. Rock magnetic criteria for the detection of biogenic magnetite, Earth and Planetary Science Letters, 120, 283–300.

MURTHY, I.R. & KRISHNAMACHARYULU, S., 1994. Identification of NRM carriers in chromite ores by alternating field and thermal demagnetization studies, Current Science, 66, 373-375.

MUXWORTHY, A.R. & DUNLOP, D.J., 2002. First-order reversal curve (FORC) diagrams for pseudo-single-domain magnetites at high temperature, Earth and Planetary Science Letters, 203, 369-382.

NEWELL, A.J., 2005. A high-precision model of first-order reversal curve (FORC) functions for single-domain ferromagnets with uniaxial anisotropy, Geochemistry, Geophysics, Geosystems, 6, Q05010, doi: 10.1029/2004GC000877.

NILSSON, A., LEE, Y.S., SNOWBALL, I. & HILL, M., 2013. Magnetostratigraphic importance of secondary chemical remanent magnetizations carried by greigite (Fe_3S_4) in Miocene sediments, New Jersey shelf (IODP Expedition 313), Geosphere, 9, 510-520.

NORD, G.L. & LAWSON, C.A., 1989. Order-disorder transition-induced twin domains and magnetic properties in ilmenite-hematite, American Mineralogist, 74, 160-176.

NOWACZYK, N.R., 2011. Dissolution of titanomagnetite and sulphidization in sediments from Lake Kinneret, Israel, Geophysical Journal International, 187, 34-44.

OGG, J.G., OGG, G. & GRADSTEIN, F.M., 2016. A Concise Geologic Time Scale: 2016, pp. 203-223, Elsevier.

ÖZDEMIR, Ö., 1990. High-temperature hysteresis and thermoremanence of single-domain maghemite, Physics of The Earth and Planetary Interiors, 65, 125-136.

PAN, Y., ZHU, R., BANERJEE, S.K., GILL, J. & WILLIAMS, Q., 2000. Rock magnetic properties related to thermal treatment of siderite: Behavior and interpretation, Journal of Geophysical Research: Solid Earth, 105, 783-794.

PASSIER, H., DE LANGE, G. & DEKKERS, M.J., 2001. Magnetic properties and geochemistry of the active oxidation front and the youngest sapropel in the eastern Mediterranean Sea, Geophysical Journal International, 145, 604-614.

PETERSEN, N. & VALI, H., 1987. Observation of shrinkage cracks in ocean floor titanomagnetites, Physics of The Earth and Planetary Interiors, 46, 197-205.

PETERSEN, N., VON DOBENECK, T. & VALI, H., 1986. Fossil bacterial magnetite in deep -sea sediments from the South Atlantic Ocean, Nature, 320, 611-615.

PIKE, C.R., ROBERTS, A.P. & VEROSUB, K.L., 1999. Characterizing interactions in fine magnetic particle systems using first order reversal curves, Journal of Applied Physics, 85, 6660-6667.

PREUSSER, F., 2008. Characterisation and evolution of the River Rhine system., Netherlands Journal of Geosciences, 87, 7-19.

PRICE, G., 1980. Exsolution microstructures in titanomagnetites and their magnetic significance, Physics of The Earth and Planetary Interiors, 23, 2-12.

PRZYROWSKI, R. & SCHÄFER, A., 2015. Quaternary fluvial basin of northern Upper Rhine Graben, Zeitschrift der Deutschen Gesellschaft für Geowissenschaften, 166, 71-98.

PYE, K., 1981. Marshrock formed by iron sulphide and siderite cementation in saltmarsh sediments, Nature, 294, 650-652.

RAMDOHR, R., 1975. Die Lagerstätten des Odenwaldes, Aufschluß, Sonderbd, 27.

REINHOLDSSON, M., SNOWBALL, I., ZILLÉN, L., LENZ, C. & CONLEY, D., 2013. Magnetic enhancement of Baltic Sea sapropels by greigite magnetofossils, Earth and Planetary Science Letters, 366, 137-150.

REITER, W., ELFERT, S., GLOTZBACH, C. & SPIEGEL, C., 2015. Plio-Pleistocene evolution of the north Alpine drainage system: new constraints from detrital thermochronology of foreland deposits, International Journal of Earth Sciences, 104, 891-907.

REYNOLDS, R., ROSENBAUM, J., VAN METRE, P., TUTTLE, M., CALLENDER, E. & GOLDIN, A., 1999. Greigite (Fe_3S_4) as an indicator of drought – The 1912–1994 sediment magnetic record from White Rock Lake, Dallas, Texas, USA, Journal of Paleolimnology, 21, 193-206.

REYNOLDS, R.L., 1977. Magnetic Titanohematite Minerals in Uranium-Bearing Sandstones. in Open-File Report 77-355.

ROBERTS, A.P., 1995. Magnetic properties of sedimentary greigite (Fe (sub 3) S (sub 4)), Earth and Planetary Science Letters, 134, 236-227.

ROBERTS, A.P., 2015. Magnetic mineral diagenesis, Earth-Science Reviews, 151, 1-47.

ROBERTS, A.P. & TURNER, G.M., 1993. Diagenetic formation of ferrimagnetic iron sulphide minerals in rapidly deposited marine sediments, South Island, New Zealand, Earth and Planetary Science Letters, 115, 257-273.

ROBERTS, A.P. & WEAVER, R., 2005. Multiple mechanisms of remagnetization involving sedimentary greigite (Fe3S4), Earth and Planetary Science Letters, 231, 263-277.

ROBERTS, A.P., CUI, Y. & VEROSUB, K.L., 1995. Wasp-waisted hysteresis loops: Mineral magnetic characteristics and discrimination of components in mixed magnetic systems, Journal of Geophysical Research: Solid Earth, 100, 17909-17924.

ROBERTS, A.P., PIKE, C.R. & VEROSUB, K.L., 2000. First-order reversal curve diagrams: A new tool for characterizing the magnetic properties of natural samples, Journal of Geophysical Research: Solid Earth, 105, 28461-28475.

ROBERTS, A. P., CHANG, L., ROWAN, C. J., HORNG, C. S. & FLORINDO, F. 2011. Magnetic properties of sedimentary greigite (Fe3S4): An update. *Reviews of Geophysics,* 49, RG1002, doi:10.1029/2010RG000336.

ROBERTS, A.P., HESLOP, D., ZHAO, X. & PIKE, C.R., 2014. Understanding fine magnetic particle systems through use of first-order reversal curve diagrams, Reviews of Geophysics, 52, 557-602.

ROBERTSON, D. & FRANCE, D., 1994. Discrimination of remanence-carrying minerals in mixtures, using isothermal remanent magnetisation acquisition curves, Physics of The Earth and Planetary Interiors, 82, 223-234.

ROBINSON, S.G., 1986. The late Pleistocene palaeoclimatic record of North Atlantic deep-sea sediments revealed by mineral-magnetic measurements, Physics of The Earth and Planetary Interiors, 42, 22-47.

ROCHETTE, P., MATHÉ, P.E., ESTEBAN, L., RAKOTO, H., BOUCHEZ, J.L., LIU, Q. & TORRENT, J., 2005. Non-saturation of the defect moment of goethite and fine-grained hematite up to 57 Teslas, Geophysical Research Letters, 32, L22309, doi:10.1029/2005GL024196.

ROLF, C., 2000. Das Kryogenmagnetometer im Magnetiklabor Grubenhagen, Geologisches Jahrbuch, E52, 161-188.

ROLF, C., HAMBACH, U. & WEIDENFELLER, M., 2008. Rock and palaeomagnetic evidence for the Plio-Pleistocene palaeoclimatic change recorded in Upper Rhine Graben sediments (Core Ludwigshafen Parkinsel), Netherlands Journal of Geosciences, 87, 41-50.

RÖSLER, W., METZLER, W. & APPEL, E., 1997. Neogene magnetic polarity stratigraphy of some fluviatile Siwalik sections, Nepal, Geophysical Journal International, 130, 89-111.

ROWAN, C.J. & ROBERTS, A.P., 2006. Magnetite dissolution, diachronous greigite formation, and secondary magnetizations from pyrite oxidation: Unravelling complex magnetizations in Neogene marine sediments from New Zealand, Earth and Planetary Science Letters, 241, 119-137.

ROWAN, C.J., ROBERTS, A.P. & BROADBENT, T., 2009. Reductive diagenesis, magnetite dissolution, greigite growth and paleomagnetic smoothing in marine sediments: A new view, Earth and Planetary Science Letters, 277, 223-235.

SAGNOTTI, L., CASCELLA, A., CIARANFI, N., MACRÌ, P., MAIORANO, P., MARINO, M. & TADDEUCCI, J., 2010. Rock magnetism and palaeomagnetism of the Montalbano Jonico section (Italy): evidence for late diagenetic growth of greigite and implications for magnetostratigraphy, Geophysical Journal International, 180, 1049-1066.

SAGNOTTI, L., ROBERTS, A.P., WEAVER, R., VEROSUB, K.L., FLORINDO, F., PIKE, C.R., CLAYTON, T. & WILSON, G.S., 2005. Apparent magnetic polarity reversals due to remagnetization resulting

from late diagenetic growth of greigite from siderite, Geophysical Journal International, 160, 89-100.

SCARDIA, G., MUTTONI, G. & SCIUNNACH, D., 2006. Subsurface magnetostratigraphy of Pleistocene sediments from the Po Plain (Italy): Constraints on rates of sedimentation and rock uplift, Geological Society of America Bulletin, 118, 1299-1312.

SCHEIDT, S., HAMBACH, U. & ROLF, C., 2015. A consistent magnetic polarity stratigraphy of late Neogene to Quaternary fluvial sediments from the Heidelberg Basin (Germany): A new time frame for the Plio–Pleistocene palaeoclimatic evolution of the Rhine Basin, Global and Planetary Change, 127, 103-116.

SCHMIDBAUER, E., 1969. Magnetic properties of oxidized Fe-Cr spinels, Zeitschrift für Geophysik. B., 35, 475-484.

SCHMIDBAUER, E., 1971. Magnetization and lattice parameters of Ti substituted Fe Cr spinels, Journal of Physics and Chemistry of Solids, 32, 71-76.

SCHNABL, P., NOVÁK, J.K., CAJZ, V., LANG, M., BALOGH, K., PÉCSKAY, Z., CHADIMA, M., ŠLECHTA, S., KOHOUT, T. & PRUNER, P., 2010. Magnetic properties of high-Ti basaltic rocks from the Krušné hory/Erzgebirge MTS.(Bohemia/Saxony), and their relation to mineral chemistry, Studia Geophysica et Geodaetica, 54, 77-94.

SCHUMACHER, M.E., 2002. Upper Rhine Graben: Role of preexisting structures during rift evolution, Tectonics, 21, doi:10.1029/2001TC900022.

SCHWARZ, E. & VAUGHAN, D., 1972. Magnetic phase relations of pyrrhotite, Journal of Geomagnetism and Geoelectricity, 24, 441-458.

SIMON, T., 2012. Herkunft und Transport der Sedimente in der Forschungsbohrung Heidelberg UniNord, LGRB-Informationen, 26.

STACEY, F.D. & BANERJEE, S.K., 1974. The Physical Principles of Rock Magnetism, edn, Vol., pp. Pages, Elsevier, Amsterdam.

STOCKHAUSEN, H., 1998. Some new aspects for the modelling of isothermal remanent magnetization acquisition curves by cumulative log Gaussian functions, Geophysical Research Letters, 25, 2217-2220.

TATZEL, M., DUNKL, I. & VON EYNATTEN, H., 2017. Provenance of Palaeo-Rhine sediments from zircon thermochronology, geochemistry, U/Pb dating and heavy mineral assemblages, Basin Research, 29, 396-417.

TAUXE, L. & KENT, D.V., 1984. Properties of a detrital remanence carried by haematite from study of modern river deposits and laboratory redeposition experiments, Geophysical Journal International, 76, 543-561.

TAUXE, L., MULLENDER, T. & PICK, T., 1996. Potbellies, wasp-waists, and superparamagnetism in magnetic hysteresis, Journal of Geophysical Research, 101, 571-583.

TAYLOR, S.N., LAGROIX, F., ROUSSEAU, D.-D. & ANTOINE, P., 2014. Mineral magnetic characterization of the Upper Pleniglacial Nussloch loess sequence (Germany): an insight into local environmental processes, Geophysical Journal International, 199, 1463-1480.

TUCKER, P. & O'REILLY, W., 1980. The laboratory simulation of deuteric oxidation of titanomagnetites: effect on magnetic properties and stability of thermoremanence, Physics of The Earth and Planetary Interiors, 23, 112-133.

TURNER, P., 1980. Continental red beds, edn, Vol. 29, pp. Pages, Elsevier, New York.

VAN HOUTEN, F.B., 1968. Iron oxides in red beds, Geological Society of America Bulletin, 79, 399-416.

VASILIEV, I., DEKKERS, M.J., KRIJGSMAN, W., FRANKE, C., LANGEREIS, C.G. & MULLENDER, T.A., 2007. Early diagenetic greigite as a recorder of the palaeomagnetic signal in Miocene—Pliocene sedimentary rocks of the Carpathian foredeep (Romania), Geophysical Journal International, 171, 613-629.

VASILIEV, I., FRANKE, C., MEELDIJK, J.D., DEKKERS, M.J., LANGEREIS, C.G. & KRIJGSMAN, W., 2008. Putative greigite magnetofossils from the Pliocene epoch, Nature Geoscience, 1, 782-786.

VERWEY, E., 1935. The crystal structure of γ-Fe$_2$O$_3$ and γ-Al$_2$O$_3$, Zeitschrift für Kristallographie-Crystalline Materials, 91, 65-69.

WEAVER, R., ROBERTS, A.P. & BARKER, A.J., 2002. A late diagenetic (syn-folding) magnetization carried by pyrrhotite: implications for paleomagnetic studies from magnetic iron sulphide-bearing sediments, Earth and Planetary Science Letters, 200, 371-386.

WEDEL, J., 2008. Pleistocene molluscs from research boreholes in the Heidelberg Basin, E & G (Quaternary Science Journal), 57, 382-402.

WEHLAND, F., STANCU, A., ROCHETTE, P., DEKKERS, M.J. & APPEL, E., 2005. Experimental evaluation of magnetic interaction in pyrrhotite bearing samples, Physics of The Earth and Planetary Interiors, 153, 181-190.

WEIDENFELLER, M., ELLWANGER, D., GABRIEL, G., HOSELMANN, C. & WIELANDT-SCHUSTER, U., 2010. Ludwigshafen-Formation. in Litholex (online database) Federal Institute for Geosciences and Natural Resources (BGR), http://www.bgr.bund.de/litholex.

WEIDENFELLER, M. & KNIPPING, M., 2008. Correlation of Pleistocene sediments from boreholes in the Ludwigshafen area, western Heidelberg Basin, E & G (Quaternary Science Journal), 57, 270-285.

WESTERHOFF, W., KEMNA, H. & BOENIGK, W., 2008. The confluence area of Rhine, Meuse, and Belgian rivers: Late Pliocene and Early Pleistocene fluvial history of the northern lower Rhine Embyment, Netherlands Journal of Geosciences, 87, 107-125.

WILKIN, R. & BARNES, H., 1997. Formation processes of framboidal pyrite, Geochimica et Cosmochimica Acta, 61, 323-339.

WILSON, G.S. & ROBERTS, A.P., 1999. Diagenesis of magnetic mineral assemblages in multiply redeposited siliciclastic marine sediments, Wanganui Basin, New Zealand, Geological Society, London, Special Publications, 151, 95-108.

WINKLHOFER, M., CHANG, L. & EDER, S.H., 2014. On the magnetocrystalline anisotropy of greigite (Fe3S4), Geochemistry, Geophysics, Geosystems, 15, 1558-1579, doi:10.1002/2013GC005121
.

Due to the language standards of the publisher of the Geophysical Journal International (…), the English language in this paper differs from that used in the other publications. This difference concerns all words alternatively written with s or with z, such as characterisation/characterization.

During the publication process, the editors of the paper changed the design of table 3.4 and did not take into account the comments of the authors on its arrangement in the final proof. Initially, the journal did not respond to contact attempts after the paper had been published online. Another version was then made available online; however, this new version still did not follow all of the instructions of the authors. After further complaints, the journal indicated that an erratum was the only practicable way to change the online version of the publication. However, the online version did not change after the release of the following erratum.

Geophysical Journal International, Volume 211, Issue 2, 1 November 2017, Pages 1139, https://doi.org/10.1093/gji/ggx346   (Published: 22 September 2017)

Erratum of the paper '*A mineral magnetic characterization of the Plio-Pleistocene fluvial infill of the Heidelberg Basin (Germany)*', by Scheidt *et al.*, published in *Geophys. J. Int.* (2017) **210**, 743–764.

In the original paper, the publisher misplaced Table 4. The paper has now been updated. The publisher apologise for this error.

Table 4.

B1/2 [mT]	μ		no	B1/2 [mT]	μ		no
36.40	1.561		19	96.43	1.984		44
36.54	1.563		23	112.50	2.051		37
42.08	1.624		172	115.33	2.062		171
46.76	1.670		32	115.98	2.064		19
50.94	1.707		36	223.38	2.349		33
51.23	1.709		74	342.37	2.534		38
60.94	1.785		32	439.89	2.643		52
65.02	1.813		45	459.71	2.662		37
66.11	1.820		27	486.49	2.687		19
75.93	1.880		45	494.41	2.694		26
81.89	1.914		53	529.71	2.724		71
85.70	1.933		53	532.48	2.726		175
87.41	1.942		74	659.72	2.819		44
89.18	1.950		26	1995.26	3.300		72
94.18	1.974		44	5793.75	3.763		96

Components arranged in order of ascending μ values, neglecting variances in σ.

4. Study 3: Environmental signals of Pliocene-Pleistocene climatic changes in Central Europe: insights from the mineral magnetic record of the Heidelberg Basin sedimentary infill (Germany)

Stephanie Scheidt [1, 2], Ulrich Hambach [2, 3, 4], Christian Rolf [5]

[1]Institute of Geology and Mineralogy, University of Cologne, 50674 Cologne, Germany

[2]Chair of Geomorphology, University of Bayreuth, 95440 Bayreuth, Germany

[3]BayCEER, University of Bayreuth, 95440 Bayreuth, Germany

[4]Laboratory for Palaeoenvironmental Reconstruction, Faculty of Sciences, University of Novi Sad, Serbia

[5]Leibniz Institute for Applied Geophysics, 30655 Hannover, Germany

Corresponding author: Stephanie Scheidt

Abstract

Earth's climate entered its present icehouse state during a time of rapid temperature decline in the late Pliocene. The progression from the greenhouse state towards the icehouse state in the Northern Hemisphere is recorded in marine and terrestrial sedimentary archives. In central and northwestern Europe, the Pliocene and Pleistocene environmental history has mainly been reconstructed in studies of palaeobotanical proxies. These data reveal a cooling trend in climatic conditions and point towards an increase in seasonality during the Pliocene. Detailed reconstruction of the Pliocene-Pleistocene climatic evolution of northwestern Europe is, however, hampered by a general lack of data. Recently, the Heidelberg Basin in the Upper Rhine Graben (URG) provides a continental palaeoclimate archive. The long sequences of mainly fluvial sediments present within the basin record the evolution of the environment and climatic conditions during the late Pliocene and the entire Pleistocene.

The work presented here interprets two previously completed studies, a comprehensive magnetic polarity stratigraphy and a mineral magnetic characterisation of the post-Pliocene sedimentary infill of the Heidelberg Basin. Both studies were performed using sedimentary material taken from drill cores obtained at three sites within the basin. The magnetic polarity stratigraphy provides a consistent temporal framework, whereas the mineral magnetic record reflects details on environmental and climatic processes. Based on these data, the Pliocene was characterised by Mediterranean to subtropical climates. Cyclic variations in the groundwater table in the Rhine flood plain resulted in redox fluctuations, which led to the decomposition of the primary detrital mineral assemblage. Authigenic Fe oxides, particularly haematite, formed during dry periods. A rapid transition into cooler and moister conditions occurred at the end of the Pliocene, as indicated by the persistence of Fe sulphides, especially greigite. A high groundwater table and the associated reducing conditions have largely persisted to the present day.

This work supplements existing knowledge of the climatic evolution of central Europe during the Pliocene-Pleistocene transition with data from a region from which little data has traditionally been available. The sequence of events recorded by the composition of the magnetic mineral assemblage and the overall condition of the magnetic constituents in the sediment reflect the progressive intensification of Northern Hemisphere glaciation (iNHG). The data are consistent with climatic data obtained by studies of terrestrial and marine sediments elsewhere in the Northern Hemisphere (e.g., Atlantic, China, Russia).

4.1. Introduction

Over the past several decades, the application of new proxy methods has improved our understanding of terrestrial environments and the evolution of climate conditions during the Pliocene-Pleistocene in central and northwestern Europe. Analyses of palaeobotanical remains (i.e., pollen/spores, leaves, fruits/seeds, and wood) enable quantitative reconstruction of atmospheric climate parameters, such as the mean annual temperature, the temperatures of the warmest and coldest months, and the mean annual precipitation (e.g., Utescher et al., 2000, Utescher et al., 2012, Mosbrugger et al., 2005). Furthermore, regional precipitation curves are also derived from the ecological categorization of the fossil teeth of small mammals (e.g., van Dam, 2006). The terrestrial records that have been recovered to date reveal a progressive cooling trend from the Miocene into the late Pliocene. During the Pliocene, mean summer temperatures and mean winter temperatures dropped by 2-3 C° and ~6°C, respectively. Thus, an increase in seasonality is inferred. Palaeoprecipitation curves point towards wet summers and dry winters. Nevertheless, the late Pliocene was characterised by mean annual temperatures that were well above those of the present day (~+4°C) and a humid subtropical climate (Utescher et al., 2000). The vegetation changed from subtropical to boreal types, indicating a change from greenhouse to icehouse climatic conditions. The Quaternary climate was characterised by cyclic changes from warmer and cooler climates, as has been described in several other papers (Zagwijn, 1985, 1992, Raymo et al. 1992, Muddelsee & Stategger 1997, Clark et al. 2006, Lisiecki & Raymo 2007, Lawrence et al. 2010).

Despite the results mentioned above, the palaeoclimatic and palaeoenvironmental history of the Late Pliocene and Early Pleistocene of the central parts of continental Europe is largely unknown. One primary obstacle to producing a detailed reconstruction of the Pliocene-Pleistocene climatic evolution of Central Europe is the lack of spatially distributed records with sufficient temporal resolution and age constraints (Utescher et al., 2012). The currently available information derives primarily from sites in northern Germany, the Netherlands and Great Britain (e.g., Zagwijn, 1974, Zagwijn, 1992, Utescher et al., 2000, Mosbrugger et al., 2005, Schreve and Candy, 2010), whereas data from sites located further south are exceptionally rare. The Pliocene successions at southern sites are either eroded or lack robust age constraints. In the case of the Alpine foreland, the Tertiary bedrock has been reworked and deposited in Quaternary-age glacial, fluvial and lacustrine deposits (Ellwanger et al., 2011). The fluvioglacial "Höhere Deckenschotter" in the Swiss midlands is considered to represent the oldest preserved remnants of the glacial cycles (Graf, 1993). An age of 1.8 Ma-2.1 Ma was determined for these deposits through the identification of the tooth of a small mammal (Bolliger et al., 1996). However, this case represents an exception in the northern Alpine realm, where the deposits are generally highly fragmented and lack robust age constraints.

To obtain new data and promote a more detailed understanding of the climate evolution of the Alps and its connection to northwestern Europe, the Heidelberg Basin Drilling Project was initiated (Ellwanger et al., 2005, Gabriel et al., 2008). The geological setting of the Heidelberg Basin and its geographical location between the North Sea Basin and the Alps provide an ideal framework for several geoscientific studies that have been performed since 2004 (e.g., Hagedorn, 2004, Buness et al., 2008, Hagedorn and Boenigk, 2008, Hahne et al., 2008, Hunze and Wonik, 2008, Knipping, 2008, Lauer et al., 2010, 2011, Reiter et al., 2013, 2015, Tatzel et al., 2015, Li et al., 2017). In this paper, we focus on conclusions regarding the climatic and environmental evolution during Pliocene-Pleistocene times. These conclusions are based on age determinations derived from magnetic polarity stratigraphy (Scheidt et al., 2015) and detailed magnetic mineral characterisations (Scheidt et al., 2017) of three drill cores from the Heidelberg Basin. To characterise the climatic history of the Heidelberg basin from its sedimentary infill, the complex nature of all of the processes involved must be considered. This requires an understanding of the origin of the sediment, the transport mechanisms, and the depositional and post-depositional processes. We combine available information from the literature with the results of mineral magnetic analyses and major element analyses. As a side benefit, this study demonstrates the potential of rock magnetic studies of fluvial sediments to reveal details of past environmental and climate conditions.

4.2. Geological setting

The Heidelberg Basin (fig. 4.1) developed as part of the European Cenozoic Rift System and is a subordinate structure of the Upper Rhine Graben (URG). Rifting-induced subsidence began during the late Oligocene (Schumacher, 2002) and led to the accumulation of several kilometre-thick sediment packages (Bartz, 1974, Buness et al., 2008). The Oligocene-age basin infill was delivered by rivers that drained the subsiding URG to the north. Later, predecessors of the Rhine and the Rhine River itself increased the sediment supply (Schirmer, 2003, Preusser, 2008). According to Przyrowski and Schäfer (2015), a meandering sediment model can generally be deduced from sedimentological analysis of wells across the basin and lithostratigraphic correlations of available mud logs. However, exceptionally thick accumulations of pelitic overbank fines are interpreted to represent anastomosing sub-environments and lacustrine environments that formed mainly during the Tertiary. Climate changes and tectonic processes affected the catchments of the rivers and, in turn, the composition of the sediment load derived from them varied over time (Reiter et al., 2015, Hagedorn and Boenigk, 2008, Tatzel et al., 2015).
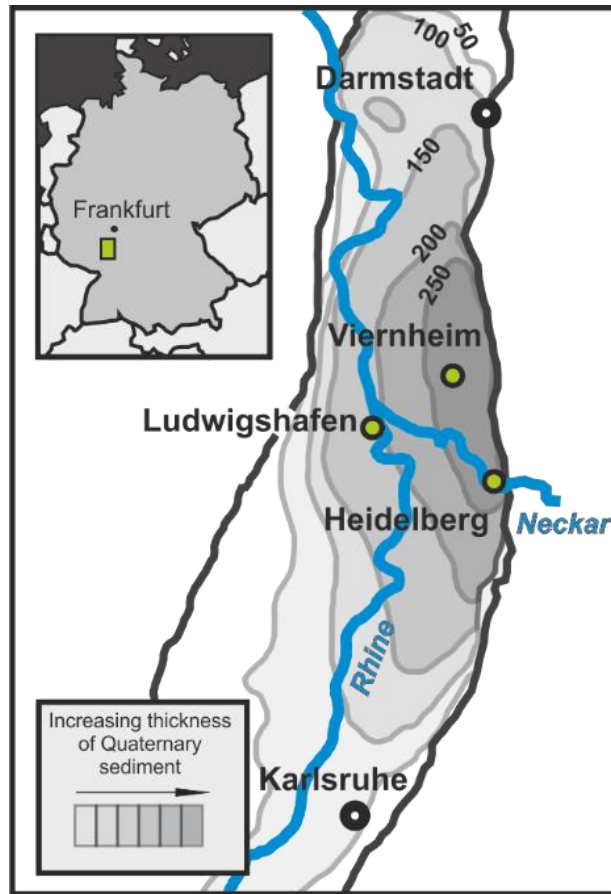
Figure 4.1:
This map of the Heidelberg Basin shows the thickness of the Quaternary infill (illustration after Bartz (1974)) and the location of the drill sites (green dots). Inset: The position of the Heidelberg Basin in Germany is indicated with a green rectangle.

The Heidelberg Basin is situated at the triple junction of three of the federal states of Germany (Hesse, Rhineland-Palatinate & Baden-Württemberg). Within this context, it is not surprising that three different nomenclatures for the lithostratigraphic units were in use until 2010, when a consistent lithostratigraphy was introduced. Exact descriptions of the new formations are given in the German lithostratigraphic lexicon (Ellwanger et al., 2010a, Ellwanger et al., 2010b, Hoselmann et al., 2010, Weidenfeller et al., 2010). An overview of the previously used units and their translation to the new nomenclature is given by (Gabriel et al., 2013). The following four lithostratigraphic units have relevance for this study.

Iffezheim Formation (IFm)

The IFm is the lowermost lithostratigraphic unit. It is composed of cyclically deposited sands, silts and clays. The carbonate-free sand is frequently kaolinitic and light in colour. Thick clayey horizons likely accumulated between the channels as floodplain deposits of an anastomosing sub-environment of the river (Przyrowski and Schäfer, 2015). Mottling is common and frequently associated with root

traces. The colouration varies between mixtures of grey, yellow, orange and red, reflecting a partly paludal origin, and pedogenetic overprints are frequently present. Fine humic clastics are occasionally preserved in the bedload sands, which are rich in fossil wood in places (Ellwanger et al., 2010b). The IFm is dominated by a stable heavy mineral assemblage that consists mainly of tourmaline, zircon, rutile and anatase. A change in the heavy mineral composition marks the onset of the following unit (Hagedorn, 2004, Hagedorn and Boenigk, 2008).

Viernheim Formation (VFm)

The VFm is characterised by the presence of the unstable heavy minerals epidote, garnet and hornblende (Hagedorn, 2004, Hagedorn and Boenigk, 2008). The deposits consist of alternating clayey silts, sands and fine gravels. The lowermost parts are predominantly pelitic; the abundance of sand-filled channels increases upward, and greenish to greyish successions are dominated by medium to fine sand at the top of the deposit. The silt layers are occasionally accompanied by peat layers. Stacks of depositional cycles indicate a meandering fluvial environment with increasing sinuosity (Przyrowski and Schäfer, 2015). The carbonate content, which is controlled by the provenance of the sediment, varies between 0% and 30%. The carbonate-rich portions of this formation are characterised by very well sorted sands with large amounts of mica (Hoselmann et al., 2010).

Ludwigshafen Formation (LFm)

The sediments of the LFm are characterised by fining upward cycles that consist of sands and greyish, carbonate-rich silts and clays. The cycles frequently end with humic sections consisting of black to brownish-black silty clay and occasional peat layers. Intercalations of aeolian fine and medium sand occur within the fluvial and limnic successions (Weidenfeller et al., 2010). The heavy mineral composition and fluvial dynamics correspond to those of the VFm (Hagedorn, 2004, Hagedorn and Boenigk, 2008, Przyrowski and Schäfer, 2015).

Mannheim Formation (MFm)

The MFm is the uppermost lithostratigraphic unit. Several fluvial cycles lie atop a basal gravel layer. The series consists of greyish, calcareous sand that is sporadically interrupted by fine-grained, partially organic-rich overbank and oxbow sediments (Ellwanger et al., 2010a). Generally, the MFm is coarser grained than the prior units and contains a reduced number of horizons of fine clastics (Przyrowski and Schäfer, 2015). The heavy mineral composition of the MFm is the same as that of the LFm (Hagedorn, 2004, Hagedorn and Boenigk, 2008).

Despite the ubiquity of these four lithostratigraphic units throughout the basin, local and regional conditions and events have resulted in lithological variations. The most prominent variations are

evident near the graben shoulder and the Neckar alluvial fan. In these area, intercalations of coarser material appear within the IFm. These reddish, gravelly sands and gravels are composed of material from the Triassic hinterland and were deposited either by waterways draining the nearby Odenwald Mountains or by the Neckar alluvial fan (Simon, 2012).

4.3. Sample materials

The present interpretation of the environmental and climatic evolution of the Heidelberg Basin sedimentary record is based on analyses of sample material described and discussed in previous studies. For this reason, only a brief overview of the sample materials is provided here. For detailed information, we refer to Scheidt et al. (2015) and Scheidt et al. (2017).

The sedimentary material discussed here was taken from drill cores from the following three sites (fig. 4.1):

(1) The Viernheim site is located in the geographical centre of the Heidelberg Basin, approximately 3 km north of the city of Viernheim (Hessian Ried, Buchnerschneise). The borehole was drilled in 2006 to a total depth (TD) of 350 m.

(2) Two cores are available from the Heidelberg drilling site. The first core (UniNord 1) was drilled in 2006 to a TD of 190.4 m. In 2009, a second core was drilled approximately 260 m north-northwest of the location of the first core. The second core contains material recovered at depths of 114-115 m and 183-500 m. Because the identification of magnetic polarity reversals indicated that the vertical stratigraphic differences were ~1 m, the two Heidelberg cores are considered as a single core in this paper. Heidelberg is situated in the centre of subsidence of the Heidelberg Basin.

(3) At the Ludwigshafen Parkinsel drilling site, several wells were brought down for groundwater exploration work. In this study, we focus on core P36, which was drilled to a TD of 301 m in 2009. The Ludwigshafen Parkinsel drilling site is located on the western margin of the Heidelberg Basin.

Samples were taken at intervals of 0.5 m from all three cores. Only coarse-grained sections (coarse sand, and gravel) were skipped. Most of the samples were sawed out from the dried, hardened core material. This process produced cubic specimens with a volume of approximately 10 cm³. Additional cylindrical samples with a diameter of 1 inch (= 2.54 cm) and a length of 2.2 cm were cut out of the unconsolidated sections of the Viernheim core. Sample material from core P36 was additionally sieved into two grain size fractions (<0.02 mm; 0.02-2 mm) and pressed into rectangular plastic boxes with a volume of 6 cm³. Further, sample material was taken from all of the cores at approximately 10-m

intervals for the preparation of magnetic extracts. Sample material for the vibrating sample magnetometer (VSM) was mainly sawed out of the cubic specimens.

For this study, core P36 and the Viernheim core were again sampled for elemental analyses. In total, 40 samples from the Viernheim core were collected at 9-m intervals; the sample density was increased near the Pliocene-Pleistocene boundary. To confirm the information, 10 samples were taken from core P36 with a spacing of 3 m near the Pliocene-Pleistocene boundary.

4.4. The age of the deposits

Determination of the ages of the Pliocene and Pleistocene sediments of the Heidelberg Basin is a challenging task. No absolute dating method is available that covers the entire time interval represented by these deposits with sufficient accuracy, and biostratigraphic methods have limited applicability because the fossil remains within the deposit are insufficiently well preserved. Given the lack of viable alternatives, a major change in the drainage system that is expressed by the onset of calcareous sediment deposition and changes in the heavy mineral composition was selected to represent the base of the Quaternary (Bartz, 1953). New information has been contributed by interdisciplinary studies that were initiated by the Heidelberg Drilling Project (Gabriel et al., 2008, Ellwanger et al., 2005). Differing assessments of the ages of the deposits are presently available. Thus, we provide a brief overview of the information available in the existing literature and point out where these studies agree and disagree.

Biostratigraphic age information determined from mollusc remains found in material from the Viernheim and Ludwigshafen drilling sites is provided by (Wedel, 2008). Knipping (2008), Hahne et al. (2008, 2012), and Heumann et al. (pers. com.) used pollen analysis to examine the core material from the Ludwigshafen Parkinsel, Heidelberg and Viernheim drilling sites, respectively. The general lack of fossils in coarse-grained sediments means that chronologic classification can only be performed for certain layers. Nevertheless, unambiguous results were obtained for the MFm and the LFm. Within the VFm, inconsistencies exist between the interpreted results obtained for the Ludwigshafen Parkinsel and Viernheim sites on the one hand and the pollen spectra of the Heidelberg site on the other. Knipping (2008) and Heumann et al. (pers. com.) confirmed that the lower boundary of the VFm essentially coincides with the Pliocene-Pleistocene transition; however, Hahne et al. (2008, 2012) determined an age of <1.77 Ma for the IFm-VFm boundary at a depth of 298.6 m and argued that the lowermost part of the Heidelberg core at a depth of 500 m depth is still Early Pleistocene in age. At first glance, the interpretation of Hahne et al. (2008, 2012) appears to be supported by preliminary interpretations of seismic reflection profiles that place the base of the Quaternary at a depth of approximately 430 m (Buness et al., 2008). However, the determination of ages by lithological

correlations performed on the basis of reflection seismic profiles alone is generally not possible. In fact, the depth of this horizon was determined by correlation with an industrial well (Schrießheim), for which the origin of the age assignments is unclear.

To account for the available research results, subsequent studies (Simon, 2012, Przyrowski and Schäfer, 2015) suggested that the lithostratigraphic boundary between the IFm and the VFm is diachronous. This conclusion is contradicted by the magnetostratigraphic study of Scheidt et al. (2015). A graphical outline is shown in figures 4.2, 4.3, and 4.4. The Matuyama-Brunhes-boundary (MBB) and the Jaramillo subchron were only successfully identified in the Heidelberg core; however, lithostratigraphic correlation allows inference of its position within the other two cores. The Olduvai subchron and the Gauss-Matuyama boundary (GMB) are defined by clear changes in polarity in each core. The GMB is shown to be essentially synchronous with the IFm-VFm lithostratigraphic boundary. Continuation of the stratigraphic framework into the Gilbert chron permits multiple correlation schemes.

By applying age-depth plots and assuming steady subsidence, we tentatively identify the most plausible scenarios, which yield ages of >5 Ma and >4 Ma for the deepest portions of the Viernheim (350 m) and Heidelberg (500 m) cores, respectively. A strong drilling-induced overprint prevents palaeomagnetic analysis of the Pliocene sediments found in the Ludwigshafen core P36. The age model of Scheidt et al. (2015) is based on strong assumptions regarding the preservation probability of the palaeomagnetic record in fluvial environments, combined with a successive correlation of the detected reversals with the geomagnetic polarity timescale (GPTS).

The proposed time-depth correlation is consistent with the biostratigraphic results of Wedel (2008), Knipping (2008) and Heumann et al. (pers. com.) and corresponds to optically stimulated luminescence (OSL) and infrared radiofluorescence (IR-RF) dating of samples of the MFm and LFm obtained from the Viernheim (Lauer et al. 2010, 2011) and Heidelberg (Li et al. 2017) cores. Stratigraphic ages interpreted from apatite fission track (AFT) age determinations of sample material obtained from the Viernheim core are also largely consistent with the magnetostratigraphy (Reiter et al., 2013). Only one age (3.0 ± 0.2 Ma) for a sample obtained from the Viernheim core at a depth of approximately 325 m and specified in a study using (U-Th-Sm)/He thermochronology (Reiter et al. 2015) does not conform to the results presented by Scheidt et al. (2015).
In this study, we refer to the age model of Scheidt et al. (2015).

4.5. Measurement procedures

The instrumentation and measurement procedures that were used to obtain the comprehensive data set used here have previously been described in Scheidt et al. (2015) and Scheidt et al. (2017).

The first article focuses on the magnetic polarity stratigraphy of the sediments of the Heidelberg Basin. Thus, that article describes the alternating field (AF) and thermal demagnetisation experiments. Further, the procedures used in performing three-component IRM analyses are described. The latter work provides information on the measurements and analyses used to characterise magnetic mineral assemblages, including the determination of the frequency dependency of magnetic susceptibility (MS), hysteresis measurements, coercivity analyses of isothermal remanent magnetisation (IRM) curves, thermomagnetic measurements, first-order reversal curve (FORC) measurements and the computer software used in these characterisations.

The S-ratio shown in this work is calculated following Bloemendal et al. (1992):

$$(1 + (BF\_IRM_{-0.3T}/IRM_{2.7T}))/2 \tag{1}$$

Here, BF_IRM 2.7T represents the remanent magnetisation obtained after saturating the sample in a field of 2.7 T, and IRM-0.3T represents the remanent magnetisation of the 300-mT backfield step. Thus, values close to 1 indicate samples that are dominated by minerals that become saturated in a field of 300 mT.

Most of the laboratory work was carried out in the Grubenhagen palaeomagnetic laboratory of the Leibniz Institute for Applied Geophysics (LIAG), Einbeck (Germany). Additional work was carried out in the palaeomagnetic laboratory of the Department of Earth and Environmental Sciences in Niederlippach, Geophysics Section of the University of Munich (Germany); in the Department of Geosciences, University of Bremen (Germany); and in the rock magnetism laboratory of the Institute of Geophysics, Academy of Sciences of the Czech Republic in Prague.

The rock magnetic data were complemented by the results of scanning electron microscopy (SEM, backscattered electrons) of materials extracted from core P36, combined with energy dispersive X-ray microanalysis (EDX). Details on these analyses are provided in Scheidt et al. (2017).

Analyses performed using a PANalytical Axios wavelength-dispersive X-ray fluorescence spectrometer (WD-XRF) complemented the experiments and analyses presented in existing studies. For this purpose, bulk sample material was milled to a fine powder. One thousand milligrams of the powder derived from each sample were subjected to a two-stage heating process that required approximately 2-3 hours. The samples were first heated to 700°C and 1030°C to cause the oxidation of certain compounds and the liberation of volatile components, respectively. After cooling, the loss on ignition (LOI) was determined from the difference in weight. The material was than mixed with 5000 mg of lithium borate (LiBO$_2$) to promote melting and 50 µl of a 400 g/l LiBr solution used as an anti-sticking agent before it was poured into a crucible made of 95% platinum and 5% gold. To form homogeneous fused beads, the samples were then subjected to a temperature of 1200°C for 20

minutes. All of the major and minor elements were determined from these specimens, except for volatile elements and some trace elements. The precision and accuracy of these elemental analyses was determined through calibration of the system using international certified reference materials; moreover, some special samples made from pure oxides were used to determine line overlap corrections.

Both of the X-ray analytical procedures were carried out in the laboratory of the Federal Institute for Geosciences and Natural Resources (BGR) (Hannover, Germany).

4.6. Results

4.6.1. Magnetic polarity stratigraphy

The palaeomagnetic analyses show that several reversals are present in all of the cores (fig. 4.2-4.4). The age-depth models indicate that minimum ages of 5.235 Ma and 4.187 Ma are highly possible for the bases of the Viernheim and Heidelberg cores, respectively (Scheidt et al., 2015). A comparable determination of the minimum age of core P36 is not possible because strong drilling-induced overprinting has obscured most of the palaeodirections within the Tertiary part of the core. The Pliocene-Pleistocene boundary, defined by the GMB, is located within the uppermost part of the IFm in the Heidelberg core. Within the Viernheim core, the lithostratigraphic and the magnetostratigraphic boundaries appear to coincide. Finally, due to the presence of coarse sediment layers at the base of the VFm, the position of the GMB cannot be confidently identified in core P36. However, normal directions are identified at the very top of the IFm; thus, the GMB is expected to occupy a similar position as in the Viernheim core.

The subsequent and overlying reversed Matuyama chron is only well defined in the lower half, which includes the Olduvai subchron in all three cores. The determination of palaeodirections in the upper part is limited by the presence of coarser layers containing sand and gravel. Large parts of the Jaramillo subchron are missing in all three cores. The location of the MBB is placed in the lowermost part of the LFm only in the Heidelberg core. Its position within the other two cores is not preserved and is thus a matter of interpretation. Scheidt et al. (2015) suggest that the MBB occurs at the top of the VFm. The subsequent and overlying Brunhes chron includes almost the entire LFm and the MFm. Excursions are not recognised.
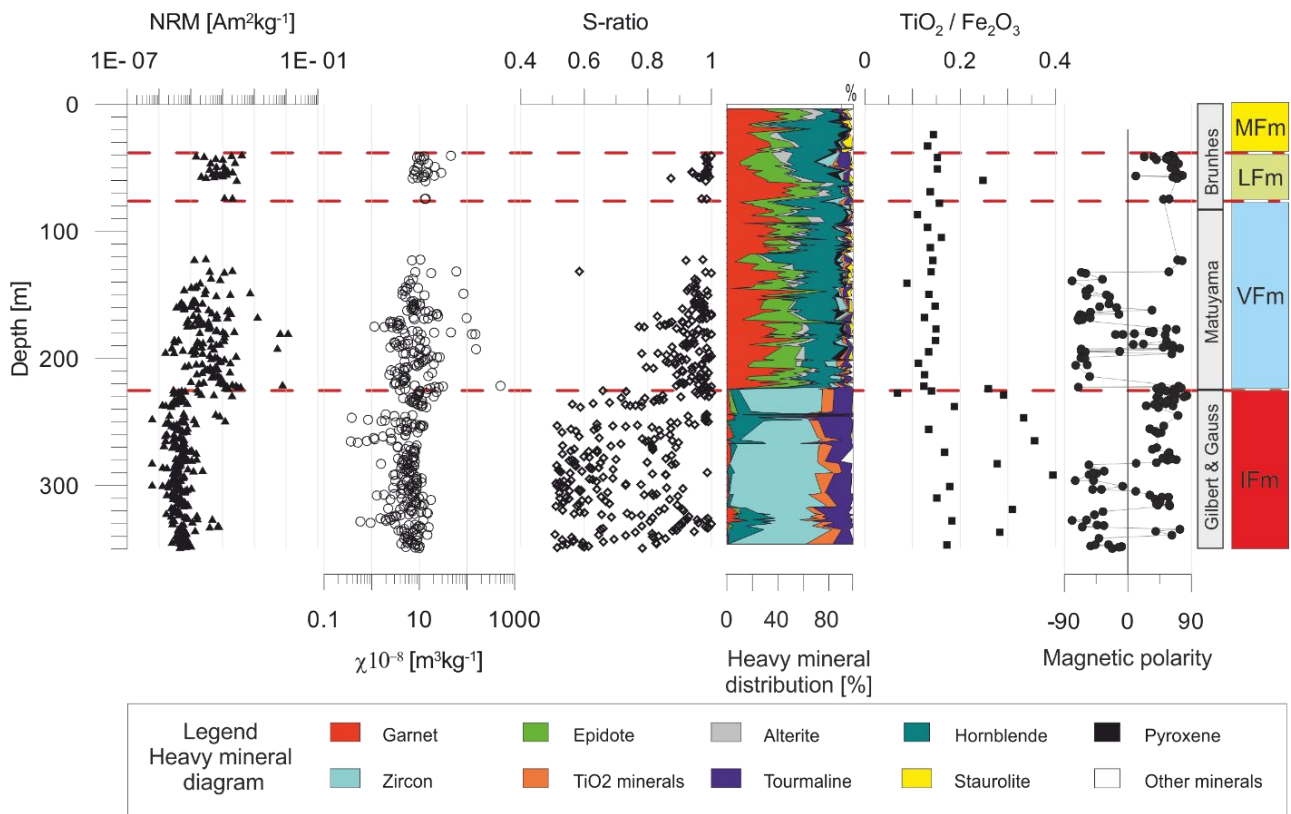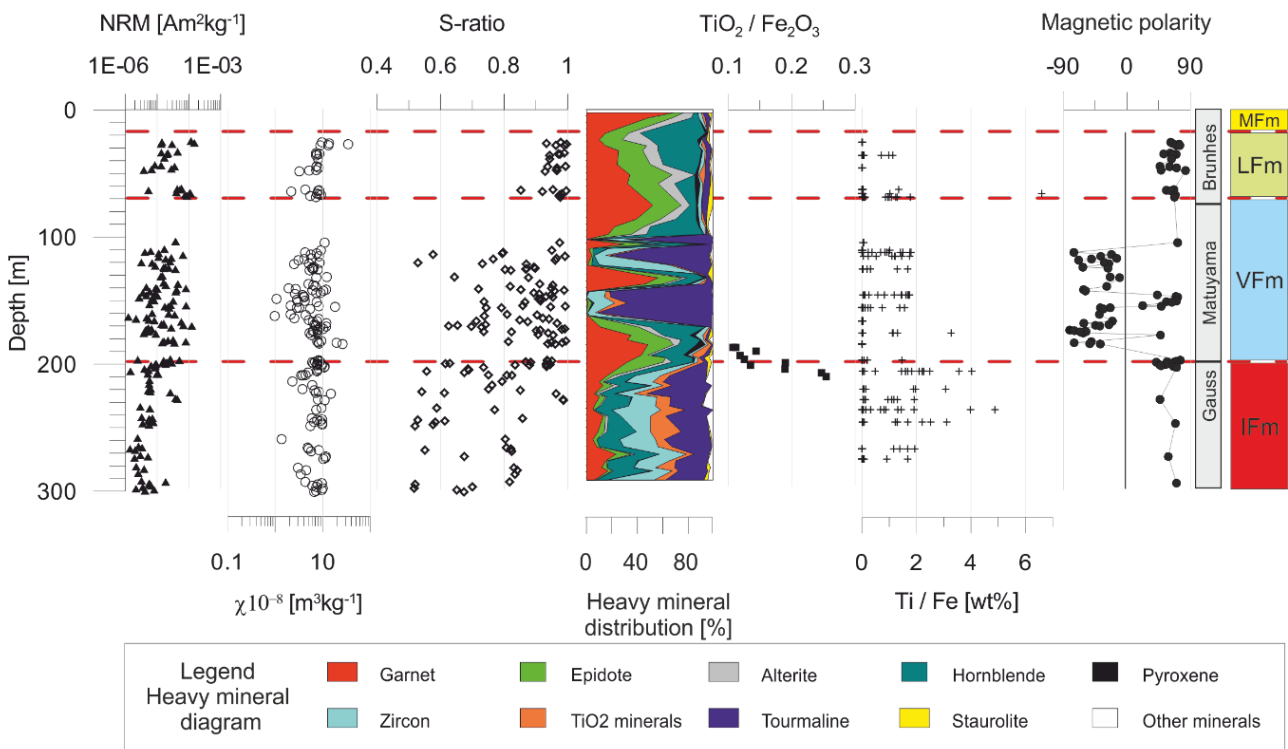
Figure 4.2:

Downcore variations in NRM, the mass specific MS, the S-ratio, the heavy mineral distribution (Hoselmann, 2008), the TiO$_2$/Fe$_2$O$_3$-ratio obtained by WD-XRF analysis, and the magnetic polarity of the Viernheim core. The magnetic polarity stratigraphy is based on directional palaeomagnetic data with MAD ≤ 12. The lithostratigraphic units are indicated on the right-hand side.
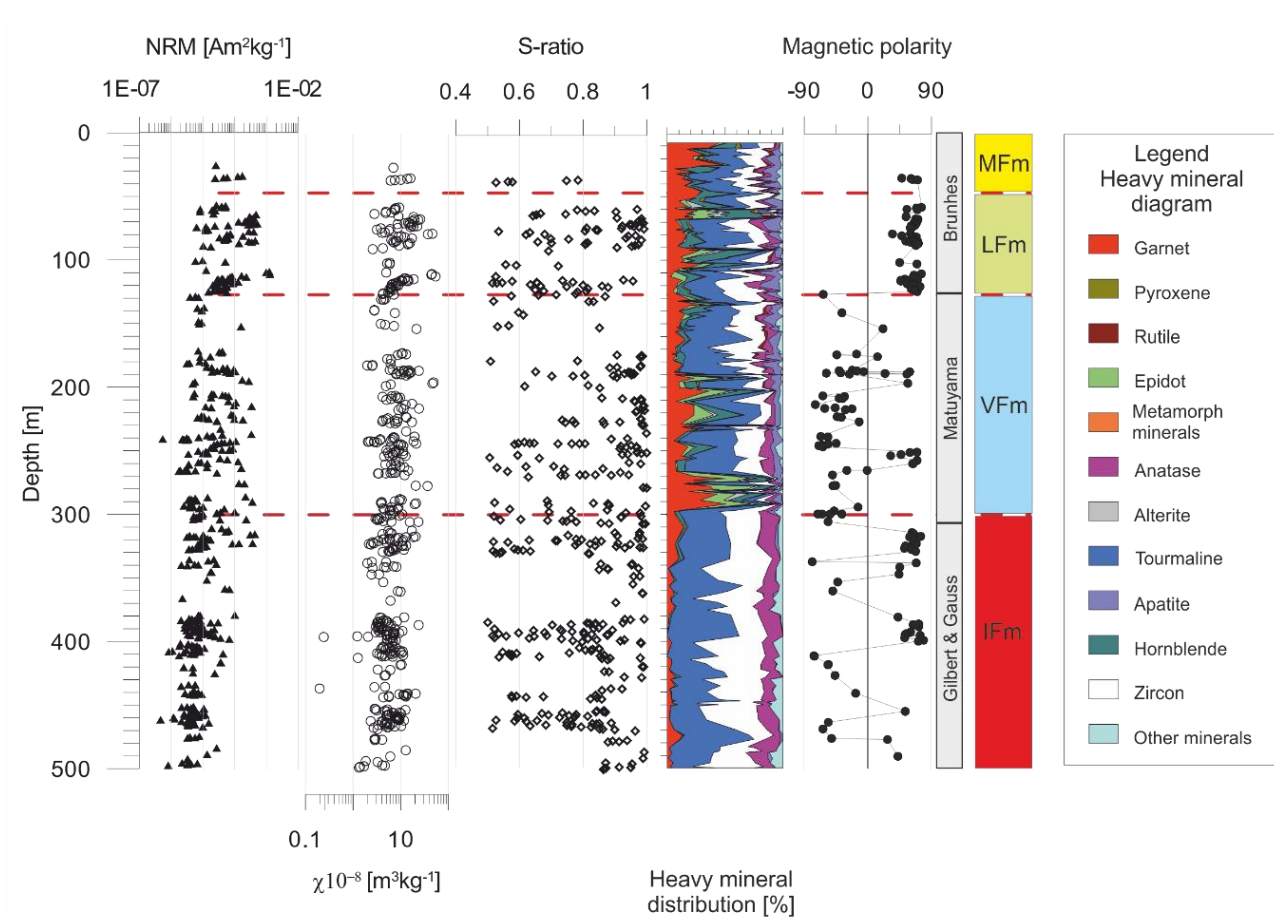
Figure 4.4:
Downcore variations in NRM, the mass specific MS, the S-ratio, the heavy mineral distribution (analysis performed by Eva Hagedorn, in Simon (2012)), and the magnetic polarity of the Heidelberg core. The methodological approach used in the heavy mineral analyses differs slightly between the Heidelberg core and the other two cores. The magnetic polarity stratigraphy is based on directional palaeomagnetic data with MAD ≤ 12. The lithostratigraphic units are indicated on the right-hand side.

Figure 4.3 (lower figure at page 138):
Downcore variations in NRM, the mass specific MS, the S-ratio, the heavy mineral distribution (Hoselmann and Weidenfeller, 2014), the TiO₂/ Fe₂O₃-ratio obtained by WD-XRF analysis, the Ti/Fe-ratio obtained by EDX analysis, and magnetic polarity of core P36. The magnetic polarity stratigraphy is based on directional palaeomagnetic data with MAD ≤ 12. The lithostratigraphic units are indicated on the right-hand side.

4.6.2. Magnetic mineralogy

The magnetic inventory of the Heidelberg Basin is made up of different combinations of magnetic minerals with varying grain sizes and chemical configurations (Scheidt et al., 2017, Scheidt et al., 2015). The mixed signals yielded by most bulk sample measurements thus do not provide detailed information on individual magnetic components. However, general trends can be clearly seen; the MS and NRM intensities of the sediments of the IFm are lower than those of the younger strata. At the top of the IFm, rapid but continuous changes occur in the bulk sample parameters, which progressively come to resemble the values characteristic of the Quaternary parts of the cores. This transition is most clearly expressed by the data from the Viernheim core (fig. 4.2) and is still visible in core P36 (fig. 4.3). In contrast, the Heidelberg core shows only minor changes in the distribution of NRM intensity and MS values along its entire length (fig. 4.4). The S-ratios of the sediments obtained from the Viernheim core and core P36 also reflect differences between the upper and lower parts of the cores. The Pliocene sediments display considerable scatter, with values between 0.5 and 1.0; the portions with low values are thus noteworthy. In comparison, relatively low S-ratios are only noted for distinct horizons within the VFm. Generally, the variability in the S-ratios is clearly smaller within the Quaternary sediments of the Viernheim core and core P36. In contrast, the S-ratio diagram of the Heidelberg core discloses a different distribution of high coercivity minerals. Within the Pliocene part of this core, S-ratios as low as 0.5 occur only within discrete intervals. In between, the values of this parameter vary between 0.8 and 1.0. Within the Quaternary part, the S-ratios display a greater degree of scatter (fig. 4.4).

Depending on the ratio of sediment supply from the Rhine, either stable or instable heavy minerals dominate the mineral assemblages of the sequences throughout the basin; thereby an irregular alternation is formed over time (Hagedorn and Boenigk, 2008, Hoselmann et al., 2008). Comparison of the rock-magnetic parameters with the heavy mineral composition unveil a rough correlation with the fluctuation of susceptibility and NRM only for core P36. However, core Viernheim has no interruptions of the instable mineral suite by the stable spectra and Heidelberg shows completely scattered data.

Detailed information on the magnetic components was obtained by thermomagnetic curves, FORC measurements and coercivity analyses of IRM acquisition curves. The combined information permits unravelling of these multi-component systems and the identification of the associated magnetic minerals (for details see Scheidt et al. (2017)). Based on these results, the sediments of the Heidelberg Basin are divided into two major parts.

The Tertiary part is exclusively represented by the IFm. The magnetic minerals found within the predominantly fine-grained clastic sediments are ferrian ilmenites, ferrian chromites, haematite, and goethite, as well as minor quantities of magnetite and maghemite (Scheidt et al., 2017, Scheidt et al., 2015). Sulphides are almost exclusively detected in core Heidelberg, during this period. Admittedly, the finding of an iron oxide pseudomorph after pyrite exhibits that sulphides were more abundant

during early diagenesis. Precise observations of magnetic extracts by SEM disclose intense dissolution; magnetite minerals remained in porous remnants and even haematite specularite suffered dissolution processes after deposition (Scheidt et al., 2017). Signs of magnetotactic bacteria have not been found in the IFm nor in the younger units.

Although the Quaternary sediments include three complete lithostratigraphic units, the magnetomineralogical fingerprint is very similar for all of them. A major proportion of the magnetic minerals have been replaced by sulphides; greigite is most prevalent, and pyrite and most likely pyrrhotite are also present. Detrital magnetites occur mainly as porous remnants. Ferrian chromites and ferrian ilmenites are also part of the magnetic mineral inventory. Preferentially in the fine-grained sections, goethite appears as a degradation product. The Heidelberg core also contains detrital haematite within discrete horizons; it is otherwise similar to the other cores.

4.6.3. X-ray analyses (EDX and WD-XRF)

The abovementioned subdivision of the successions into two major parts is also recognised in X-ray analyses. The downcore Fe/Ti ratios of single magnetic minerals exhibit a similar distribution pattern as the Fe_2O_3/TiO_2 ratios of bulk sample material (fig. 4.2 and 4.3). In both cases, the variability decreases considerably at the Pliocene-Pleistocene boundary. In contrast to the EDX analyses, the WD-XRF analyses permit consideration of grain size-specific dependence of the bulk sample material. The inferred linear trend indicates an inversely proportional relationship of the contents of Fe_2O_3 and TiO_2 to the grain size of the bulk sample material (fig. 4.5). It is noteworthy that the finest sediments within the IFm are characterised by higher Fe_2O_3 values than the sediments

Figure 4.5:
TiO_2 content versus Fe_2O_3 content derived from WD-XRF analyses of sample material obtained from the Viernheim core and core P36. Variations arise as a function of the grain size spectra of the bulk sample material and the lithostratigraphic units. IFm: red, VFm: blue; LFm: yellow; MFm: green.

with comparable grain sizes within the other lithostratigraphic formations. Moreover, the IFm sediments show generally higher TiO_2 values.
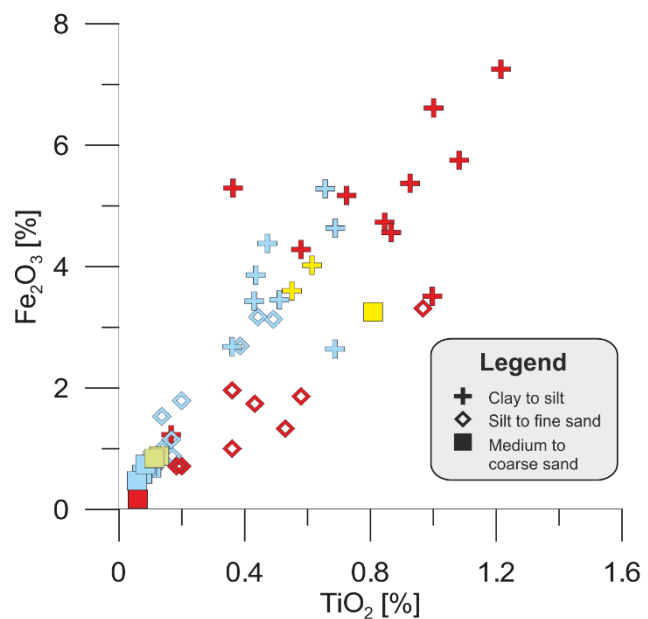
4.7. Discussion

Fluvial deposits are not generally preferred for the reconstruction of past environmental and climatic conditions using rock magnetic techniques. The main reasons are related to the highly energetic depositional environments in which fluvial sediments are laid down. These environments feature a complex combination of processes that are involved in the genesis and diagenesis of fluvial sedimentary materials and produce records with superimposed signals.

The primary compositions of the magnetic minerals in fluvial deposits depend upon their source areas. However, any given magnetic inventory is subject to two main controlling factors, which are the condition of the remainder of the primary magnetic mineral assemblage after repeated burial-transportation cycles from the source of these minerals to their sink, and the amounts of magnetic phases that form during diagenesis. Both of these factors are subject to numerous influences, including the mechanisms by which minerals form and the reactivity of the existing iron minerals. These influences include temperature, the chemical compositions of the educts, microbial activity, the Eh-pH conditions in the interstitial spaces, and the availability of reactants (Canfield et al., 1992, Florindo et al., 2003, Roberts, 2015, Ginn et al., 2017). In fluvial systems, all of these factors are controlled by the dynamic modifications of the riverbed that occur in response to climate-related boundary conditions, such as water discharge and sediment supply (Bogaart and Van Balen, 2000). The shifts in sedimentary sub-environments that are driven by these modifications and the related depositional and diagenesis conditions affect vegetation cover, drainage conditions, and water table fluctuations and result in conformities, superimposed grain size effects and small-scale temporal and spatial heterogeneities in magnetic minerals (Boersma et al., 1972, Simonson and Boersma, 1972, Bouma, 1983, Van Breemen, 1988, Kraus and Aslan, 1993, Fimmen et al., 2008).

Precise reconstructions of the chronology of past depositional and diagenetic events in fluvial systems is usually hardly possible; however, indications of the driving factors may be present. In this study, the spatially limited nature of the information provided by the drill cores makes it nearly impossible to differentiate between microscale (tens to hundreds of metres) and mesoscale (hundreds to thousands of metres) variations. These variations arise from short-lived local and sub-basin processes, respectively (Kraus, 1999, Kraus, 2002). The analysis of cores from different areas within a basin, however, provides a means of distinguishing local features from basin-scale processes; the latter are largely controlled by climate changes, tectonic effects and modifications to the upstream portions of the catchment areas (Kraus, 2002, Hagedorn and Boenigk, 2008).

In the following, we integrate the results of our rock magnetic survey of the Heidelberg Basin sedimentary record into the environmental evolution of the late Pliocene and Pleistocene, as described in the literature. Sedimentological and palaeontological data provide especially important constraints

in understanding past environmental conditions. We show that the two clearly distinguishable parts of the rock magnetic record reflect two major phases with strongly contrasting depositional and diagenetic environments. Subsequently, we discuss the significance of the new data in reconstructing the climatic evolution of Central Europe.

4.7.1. The development of the Heidelberg Basin during the Pliocene and Pleistocene

In the late Neogene, the proto-Rhine was already established in the URG and transported sediments from the south into the Heidelberg Basin and thence to the North Sea (Preusser, 2008). A recent study by Reiter et al. (2015) suggests that the southern Molasse Basin or the central Alps supplied detritus to the Pliocene Palaeo-Rhine system, perhaps as early as ca. 4.2 Ma. Between 3.6 Ma and 2.59 Ma, the northern margin of the Alps (subalpine Molasse and/or Rhenodanubic Flysch units) likely supplied sediment to the Pliocene Rhine River. The prevailing meander environment was accompanied by anastomosing sub-environments and wide interconnected lakes of restricted extent and depth (Przyrowski and Schäfer, 2015). Up to the end of the Pliocene, the centre and the western margin of the Heidelberg Basin were characterised by thick, weakly vertically differentiated floodplain deposits. Triggered by ongoing subsidence and climatically controlled variations in discharge and sediment load, a vertical stack of fining-up sequences terminated by palaeosols with low degrees of profile differentiation formed (Kraus and Aslan, 1993). However, parts of the deposits were subjected to strong post-sedimentary overprinting (Hoselmann, 2008) when the discharge and channel activity rapidly decreased, as indicated by the presence of iron pisolites in orange to yellow-brown horizons and the frequent occurrence of varying degrees of mottling, accompanied by thin, predominantly greyish layers. Gleyification occurred in the alluvial plain adjacent to the stream; the occurrence of this process indicates the mobilisation of iron within the sediments, driven by water table fluctuations (Bouma, 1983, Van Breemen, 1988, Kraus and Aslan, 1993, Nawaz et al., 2014).

The pedological evidence is consistent with the rock magnetic analyses of the Viernheim and Ludwigshafen cores, which indicate pervasive changes in the magnetic mineral assemblage by redox fluctuations. Thus, sulphide formation occurred at the expense of magnetite during times of reducing diagenesis. This stage of diagenesis is documented by the given magnetic mineral assemblage. Magnetite and Ti-magnetite are largely absent, other than as host minerals; instead, only a few remainders of titanium- and chromium-enriched detrital ferrian ilmenites and ferrian chromites are present that point towards excessive iron leaching. This stage of reducing diagenesis was followed by the recurrence of oxic conditions, in which the sulphide minerals broke down. Thus, only small amounts of sulphide minerals are preserved in the IFm of the Viernheim core and core P36. Repetition of these processes during the alternation of oxic and reducing conditions led to the dissolution and re-oxidation of both detrital and authigenic magnetic minerals and resulted in the formation of poorly

crystalline Fe(III) phases (Van Breemen, 1988, Isambert et al., 2003, Poulton et al., 2004, Ginn et al., 2017). It should be noted that, although no evidence of microbial processes, such as magnetofossils, could be identified in this study, the presence of Fe(III) phases promotes microbial activity in sediments (Byrne et al., 2015, Ginn et al., 2017) thus, microbial activity likely played an important role in the diagenesis of the studied sediments. During times in which arid and dry conditions prevailed, the cyclic series of processes was finally completed by the oxidation and successive transformation of the poorly crystalline Fe(III) phases and the remainders of detrital magnetite/maghemite into maghemite and haematite, respectively (Banerjee, 1965, Turner, 1980, Liu et al., 2008, Liu et al., 2010).

Indications of the repeated occurrence of the processes described above are provided by the identification of a pseudomorph of haematite after pyrite that provides conclusive evidence of the recurrence of oxic conditions after the formation of sulphides. In turn, the slightly pitted surfaces of haematite (specularite) disclose the operation of reducing dissolution processes after the formation of these oxide minerals (Scheidt et al. 2017). Finally, the low MS and NRM values and the small yields of the magnetic mineral extraction procedure are also readily explained in terms of redox fluctuations. Further evidence is provided by the total iron values of the IFm indicated by the X-ray elemental analyses. Although only a small number of detrital magnetic minerals are present in the sediment, the high measured percentages of iron suggest that most of the initially deposited ferrimagnetic minerals were transformed into haematite and hydrous ferric oxides, such as goethite, limonite and ferrihydrite. This sequence of events is also clearly indicated by the deep red, yellow, and orange colouration of the sediments.

All things considered, we propose that the Viernheim core and core P36 are heavily influenced by redox fluctuations that were induced by the recurrent rise and fall of the groundwater table in the Pliocene. Because spectral analysis using the sliding-window technique reveals significant cyclicality within the IFm (Hunze and Wonik, 2008), we suggest that the inferred redox fluctuations were mainly controlled by supra-seasonal (sub-orbital to orbital) climatic cycles. No indications of cooler periods that interrupted the generally warm climatic conditions of the Pliocene (De Schepper et al. (2013), and references therein) are provided by the magnetic parameters. Our results also do not reflect the intensification of seasonality between 2.8 and 2.5 Ma (Williams et al., 2009). The evidence of this change in seasonality may have been erased by the pervasive transformation processes. However, the discontinuous nature of the sedimentary record and the coarseness of the sampling interval (ca. 50 cm) may also serve to eliminate high-frequency signals.

In contrast to the environmental situation described above, the sedimentary material contained in the Heidelberg core suggests that different environmental conditions prevailed during most of the Pliocene. Greyish to brownish, partly organic-rich sandy layers were likely produced by high-sinuosity meandering rivers and extensive lake basins (Przyrowski and Schäfer, 2015). The alternation with

hydromorphic soils deposited in the floodplain environment is reflected in the S-ratio variations (fig. 4.4). However, at the end of the Pliocene, haematite-rich debris from the widespread Triassic Bundsandstein formation in the hinterland (Hagedorn and Boenigk, 2008, Simon, 2012, Reiter et al., 2013) began to affect the S-ratios of the Heidelberg core. Thus, the small values that occur from a depth of approximately 315 m upwards do not indicate hot and dry climatic conditions; instead, they reflect an increase in the impact of the Odenwald sediment supply and the Neckar alluvial fan (Simon, 2012) during times of intensified erosion. We attribute the frequent occurrence of sulphide minerals, especially greigite, throughout the Pliocene part of the core to the prevalence of locally stable diagenetic conditions during Pliocene times. High subsidence rates (Kraus, 2002) and the continuous water supply from the Rhine and Neckar Rivers may have caused higher water levels at the Heidelberg core than at the locations of the Viernheim core and core P36 (Van Breemen, 1988, Ginn et al., 2017). In this regard, the hydromorphic soil horizons identified within the Heidelberg core reflect the periodic drying of normally saturated soils within a landscape with spatially restricted and erratically distributed lacustrine environments. These observations may point towards the occurrence of extreme climate events. However, sliding-window spectral analysis of the natural radioactivity of the sediments reveals the presence of strong cyclicity over the entire IFm within the Heidelberg core, as in the other two cores (Hunze and Wonik, 2008).

Close to the time of the Pliocene-Pleistocene transition, the subsidence of the southern part of the URG (Dèzes et al., 2004) results in the extension of the drainage area of the Rhine River by the northward deflection of the Aare River (Sissingh, 1998, Giamboni et al., 2004, Preusser, 2008, Ziegler and Fraefel, 2009, Reiter et al., 2013, Reiter et al., 2015). This development is reflected by a prominent change in the sediment provenance, which can be recognised in the heavy mineral spectra. Until that time, the Variscan graben shoulders of the URG supplied sedimentary materials, which are characterised by a stable heavy mineral assemblage (zircon, tourmaline, and rutile-anatase). Subsequently, an unstable heavy mineral suite (garnet, epidote, and hornblende) originating from the Molasse Basin or the northern Central Alps is preserved (Hagedorn, 2004, Hagedorn and Boenigk, 2008, Hoselmann, 2008, Reiter et al., 2015). Prior to the recent identification of the GMB near the top of the IFm (Scheidt et al., 2015), this dominant change in the mineral association was taken to represent the base of the Quaternary (Bartz, 1953). However, the Pliocene-Pleistocene boundary defined by the magnetic reversal, and the base of the Quaternary defined by the change in the heavy mineral composition may coincide, if the top of the IFm is eroded. At first glance, the proximity of the extension of the drainage area to the Pliocene-Pleistocene boundary raises the question as to whether its effects on the magnetic signals can be distinguished from the climatically induced signal that is expected at the beginning of the Quaternary. Rolf et al. (2008) identified a good correlation between

the MS values of core P34 (a sister core of P36) and the heavy mineral signature. Likewise, the distribution of the susceptibility values of core P36 recalls the shape of the heavy mineral diagram. For the other two cores, the correlation cannot be discerned clearly because only core P36 shows the recurrence of the stable heavy mineral signature during the Pleistocene. These intercalations result from a relocation of the riverbed of the palaeo-Rhine that allows for the predominant accumulation of sedimentary material derived from the western graben shoulder (Hoselmann and Weidenfeller, 2014). However, the change in provenance does not influence the measured Fe/Ti ratios (fig. 4.2). Thus, the enrichment of titanium with respect to iron does not depend on the source areas of the deposited sediments; instead, it results from climatic controls on diagenetic conditions.

Closer examination indicates that the rock magnetic parameters increase (indicative for soft magnetic minerals) before the effects of the increase in the catchment area are seen. Consequently, we propose that most of the change in the bulk sediment magnetic parameters is driven by climatic aspects, including changes in the hydrological regime. Thus, the alternating oxidizing-reducing conditions transitioned to dominantly reducing ones. The sediment layers at the top of the IFm were less affected by pervasive redox cycles than the older parts; thus, they preserve larger amounts of ferrimagnetic constituents. The increased S-ratios in the Viernheim core and core P36 correlate roughly with the transition from red and orange sediments to grey colours. Thus, the conditions required for the formation of haematite disappeared quickly. Sedimentary facies analyses (Hoselmann, 2008, Przyrowski and Schäfer, 2015) support this interpretation through the recognition of changes in the depositional dynamics. We tentatively propose that the change in the hydrological regime was related to an increase in the continuity of the water supply, which may have been related to the early glaciation of the Alps. Because Reiter et al. (2015) suggested an early connection to the Alpine region from 4.2 Ma onwards, the later extension of the drainage area of the Rhine River does not necessarily contradict this idea. The water from the Alps may have followed flow paths other than the larger rivers during most of the Pliocene; alternatively, and more likely, the significant extension of glacial ice during the latest Pliocene in the high Alps provided greater amounts of water and resulted in a more continuous water supply. This hypothesis certainly needs confirmation from additional data.

The sequence contained in the Heidelberg core displays only minor changes around the Pliocene-Pleistocene boundary. On the one hand, the smaller contrast between the magnitude of the NRM and the susceptibility values can be explained by the presence of larger amounts of ferrimagnetic minerals in the Pliocene sediments. On the other hand, the heavy mineral spectrum of the Pleistocene lithostratigraphic formations of the Heidelberg core indicates larger proportions of sedimentary material derived from the graben margin and the Neckar catchment (Hagedorn, 2004, Hagedorn and

Boenigk, 2008, Simon, 2012). Correlation of the NRM and MS values with the heavy mineral signature of core P36 shows that sediments characterised by this stable mineral suite tend to show lower values relative to the unstable heavy mineral spectrum (fig. 4.3). Because these two options are not mutually exclusive, we assume the minor variability between the bulk sample parameters of the Pliocene and Pleistocene part of the Heidelberg core to be due to both, the primary composition and the diagenetic overprint. The S-ratios of Heidelberg core are virtually not affected by any change around the Pliocene-Pleistocene boundary. Due to ongoing deposition of haematite-rich debris, no climatic signals are extractable.

The Pleistocene sediments are characterised by a rather monotonous series that display predominantly greyish and greenish colours. Only the Heidelberg core shows intercalations of red-coloured Tertiary material derived from the graben shoulders or the Neckar alluvial fan. The higher NRM and susceptibility values result from the persistent presence of greigite in the Quaternary sediments. The greigite appears to be diagenetic, though an extracellular biogenic origin is also possible. Magnetofossils were not identified. The formation and preservation of greigite point towards continuous reducing conditions, high accumulation rates, fast burial, and reactant-limited conditions (Berner, 1970, Kao et al., 2004, Roberts, 2015). Goethite is also found in the Pleistocene sediments, but there are reasons to assume that at least some of this mineral formed as a breakdown product of sulphides during storage of the core. Overall, the Pleistocene magnetic mineral assemblage points towards clearly cooler and moister diagenetic conditions than those that prevailed in late Pliocene times. The variations in the sources of sediments described in Reiter et al. (2015) are not reflected in the rock magnetic record. Nor do the cores contain evidence of the multiple warm-climate peaks and cold-climate troughs that have been identified in British terrestrial records (Schreve and Candy, 2010) and southern Europe sediment cores (Tzedakis et al., 2006). However, it is possible that horizons with smaller S-ratios within the VFm of the Viernheim core and core P36 represent (fig. 4.2-4.3) warm periods (Larrasoana et al., 2003); however, insufficient data obtained using these approaches are presently available.

4.7.2. Implications for the reconstruction of climatic conditions of Central Europe during the Pliocene-Pleistocene

A major obstacle to the production of a detailed reconstruction of the Pliocene-Pleistocene climatic evolution of central and northwestern Europe is the lack of sufficiently resolved records with well-constrained age models (Utescher et al., 2012). To date, (semi-)continuous successions reflecting the late Pliocene and early Pleistocene climate evolution have only been available from the northern parts of northwestern Europe (e.g., Utescher et al. 2000, Zagwijn 1985, 1992, Heumann and Litt, 2002, Walker et al., 1994, Schreve and Candy, 2010). Further south, even small, isolated outcrops are

extremely rare. This is particularly true in the Alpine realm, where glaciofluvial erosion and the redeposition of unconsolidated sediments have substantially reshaped the landscape. The Heidelberg Basin drill cores now provide desperately needed data from southwestern Germany and the more southerly regions where large fractions of the accumulated sedimentary material originated. These results have implications for Pliocene and Pleistocene climatic conditions in the portions of central and northwestern Europe where records have not yet been obtained. Our knowledge would increase further through sampling at finer intervals and the inclusion of the still-pending palynological data. Combining these results with pollen data might provide crucial information that would guide the next step towards the final correlation of the stratigraphic positions of the glaciations of Northern Europe and the Alpine region.

Another important benefit of the data from the Heidelberg Basin cores is the identification of the timing of the intensification of the Northern Hemisphere glaciation (iNHG) in a terrestrial record in Central Europe. As described above (section 4.7.1), the data document a rapid change in climatic conditions at the end of the Pliocene. This development is consistent with the increases in erosion rates that have been identified in various sedimentary archives throughout the entire Northern Hemisphere (fig 4.6) and in global trends (Herman & Champagnac, 2016).

The iNHG has been recognised to have occurred at approximately 2.7 Ma in sediments of Lake El'gygytgyn in Russia (Brigham-Grette et al., 2013), and the red clay sequence of the Chinese loess plateau (Ding et al., 2005, Nie et al., 2014, Nie et al., 2016), as well as the supply of dust from the North American continent into the North Atlantic (Lang et al., 2014). In marine environments, changes in sea surface temperatures and the occurrence of ice-rafted debris (IRD) also indicate the onset of glaciations in the north at approximately 2.7 Ma (e.g., Bailey et al., 2013, Dowsett and Poore, 1990, Dowsett and Poore, 1991, Haug et al., 2005, Jansen et al., 2000, Kleiven et al., 2002, Maslin et al., 1998, Raymo, 1994, Tiedemann et al., 1994). Naturally, these studies represent a few examples of a vast number of works that provide evidence on the chronology of the iNHG. We do not review this topic further here, and we also do not discuss the forcing mechanisms that produced the iNHG. For information on these topics, we refer the reader to the literature (e.g., Raymo, 1994, Ravelo et al., 2007, Lisiecki and Raymo, 2007, De Schepper et al., 2014). Instead, we note that a tentative integration of the evolution of the Heidelberg Basin into the palaeoclimatic history of the Northern Hemisphere supports recent reconstructions of the transition of the climate from a greenhouse state to an icehouse state.
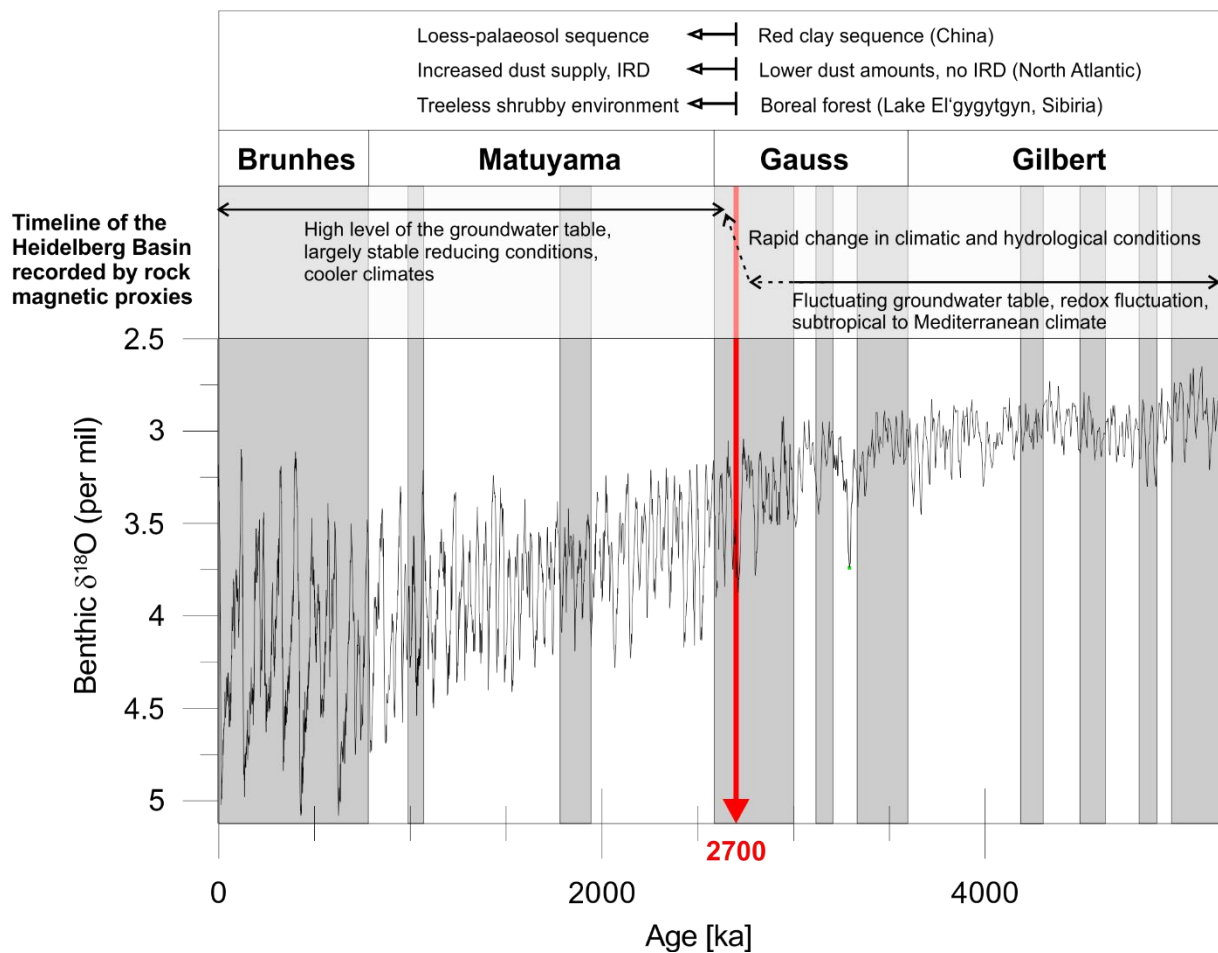
Figure 4.6:
Overview of proxy records that reflect the transition from a greenhouse state to an icehouse state at approximately 2.7 Ma. This transition is indicated by rock magnetic proxies of the Heidelberg Basin, changes in aeolian deposits in China (Nie et al. 2016*), geological evidence from marine drill cores obtained from the North Atlantic (*Lang et al. 2014*), and vegetation changes in Siberia (*Brigham-Grette et al., 2013*). The benthic δ¹⁸O records* (Lisiecki and Raymo, 2005) *represent marine responses to global climate change.*

The information provided by this study should be considered in future simulations of the continental climatic development; to date, such studies have been based primarily on information from adjacent regions (e.g., Haywood et al., 2000, Jost et al., 2009, Popescu et al., 2010).

Taken together, the sedimentary archive of the Heidelberg Basin may provide information of crucial importance in improving our understanding of the Pliocene and Pleistocene climatic development on local (Heidelberg Basin), regional (southwestern Germany), and even hemispheric contexts.

4.8. Conclusion

The data obtained from the Heidelberg Basin succession represent the first (semi-)continuous documentation of the evolution of environmental and climate conditions from the late Pliocene to the present day in southern part of Central Europe. We use data from two completed studies on magnetic polarity stratigraphy and magnetomineralogy to trace the environmental development of the region. The climatic conditions of the late Pliocene were likely warm and humid and alternated with dry periods. The floodplain deposits of this age reflect the effects of water table fluctuations that presumably resulted from supra-seasonal (sub-orbital to orbital) climatic cycles. The redox fluctuations that were produced in this way led to the transformation of most of the detrital iron minerals into low-ordered $Fe(III)$ phases. During hot and dry periods, authigenic haematite formed. The iNHG began at the very end of the Pliocene, when the diagenetic conditions responded to rapid cooling and a change in the hydrological regime. The persistent reducing conditions promoted the preservation of Fe sulphides, particularly greigite; however, authigenic haematite ceased to form. These conditions have largely persisted until the present day. Variations within the environmental magnetic record cannot directly be assigned to changes in climate during the Quaternary without further information (e.g., palynology, clay mineralogy), that is not yet available. We are confident that further investigations will enable more detailed reconstructions. However, considering only the environmental magnetic evidence, it appears that the evolution of the Heidelberg Basin reflects palaeoclimatic trends that agree with those obtained by studies performed elsewhere in the Northern Hemisphere. Thus, this study demonstrates that fluvial sediments can preserve rock magnetic data that reflect environmental and climate changes; this possibility has widely been discounted previously.

References

BAILEY, I., HOLE, G. M., FOSTER, G. L., WILSON, P. A., STOREY, C. D., TRUEMAN, C. N. & RAYMO, M. E. 2013. An alternative suggestion for the Pliocene onset of major northern hemisphere glaciation based on the geochemical provenance of North Atlantic Ocean ice-rafted debris. *Quaternary Science Reviews,* 75**,** 181-194.

BANERJEE, S. K. 1965. On the Transition of Magnetite to Haematite and its Implications to Rockmagnetism. *Journal of geomagnetism and geoelectricity,* 17**,** 357-361.

BARTZ, J. 1953. Revision des Bohr-Profils der Heidelberger Radium-Sol-Therme. *Jahresberichte und Mitteilungen des Oberrheinischen Geologischen Vereins***,** 101-125.

BARTZ, J. 1974. Die Mächtigkeit des Quartärs im Oberrheingraben. *In:* ILLIES, J. H. & FUCHS, K. (eds.) *Approaches to Taphrogenesis.* Stuttgart: Schweizerbart.

BERNER, R. A. 1970. Sedimentary pyrite formation. *American Journal of Science,* 268**,** 1-23.

BOERSMA, L., SIMONSON, G. & WATTS, D. 1972. Soil morphology and water table relations: I. Annual water table fluctuations. *Soil Science Society of America Journal,* 36**,** 644-648.

BOGAART, P. W. & VAN BALEN, R. T. 2000. Numerical modeling of the response of alluvial rivers to Quaternary climate change. *Global and Planetary Change,* 27**,** 147-163.

BOLLIGER, T., FEJFAR, O., GRAF, H. & KÄLIN, D. 1996. Vorläufige Mitteilung über Funde von pliozänen Kleinsäugern aus den höheren Deckenschottern des Irchels (Kt. Zürich). *Eclogae Geologicae Helvetiae,* 89**,** 1043-1048.

BOUMA, J. 1983. Hydrology and soil genesis of soils with aquic moisture regimes. *Developments in Soil Science,* 11**,** 253-281.

BRIGHAM-GRETTE, J., MELLES, M., MINYUK, P., ANDREEV, A., TARASOV, P., DECONTO, R., KOENIG, S., NOWACZYK, N. R., WENNRICH, V., ROSÉN, P., HALTIA, E., COOK, T., GEBHARDT, C., MEYER-JACOB, C., SNYDER, J. & HERZSCHUH, U. 2013. Pliocene Warmth, Polar Amplification, and Stepped Pleistocene Cooling Recorded in NE Arctic Russia. *Science,* 340**,** 1421-1427.

BUNESS, H., GABRIEL, G. & ELLWANGER, D. 2008. The Heidelberg Basin drilling project: Geophysical pre-site surveys. *E & G (Quaternary Science Journal),* 57**,** 338-366.

BYRNE, J. M., KLUEGLEIN, N., PEARCE, C., ROSSO, K. M., APPEL, E. & KAPPLER, A. 2015. Redox cycling of Fe (II) and Fe (III) in magnetite by Fe-metabolizing bacteria. *Science,* 347**,** 1473-1476.

CANFIELD, D. E., RAISWELL, R. & BOTTRELL, S. H. 1992. The reactivity of sedimentary iron minerals toward sulfide. *American Journal of Science,* 292**,** 659-683.

CLARK, P. U., ARCHER, D., POLLARD, D., BLUM, J. D., RIAL, J. A., BROVKIN, V., MIX, A. C., PISIAS, N. G. & ROY, M. 2006. The middle Pleistocene transition: characteristics, mechanisms, and implications for long-term changes in atmospheric pCO_2. *Quaternary Science Reviews,* 25**,** 3150-3184.

DE SCHEPPER, S., GIBBARD, P. L., SALZMANN, U. & EHLERS, J. 2014. A global synthesis of the marine and terrestrial evidence for glaciation during the Pliocene Epoch. *Earth-Science Reviews,* 135**,** 83-102.

DE SCHEPPER, S., GROENEVELD, J., NAAFS, B. D. A., VAN RENTERGHEM, C., HENNISSEN, J., HEAD, M. J., LOUWYE, S. & FABIAN, K. 2013. Northern hemisphere glaciation during the globally warm early late Pliocene. *PloS one,* 8**,** e81508.

DÈZES, P., SCHMID, S. & ZIEGLER, P. 2004. Evolution of the European Cenozoic Rift System: interaction of the Alpine and Pyrenean orogens with their foreland lithosphere. *Tectonophysics,* 389**,** 1-33.

DING, Z., DERBYSHIRE, E., YANG, S., SUN, J. & LIU, T. 2005. Stepwise expansion of desert environment across northern China in the past 3.5 Ma and implications for monsoon evolution. *Earth and Planetary Science Letters,* 237**,** 45-55.

DOWSETT, H. J. & POORE, R. Z. 1991. Pliocene sea surface temperatures of the north atlantic ocean at 3.0 Ma. *Quaternary Science Reviews,* 10**,** 189-204.

ELLWANGER, D., GABRIEL, G., HOSELMANN, C., LÄMMERMANN-BARTHEL, J. & WEIDENFELLER, M. 2005. The Heidelberg drilling project (Upper Rhine Graben, Germany). *Quaternaire. Revue de l'Association française pour l'étude du Quaternaire,* 16**,** 191-199.

ELLWANGER, D., GABRIEL, G., HOSELMANN, C., WEIDENFELLER, M. & WIELANDT-SCHUSTER, U. 2010a. Mannheim-Formation. *Litholex (online database).* 03.11.2010 ed. http://www.bgr.bund.de/litholex: Federal Institute for Geosciences and Natural Resources (BGR).

ELLWANGER, D., GRIMM, M., HOSELMANN, C., HOTTENROTT, M., WEIDENFELLER, M. & WIELANDT-SCHUSTER, U. 2010b. Iffezheim-Formation. *Litholex (online database).* 03.11.2010 ed. http://www.bgr.bund.de/litholex: Federal Institute for Geosciences and Natural Resources (BGR).

ELLWANGER, D., WIELANDT-SCHUSTER, U., FRANZ, M. & SIMON, T. 2011. The Quaternary of the southwest German Alpine Foreland (Bodensee-Oberschwaben, Baden-Württemberg, Southwest Germany). *E & G (Quaternary Science Journal),* 60**,** 306–328.

FIMMEN, R. L., VASUDEVAN, D., WILLIAMS, M. A. & WEST, L. T. 2008. Rhizogenic Fe–C redox cycling: a hypothetical biogeochemical mechanism that drives crustal weathering in upland soils. *Biogeochemistry,* 87**,** 127-141.

FLORINDO, F., ROBERTS, A. P. & PALMER, M. R. 2003. Magnetite dissolution in siliceous sediments, Geochemistry, Geophysics, Geosystems, 4, 1053, doi: 10.1029/2003GC000516, 7

GABRIEL, G., ELLWANGER, D., HOSELMANN, C. & WEIDENFELLER, M. 2008. Preface: The Heidelberg Basin Drilling Project. *E & G (Quaternary Science Journal),* 57**,** 253-260.

GABRIEL, G., ELLWANGER, D., HOSELMANN, C., WEIDENFELLER, M. & WIELANDT-SCHUSTER, U. 2013. The Heidelberg Basin, Upper Rhine Graben (Germany): a unique archive of Quaternary sediments in Central Europe. *Quaternary International,* 292**,** 43-58.

GIAMBONI, M., USTASZEWSKI, K., SCHMID, S., SCHUMACHER, M. & WETZEL, A. 2004. Plio-Pleistocene transpressional reactivation of Paleozoic and Paleogene structures in the Rhine-Bresse transform zone (northern Switzerland and eastern France). *International Journal of Earth Sciences,* 93**,** 207-223.

GINN, B., MEILE, C., WILMOTH, J., TANG, Y. & THOMPSON, A. 2017. Rapid Iron Reduction Rates Are Stimulated by High-Amplitude Redox Fluctuations in a Tropical Forest Soil. *Environmental Science & Technology,* 51**,** 3250-3259.

GRAF, H. R. 1993. *Die Deckenschotter der zentralen Nordschweiz*. Doktorarbeit. ETH Zurich

HAGEDORN, E.-M. 2004. *Sedimentpetrographie und Lithofazies der Jungtertiären und Quartären Sedimente im Oberrheingebiet.* Dissertation, Universität zu Köln.

HAGEDORN, E.-M. & BOENIGK, W. 2008. The Pliocene and Quaternary sedimentary and fluvial history in the Upper Rhine Graben based on heavy mineral analyses. *Netherlands Journal of Geosciences,* 87**,** 19-30.

HAHNE, J., ELLWANGER, D., FRANZ, M., STRITZKE, R. & WIELAND-SCHUSTER, U. 2012. Pollenanalytische Untersuchungsergebnisse aus dem baden-württembergischen Rheinsystem

Oberrheingraben, Hochrhein, Oberschwaben - eine Zusammenfassung des aktuellen Kenntnisstandes. *LGRB-Informationen,* 26**,** 33.

HAHNE, J., ELLWANGER, D. & STRITZKE, R. 2008. Evidence for a Waalian thermomer pollen record from the research borehole Heidelberg UniNord, Upper Rhine Graben, Baden-Württemberg. *E & G (Quaternary Science Journal),* 57**,** 403-410.

HAUG, G. H., GANOPOLSKI, A., SIGMAN, D. M., ROSELL-MELE, A., SWANN, G. E., TIEDEMANN, R., JACCARD, S. L., BOLLMANN, J., MASLIN, M. A. & LENG, M. J. 2005. North Pacific seasonality and the glaciation of North America 2.7 million years ago. *Nature,* 433**,** 821-825.

HAYWOOD, A., SELLWOOD, B. & VALDES, P. 2000. Regional warming: Pliocene (3 Ma) paleoclimate of Europe and the Mediterranean. *Geology,* 28**,** 1063-1066.

HERMAN, F. & CHAMPAGNAC, J. D. 2016. Plio-Pleistocene increase of erosion rates in mountain belts in response to climate change. *Terra Nova,* 28**,** 2-10.

HEUMANN, G. & LITT, T. 2002. Stratigraphy and paleoecology of the Late Pliocene and Early Pleistocene in the open-cast mine Hambach (Lower Rhine Basin). *Netherlands Journal of Geosciences,* 81**,** 193-199.

HOSELMANN, C. 2008. The Pliocene and Pleistocene fluvial evolution in the northern Upper Rhine Graben based on results of the research borehole at Viernheim (Hessen, Germany). *E & G (Quaternary Science Journal),* 57**,** 286-315.

HOSELMANN, C., ELLWANGER, D., GABRIEL, G., LAUER, T., WEDEL, J. & WEIDENFELLER, M. Forschungsbohrungen im nördlichen Oberrheingraben (Heidelberger Becken) - neue Erkenntnisse zur geologischen Entwicklung. Hauptversammlung der Deutschen Quartärvereinigung e.V. (DEUQUA), 31.08.2008-06.09.2008 2008 Wien. Abhandlungen der Geologischen Bundesanstalt, 95-98.

HOSELMANN, C., ELLWANGER, D., GABRIEL, G., WEIDENFELLER, M. & WIELANDT-SCHUSTER, U. 2010. Viernheim-Formation. *Litholex (online database).* 03-11-2010 ed. http://www.bgr.bund.de/litholex: Federal Institute for Geosciences and Natural Resources (BGR).

HOSELMANN, C. & WEIDENFELLER, M. 2014. Schwermineralogische Provenienz-Analyse im nördlichen Oberrheingraben (Poster). *DEUQUA (37. Hauptversammlung der Deutschen Quartärvereinigung).* Innsbruck (24.-29.09.2014).

HUNZE, S. & WONIK, T. 2008. Sediment Input into the Heidelberg Basin as determined from Downhole Logs. *E & G (Quaternary Science Journal),* 57**,** 367-381.

ISAMBERT, A., LETARD, I., GLOTER, A., VALET, J.-P. & GUYOT, F. 2003. Mechanisms of oxidation of natural greigite (Fe_3S_4). *EGS - AGU - EUG Joint Assembly,* 2003EAEJA.....8904I.

JANSEN, E., FRONVAL, T., RACK, F. & CHANNELL, J. E. 2000. Pliocene-Pleistocene ice rafting history and cyclicity in the Nordic Seas during the last 3.5 Myr. *Paleoceanography,* 15(6), 709–721, doi: 10.1029/1999PA000435.

JOST, A., FAUQUETTE, S., KAGEYAMA, M., KRINNER, G., RAMSTEIN, G., SUC, J.-P. & VIOLETTE, S. 2009. High resolution climate and vegetation simulations of the Mid-Pliocene, a model-data comparison over western Europe and the Mediterranean region. *Climate of the Past,* 5**,** 585-606.

KAO, S.-J., HORNG, C.-S., ROBERTS, A. P. & LIU, K.-K. 2004. Carbon–sulfur–iron relationships in sedimentary rocks from southwestern Taiwan: influence of geochemical environment on greigite and pyrrhotite formation. *Chemical Geology,* 203**,** 153-168.

KLEIVEN, H. F., JANSEN, E., FRONVAL, T. & SMITH, T. 2002. Intensification of Northern Hemisphere glaciations in the circum Atlantic region (3.5–2.4 Ma)–ice-rafted detritus evidence. *Palaeogeography, Palaeoclimatology, Palaeoecology,* 184**,** 213-223.

KNAB, M., HOFFMANN, V. & APPEL, E. 2000. Magnetic susceptibility as a proxy for heavy metal contamination in roadside soils. *Geologica Carpathica Bratislava, June,* 51**,** 199.

KNIPPING, M. 2008. Early and Middle Pleistocene pollen assemblages of deep core drillings in the northern Upper Rhine Graben, Germany. *Netherlands Journal of Geosciences,* 87**,** 51-65.

KRAUS, M. J. 1999. Paleosols in clastic sedimentary rocks: their geologic applications. *Earth-Science Reviews,* 47**,** 41-70.

KRAUS, M. J. 2002. Basin-scale changes in floodplain paleosols: implications for interpreting alluvial architecture. *Journal of Sedimentary Research,* 72**,** 500-509.

KRAUS, M. J. & ASLAN, A. 1993. Eocene hydromorphic paleosols: significance for interpreting ancient floodplain processes. *Journal of Sedimentary Research,* 63**,** 453-463.

LANG, D. C., BAILEY, I., WILSON, P. A., BEER, C. J., BOLTON, C. T., FRIEDRICH, O., NEWSAM, C., SPENCER, M. R., GUTJAHR, M., FOSTER, G. L., COOPER, M. J. & MILTON, J. A. 2014. The transition on North America from the warm humid Pliocene to the glaciated Quaternary traced by eolian dust deposition at a benchmark North Atlantic Ocean drill site. *Quaternary Science Reviews,* 93**,** 125-141.

LARRASOANA, J. C., ROBERTS, A. P., STONER, J. S., RICHTER, C. & WEHAUSEN, R. 2003. A new proxy for bottom-water ventilation in the eastern Mediterranean based on diagenetically controlled magnetic properties of sapropel-bearing sediments. *Palaeogeography, Palaeoclimatology, Palaeoecology,* 190**,** 221-242.

LAUER, T., FRECHEN, M., HOSELMANN, C. & TSUKAMOTO, S. 2010. Fluvial aggradation phases in the Upper Rhine Graben—new insights by quartz OSL dating. *Proceedings of the Geologists' Association,* 121**,** 154-161.

LAUER, T., KRBETSCHEK, M., FRECHEN, M., TSUKAMOTO, S., HOSELMANN, C. & WEIDENFELLER, M. 2011. Infrared radiofluorescence (IR-RF) dating of middle pleistocene fluvial archives of the Heidelberg Basin (Southwest Germany). *Geochronologia,* 38**,** 23–33.

LAWRENCE, K., SOSDIAN, S., WHITE, H. & ROSENTHAL, Y. 2010. North Atlantic climate evolution through the Plio-Pleistocene climate transitions. *Earth and Planetary Science Letters,* 300**,** 329-342.

LI, Y., TSUKAMOTO, S., FRECHEN, M. & GABRIEL, G. 2018. Timing of fluvial sedimentation in the Upper Rhine Graben since the Middle Pleistocene: constraints from quartz and feldspar luminescence dating. *Boreas,* 47**,** 256-270.

LISIECKI, L. E. & RAYMO, M. E. 2005. A Pliocene-Pleistocene stacl of 57 globally distributed benthic δ^{18} O records. *Paleoceanography,* 20, PA1003, doi: 10.1029/2004PA001071.

LISIECKI, L. E. & RAYMO, M. E. 2007. Plio–Pleistocene climate evolution: trends and transitions in glacial cycle dynamics. *Quaternary Science Reviews,* 26**,** 56-69.

LIU, Q., BARRÓN, V., TORRENT, J., EECKHOUT, S. G. & DENG, C. 2008. Magnetism of intermediate hydromaghemite in the transformation of 2-line ferrihydrite into hematite and its paleoenvironmental implications. *Journal of Geophysical Research B: Solid Earth,* 113, B01103, doi:10.1029/2007JB005207.

LIU, X., SHAW, J., JIANG, J., BLOEMENDAL, J., HESSE, P., ROLPH, T. & MAO, X. 2010. Analysis on variety and characteristics of maghemite. *Science China Earth Sciences,* 53**,** 1153-1162.

MASLIN, M., LI, X., LOUTRE, M.-F. & BERGER, A. 1998. The contribution of orbital forcing to the progressive intensification of Northern Hemisphere glaciation. *Quaternary Science Reviews,* 17**,** 411-426.

MOSBRUGGER, V., UTESCHER, T. & DILCHER, D. L. 2005. Cenozoic continental climatic evolution of Central Europe. *Proceedings of the National Academy of Sciences of the United States of America,* 102**,** 14964-14969.

MUDELSEE, M. & SCHULZ, M. 1997. The Mid-Pleistocene climate transition: onset of 100 ka cycle lags ice volume build-up by 280 ka. *Earth and Planetary Science Letters,* 151**,** 117-123.

NAWAZ, M. F., BOURRIE, G. & GUL, S. 2014. Factors affecting redox reactions in hydromorphic soils. A review. *Pakistan Journal of Agricultural Sciences,* 51**,** 517-523.

NIE, J., ZHANG, R., NECULA, C., HESLOP, D., LIU, Q., GONG, L. & BANERJEE, S. K. 2014. Late Miocene–early Pleistocene paleoclimate history of the Chinese Loess Plateau revealed by remanence unmixing. *Geophysical Research Letters,* 41**,** 2163-2168.

POPESCU, S.-M., BILTEKIN, D., WINTER, H., SUC, J.-P., MELINTE-DOBRINESCU, M. C., KLOTZ, S., RABINEAU, M., COMBOURIEU-NEBOUT, N., CLAUZON, G. & DEACONU, F. 2010. Pliocene and Lower Pleistocene vegetation and climate changes at the European scale: Long pollen records and climatostratigraphy. *Quaternary International,* 219**,** 152-167.

POULTON, S. W., KROM, M. D. & RAISWELL, R. 2004. A revised scheme for the reactivity of iron (oxyhydr) oxide minerals towards dissolved sulfide. *Geochimica et Cosmochimica Acta,* 68**,** 3703-3715.

PREUSSER, F. 2008. Characterisation and evolution of the River Rhine system. *Netherlands Journal of Geosciences,* 87**,** 7-19.

PRZYROWSKI, R. & SCHÄFER, A. 2015. Quaternary fluvial basin of northern Upper Rhine Graben. *Zeitschrift der Deutschen Gesellschaft für Geowissenschaften,* 166**,** 71-98.

RAVELO, A., BILLUPS, K., DEKENS, P., HERBERT, T. & LAWRENCE, K. 2007. Onto the ice ages: proxy evidence for the onset of Northern Hemisphere glaciation. *Deep Time Perspectives on Climate Change. The Micropalaeontological Society***,** 563-574.

RAYMO, M. E. 1994. The Initiation of Northern Hemisphere Glaciation. *Annual Review of Earth and Planetary Sciences,* 22**,** 353-383.

RAYMO, M. E., HODELL, D. & JANSEN, E. 1992. Response of deep ocean circulation to initiation of Northern Hemisphere glaciation (3–2 Ma). *Paleoceanography,* 7(5), 645–672, doi: 10.1029/92PA01609.

REITER, W., ELFERT, S., GLOTZBACH, C., BERNET, M. & SPIEGEL, C. 2013. Relations between denudation, glaciation, and sediment deposition: implications from the Plio-Pleistocene Central Alps. *Basin Research,* 25**,** 659-674.

REITER, W., ELFERT, S., GLOTZBACH, C. & SPIEGEL, C. 2015. Plio-Pleistocene evolution of the north Alpine drainage system: new constraints from detrital thermochronology of foreland deposits. *International Journal of Earth Sciences,* 104**,** 891-907.

ROBERTS, A. P. 2015. Magnetic mineral diagenesis. *Earth-Science Reviews,* 151**,** 1-47.

ROLF, C., HAMBACH, U. & WEIDENFELLER, M. 2008. Rock and palaeomagnetic evidence for the Plio-Pleistocene palaeoclimatic change recorded in Upper Rhine Graben sediments (Core Ludwigshafen Parkinsel). *Netherlands Journal of Geosciences,* 87**,** 41-50.

SCHEIDT, S., EGLI, R., FREDERICHS, T., HAMBACH, U. & ROLF, C. 2017. A mineral magnetic characterization of the Plio-Pleistocene fluvial infill of the Heidelberg Basin (Germany). *Geophysical Journal International,* 210**,** 743-764.

SCHEIDT, S., HAMBACH, U. & ROLF, C. 2015. A consistent magnetic polarity stratigraphy of late Neogene to Quaternary fluvial sediments from the Heidelberg Basin (Germany): A new time frame for the Plio–Pleistocene palaeoclimatic evolution of the Rhine Basin. *Global and Planetary Change,* 127**,** 103-116.

SCHIRMER, W. 2003. Stadien der Rheingeschichte. *In:* SCHIRMER, W. (ed.) *Landschaftsgeschichte im europäischen Rheinland.* GeoArchaeoRhein.

SCHREVE, D. & CANDY, I. 2010. Interglacial climates: Advances in our understanding of warm climate episodes. *Progress in Physical Geography,* 34**,** 845-856.

SCHUMACHER, M. E. 2002. Upper Rhine Graben: Role of preexisting structures during rift evolution. *Tectonics,* 21**,** 6-1-6-17.

SIMON, T. 2012. Herkunft und Transport der Sedimente in der Forschungsbohrung Heidelberg UniNord. *LGRB-Informationen,* 26.

SIMONSON, G. & BOERSMA, L. 1972. Soil morphology and water table relations: II. Correlation between annual water table fluctuations and profile features. *Soil Science Society of America Journal,* 36**,** 649-653.

SISSINGH, W. 1998. Comparative tertiary stratigraphy of the Rhine Graben, Bresse Graben and Molasse Basin: correlation of Alpine foreland events. *Tectonophysics,* 300**,** 249-284.

TATZEL, M., DUNKL, I. & VON EYNATTEN, H. 2017. Provenance of Palaeo-Rhine sediments from zircon thermochronology, geochemistry, U/Pb dating and heavy mineral assemblages. *Basin Research,* 29**,** 396-417.

TIEDEMANN, R., SARNTHEIN, M. & SHACKLETON, N. J. 1994. Astronomic timescale for the Pliocene Atlantic $\delta^{18}O$ and dust flux records of Ocean Drilling Program Site 659. *Paleoceanography,* 9(4), 619–638, doi: 10.1029/94PA00208.

TURNER, P. 1980. *Continental red beds,* New York, Elsevier.

TZEDAKIS, P., HOOGHIEMSTRA, H. & PÄLIKE, H. 2006. The last 1.35 million years at Tenaghi Philippon: revised chronostratigraphy and long-term vegetation trends. *Quaternary Science Reviews,* 25**,** 3416-3430.

UTESCHER, T., ASHRAF, A. R., DREIST, A., DYBKJAER, K., MOSBRUGGER, V., PROSS, J. & WILDE, V. 2012. Variability of neogene continental climates in Northwest Europe-a detailed study based on microfloras. *Turkish Journal of Earth Sciences,* 21**,** 289-314.

VAN BREEMEN, N. 1988. Long-term chemical, mineralogical, and morphological effects of iron-redox processes in periodically flooded soils. *Iron in Soils and Clay Minerals.* Springer.

VAN DAM, J. A. 2006. Geographic and temporal patterns in the late Neogene (12–3 Ma) aridification of Europe: the use of small mammals as paleoprecipitation proxies. *Palaeogeography, Palaeoclimatology, Palaeoecology,* 238**,** 190-218.

WALKER, M. J. C., BOHNCKE, S. J. P., COOPE, G. R., O'CONNELL, M., USINGER, H. & VERBRUGGEN, C. 1994. The Devensian/Weichselian Late-glacial in northwest Europe (Ireland, Britain, north Belgium, The Netherlands, northwest Germany). *Journal of Quaternary Science,* 9**,** 109-118.

WEDEL, J. 2008. Pleistocene molluscs from research boreholes in the Heidelberg Basin. *E & G (Quaternary Science Journal),* 57**,** 382-402.

WEIDENFELLER, M., ELLWANGER, D., GABRIEL, G., HOSELMANN, C. & WIELANDT-SCHUSTER, U. 2010. Ludwigshafen-Formation. *Litholex (online database).* 02.11.2010 ed. http://www.bgr.bund.de/litholex: Federal Institute for Geosciences and Natural Resources (BGR).

WILLIAMS, M., HAYWOOD, A. M., HARPER, E. M., JOHNSON, A. L., KNOWLES, T., LENG, M. J., LUNT, D. J., OKAMURA, B., TAYLOR, P. D. & ZALASIEWICZ, J. 2009. Pliocene climate and seasonality in North Atlantic shelf seas. *Philosophical Transactions of the Royal Society of London A: Mathematical, Physical and Engineering Sciences,* 367**,** 85-108.

ZAGWIJN, W. 1974. The Pliocene-Pleistocene boundary in western and southern Europe. *Boreas,* 6-3**,** 75-97.

ZAGWIJN, W. 1985. An outline of the Quaternary stratigraphy of the Netherlands. *Geologie en Mijnbouw,* 64**,** 17-24.

ZAGWIJN, W. 1992. The beginning of the Ice Age in Europe and its major subdivisions. *Quaternary Science Reviews,* 11**,** 583-591.

ZIEGLER, P. A. & FRAEFEL, M. 2009. Response of drainage systems to Neogene evolution of the Jura fold-thrust belt and Upper Rhine Graben. *Swiss Journal of Geosciences,* 102**,** 57-75.

Remarks to study 3

The planned focus of the third publication was developed during a meeting of the mentorship team. This manuscript was expected to include the environmental information derived from palynological and clay mineralogical studies. The co-authors responsible for these respective parts were not able to cooperate the relevant data within the specified temporal framework. Because this problem became evident in the early stages of writing the manuscript, the paper was written without the desired information. This gap particularly affects the interpretation of the Quaternary part of the succession. Presumably, assignment of the variations in the mineral magnetic record to warmer or cooler climatic phases will become possible as soon as the data are available. The authors plan to wait to submit the paper for publication until the missing information has been incorporated.

Danksagung

(Eidesstattliche) Versicherungen und Erklärungen

(§ 9 Satz 2 Nr. 3 PromO BayNAT)

Hiermit versichere ich eidesstattlich, dass ich die Arbeit selbständig verfasst und keine anderen als die von mir angegebenen Quellen und Hilfsmittel benutzt habe (vgl. Art. 64 Abs 1 Satz 6 BayHSchG).

(§ 9 Satz 2 Nr. 3 PromO BayNAT)

Hiermit erkläre ich, dass ich die Dissertation nicht bereits zur Erlangung eines akademischen Grades eingereicht habe und dass ich nicht bereits diese oder eine gleichartige Doktorprüfung endgültig nicht bestanden habe.

(§ 9 Satz 2 Nr. 4 PromO BayNAT)

Hiermit erkläre ich, dass ich Hilfe von gewerblichen Promotionsberatern bzw. - vermittlern oder ähnlichen Dienstleistern weder bisher in Anspruch genommen habe noch künftig in Anspruch nehmen werde.

(§ 9 Satz 2 Nr. 7 PromO BayNAT)

Hiermit erkläre ich mein Einverständnis, dass die elektronische Fassung meiner Dissertation unter Wahrung meiner Urheberrechte und des Datenschutzes einer gesonderten Überprüfung unterzogen werden kann.

(§ 9 Satz 2 Nr. 8 PromO BayNAT)

Hiermit erkläre ich mein Einverständnis, dass bei Verdacht wissenschaftlichen Fehlverhaltens Ermittlungen durch universitätsinterne Organe der wissenschaftlichen Selbstkontrolle stattfinden können.

……………………………………………………………………………….

Ort, Datum, Unterschrift